Cellular structure and sexual development of somatosensory cortex

Dissertation

Zur Erlangung des akademischen Grades

Doctor rerum naturalium

(Dr. rer. nat.)

im Fach Biologie

eingereicht an der

Lebenswissenschaftlichen Fakultät

der Humboldt-Universität zu Berlin

von

M.Sc.

Johanna Sigl-Glöckner

Präsidentin der Humboldt-Universität zu Berlin

Prof. Dr.-In. Dr. Sabine Kunst

Dekan der Lebenswissenschaftlichen Fakultät

Prof. Dr. Bernhard Grimm

Gutachter/innen:

1. Prof. Michael Brecht
2. Prof. Christine Heim
3. Prof. Benjamin Judkewitz

Tag der mündlichen Prüfung: 12. Dezember 2019

Cellular structure and sexual development of somatosensory cortex

Doctoral candidate:

Johanna Sigl-Glöckner

Supervisor:

Prof. Dr. Michael Brecht

September 2019

Bernstein Center for Computational Neuroscience

Animal Physiology / Systems Neurobiology and Neural Computation

Humboldt Universität zu Berlin, Berlin, Germany

NeuroCure Cluster of Excellence

Boehringer Ingelheim Fonds
Stiftung für medizinische Grundlagenforschung

Abstract

For more than a century, neuroscientists have recognized that within the mammalian neocortex, there are local groups of neurons that serve distinct functions. Key for constructing such functionally specialized cortical circuits are different neuronal cell-types, which process information depending on their physiology, morphology and synaptic connectivity. This doctoral thesis explores two functionally distinct circuits within the neocortex, namely its input (Chapters 2 to 4) and output (Chapter 5) structures, layer 4 and layer 5 respectively. The first part of the thesis comprises three studies that examine the processing of genital touch in the cortical input layer, layer 4. Specifically, we investigated how layer 4 and its inputs are structurally refined during puberty, a time when genital touch gains biological relevance. Earlier work from layer 4 of barrel cortex – the whisker subdivision of the cortical body representation – suggested that somatosensory cortex contains a topographic representation of the body surface, which is established early in development and remains stable thereafter. We find, however, that the part of this body map that processes genital touch expands significantly during puberty and that this expansion could be advanced by the early experience of sexual touch. To elucidate the underlying mechanism driving genital cortex expansion, we examined the sensory innervation of the mouse penis. Comparing pre- and postpubertal mice, we find no difference in the number of peripheral fibers within the dorsal nerve of the penis. Finally, chronic imaging of excitatory neurons within layer 4 revealed cell-type specific functional and structural changes within genital cortex during puberty, which could be significantly accelerated by a brief period of early sexual experience. The second part of this thesis focuses on the cellular specialization of the cortical output layer, layer 5. Layer 5 is populated by different types of excitatory projection neurons, which broadcast cortical output to other brain structures. Because our understanding of the different types of projection neurons in layer 5 is still incomplete, we investigated genomic differences as novel mechanism underlying projection neuron diversity. Our data suggests that the exceptionally large size of some of these projection neurons may be associated with an increase in DNA content, a phenomenon referred to as polyploidy. Overall, the data presented in this thesis highlights two novel instances of cellular specialization in the cortex: (i) Within the cortical input layer, layer 4, we observed development and experience driven changes in the area which processes genital touch. (ii) Within the cortical output layer, layer 5, we identified putatively polyploid projection neurons, which may have developed to facilitate an increase in cell size.

Zusammenfassung

Seit dem Anfang des neunzehnten Jahrhunderts ist bekannt, dass die Großhirnrinde von Säugetieren aus einer Vielzahl lokaler Schaltkreise besteht, die bestimmte Funktionen in der Verarbeitung neuronaler Signale haben. Solche Schaltkreise bestehen aus unterschiedlichen Zellarten, deren charakteristische Physiologie, Morphologie und Konnektivität die Verarbeitung eintreffender neuronaler Signale bestimmen. Im Rahmen dieser Doktorarbeit wurde die zelluläre Spezialisierung zweier kortikaler Schaltkreise untersucht: einerseits die der Eingangsschicht oder Schicht 4 (Kapitel 2 bis 4) und andererseits die der Ausgangsschicht oder Schicht 5 (Kapitel 5). Der erste Teil der Dissertation umfasst drei Publikationen, welche die Verarbeitung von genitalen Berührungen in der kortikalen Schicht 4 von Nagern als Forschungsgegenstand haben. Die Arbeiten konzentrieren sich auf strukturelle Veränderungen während der Pubertät, da sich die Bedeutung genitaler Berührungen in dieser Zeit stark verändert. Die Erforschung des „Barrel Cortex“ – des Teils der Hirnrinde, welcher bei Nagern Reize der Schnurrhaare verarbeitet – führte zu der Erkenntnis, dass der somatosensorische Kortex eine topographische Repräsentation der Körperoberfläche enthält. Diese wird kurz nach der Geburt gebildet und weist danach kaum Veränderungen auf. Erstaunlicherweise vergrößert sich während der Pubertät der Bereich dieser Körperkarte, der genitale Berührungen verarbeitet. Dieser Prozess kann durch frühe sexuelle Berührungen beschleunigt werden. Diese Beobachtungen lassen sich jedoch nicht auf Veränderungen der sensorischen Innervation der Geschlechtsorgane zurückführen. So konnten wir bei der Anzahl peripherer Nervenfasern keinen Unterschied zwischen pre- und postpubertären Penissen feststellen. Zuletzt konnten wir mithilfe chronischer Bildgebung bei Mäusen zelltypabhängige strukturelle und funktionelle Veränderungen in Schicht 4 des Genitalkortexes während der Pubertät nachweisen, welche wiederum durch eine kurze Episode sexueller Berührungen beschleunigt werden konnten. Im zweiten Teil dieser Dissertation wurde die kortikale Ausgangsstruktur untersucht. Diese ist von verschiedenen Projektionsneuronen besiedelt, welche kortikale Signale an andere Hirnregionen weiterleiten. Angesichts der drastischen Größenunterschiede dieser Projektionsneurone haben wir deren Genomgröße untersucht. Unsere Ergebnisse legen nahe, dass einige außerordentlich große Projektionsneurone polyploid sind. Dies bedeutet, dass sie zusätzliche Kopien ihres gesamten Chromosomensatzes enthalten. Insgesamt wurden in dieser Dissertation zwei neue Formen zellulärer Spezialisierung in der Hirnrinde aufgezeigt: (i) Schicht 4 weist zelltypspezifische entwicklungs- und erfahrungsabhängige Veränderungen im Genitalfeld auf. (ii) Schicht 5 enthält Projektionsneurone, deren erstaunliche Zellgröße auf ein polyploides Genom zurückzuführen ist.

Table of Contents

List of Figures

Thesis Outline

Chapter 1 provides a brief introduction to the cellular architecture of the rodent cortex, focusing on its input and output structures. With regards to its input layer, the topographic processing of genital touch in somatosensory cortex is discussed. With regards to its output layer, its excitatory cell-type diversity is introduced as well as the concept of polyploidy as determinant of cell size. **Chapters 2 to 4** constitute the first part of the thesis. **Chapter 2** examines the effect of sexual experience and hormones on the development of genital cortex. **Chapter 3** investigates the peripheral innervation of male mouse genitals and their cortical magnification. **Chapter 4** explores the pubertal maturation of genital cortex in a cell-type specific manner using in vivo imaging. **Chapter 5** constitutes the second part of the thesis. It examines polyploidy as novel mechanism to increase cell-type diversity in cortical layer 5. Finally, **Chapter 6** summarizes the main findings of this thesis and provides a brief overall discussion.

1 General Introduction

Similar to other complex systems, the brain has many levels of mechanistic organization. It contains large structures, like the cerebral cortex and the cerebellum, which can be decomposed into functionally specialized areas. Such brain areas contain neuronal circuits made up diverse neuronal subtypes. To understand how the functional specialization of neuronal circuits emerges, it is key to understand their component cell-types. This thesis focuses on two novel forms of cellular specialization within the primary sensory areas of the rodent neocortex. On the one hand, we investigated how the part of the cortical input layer, layer 4, that processes genital touch is uniquely shaped by sexual maturation. On the other hand, we explored how an unusual type of genomic variation, namely polyploidy, contributes to the cellular diversity within the cortical output layer, layer 5.

1.1 Constructing cortical circuits

1.1.1 Cortical Areas

In order to understand how cortical circuits serve their specialized function, it is essential to understand how the cortex is organized. Many important organizational concepts date back to the pioneering work of Korbinian Brodmann at the beginning of the 20th century. He was among the first to recognized that the human neocortex can be tangentially separated into different areas, which can be distinguished based on their unique cellular architecture (Figure 1A, Brodmann, 1909). Brodmann also already suggested that it is the grouping of different types of nerve cells and not their individual morphology that provides neocortical areas with the ability to serve some back then still unknown function (Brodmann, 1909; Zilles, 2018). Furthermore, his comparative neuroanatomical studies on humans, primates and other mammals demonstrated the strong homology of cortical parcellation across species (Amunts and Zilles,

2015), paving the way for decades of research on cortical architecture in model organisms such as rats and mice. Today, modern neuroscientific techniques have provided much insight into the cellular and molecular underpinnings of different cortical areas and their component circuits (Molyneaux et al., 2007; Kim et al., 2015; Tasic et al., 2016), which processes information depending on their cellular composition and synaptic connectivity (Douglas and Martin, 2004; Harris and Mrsic-Flogel, 2013). This thesis focuses on specific cortical circuits within the primary sensory cortices (Figure 1B), which receive sensory signals relayed from peripheral receptors: primary somatosensory cortex, primary visual cortex and primary auditory cortex.

1.1.2 Cortical layers and cell-types

In addition to the horizontal arrangement of areas, the neocortical sheet can be vertically separated into six layers, which run parallel to its surface. This second key principle of cortical organization was first described by Ramon J Cajal at the end of the 19th century. He found that each layer can be distinguished by the types of excitatory neurons whose cell bodies reside within it and by the shape of their dendrites and axons (Figure 1C, y Cajal, 1923; De Carlos and Borrell, 2007). In recent years, tremendous progress has been made elucidating how excitatory cell-types vary between layers in terms of morphology, gene expression, connectivity and physiology (Molyneaux et al., 2007; Jabaudon, 2017). Together, these characteristics determine how each cell-type processes neural signals, which travel vertically across the layers of primary sensory cortices. Along the way, each layer performs distinct computations on the signal depending on its inhabitant cell-types. Overall, there are some striking communalities in terms of the cellular architecture and processing of each layer across primary sensory cortices (Douglas and Martin, 2004; Harris and Mrsic-Flogel, 2013). This thesis focuses on two of the six layers, which can also be conceived as functionally distinct cortical structures. **Chapters 2 to 4** examine the cortical input layer, layer 4, which acts as main entry point into the cortex. Signals from the peripheral sensory receptors arrive most densely in layer 4 (Petreanu et al., 2009; Smith et al., 2012; Constantinople and Bruno, 2013), where excitatory neurons are thought to encode core stimulus properties (Welker and Woolsey, 1974). The precise cellular layout and development of layer 4 will be introduced in **Chapter 1.2**. **Chapter 5** of this thesis focuses on the cortical output layer, layer 5, which is populated by different types of excitatory pyramidal neurons, whose precisely directed axonal arbors broadcast cortical output to many near and far targets including the hindbrain and spinal cord (Kim et al., 2015; Gerfen et al., 2018). **Chapter 1.3** will introduce cellular diversity within layer 5.

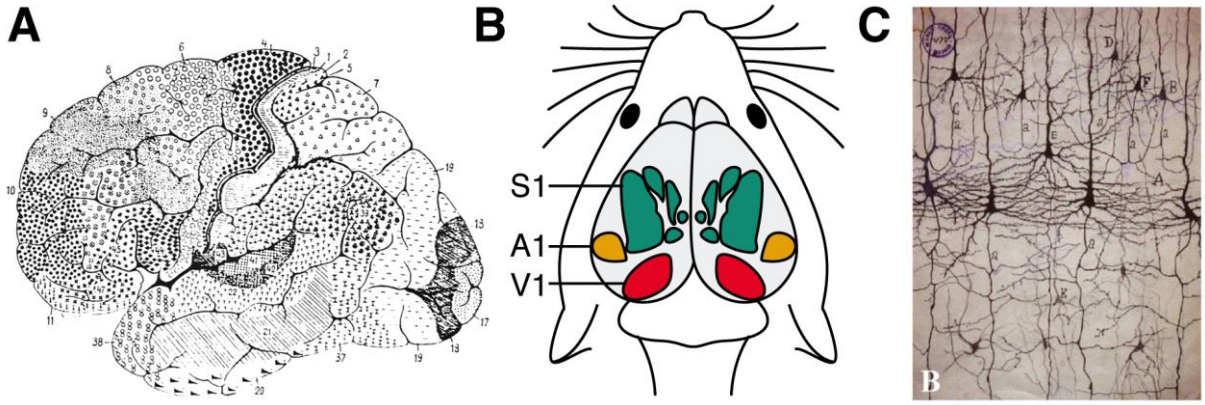

Figure 1. The mammalian neocortex is made up of areas and layers.
A) Brodmann's map of 43 cytoarchitectonically distinct cortical areas in the human brain (Brodmann, 1909).
B) The rodent cortex contains three primary sensory cortical areas: primary somatosensory cortex (S1, green), primary visual cortex (V1, red) and primary auditory cortex (A1, orange).
C) Drawing of morphologically distinct neuronal subtypes in the different layers of the cortex by Ramon J Cajal (y Cajal, 1923; López-Muñoz et al., 2006).

1.2 Pubertal development of genital cortex

Chapters 2 to 4 of this thesis focus on layer 4 of the rodent primary somatosensory cortex (Figure 1B, green). Layer 4 of primary somatosensory cortex is populated by two types of specialized excitatory neurons, which have classically been conceived as rigidly relaying incoming physical stimulation from the body surface (Harding-Forrester and Feldman, 2018). This belief is based almost entirely on findings involving mechanically controlled stimulation of the rodent whisker system. We argue that this approach might deliver an incomplete account of the function of layer 4 in primary somatosensory cortex, because it often does not investigate this circuit in a biologically relevant context. Therefore, we study the sensory perception of genitals, a body part that has largely been neglected in sensory neuroscience. At the same time, genitals represent an exceptionally interesting model, because they acquire great biological relevance during puberty, a late but all the more critical period in the lifespan of animals and humans. Moreover, sexual maturation is probably not exclusively age-dependent. Instead the onset of puberty in rodents is at least partly controlled by social cues, such as pheromones and touch (Bronson and Maruniak, 1975; Levin and Johnston, 1986; Vandenbergh, 2012; Lenschow et al., 2017). In humans, early childhood sexual abuse has been linked with early menarche in girls (Noll et al., 2017). These related observations highlight the great importance of investigating how genital touch is processed by the cortex during puberty and how this processing is affected by sensory experience.

1.2.1 Beyond whiskers: the rodent somatosensory body map

To find out how genital touch is processed in the input layer of primary somatosensory cortex, we leverage a unique organizational feature of this cortical structure, which allows the localization of neurons that exclusively respond to touch of a specific body part. Within its input layer, layer 4, there is a topographic map of the body surface, where neighboring excitatory neurons receive signals from neighboring receptor cells on the peripheral sensory surface (Harding-Forrester and Feldman, 2018). Seminal studies in the 80's revealed that in rodents the majority of this topographic map is dedicated to the representation of the whisker pad on the animals snout (Welker, 1976; Chapin and Lin, 1984). Specifically, discrete cytoarchitectonic clusters of neurons called barrels each represent a specific whisker on the animals snout (Woolsey and Van der Loos, 1970; Van Der Loos and Woolsey, 1973). Histological staining of mitochondrial enzymes enriched in layer 4 excitatory neurons nicely reveals these whisker barrels as well as modules representing other body parts (Figure 2A,B). The topographic arrangement of inputs is relayed from the body surface via the lemniscal pathway with synapses in the brainstem and the ventral posteromedial nucleus of the thalamus (Figure 2C, Feldman and Brecht, 2005). Despite the great biological relevance of genitals, its cortical representation in rodents was only recently identified in its topographically appropriate location, between the trunk and the hindpaw (Figure 2A, Lenschow et al., 2016; Lauer et al., 2017).

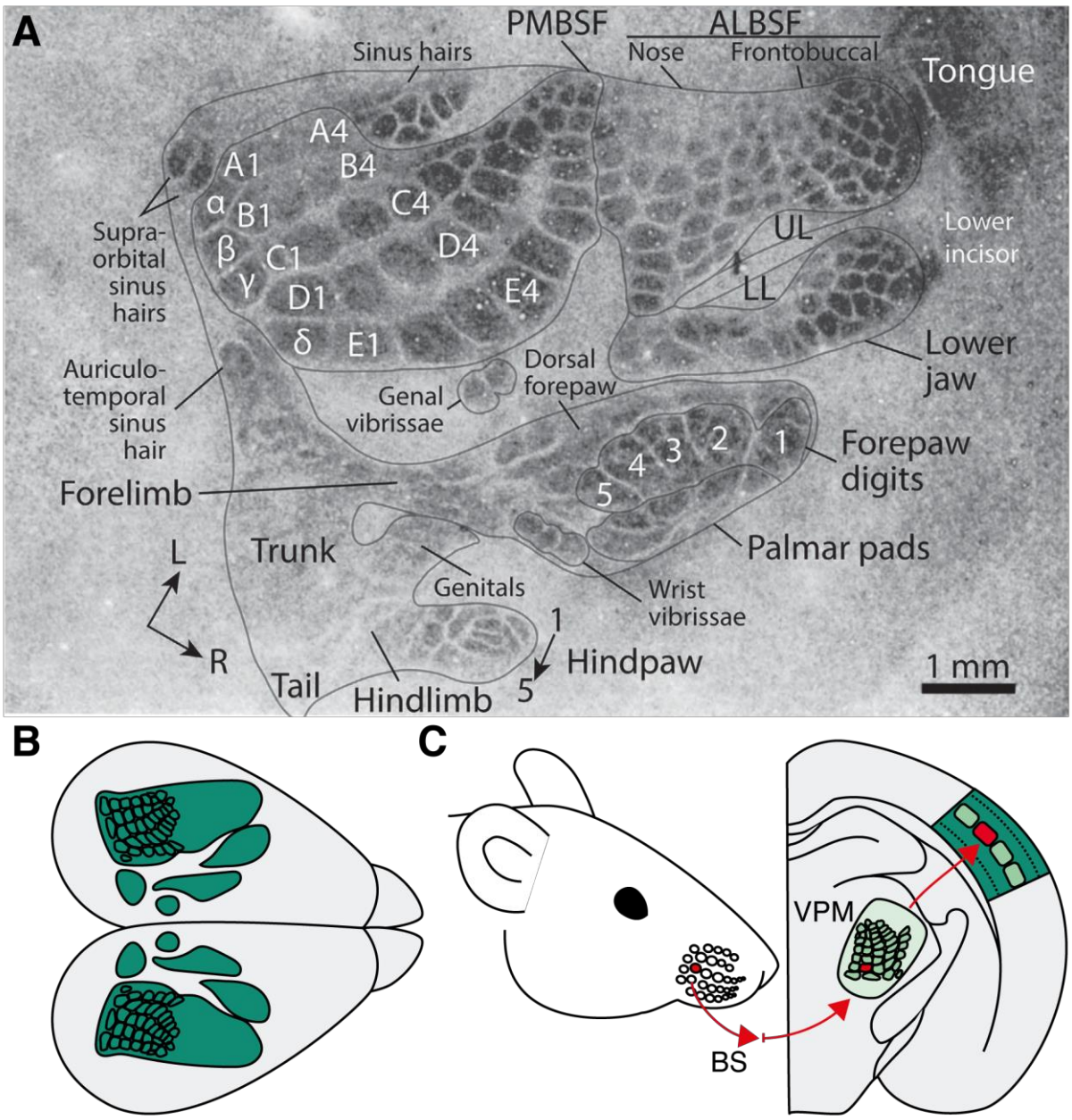

Figure 2. Topographic representation of the body in layer 4 of somatosensory cortex.

A) Cytochrome oxidase staining of tangential brain sections reveals dense clusters of layer 4 excitatory neurons, which receive input from peripheral receptors innervating the skin of different body parts. A large part of the map comprises the representation of whiskers on the animals snout (Harding-Forrester and Feldman, 2018).

B) Schematic of the rodent somatosensory cortex of the left and right hemisphere.

C) Illustration of topographic projections from the periphery to layer 4. Sensory inputs are sent from the whiskers on the animal's snout (left) to the cortex (coronal view, right) via synapses in the brainstem (BS) and ventral posteromedial nucleus (VPM) of the thalamus. Inputs from a specific whisker (left, red) cluster within a specific barrel (right, red) within layer 4 of somatosensory cortex.

1.2.2 Pubertal expansion of genital cortex depends on hormones and sexual experience

In addition to providing the first orderly mapping of rodent genital cortex, Lenschow et al. (2016) made a stunning observation. Based on histological sections stained with cytochrome oxidase, the authors showed that the area of primary somatosensory cortical layer 4 that represents the genital was larger in postpubertal rats compared to prepubertal rats. This observation was highly unusual, since the topographic body map in layer 4 is classically conceived as particularly stable to changes in sensory inputs (Glazewski and Fox, 1996; Feldman and Brecht, 2005). After early establishment (Li and Crair, 2011) and a short critical period, which ends with the first postnatal week (Fox, 1992), only gross changes in sensory inputs, such as lesioning or whisker trimming, result in plasticity of the layer 4 body map (Van Der Loos and Woolsey, 1973; Lee Weller and Johnson, 1975; Waite and Taylor, 1978). Even then, plasticity is largely reflected in adjustments in the receptive field properties of excitatory neurons (Xerri, 2008; Harding-Forrester and Feldman, 2018). Especially, the anatomical organization of the layer 4 body map has so far been described as excessively stable, rendering the observation that genital cortex is larger in post- compared to prepubertal rats highly unusual.

In **Chapter 2** of this thesis I present a study that investigates the hormonal and behavioral control of pubertal changes in layer 4 of genital cortex. Specifically, we asked whether the larger size of genital cortex in postpubertal rats was related to mechanisms orchestrating sexual maturation of the whole organism. During puberty, external genitals undergo highly relevant biological changes, which are controlled by sex hormones (Berthold, 1849). At the same time, sex hormones also control the sexual differentiation of the brain (Terasawa and Kurian, 2012; Juraska et al., 2013), potentially including the pubertal development of genital cortex. Moreover, puberty is not purely age-dependent but heavily influenced by social and sexual cues (Bronson and Maruniak, 1975; Drickamer and Murphy, 1978; Kaneko et al., 1980; Mucignat-Caretta et al., 1995). Co-housing prepubertal female mice with sexually experience adult males advanced pubertal timing via the synergistic action of tactile and pheromonal cues (Bronson and Maruniak, 1975). The observation that sexual touch contributes to the puberty advancing effect of co-housing makes layer 4 of genital cortex, the key area for processing genital touch, an even more interesting target for investigating effects of pubertal maturation on the brain. **Chapter 2** of the thesis addresses the role of sex hormones and sexual experience in maturation of genital cortex during puberty using histological staining. Specifically, we asked: (i) Do sex hormones control the expansion of genital cortex during puberty? (ii) Does sexual experience modulate genital cortex growth? (iii) Can artificial sexual touch of the genitals mimic potential

effects of sexual experience on genital cortex? Overall, the results of this study revealed that genital cortex grows significantly during puberty and that this expansion is strongly dependent on both hormones and touch.

Published as: Lenschow C., **Sigl-Glöckner J.**, Brecht M. (**2017**) Development of rat female genital cortex and control of female puberty by sexual touch. *PLoS Biol* 15(9): e2001283.

1.2.3 Sensory innervation of the pre- and postpubertal mouse penis

The observation that the cortical representation of the genitals appears to change in size during puberty (Lenschow et al., 2016, 2017) also prompts the question whether this phenomenon is rooted in changes of the peripheral innervation of the external genitals (**Chapter 3**)**.** One reason being that the size of subregions within S1 is proportional to the density of peripheral receptors innervating skin covering the respective body part, which has been shown for the whisker system of rats and mice (Lee and Woolsey, 1975; Van Der Loos et al., 1986; Meyer et al., 2013). Moreover, the density of peripheral innervation reflects the relative behavioral salience of the different body parts (Krubitzer et al., 2011). This principle is nicely illustrated by the rodent whisker system: rodents are nocturnal animals, which relay heavily their whiskers to explore the environment. Therefore, the whiskers are innervated densely by sensory fibers. Accordingly, the cortical representation the whisker pad in layer 4 occupies a large part of the primary somatosensory cortex body map (Figure 2A).

Given the relationship between peripheral innervation and cortical field size, we investigate in **Chapter 3** whether the expansion of genital cortex is accompanied by concurrent changes in the peripheral sensory innervation of the genital organs. During puberty, genitals change markedly in size and shape (Tomova et al., 2010; Han and Lee, 2014). Interestingly, there is evidence pointing towards a role of sex hormones in the structure and physiology of the peripheral nerve fibers innervating female rat genitals (Adler et al., 1977; Ting et al., 2004; Liao and Smith, 2011). In contrast, the effect of hormones and more specifically sexual maturation has received little attention in male rodents, despite the fact that this question is particularly approachable in here. Unlike the scattered innervation of female genitals, the sensations of the penis is provided by a compact, central bundle of fibers which forms the dorsal penile nerve (Calaresu, 1970), the integrity of which is essential for sexual function, including erection and ejaculation (Herbert, 1973; Chen et al., 2018). Leveraging these advantages of the mouse dorsal penile nerve, we performed histological staining to find out whether the density

of the nerve fibers in the dorsal penile nerve is different between pre- and postpubertal mice. Furthermore, we investigated the cortical magnification of the fibers innervating the genitals, which refers to the ratio between the devoted area of the cortical sheet and the number of peripheral fibers. Overall the results of this study indicate that the sensory innervation of the mouse penis is stable despite its significant growth during puberty. These findings suggest that the pubertal expansion of genital cortex layer 4 is independent of the peripheral innervation of the genitals.

Published as: Purkart, L., **Sigl-Glöckner, J**. & Brecht, M. (**in revision**). Constant innervation despite pubertal growth of the mouse penis *(Journal of Comparative Neurology)*.

1.2.4 Chronic imaging of cell-type specific changes during genital cortex development

The third and final study contributing to the first part of this thesis (**Chapter 4**) investigates the cellular mechanisms underlying the pubertal maturation of the genital field within cortical layer 4. As mentioned above, layer 4 of somatosensory cortex is classically conceived as rigid relay of incoming sensory information, where plasticity can, if at all, be detected physiologically (Xerri, 2008; Harding-Forrester and Feldman, 2018). Yet we made the highly unusual observation that the cortical field representing the genital within layer 4 of somatosensory cortex grows during puberty (Lenschow et al., 2016; Lauer et al., 2017). This observation is based on the inspection of histological sections of pre and postpubertal rats, where we used two different approaches to measure the size of the cortical genital field. We applied cytochrome oxidase staining, which is thought to mark highly active neurons in layer 4 and has long been used to reveal the topographic body map in layer 4 (Figure 2A, Wong-Riley, 1989). In addition, we confirmed our findings using Vglut2 antibody staining (Lenschow et al., 2017), which visualizes the topographically ordered thalamocortical fibers carrying sensory input from the body surface to excitatory neurons within cortical layer 4 (Antón-Bolaños et al., 2018).

Interestingly, the formation of the layer 4 body map critically depends on the coordinated maturation of thalamus and cortex. During development, thalamocortical afferents grow towards layer 4 of primary somatosensory cortex, where they synapse onto excitatory neurons that are arranged into clusters representing the different body parts (Simi and Studer, 2018). In the absence of primary thalamocortical afferents, excitatory neurons within layer 4 acquire a secondary somatosensory identity in terms of electrophysiological properties and molecular profile (Pouchelon et al., 2014). In addition, the thalamic input even appears to shape the

morphology of layer 4 excitatory neurons, which all have a pyramidal shape at the beginning. Upon receiving thalamic input, many of those retract their apical dendrite to become typical spiny stellate neurons to which layer 4 owes its granular appearance (Brodmann, 1909; Callaway and Borrell, 2011). Given, that thalamocortical input appears to strongly impact the cellular specialization of excitatory neurons within layer 4, we explored, whether the growth of genital cortex is accompanied by concurrent, cell-type specific changes within layer 4. In **Chapter 4** of this thesis, we address this question by performing chronic two-photon imaging of genital cortex in layer-4-specific transgenic mice. This approach allowed us to visualize cell-type specific structural and functions changes within genital cortex across the entire duration of sexual maturation. Furthermore, we could specifically investigate how first sexual experience, an event often considered to produce long lasting memories, shapes the pubertal maturation of genital cortex.

Published as: **Sigl-Glöckner J.,** Meier E., Takahashi N., Sachdev R., Larkum M. & Brecht M. (**accepted**). Effects of sexual experience and puberty on mouse genital cortex revealed by chronic imaging. *Current Biology*.

1.3 Polyploidy in Layer 5 pyramidal neurons

In **Chapter 5** of this thesis, we turn away from the cortical input layer and instead focus on the cortical output layer, layer 5, and its cellular composition across primary sensory cortical areas (Figure 1B). Layer 5 is composed of variety of distinct neuronal subtypes including excitatory projection neurons, which send cortical output to near and far brain areas (Molnár and Cheung, 2006; Kim et al., 2015). In order to understand how the functional specialization of layer 5 emerges, it is of great importance to disentangle these multiple excitatory subtypes. Based on the belief that physiology is rooted in anatomy (Brodmann, 1909), the early neuroanatomists already conceived that neuronal cell size varied significantly between cytoarchitectonic areas and layers and that such differences might be functionally meaningful. Within the human and cat cortex, the largest cells were found within layer 5 of motor cortex (Figure 3A, Betz, 1874; Brodmann, 1909; Udaka et al., 1986). In rodents two kinds of layer 5 projection neurons can be broadly distinguished based on their molecular profile, physiology, somatodendritic morphology and, importantly, also cell size (Chagnac-Amitai et al., 1990; Molnár and Cheung, 2006; Molyneaux et al., 2007). In the upper half of layer 5 (layer 5a) there are small, slender-tufted pyramidal neurons (Figure 3B, left), projecting to inter- and subcortical areas. In contrast,

the deeper half of layer 5 (layer 5b) contains large, thick-tufted pyramidal neurons (Figure 3B, right) that possess a large dendritic tree (Chagnac-Amitai et al., 1990). These neurons project to some of the most distant cortical targets, including the brainstem and spinal cord. Interestingly, previous research has suggested, that their large cell size may be linked to differences in projection site, morphology and physiology (Klein et al., 1986; Hallman et al., 1988; Mason et al., 1990).

Therefore, we explored whether variations in cell size indeed represent different underlying cell-types. One of the most important determinants of cell size is DNA content (Epstein, 1967). In order to increase their volume, many types of cells undergo endoreduplication in the cell cycle: by duplicating their genomic DNA without dividing they become polyploid (Figure 3C, Epstein, 1967; Beaulieu et al., 2008). Accordingly, endoreduplication of a mammalian nerve cell, which typically has two sets of chromosomes (diploid = 2C, Figure 3C), results in four copies of each chromosome (tetraploid = 4C, Figure 3C). It has been proposed that a polyploid genome and the accompanying increase in size allows cells to functionally adapt to environmental needs, such as increased metabolic requirements (Edgar and Orr-Weaver, 2001; Selmecki et al., 2015). While polyploid cells are highly abundant in some tissues, there are only few reports of polyploidy in neurons (Mosch et al., 2007; López-Sánchez and Frade, 2013). Nevertheless, one of the cell-types which have been reported to contain a polyploid genome are the giant Betz cells in cat motor cortex described above (Figure 3A, Lentz and Lapham, 1969). Despite these findings, systematic surveys of polyploidy as a conserved mechanism to increase cell size and cell diversity in the mammalian brain are still missing, largely due to the absence of robust techniques to asses DNA content in postmitotic interphase neurons. In **Chapter 5,** we therefore combined a number of different techniques including histological staining of DNA content, immunohistochemistry, flow cytometry and in situ hybridization to reveal whether polyploidy also contributes to cellular diversity within rat cortical layer 5, potentially contributing to their functional specialization as large, long distance projection neurons.

Published as: **Sigl-Glöckner J.** & Brecht M. (**2017**) Polyploidy and the Cellular and Areal Diversity of Rat Cortical Layer 5 Pyramidal Neurons. *Cell Reports* 20.11: 2575-2583.

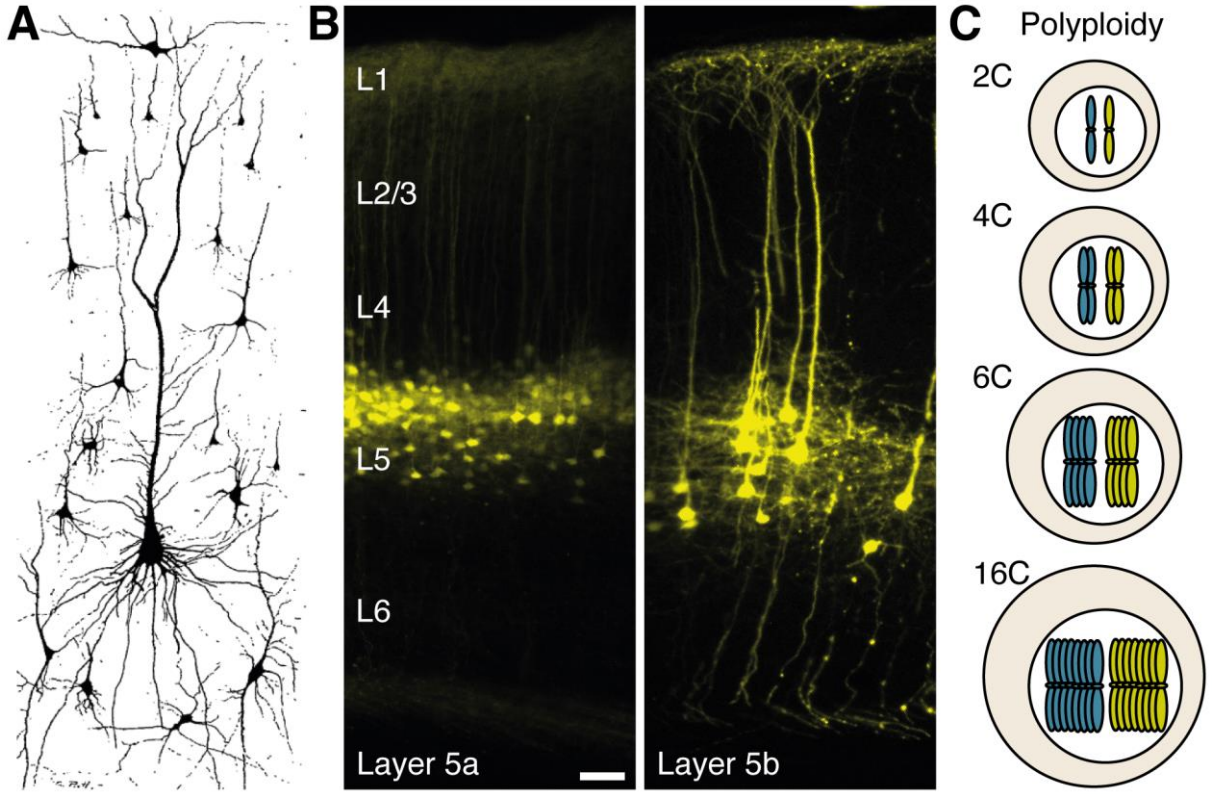

Figure 3. Polyploidy may underly differences in layer 5 pyramidal cell size.

A) Camera lucida drawing of a giant Betz cell in deep layers of the human and cortex stained with the Golgi-Cox method (Walshe and M R Walshe, 1942). Note its large cell body.

B) Coronal brain sections of transgenic mice specific for slender-tufted pyramidal neurons in layer 5a (SIM-cre, left) and thick-tufted pyramidal neurons in layer 5b (TLX-Cre, right) labelled with GFP (mice from http://connectivity.brain-map.org/transgenic). Scale bar = 50 µm.

C) Schematic illustrating polyploidy as mechanism underlying increasing cell size. In a normal, diploid mammalian cell there are two sets of chromosomes, one donated by each parent (blue and yellow). Duplication of this genome will incrementally produce additional sets of chromosomes.

2 Development of rat female genital cortex

This work was originally published as:

Lenschow C., **Sigl-Glöckner J**., Brecht M. (2017) Development of rat female genital cortex and control of female puberty by sexual touch. *PLoS Biol* 15(9): e2001283. https://doi.org/10.1371/journal.pbio.2001283

PLOS BIOLOGY

RESEARCH ARTICLE

Development of rat female genital cortex and control of female puberty by sexual touch

Constanze Lenschow[1¤]*, Johanna Sigl-Glöckner[1], Michael Brecht[1,2]*

1 Bernstein Center for Computational Neuroscience Berlin, Humboldt-Universität zu Berlin, Berlin, Germany, **2** NeuroCure Cluster of Excellence, Humboldt-Universität zu Berlin, Berlin, Germany

¤ Current address: Champalimaud Centre for the Unknown, Lisbon, Portugal
* constanze.lenschow@research.fchampalimaud.org (CL); michael.brecht@bccn-berlin.de (MB)

Citation: Lenschow C, Sigl-Glöckner J, Brecht M (2017) Development of rat female genital cortex and control of female puberty by sexual touch. PLoS Biol 15(9): e2001283. https://doi.org/10.1371/journal.pbio.2001283

Academic Editor: David Kleinfeld, University of California San Diego, United States of America

Received: October 6, 2016

Accepted: August 17, 2017

Published: September 21, 2017

Data Availability Statement: All relevant data are within the paper and its Supporting Information files.

Funding: DFG http://www.dfg.de/en/funded_projects/prizewinners/leibniz_prize/index.html (grant number Leibniz Prize BR3479/4-1). Received by MB. The funder had no role in study design, data collection and analysis, decision to publish, or preparation of the manuscript.

Competing interests: The authors have declared that no competing interests exist.

Abstract

Rat somatosensory cortex contains a large sexually monomorphic genital representation. Genital cortex undergoes an unusual 2-fold expansion during puberty. Here, we investigate genital cortex development and female rat sexual maturation. Ovariectomies and estradiol injections suggested sex hormones cause the pubertal genital cortex expansion but not its maintenance at adult size. Genital cortex expanded by thalamic afferents invading surrounding dysgranular cortex. Genital touch was a dominant factor driving female sexual maturation. Raising female rats in contact with adult males promoted genital cortex expansion, whereas contact to adult females or nontactile (audio-visual-olfactory) male cues did not. Genital touch imposed by human experimenters powerfully advanced female genital cortex development and sexual maturation. Long-term blocking of genital cortex by tetrodotoxin in pubescent females housed with males prevented genital cortex expansion and decelerated vaginal opening. Sex hormones, sexual experience, and neural activity shape genital cortex, which contributes to the puberty promoting effects of sexual touch.

Author summary

We recently identified the somatosensory representation of rat genitals; remarkably, this cortical region—genital cortex—is sexually monomorphic, despite the marked sexual dimorphism of external genitals in rats. Most intriguing was the observation that genital cortex doubles in size during puberty. In order to shed light on this unusual expansion, we studied genital cortex development and sexual maturation in the female rat. We first showed that sex hormones are likely to cause the pubertal expansion of genital cortex. Next, we examined whether sexual experience affects the development of female genital cortex. Raising females together with adult males advanced genital cortex expansion, but cohousing with adult females or exposure to nontactile male cues was not sufficient to drive genital cortex growth. Surprisingly, artificial genital touch led to an early onset of female puberty and growth of genital cortex. In line with this finding, we find that if genital cortex activity is blocked, the advancing effects of adult males on puberty and genital cortex growth are inhibited. Together, our results point to an important role of genital cortex in the puberty-promoting effects of sexual touch.

PLOS BIOLOGY

Abbreviations: GnRH, gonadotropin releasing hormone; P, postnatal day; PMBSF, posteromedial barrel subfield; S1, somatosensory cortex; TTX, tetrodotoxin; VGluT2, vesicular glutamate transporter 2.

Introduction

Early analysis of the development of visual cortex by Hubel and Wiesel focused on binocular interactions and showed that both anatomy and physiology of ocular dominance is plastic and shaped in a visually-driven, activity-dependent process [1]. In a similar vein, the development of circuits in the somatosensory cortex (S1) was studied. It was recognized early on that precise topographic (barrel) representation of the whisker pattern in cortical input layer 4 [2] is imposed by peripheral inputs and has an early and brief critical period, after which it can no longer be changed [3]. Subsequent work identified neurogenetic mechanisms of cortical pattern formation [4]. With few exceptions, [5] most of the work provided little evidence for neural activity dependent processes in the development of S1. From work on the barrel cortex a consensus emerged that cortical input layer 4 has an earlier critical period and shows less plasticity than other cortical layers [6]. In the light of aforementioned results, the recently described developmental pattern of cortical input layer 4 of genital S1 was very surprising. Specifically, layer 4 of rat genital cortex showed a major expansion during puberty [7]. We wondered if this very late development of genital cortex has implications for the role of activity in cortical development and might even allow early sexual experience to impact on cortical development.

We were also interested in the relationship between somatosensory genital cortex development and female sexual maturation. In rodents, puberty has been intensely studied and much is known about changes in subcortical structures, such as the hypothalamus, that are associated with puberty [8]; there is, however, virtually no information available about changes in cortical circuits during puberty. A host of studies in a wide variety of species came to the conclusion that sexual maturation is not a purely age-dependent process but is also under social control. In mice, studies on female sexual development showed puberty advancing effects of male (primer) pheromones [9] and puberty delaying effects of adult female pheromones [10]. Most of the research on the social control of puberty has focused on pheromones [10] and identified the vomeronasal organ as key mediator of such effects in mice [11]. There is also evidence, however, that tactile interactions and sexual touch can powerfully influence sexual development. For example, the extreme reproductive suppression in the eusocial mole rat appears to be mediated by tactile rather than olfactory cues [12]. In a landmark study on mice, Bronson and Maruniak [13] showed that the puberty advancing effects of male pheromones alone are small. Bronson and Maruniak [13] suggested that the advance in female puberty caused by adult males results from a synergistic interaction of pheromones and tactile stimulation; Bronson and Maruniak [13] also ruled out a role of visual and auditory cues. The underlying neural mechanisms and pathways mediating male touch induced advance of female puberty are still unknown.

In primates, the evidence for pheromonal effects on puberty is rather mixed [14]. Sexual touch, on the other hand, is strictly regulated in most human cultures and this is particularly true during development. It has also become painfully clear that sexual abuse and inappropriate sexual contact during development have long-lasting detrimental consequences [15,16]. Presumably the long-lasting problems from inappropriate sexual contact during development reflect brain changes resulting from sexual experience. Remarkably, structural brain imaging in humans with a history of sexual abuse identified a thinning of putative human genital cortex, as a cortical consequence of childhood sexual abuse [17].

Here we ask the following questions: (1) Are sex hormones required for the pubertal expansion of female genital cortex? (2) What are the structural events underlying genital map changes? (3) Does sexual experience affect the development of female genital cortex? (4) Does activity in female genital cortex affect female puberty and does it mediate the female puberty advancing effects of male sexual touch?

Results

Pubertal expansion, but not maintenance of an adult size genital cortex, requires sex hormones

As a first step in our analysis we performed additional experiments to confirm our recently reported data on the growth of genital cortex during puberty [7]. To this end we analyzed the layer 4 cortical input maps in the S1 of 6 young (approximate postnatal day [P] 21) and 7 old (approximately P42) female rats. Specifically, we performed cytochrome oxidase staining, which reveals granular layer 4 regions (S1A–S1D Fig). We confirmed our earlier conclusions: whereas the clitoris representation in young prepubescent animals was rather small (Fig 1A), it appears to be twice as big in adult animals (P42, Fig 1B and 1E; $P < 0.01$, Student t test). In contrast, the size of the entire S1 did not differ significantly between young and old females (Fig 1G; $P = 0.3$, Student t test).

Next, we examined whether sex hormones play a role during the pubertal expansion of genital cortex. Hence, we ovariectomized females before (at P21) and after puberty (at P42). Twenty days after the ovariectomy animals were killed, brains were removed and tangential sections through the S1 were prepared and stained for cytochrome oxidase activity (S1C and S1D Fig). We obtained detailed anatomical maps of layer 4 from 7 prepubertal (Fig 1C) and 6 postpubertal (Fig 1D) ovariectomized females. Fig 1C shows a drawing of a complete S1 (thick outline) body map of a female aged P42, in which we removed the ovaries before puberty (at P21). The size of the cortical clitoris representation is small and comparable to the one of the young female, as depicted in Fig 1A. The somatosensory cortical map obtained from a female rat ovariectomized after puberty at P42 (Fig 1D) allows 2 observations: (1) the clitoris representation is much larger than the one of the female rat ovariectomized before puberty; (2) the size of the genital cortex is comparable to the genital cortex size of an adult female (Fig 1B). The population data (Fig 1E) suggest the same conclusions. The clitoris representation in females ovariectomized before puberty (mean genital cortex of S1 1.07% ± 0.09) was comparable to young females (1.07% ± 0.06) but significantly ($P < 0.01$, Student t test) smaller than the genital cortex size in animals, which were ovariectomized after puberty (1.6% ± 0.15; Fig 1F). Comparison of the genital cortex to the posteromedial barrel subfield (PMBSF), instead of the whole S1, led to the same results (S2A–S2C Fig) with no difference in the variability (S1 Table).

We conclude that sex hormones are required for the pubertal expansion of female genital cortex but not for the maintenance of an adult size female genital cortex.

Systemic estrogen treatment accelerates genital cortex growth and advances female puberty

A strong impact of sex hormones on the onset of puberty has been reported using systemic estradiol injections during prepuberty [18]. We wondered to what extent systemic estrogen treatment can accelerate genital cortex growth. Female rats enter puberty typically at the age of P34 to P38 [19]. On that account and based on the study by Ramirez and Sawyer [18], we chose to treat females aged P26 for 5 days with estrogen and to test a possible effect on genital cortex at P30. Prepubescent females (P26) were injected over 5 days with either in sesame oil dissolved estradiol (Fig 2A, upper panel; $n = 7$ animals; 0.5 μg estradiol, dissolved in 0.4 ml of sesame oil, per 100 g body weight) or with sesame oil alone (Fig 2B, upper panel; $n = 7$ animals; 0.4 ml of sesame oil, per 100 g body weight). During the fifth day of treatment animals were killed and cortical hemispheres were flattened, tangentially sectioned and processed for cytochrome oxidase activity (S3A and S3B Fig). In order to obtain cortical body maps, granular

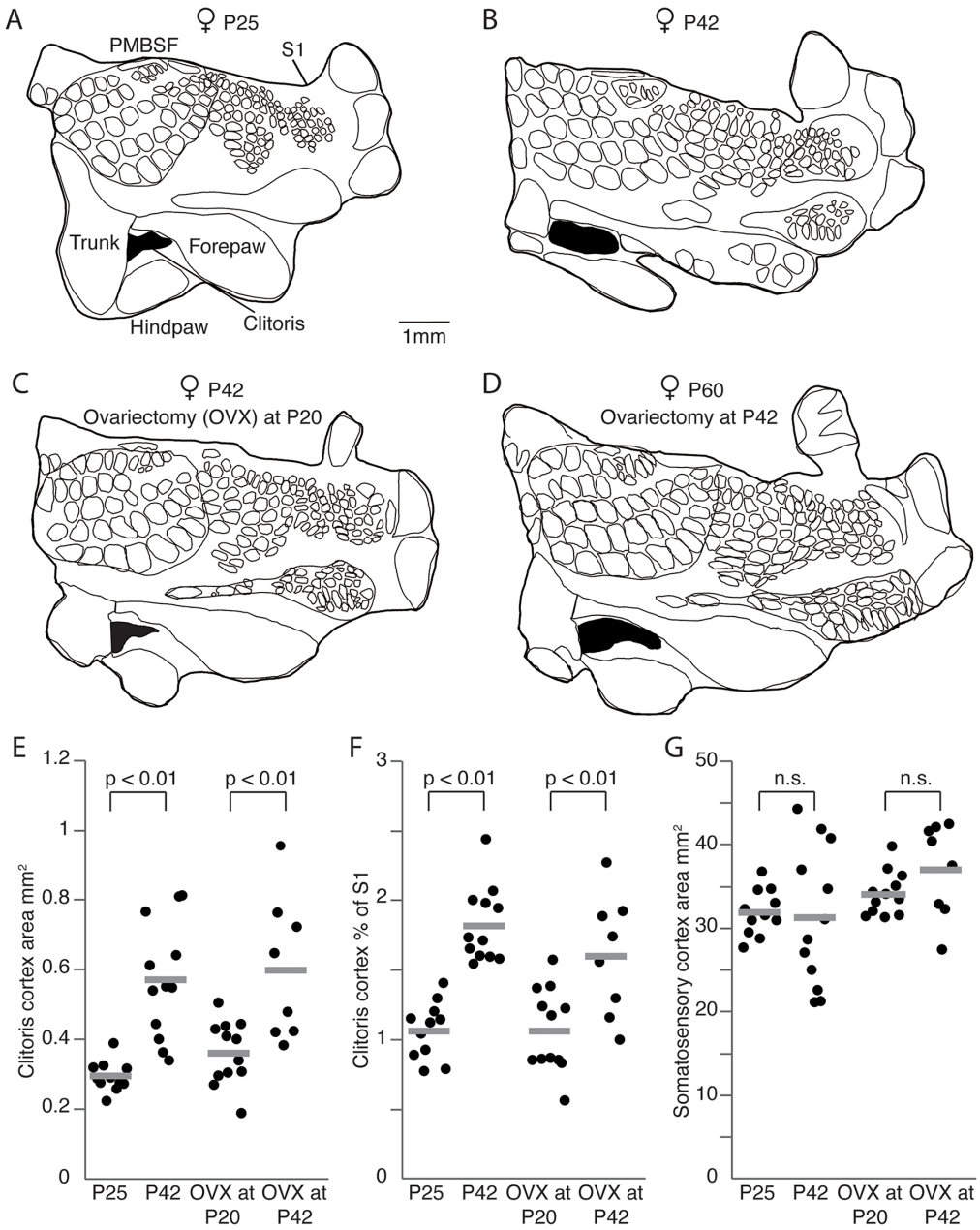

Fig 1. Pubertal expansion of genital cortex, but not its maintenance in adults requires sex hormones. (A) Outline of a somatosensory cortex (S1) map obtained from a female, aged postnatal day (P)25. Genital cortex is labeled in black. (B) Same as (A), but for an adult female (P42). Note the remarkable size difference of the genital cortex compared to the P25 female. (C) Outline of a S1 map from the brain of an adult female (P42), in which the ovaries were removed at P20. (D) Same as (B), but for an adult female (P60), in which the ovaries were removed at P42. The area of the genital cortex is similar to a nontreated adult female (B) and is bigger than in female rats ovariectomized before puberty (C). (E) Absolute area of clitoris in hemispheres of P25, P42 females, and females which were ovariectomized at either P20 or P42. (F) Fraction of genital cortex of the entire S1 in

hemispheres of P25, P42 females, and females which were ovariectomized at either P20 or P42. Note that there is a substantial growth of the genital cortex between P25 and P42 animals. Female rats ovariectomized during prepuberty had smaller genital cortices than animals ovariectomized after puberty. (G) Absolute area of S1 in hemispheres of P25, P42, in prepuberty (P20) ovariectomized, and postpuberty (P42) ovariectomized female rats. See also S1 and S2 Figs, S1 Table, and S1 Data.

https://doi.org/10.1371/journal.pbio.2001283.g001

somatosensory regions were reconstructed through serial sections. To exclude experimenter biases cortical maps were drawn and analyzed by an experimenter blind to the condition estradiol versus oil treated animals.

The lower panel in Fig 2A shows a cortical map obtained from an oil-treated female. A cortical map obtained from a female, which was injected with estradiol, is shown in the lower panel of Fig 2B. The size of the clitoris representation is much larger in the estrogen treated female. Population data for all hemispheres confirm this result. The absolute area of genital cortex (Fig 2C; mean absolute area in oil injected animals was 033mm ^{2} ± 002 5 and in estradiol injected animals 05mm ^{2} ± 002 8, $P < 0001$, Student *t* test) and the mean percentage of genital cortex of S1 (Fig 2D; mean genital cortex of S1 in estradiol treated animals was 1.6% ± 009 and in sesame oil injected animals 1.01% ± 006, $P < 0001$, Student *t* test) was significantly greater in estradiol injected animals compared with control animals (oil treated). The size of S1 was not different (Fig 2E; mean area of S1 in oil treated animals was 32.9mm ^{2} ± 07 6 and in estradiol treated animals 31.2mm^2 ± 06 8, $P = 01$, Student *t* test).

We also assessed parameters indicative of sexual maturation and the onset of puberty. Thus, we evaluated vaginal opening (an open vagina is typically seen in females, which have entered puberty, [18]) and the weight of the uterus, which is heavier in females after puberty [18]. Accordingly, we documented vaginal opening before, during and after the daily injections. In Fig 2F, 2 photographs show the clitoris and vagina of an oil treated female before the beginning of daily injections (P25, upper panel) and afterwards (P30, lower panel). Vagina and clitoris for an estrogen treated animal are shown in Fig 2G, respectively. Whereas the vagina of the oil treated female was still closed at P30, the estradiol injected animal shows an open vagina at this stage (Fig 2G, lower panel), indicating that the onset of puberty took place. To quantify vaginal opening, we gave the following scores for every vaginal opening stage (Fig 2H): a score of 0 points to a closed vagina, whereas a score of 1 indicates an open vagina. A score of 05 represents the intermediate state, during which the vagina was about to open. The majority of oil treated females (6 out of 7) showed a closed vagina at P30, whereas most of the estrogen injected animals displayed an open vagina (6 out of 7, $P < 0001$, Mann–Whitney U test). We also removed and weighed the uteri. On average, the oil-treated animals had lighter uteri (015g ± 007, Fig 2I) compared to animals, which received daily estradiol injections (029g ± 008), but this difference did not reach significance ($P = 008$, Student *t* test). Taken together these data suggest that systemic estradiol accelerates genital cortex growth and advances the onset of puberty.

Genital cortex growth is due to the invasion of dysgranular cortex by putative genital thalamic afferents

Which cellular changes underlie the unusual genital cortex expansion during puberty? To answer this question, we first stained alternating tangential sections of flattened cortices for cytochrome oxidase activity (S4A Fig) and with vesicular glutamate transporter 2 (VGluT2) antibodies (S4B Fig). While cytochrome oxidase reports constitutive layer 4 metabolic activity, VGluT2 is expressed in thalamocortical terminals [20] and, hence, labels thalamic afferents. S4A Fig (upper panel) shows a tangential section through S1 of a young animal (P14) stained for cytochrome oxidase activity and in S4B Fig (upper panel) the subsequent section is shown

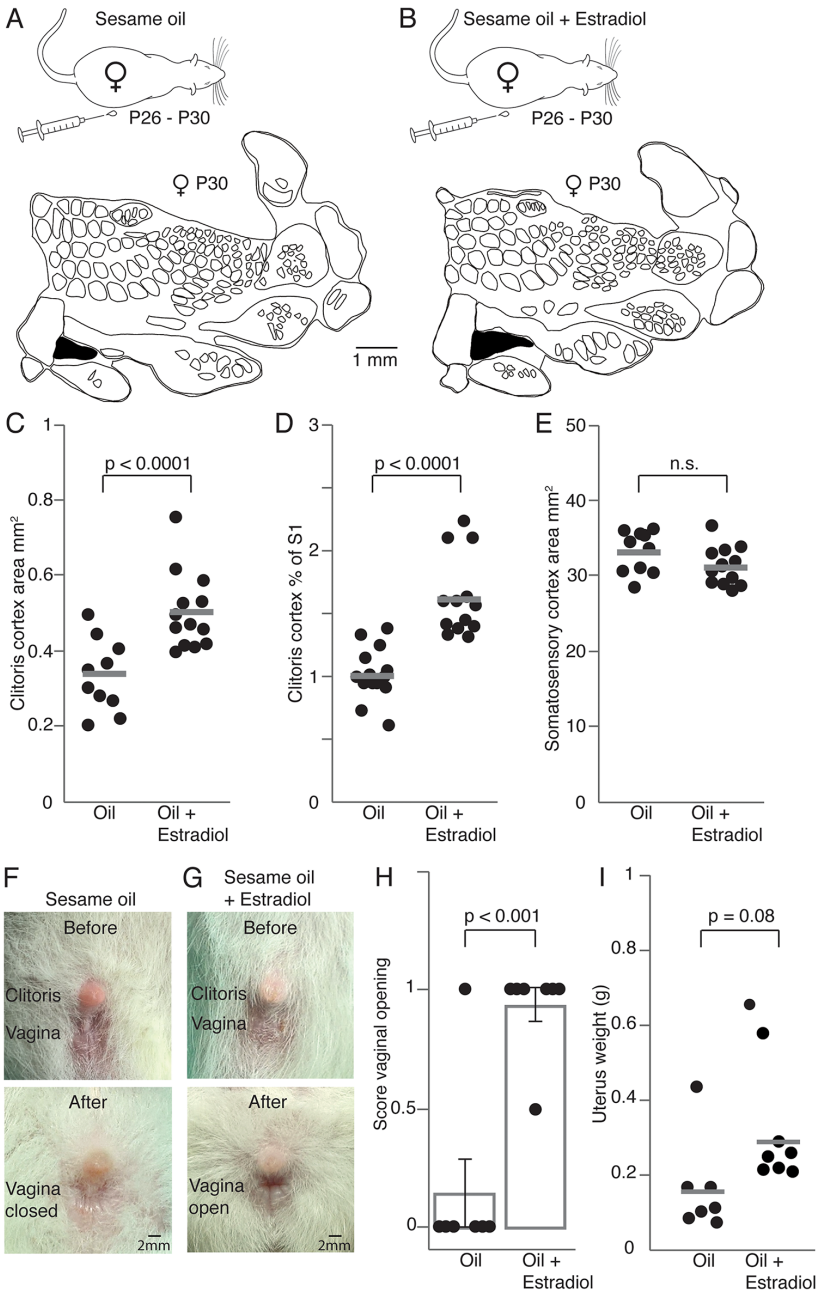

Fig 2. Systemic estradiol application drives genital cortex growth and advances puberty. (A) Upper panel: Control rats received daily subcutaneous injection of sesame oil for 5 days (postnatal day [P]26–P30). Lower panel: Outline of a somatosensory cortex (S1) map from the brain of a P30 female treated only with oil. The genital cortex is labeled in black. (B) Same as (A), but prepubescent rats were injected with sesame oil containing estradiol. (C) Absolute area of the clitoris representation in hemispheres of P30 females, which received daily injections (over 5 days) of either sesame oil alone or sesame oil containing estradiol. The

genital cortex appears bigger in the estradiol group. (D) Same as (C), but the fraction of genital cortex of the entire S1 is plotted. (E) Absolute area of S1 in hemispheres of animals that received either daily oil or estradiol injections. There is no difference between the 2 groups. (F) Pictures of clitoris and vagina, before and after sesame oil treatment. Note that the vagina stays closed at P30 when animals were injected with sesame oil alone. (G) Same as (F), but for the vagina of estradiol treated animals. The vagina is already open at P30 (lower picture). (H) Mean scores for vaginal opening. A score of 0 represents a closed vagina, whereas a score of 1 stands for an opened vagina. The intermediate state (between open and closed vagina) has a score of 0.5. The vagina stayed closed in almost all control animals (treated with oil) whereas the majority of estradiol animals, showed an open vagina at P30. Each dot represents the score of vaginal opening for one animal. (I) Uterus weights of oil and estradiol treated animals. The uterus in estradiol treated animals is heavier, although this difference was not significant. Each dot represents the uterus weight from one animal. See also S3 Fig and S1 Data.

https://doi.org/10.1371/journal.pbio.2001283.g002

labeled for VGluT2. The labeled structures have the same layout and size, as confirmed by quantitatively analyzed drawings (S4A and S4B Fig, lower panels). In old animals, alternating staining for cytochrome oxidase activity and with VGluT2 also led to completely overlapping results. We conclude from these observations that pubertal genital cortex growth leads to an expansion of the cortical area innervated by thalamic afferents.

Next, we asked, how the genital cortex is able to increase its thalamically innervated area so drastically. Does the genital cortex expand like a balloon, pushing the neighboring cortex aside? Alternatively, do genital afferents invade neighboring territories? To address this issue, we analyzed S1 maps from young and old animals in more detail (Fig 1A and 1B). Specifically, we measured the space between fore- and hindpaw, as shown in Fig 3A and 3B, and named it interlimb cortex. The interlimb cortex (grey zone) is dysgranular in structure (i.e., does not have a distinct layer 4) and is larger in the map of a young animal (P25; Fig 3A, upper panel) than in the one of an old animal (P48; Fig 3B, upper panel). This size decrease is very surprising, as S1 grows overall by approximately 15% during puberty (note that this growth in S1 did not reach significance between young and old females; Fig 1). Cytochrome oxidase stained sections (Fig 3A and 3B, lower panels) confirm this result. Whereas the absolute genital cortex area almost doubles in size from P21 to P42 (Fig 3C), the absolute interlimb cortex area slightly decreases (Fig 3D; mean interlimb cortex area in S1 maps of young animals was 0.64 $mm^2 \pm$ 0.06 and in old animals 0.56 $mm^2 \pm 0.1$). Interestingly, the ratio of the genital cortex to the interlimb cortex significantly increases during puberty (Fig 3E; mean ratio of genital cortex to the interlimb area in young animals was 0.35 ± 0.035 and in old animals 0.51 ± 0.017; $P < 0.001$, Student *t* test). The simultaneous increase of genital cortex and decrease of interlimb cortex suggest that the pubertal genital cortex growth reflects an invasion of dysgranular interlimb cortex by putative genital thalamic afferents.

Genital cortex growth in prepubescent females is accelerated by tactile cues from males

Although sex hormones have been identified as important players during the onset of puberty, there is also evidence that somatosensory stimuli (olfactory or tactile) can influence sexual development. Thus, we assessed if sexual experience affects the development of female genital cortex. To this end, we chose the following experimental paradigm, which is inspired by the seminal work of Bronson and Maruniak [13]. Prepubescent females (P21) were cohoused for 9 days with (1) sexually experienced females (Fig 4A, upper panel), or with (2) sexually experienced males (Fig 4A, middle panel), or with (3) sexually experienced males separated by a wire mesh (Fig 4A, lower panel). In the first 2 groups, the animals had direct contact to interaction partners. In the third group, animals were cohoused but had no tactile access to them because of a wire mesh dividing the cage (Fig 4A, lower panel). Importantly, bedding was swapped

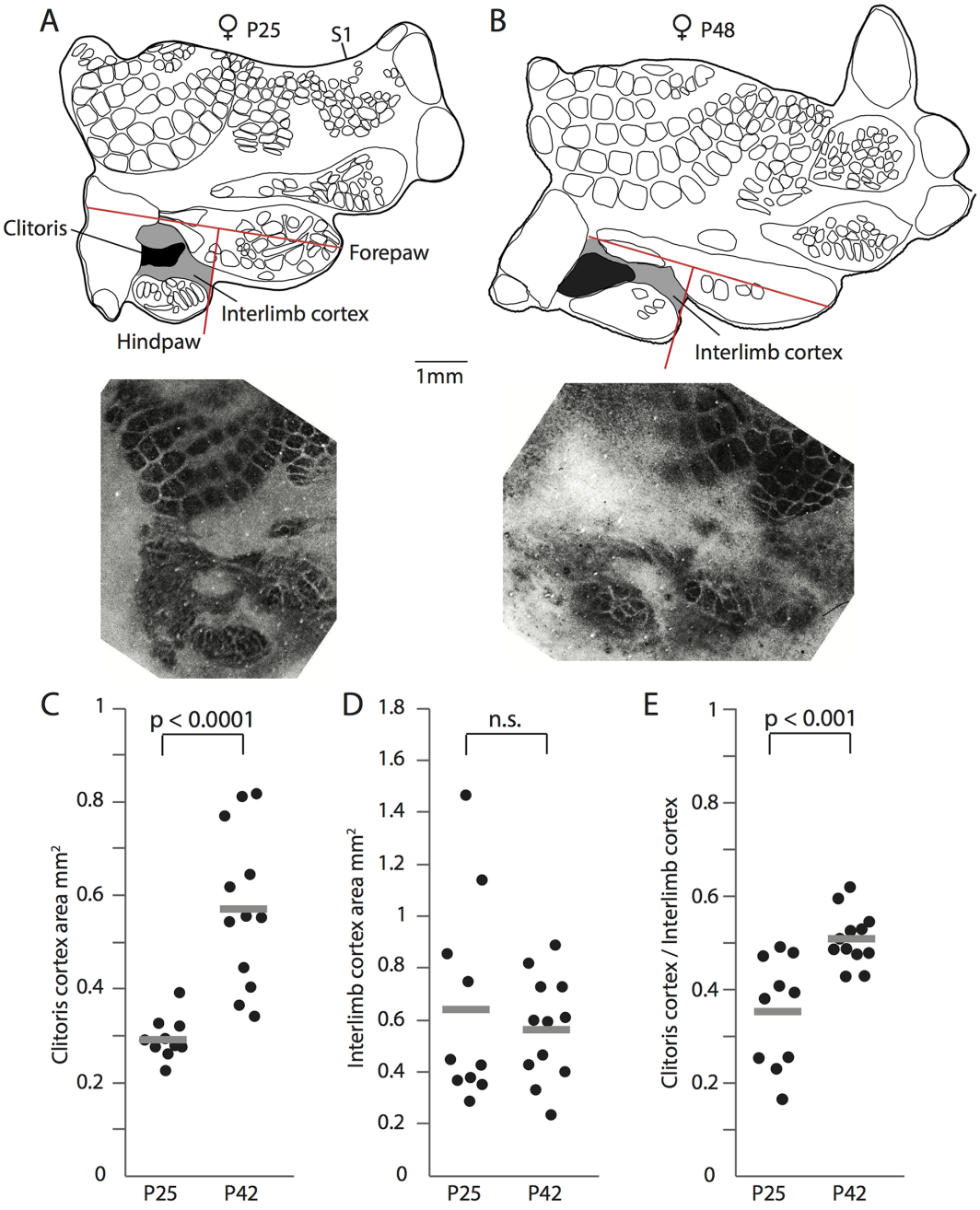

Fig 3. Genital cortex growth is due to the invasion of dysgranular territories. (A) Upper panel: Map of somatosensory cortex (S1) obtained from a female aged postnatal day (P) 25. Genital cortex is labeled in black. The interlimb cortex is marked in grey. The upper red lines marks the forepaw axis. The lower red line is rectangular to the forepaw axis, terminates at the anterior end of the hindpaw representation, and was used to demarcate interlimb cortex. Lower panel: Corresponding for cytchrome c stained tangential section, which shows best the clitoris area. (B) Same as (A), but for an animal aged P48. Note that the interlimb cortex area is smaller than in the

young animal and that the clitoris representation is larger. (C) Absolute area of the clitoris representation in hemispheres of young (P25) and old (P42) animals. The clitoris representation almost doubles in size. (D) Same as (C), but the absolute area of the interlimb cortex is plotted. The interlimb cortex is slightly smaller in area in old animals than in young animals. (E) The ratio of the genital cortex to the interlimb cortex increases after puberty in P42 animals. See also S4 Fig and S1 Data.

https://doi.org/10.1371/journal.pbio.2001283.g003

between the 2 cage compartments daily, such that females received full exposure to pheromonal cues. Females were also able to see and hear the adult male. At the age of P30 animals were killed. Brains were removed and tangential sections through layer 4 of S1 were prepared and stained for cytochrome oxidase activity. The experimenter reconstructing and analyzing cortical maps was again blind to the experimental condition.

In Fig 4B somatosensory cortical maps are shown for all 3 experimental conditions (upper panel: map obtained from a female cohoused with a female; middle panel: map from a female cohoused with a male; lower panel: map from a female, which sat together with a male, but with a wire-mesh separating the animals). Note that the cortical clitoris representation is the largest in the map of the female cohoused together with a sexually experienced male. In fact, the cortical clitoris representation (Fig 4C) and the fraction of clitoris of the entire S1 (Fig 4D) increased significantly more, when prepubescent females received male tactile cues (filled blue circles, mean genital cortex of S1 1.9% ± 01) compared to female tactile cues (filled red circles, mean genital cortex of S1 1.36% ± 01). Interestingly, pheromones and audio-visual contact alone were insufficient to drive genital cortex growth (open blue circle, mean genital cortex of S1 1.3% ± 01). A 1-way ANOVA also reported a significant difference between prepubescent females cohoused with either males, females, or males without having tactile contact ($P = 001$). The overall size of S1 (Fig 4E) did not differ between groups ($P = 06$7; 1-way ANOVA). Note that the relative size of genital cortex of the young females, which were cohoused with sexually experienced males (mean genital cortex of S1 1.9% ± 01, Fig 4D filled blue circles), is similar to that of the adult females (mean genital cortex of S1 1.8% ± 01, Fig 1B), even though we killed these animals at P30, which would correspond to midpuberty group raised animals. These findings suggest, that male sexual touch strongly advances female genital cortex growth.

Artificial genital touch drives genital cortex expansion and promotes female sexual maturation

We were surprised to observe such big effects following cohousing with sexually experienced males, while male olfactory cues had no impact on genital cortex development. These observations made us wonder about the relative contributions of tactile and other cues on female sexual maturation and genital cortex development. What are the contact cues that drive genital cortex expansion and promote female sexual maturation? It has previously been shown, that gentle touch of female genitals creates conditioned place preference in female rats [21] and increases 5kHz range trill calls emitted by hormonally primed females [22]. Similarly, we set up an experiment, where prepubescent female rats (P23) were exposed to artificial genital touch (Fig 5). During a 10-minute session, animals were freely moving in a small U-shaped environment, while the female experimenter repeatedly touched the animals' clitoris and vulva with a lubricated brush (artificial genital touch, Fig 5B). Control animals were placed in the same environment for 10 minutes without genital touch (Fig 5A). For 7 days, each animal completed 3 sessions distributed across the day. Animals were killed at P30 and S1 maps were reconstructed with the experimenter being blind to the condition. Control animals (Fig 5C) had a smaller genital cortex than animals, which received artificial genital touch (Fig 5D). Such differences in absolute (Fig 5E) and relative size of genital cortex (Fig 5F) were significant. The effect size was comparable to the differences observed between male and female touch in Fig 4;

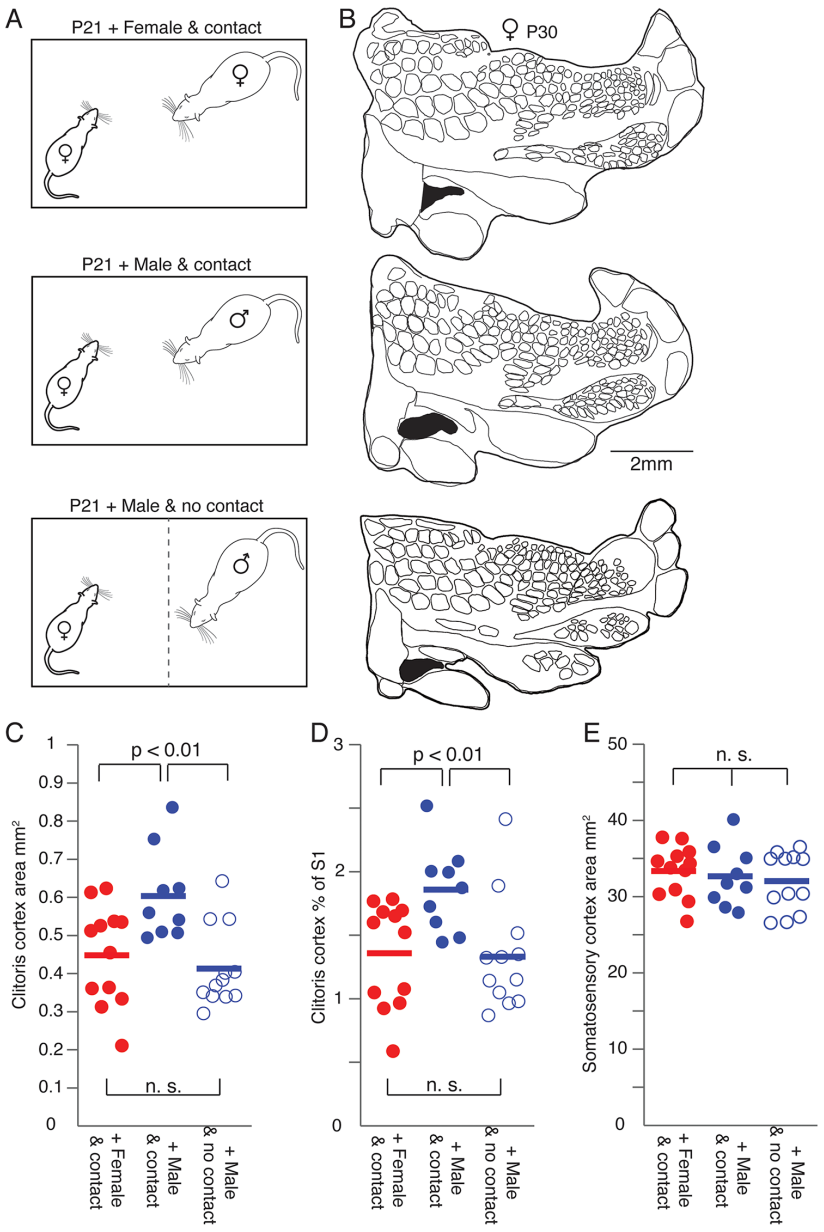

Fig 4. Genital cortex growth in prepubescent females is accelerated by tactile cues from males. (A) Prepubescent animals (postnatal day [P]21) were cohoused for 9 days with either an adult, sexually experienced female (upper panel) or a sexually experienced adult male (middle panel). Whereas tactile contact was allowed in both of these groups, the third group of prepubescent rats was only exposed to olfactory (by a daily exchange of bedding between the cage compartments), visual, and auditory cues of a sexually experienced adult male (lower panel). (B) Upper panel: Outline of a somatosensory cortex (S1) map from the brain of a P30 female cohoused with a sexually experienced adult female. Genital cortex is labeled in black. Middle panel: Map from a brain of a P30 female cohoused with a sexually experienced adult male. Lower panel: Outline of a S1 map obtained from a P30 female exposed to olfactory, visual, and auditory cues

but not tactile cues from a sexually experienced adult male. (C) Absolute area of genital cortex in hemispheres of P30 females cohoused with either a female (female and contact), a male (male and contact), or with a male without having tactile contact (male and no contact). Note that the size of genital cortex in the brains of animals who were cohoused in tactile contact with a male is significantly larger compared to the other 2 groups (female and contact, and male and no contact). (D) Same as (C), but the fraction of genital cortex of the entire S1 is shown. (E) Same as (C), but the absolute area of S1 is plotted. There is no difference between the 3 groups. See also S1 Data.

https://doi.org/10.1371/journal.pbio.2001283.g004

the size of the entire S1 was not different (Fig 5G). Artificial genital touch also affected female sexual maturation. While there was no significant change in vaginal opening (Fig 5J), the uteri were significantly heavier following artificial genital touch, as compared with control rats (Fig 5H and 5I).

Blockade of neuronal activity prevents genital cortex growth and delays vaginal opening

In order to better understand the role of female genital cortex during puberty, we blocked genital cortex activity over a certain time during prepuberty (P23–P30). To do so, P21 animals received Elvax implants over the area of genital cortex. Elvax sheets were developed for the slow, gradual release of drugs [23]. Elvax sheets were either soaked with tetrodotoxin (TTX) (Fig 6B), which blocks voltage dependent sodium channels, or impregnated with Ringer, as a control condition (Fig 6A). After recovery, the implanted females were cohoused with sexually experienced males until the age of P30 S1 maps of the brains were obtained as described above. The experimenter reconstructing cortical maps was again blind to the experimental condition. A map from a control animal treated with ringer is shown in Fig 6C , while Fig 6D shows a cortical map obtained from a TTX treated female. In animals, in which genital cortex was blocked with TTX, the area of clitoris representation (Fig 6E ; mean area in maps of control animals was 048mm ^{2} ± 002 and in S1 of TTX treated animals 032mm ^{2} ± 0013; $P < 0001$, Student *t* test) and the relative size (Fig 6F) was smaller than in control animals. The area of S1 did not show any differences (Fig 6G ; mean area of S1 in Ringer treated animals was 32.4mm^2 ± 1.4 and in TTX implanted animals 33.1mm^2 ± 1.1; $P = 07$, Student *t* test). The difference between hemispheres from control (mean genital cortex of S1 was 1.49% ± 005) and TTX treated animals (mean genital cortex of S1 was 1.02% ± 005) was marked ($P < 0001$, Student *t* test). These results immediately suggest 2 conclusions. First, the fact that there was a difference between control and TTX treated animals indicates that our TTX treatment was effective. Second, the data indicate that the pubertal expansion of genital cortex requires cortical activity.

Next, we wondered if an intact genital cortex is required for female sexual maturation. Therefore, we determined the status of puberty in control and TTX treated animals. Accordingly, pictures of vagina and clitoris were taken before implantation and after the behavioral experiment. Five out of 13 animals, which received a ringer soaked Elvax sheet above genital cortex, showed an open vagina at the end of the experiment. The vagina before (left panel) and after the experiment (right panel) for one of those females is shown in Fig 6H . In contrast, only 1 of the animals ($n = 11$), whose genital cortices were blocked with TTX, had an open vagina. Fig 6I shows the pictures of 1 TTX animal before (left panel) and after (right panel) the treatment. The scores of vaginal opening are plotted in Fig 6J . The vaginas were closed in 9 out of 11 animals treated with TTX, and we observed a vagina that was about to open in only 1 TTX treated animal. In contrast, only 2 out of 13 animals in the Ringer group had the vagina still closed at the end of the experiment. The uterine weights (Fig 6K) were not significantly

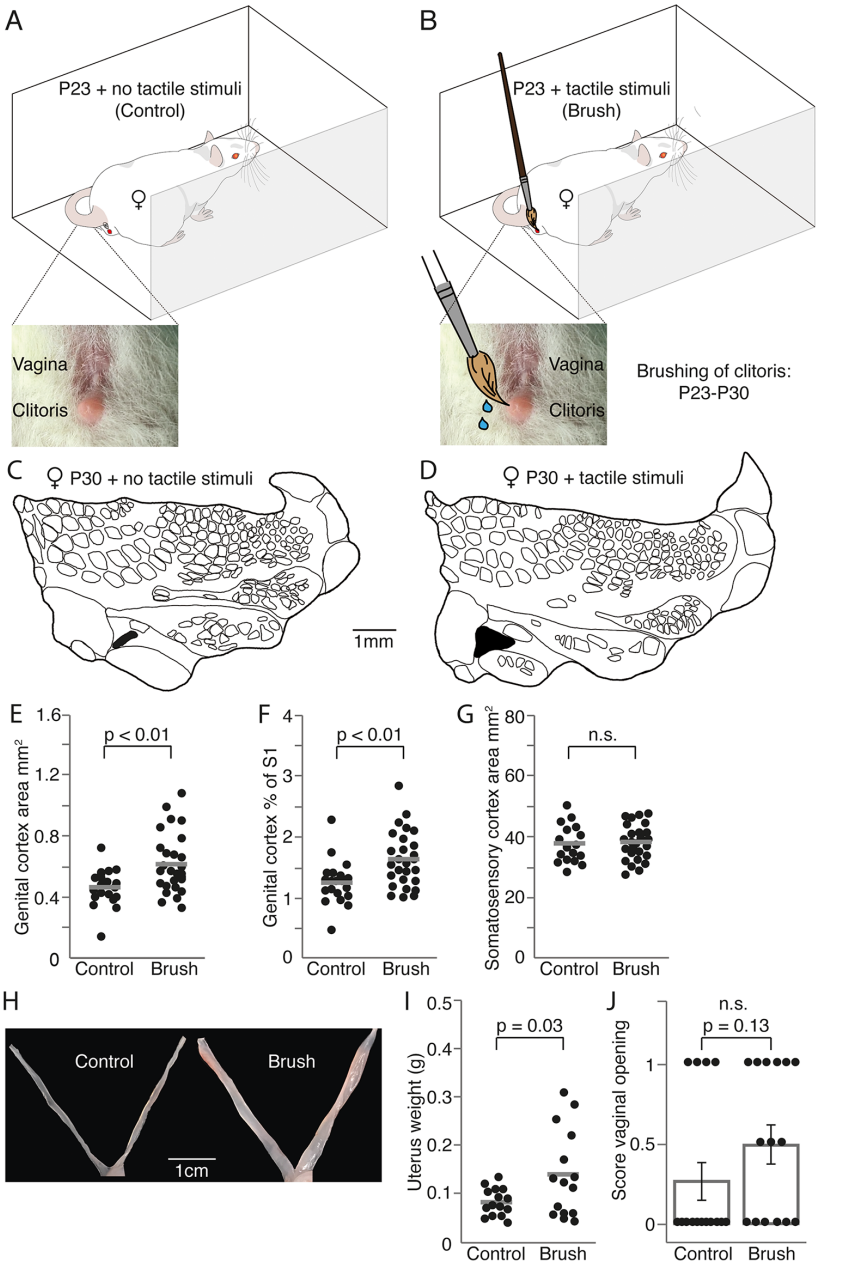

Fig 5. Artificial genital touch drives genital cortex expansion and promotes female sexual maturation. (A) Control, prepubescent female rats (postnatal day [P]23) were placed each day 3 times for 10 minutes in a box across 7 days without further treatment. (B) Artificial genital touch; prepubescent female rats (P23) were placed each day 3 times for 10 minutes in a box across for 7 days, and their clitoris and vulva were stroked with a lubricated brush by a human (female) experimenter. (C) Outline of a somatosensory cortex (S1) map from the brain of a P30 female who received the control treatment described in A. Genital cortex is depicted in black. (D) Same as (C), but example map stems from the brain of a P30 female, whose genitals were brushed

as described in (B). (E), Absolute area of clitoris representation in hemispheres of P30 females, which underwent control (A) or artificial genital touch (B) treatment. (F) Same as (E), but the fraction of genital cortex of the S1 is plotted. (G) Same as (E), but the absolute area of S1 is shown for the 2 groups. There is no difference in S1 size. (H) Mean scores for vaginal opening for P30 females, which underwent control (A) or artificial genital touch (B) treatment. (I) Picture showing the uterus of a female, which underwent control (A) or artificial genital touch (B) treatment. (J) Uterine weights of females that underwent control (A) or artificial genital touch (B) treatment. See also S1 Data.

https://doi.org/10.1371/journal.pbio.2001283.g005

different, however. Thus, genital cortex activity might relay effects of male sexual touch on vaginal opening in rat female puberty.

The relation between relative genital cortex size, estrogens, and uterine weight

In order to obtain insight in the relationship between female sexual maturation and genital cortex development, we plotted genital cortex size against uterine weight in all experiments, in which we collected such data (S5 Fig). As shown in S5A Fig, there was no tight relationship between relative genital cortex size and uterine weight. Nonetheless, it was obvious that a large uterine weight (≥015 g) is rarely associated with a small (≤1%) relative genital cortex size. If one compared genital cortex size and uterine weight across specific experimental conditions (S5B Fig), it was noticeable that animals with TTX treatment of genital cortex (the experiment described in Fig 6) never had very large genital cortices, even for cases with a large uterus.

Discussion

Our data confirm a major pubertal expansion of female genital cortex, which—unlike the maintenance of large genital cortex in adults—requires intact ovaries and sex hormones. The larger area of genital cortex in adults reflects an invasion of adjacent territories by thalamic afferents. Such changes in female genital cortex are advanced by sexual touch and require cortical activity. Most interestingly, blockade of genital cortex delays female sexual maturation, suggesting that genital cortex is the neural structure that mediates the puberty advancing effects of male sexual touch.

The expansion of layer 4 of genital cortex in puberty [7] is an unusual pattern in the development of layer 4 in S1. In contrast, the barrel representation is characterized by a brief directly postnatal critical period, after which the barrel pattern can no longer be changed [3]. Our data show that intact ovaries and, hence, presumably the sex hormones emitted by the ovaries are required for the pubertal expansion of genital cortex. The interpretation that sex hormones drive pubertal expansion is greatly strengthened by observations following the injection of estradiol, which mimics the pubertal expansion of genital cortex. The mechanisms, by which sex hormones, and in particular estrogens, drive pubertal expansion of genital cortex, are yet to be determined; both, a direct sex hormone effect on genital cortex and an indirect effect via growth stimulation of sex organs (i.e., the clitoris) by sex hormones are conceivable. Thus, it is possible that cortical changes follow similar mechanism, as described for the hippocampus, in which a rapid potentiation of excitatory synapses is achieved by estrogen [24] with different underlying mechanism in male and female rats [25]. From human studies, it is known that the hippocampus changes in size along the reproductive cycle with the biggest hippocampus being present when blood estrogen levels are highest [26].

The data discussed below indicate that at least some stage of cortical activity seems to be required for genital cortex expansion. The visualization of thalamic afferents by VGluT2 antibodies showed that cytochrome oxidase staining reveals maps completely congruent with thalamic innervation. Thus, the size increase of genital cortex in adults indicates that a larger

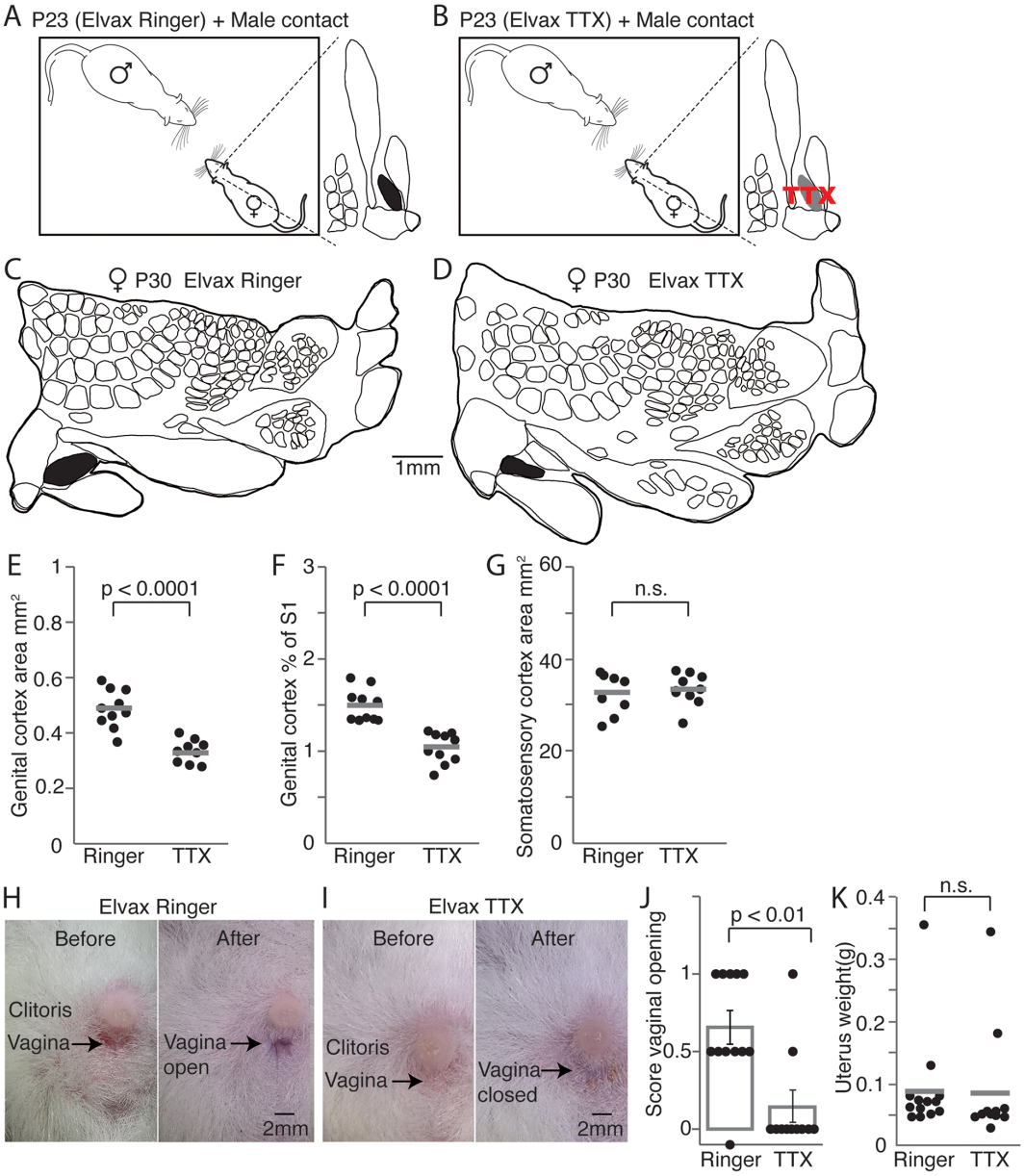

Fig 6. Blocking neuronal activity in genital cortex prevents area growth and delays female sexual maturation. (A) Prepubescent animals (postnatal day [P]23) received Ringer impregnated Elvax sheets above genital cortex and were cohoused together with a sexually experienced adult male for 7 days. (B) Same as (A), but Elvax implants released tetrodotoxin (TTX), which blocked neuronal activity in genital cortex. (C) Outline of a somatosensory cortex (S1) map from the brain of a P30 female, who received a ringer soaked implant above genital cortex and was cohoused with a sexually experienced adult male. Genital cortex is depicted in black. (D) Same as (C), but example map stems from the brain of a P30 female, whose genital cortex was blocked through a TTX containing implant. (E) Absolute area of clitoris representation in hemispheres of P30 females, which were cohoused with sexually experienced adult males and received beforehand either Elvax implants containing Ringer or TTX. Note that genital cortices in Ringer treated animals show significant larger growth compared with animals that received TTX implants above genital cortex. (F) Same as (E), but the fraction of genital cortex

of the S1 is plotted. (G) Same as (E), but the absolute area of S1 is shown for the 2 groups. There is no difference in S1 size. (H) Pictures of clitoris and vagina taken before implanting animals with Ringer containing Elvax sheets (P23) and after cohousing them for 7 days with sexually experienced adult males. Note that the vagina was already open at P30. (I) Same as (H), but pictures show clitoris and vagina of an animal, who received a TTX-soaked Elvax implant above genital cortex. The vagina stayed closed when blocking genital cortex, while cohousing the prepubescent animals with a sexually experienced adult male. (J) Mean scores for vaginal opening. A score of 0 represents a closed vagina, whereas a score of 1 stands for an opened vagina. The intermediate state (between open and closed vagina) has a score of 0.5. The majority of females, which received a Ringer soaked implant above genital cortex, showed either an opened vagina or a half opened vagina, which was about to open after being cohoused for 7 days with sexually experienced adult males. In contrast, almost all animals implanted with TTX Elvax sheets had the vagina closed at P30. Each dot represents the score of vaginal opening for 1 animal. (K) Uterine weights of females with implanted Ringer or TTX Elvax sheets after being cohoused with sexually experienced adult males. No significant difference ($P = 0.98$, Student t test) was found between the groups. See also S1 Data.

https://doi.org/10.1371/journal.pbio.2001283.g006

cortical area is innervated by thalamic afferents. The detailed analysis of body maps in young and adult animals is strongly suggestive that the size increase of genital cortex results from an invasion scenario, in which putative genital afferents innervate neighboring dysgranular cortex.

Female genital cortex development is strongly affected by tactile sexual experience. Housing pubescent females with a sexually experienced adult male strongly advances the growth of genital cortex. Even though we killed such females at P30 (which corresponds in group-housed animals to midpuberty), they had genital cortices larger than average adult size (compare Figs 2D and 4D). This advancement of puberty was induced specifically by direct male contact and was not seen in animals cohoused but not touched by males, or in animals cohoused with females. In line with the idea that genital cortex is altered by sexual experience, we find that blockade of genital cortex prevents the pubertal layer 4 expansion of genital cortex. The requirement of experience and cortical activity for the appropriate development of adult somatotopy is similar to the requirement of cortical activity for the development of ocular dominance columns in the visual system [27]. It is notably different, however, from the development of the early postnatal development of the barrel pattern in S1, which occurs despite manipulation of peripheral [28] or cortical inputs [29]. Thus, genital cortex does seem to differ from barrel cortex not only in the timing of the critical period, but also the cellular mechanisms mediating genital cortex plasticity seem to differ from barrel cortex.

Whereas our blocking experiments show that genital cortex activity is crucial for the pubertal layer 4 expansion, it is questionable to what extent this plasticity is functionally meaningful. Decorticated animals are still able to mount and reproduce. However, subtle changes in the pattern of reproduction [30,31] are observed. Furthermore, somatosensory feedback from the penis was shown to be critical for the achievement of intromission, and somatosensory feedback from the preputial region is needed for the execution of copulatory thrusting [32]. Blocking genital cortex activity during the critical period of puberty may cause changes in the pattern of reproduction during adulthood, i.e., that the number of intromissions and time to ejaculation might be affected (in males); lordosis or place preference behavior could be affected in females.

As shown many decades ago, the social signals powerfully control the advance of puberty [33]. While it became clear that pheromonal stimuli mediated by the vomeronasal organ [11] contribute to the male induced advance in female puberty in mice, the hastening effects of puberty induced by male pheromones alone are minor. Bronson and Maruniak [13] suggested that tactile male cues synergistically with pheromones advance female puberty. Further work showed that androgenized female mice [34], but not castrated male mice [13], provide the tactile female puberty promoting cues. Our artificial genital touch experiment showed a major effect of genital touch on female sexual maturation. The effects of artificial genital touch on uterine weight (Fig 5I) were even larger than the male effects seen in some of our control

experiments (Fig 6K). Thus, our data point to genital touch as a dominant cue for inducing puberty and question the idea that a sensory synergism is required [13]. Our data show that an intact female genital cortex promotes vaginal opening. Thus, the data suggest that genital cortex might be a tactile gateway through which sexual touch promotes female puberty. This question requires further investigation, however, as we did not observe an effect of genital cortex blockade on uterine weight, as described previously in rats [33]. The receptive field properties of genital cortex appear to be tuned to sexual tactile contacts associated with mating [7] and, hence, seem well-suited to relay signals arising from sexual touch. The ensemble of our systemic female hormone application effects on genital cortex growth and our puberty advancing effects established by genital touch leads to speculation about a possible bidirectional connection between genital cortex and the medial preoptic nucleus of the hypothalamus. This region contains gonadotropin releasing hormone (GnRH) neurons whose activity produces high frequency of GnRH release which, in turn, causes gametogenesis and an increase in gonadal steroid hormone secretion [35].

Materials and methods

Ethics statement

All experimental procedures were performed according to German guidelines on animal welfare under the supervision of local ethics committees (animal permit numbers: G0193/14 and G0244/16).

Animals

All experiments were conducted on Wistar rats purchased from Janvier Labs. All animals were kept on a 12 hour to 12 hour, normal light/dark cycle with lights off at 1000 PM. Rats had ad libitum access to food and water.

Ovariectomies

Ovariectomies were performed in prepubescent (P21) and adult Wistar rats (P42). For the surgery, animals were anesthetized by injection of an initial dose of 100 mg/kg ketamine and 7.5 mg/kg xylazine. Respiration, blink, and pinch reflex were observed throughout the surgery and, if needed, animals were injected with an extra shot (25%) of ketamine/xylazine mixture (Sigma-Aldrich, St. Louis, MO) or a 25% dose of ketamine (Sigma-Aldrich) alone. Monitoring of temperature was done using a rectal probe and could be maintained with a heating pad (Stoelting, Wood Dale, IL) to 34˚C–36˚C.

To remove ovaries a small incision was made bilaterally on the animal's bag. The white fat pad, to which the ovaries are attached to, was pulled out through the body wall. Ovaries were grabbed with forceps and removed from the fallopian tube using small scissors. After successful removal, the white fat pad with fallopian tube was put back through the body wall. The incision was sutured using a self-resorbing thread. The wound was disinfected and looked after in the days following surgery.

Estradiol treatment

Immature Wistar rats (P26) were divided randomly into groups of 3–4 animals. All animals were weighed daily and the vagina opening was assessed by visual inspection and defined as a complete separation of the membranous sheath covering the vaginal orifice [36]. Photos of clitoris and vagina were taken before the first injection and after the experiment. The assessment of vaginal opening was not blind but the different stages were very clear to detect.

Animals in the testing group were injected subcutaneously every morning with 0.5 μg 17β-estradiol (Sigma-Aldrich), dissolved in 0.4 ml of sesame oil (Sigma-Aldrich), per 100 g body weight. Rats in the control group received the same amount of sesame oil. On day 5 of the treatment, animals were deeply anaesthetized, perfused, and their brains processed, as described below. In addition, uteri of every animal in experiment was taken out while perfusion and weighed.

Experiments on sexual touch during development

Wistar rats aged P21 were divided into 3 groups. Each animal of group 1 was housed for 9 days together with a sexually experienced adult female rat (approximately P60). Every rat of group 2 was put for 9 days together with a sexually experienced adult male rat (approximately P60). Group 3 rats were also housed together with a sexually experienced adult male rat (approximately P60), but the cages were separated by a wire-mesh. Whereas the animals of group 1 and 2 were able to interact fully with their housing partner, the rats in group 3 could not touch the male they were housed together with. However, they were able to smell, see, and hear the male through the wire-mesh.

Vaginal opening was documented as described above, and pictures of clitoris and vagina were taken before and after the experiment. After 9 days, at the age of P30, animals of all groups were anaesthetized, perfused, and their brains histologically processed as described below. Uteri of all animals were taken out while perfusion and weighed.

Artificial genital touch

Prepubescent female Wistar rats (P23) were divided into 2 groups. Control animals were placed 3 times for 10 minutes in a small U-shaped arena over 7 days without further treatment and were then returned to their home cage. Animals in the artificial genital touch group were placed 3 times for 10 minutes in a small arena over 7 days, and their clitoris and vulva were contacted with a lubricated brush by a human (female) experimenter (similar to Parada, 2010 [21]). After 7 days (at the age of P30), animals of all groups were anaesthetized, perfused, and their brains histologically processed, as described below. Uteri of all animals were taken out while perfusing and weighed.

Experiments on blockade of S1 with TTX/Elvax

Animals (P21) were divided into 2 groups. The control group received a chronic Ringer-impregnated Elvax sheet above genital cortex and the rats in the testing group were implanted with a TTX-impregnated Elvax sheet above genital cortex.

Elvax implants were prepared as described before [29, 37, 38]. Briefly Elvax 40p (ethylene-vinyl acetate copolymer; DuPont, Wilmington, DE) was washed for one week in 96% of Ethanol and afterwards dissolved in methylene chloride to obtain a 10% solution. TTX (Abcam, Cambridge, UK) or Ringer (control) was then added in order to achieve a final concentration of 2%. The TTX or Ringer containing Elvax mixture was poured into a glass mold and quickly frozen for 1 hour at −80˚C. After 30 minutes, the blocks were removed from the mold and put for another 3 days into the −80˚C freezer. On day 3, the Elvax TTX or control blocks were transferred to the −20˚C and stored for another 3–4 days. Subsequently, the TTX and Ringer impregnated blocks were cut on a vibratome (Leica, Wetzlar, Germany) into 150 μm sheets, which were cut into 2 mm squares using a scalpel. Before surgical implantation all Elvax sheets were washed for at least 8 hours in distilled water.

For surgical implantation P21 Wistar rats were anesthetized by injection of an initial dose of 100 mg/kg ketamine and 7.5 mg/kg xylazine. Respiration, blink, and pinch reflex were

observed throughout the surgery and, if needed, animals were injected with an extra shot (25%) of ketamine/xylazine mixture or a 25% dose of ketamine alone. Monitoring of temperature was done using a rectal probe and could be maintained with a heating pad to 34˚C–36˚C. Lidocaine was locally injected in the scalp, which was then removed. A craniotomy was performed above genital cortex, and the dura was removed using a bend syringe. The TTX or Ringer impregnated sheets were placed on the brain surface and covered with silicone (Kwik-Cast; World Precision Instruments, Sarasota, FL). The exposed skull was finally covered with dental cement. Animals were allowed to recover from surgery for 2 days. Photos of clitoris and vagina were taken before the behavioral experiment. At the age of P23, implanted animals were put together with a sexually experienced male. After 7 days (at the age of P30), TTX and control animals were anaesthetized and their vaginal opening was documented as described above. Along with the perfusion, the uteri of the animals were cut out and weighed. Brains were histologically processed as described below.

Histology

At the end of the above-described experiments, animals were anaesthetized using a 20% urethane solution and perfused with phosphate buffer followed by a 2% paraformaldehyde solution (PFA). Brains were removed, hemispheres were separated, and cortices were flattened between 2 glass slides separated by clay spacers [39]. Glass slides were weighed down with small ceramic weights for approximately 3 hours. Afterwards, flattened cortices were stored overnight in 2% PFA and 80 μm sections were cut on a Vibratome (Leica). Sections were stained for cytochrome-oxidase activity using the protocol of Divac et al. [40]. After the staining procedure, sections were mounted on gelatin coated glass slides with Mowiol mounting medium. Subsequently, pictures were taken on an Olympus BX51 microscope and layer 4 areas of S1 were drawn by using a Neurolucida software. S1 maps were reconstructed through serial sections. To exclude experimenter biases, cortical maps were drawn and analyzed by an experimenter blind to the conditions (e.g., estradiol versus sesame oil control group; TTX versus Ringer-treated group).

For the alternating staining procedure with cytochrome c and VGluT2, immunohistochemical labeling was performed using standard procedures. Briefly, brain sections, which should be labeled for VGluT2, were preincubated for an hour at room temperature in a blocking solution (0.1 M PBS, 2% bovine serum albumin, and 0.5% Triton X-100). Afterwards, primary antibodies were diluted in a solution containing 0.5% Triton X-100 and 1% bovine serum albumin. The primary antibody against VGluT2 was incubated with the free-floating sections for at least 24 hours under mild shaking at 4˚C. Incubations with the primary antibody was followed by detection with a secondary antibody coupled to the fluorophore Alexa 488. The secondary antibody was diluted (1:500) in 0.5% Triton X-100 and the reaction was allowed to proceed for 2 hours in the dark at room temperature. After the staining procedure, sections were mounted on gelatin coated glass slides with Mowiol mounting medium.

Quantification of somatosensory areas and sizes

The area of various somatosensory regions was measured by outlining the anatomical region of interest and calculating its area using Neurolucida area calculating tool. The area of the following cortical representations was measured: hindpaw, forepaw, trunk, interlimb cortex, and clitoris. The fraction of genital cortex of the whole S1 area was calculated by dividing the clitoris area by the value of the S1 area. The same was done for the fraction of genital cortex of the interlimb cortex. All statistic tests were conducted in Matlab.

Scoring of vaginal opening

In order to quantify the state of vaginal opening after the above described experiments, we assigned different states with vaginal opening scores. A score of 0 points to a closed vagina, whereas a score of 0.5 describes a vagina, which was about to open. Finally, a score of 1 represents an open vagina.

Supporting information

S1 Fig. Micrographs showing the pubertal expansion of genital cortex, but not its maintenance in adults requires sex hormones. Figure S1 related to Fig 1: Micrographs showing the pubertal expansion of genital cortex, but not its maintenance in adults requires sex hormones. **A**, Upper panel: Tangential section through S1 of a P25 old animal stained for cytochrome oxidase activity. Lower panel: The corresponding map drawn from the section shown above, genital cortex shown in black.**B**, Same as A, but the section and map stems from an animal aged P42. The genital cortex is larger than in the P25 animal. **C**, Same as A for an animal aged P42, which was ovariectomized before puberty at P20. Note that the size of the genital cortex is comparable to the genital cortex of the youngfemale shown in A. **D**, Same as A for an animal aged P60, which was ovariectomized after puberty at P42. The clitoris representation is greater than in the young ovariectomized animal (C) but comparable in size to the P42 aged animal (B).
(TIF)

S2 Fig. Comparison of normalization of genital cortex to primary somatosensory cortex (S1) and posteromedial barrel subfield (PMBSF). Figure S2 related to Fig 1: Comparison of normalization of genital cortex to primary somatosensory cortex (S1) and posteromedial barrel subfield (PMBSF).**A**, Fraction of genital cortex of the entire S1 in hemispheres of P25, P42 females and females which were ovariectomized at either P20 or P42. **B**, Same as A but fraction of genital cortex of the PMBSF is shown. Note that the same effects are seen as in A, namely a substantial growth of the genital cortex between P25 and P42 animals. Female rats ovariectomized during prepuberty had smaller genital cortices than animals ovariectomized after puberty. Graphically distribution looks similar in A and B and no big difference in the variability can be make out. See also S1 Table. **C**, Absolute area of PMBSF in hemispheres of P25, P42, in prepuberty (P20) ovariectomized and postpuberty (P42) ovariectomized female rats. See also S1 Data.
(TIF)

S3 Fig. Micrographs showing systemic estradiol application drives genital cortex growth and advances puberty. Figure S3 related to Fig 2: Micrographs showing systemic estradiol application drives genital cortex growth and advances puberty.**A**, Upper panel: Tangential section through S1 of a hemisphere obtained from an animal which received subcutaneous sesame oil injections over 5 days. The section was stained for cytochrome c and shows the reconstructed clitoris area best. Lower panel: Corresponding reconstructed map from the section plotted above. **B**, Same as A, but the section and drawn map are obtained from an animal which received daily estradiol injections. Note that the clitoris area is greater compared to the example section and map shown in A.
(TIF)

S4 Fig. Genital cortex growth is due to the invasion of dysgranular territories by putative genital thalamic afferents. Figure S4 related to Fig 3: Genital cortex growth is due to the invasion of dysgranular territories by putative genital thalamic afferents.**A**, Upper, tangential

section through S1 of an animal aged P14. The section was stained for cytochrome oxidase activity. Lower, map of the somatosensory areas drawn on the section shown above. **B**, Upper, adjacent tangential section through S1 obtained from the same hemisphere, which is shown in A. The section was stained with antibodies (green fluorescence) against VGluT2 (vesicular glutamate transporter 2), which is expressed in thalamocortical afferents. Lower, map of the somatosensory areas drawn on the section shown above. Note that the reconstructed areas correspond in size when comparing A and B.
(TIF)

S5 Fig. Genital cortex size and uterine weight. Figure S5 related to Figs 5 & 6: Genital cortex size and uterine weight.**A**, Genital cortex size is plotted against uterine weight for all experiments. No tight relationship can be observed. Note that a large uterine weight ($\geq$ 015 g) is rarely associated with a small ($\leq$ 1%) relative genital cortex size.**B**, Same as A, but for specific experimental conditions See also S1 Data.
(TIF)

S1 Table. Table S1 related to Fig 1: Variation coefficient.
(TIF)

S1 Data. All supporting data. Individual data for Figs 1, 2, 3, 4, 5 and 6 and S2 and S5 Figs.
(XLSX)

Acknowledgments

We thank Undine Schneeweiß and Juliane Diederichs for excellent technical assistance, and Edith Chorev and Simon Lauer for help with the perfusions. For comments on the manuscript, we thank Andreea Neukirchner and Ann Clemens. We want to additionally thank Ann Clemens for providing a few ovariectomized animals.

Author Contributions

Conceptualization: Constanze Lenschow, Michael Brecht.

Funding acquisition: Michael Brecht.

Investigation: Constanze Lenschow, Johanna Sigl-Glöckner, Michael Brecht.

Supervision: Michael Brecht.

Writing – original draft: Constanze Lenschow, Michael Brecht.

Writing – review & editing: Constanze Lenschow, Michael Brecht.

References

1. Wiesel TN. The postnatal development of the visual cortex and the influence of environment. Biosci Rep. 1982; 2: 351–377. PMID: 7049262
2. Woolsey TA, Van der Loos H. The structural organization of layer IV in the somatosensory region (SI) of mouse cerebral cortex. The description of a cortical field composed of discrete cytoarchitectonic units. Brain Res. 1970; 17: 205–242. PMID: 4904874
3. Van der Loos H and Woolsey TA. Somatosensory cortex: structural alterations following early injury to sense organs. Science 1973; 179: 395–398. PMID: 4682966
4. Van der Loos H, Welker E, Dörfl J, Rumo G. Selective breeding for variations in patterns of mystacial vibrissae of mice. Bilaterally symmetrical strains derived from ICR stock. J Hered. 1986; 77: 66–82. PMID: 3711643
5. Schlaggar BL, Fox K, O'Leary DD. Postsynaptic control of plasticity in developing somatosensory cortex. Nature 1993; 364: 623–626. https://doi.org/10.1038/364623a0 PMID: 8102476

6. Feldman DE and Brecht M. Map plasticity in somatosensory cortex. Science 2005; 310: 810–815. https://doi.org/10.1126/science.1115807 PMID: 16272113
7. Lenschow C, Copley S, Gardiner JM, Talbot ZN, Vitenzon A, Brecht M. Sexually monomorphic maps and dimorphic responses in rat genital cortex. Curr Biol. 2016; 26: 106–113. https://doi.org/10.1016/j.cub.2015.11.041 PMID: 26725197
8. Fink G. Handbook of neuroendocrinology (Academic Press). 2012.
9. Vandenbergh JG. Effect of the presence of a male on the sexual maturation of female mice. Endocrinology 1967; 81: 345–349. https://doi.org/10.1210/endo-81-2-345 PMID: 4952008
10. Kaneko N, Debski EA, Wilson MC, Whitten WK. Puberty acceleration in mice. II. Evidence that the vomeronasal organ is a receptor for the primer pheromone in male mouse urine. Biol Reprod. 1980; 22: 873–878. PMID: 7397305
11. Faulkes CG and Abbott DH. Evidence that primer pheromones do not cause social suppression of reproduction in male and female naked mole-rats (Heterocephalus glaber). J Reprod Fertil. 1993; 99: 225–230. PMID: 8283442
12. Faulkes CG and Abbott DH. Evidence that primer pheromones do not cause social suppression of reproduction in male and female naked mole-rats (Heterocephalus glaber). J Reprod Fertil. 1993; 99: 225–230. PMID: 8283442
13. Bronson FH, Maruniak JA. Male-induced puberty in female mice: evidence for a synergistic action of social cues. Biol Reprod. 1975; 13: 94–98. PMID: 1222186
14. Rogel MJ. A critical evaluation of the possibility of higher primate reproductive and sexual pheromones. Psychol bull. 1978; 85: 810. PMID: 98777
15. Scott KM, Smith DR, Ellis PM. Prospectively ascertained child maltreatment and its association with DSM-IV mental disorders in young adults. Arch Gen Psychiatry 2010; 67:712–719. https://doi.org/10.1001/archgenpsychiatry.2010.71 PMID: 20603452
16. Shonkoff JP, Garner AS. Committee on Psychosocial Aspects of Child and Family Health; Committee on Early Childhood, Adoption, and Dependent Care; Section on Developmental and Behavioral Pediatrics: The lifelong effects of early childhood adversity and toxic stress. Pediatrics 2012; 129: e232–e246. https://doi.org/10.1542/peds.2011-2663 PMID: 22201156
17. Heim CM, Mayberg HS, Mletzko T, Nemeroff CB, Pruessner JC. Decreased cortical representation of genital somatosensory field after childhood sexual abuse. Am J Psychiatry. 2013; 6: 616–623.
18. Ramirez VD, Sawyer CH. Advancement of Puberty in the female rat by estrogen. Endocrinology 1965; 76: 1158–1168. https://doi.org/10.1210/endo-76-6-1158 PMID: 14301523
19. Engelbregt MJ, Houdijk ME, Popp-Snijders C, Delemarre-van de Waal HA. The effect of intra uterine growth retardation and postnatal undernutrition on onset of puberty in male and female rats. Pediatr Res. 2000; 48: 803–807. https://doi.org/10.1203/00006450-200012000-00017 PMID: 11102550
20. Nahmani M, Erisir A. VGluT2 immunochemistry identifies thalamocortical terminals in layer 4 of adult and developing visual cortex. J Comp Neurol. 2002; 484: 458–473.
21. Parada M, Chamas L, Censi S, Coria-Avila G, Pfaus JG. Clitoral stimulation induces conditioned place preference and Fos activation in the rat. Horm Behav. 2010; 2: 112–118.
22. Gerson CA, Scardachio T, Quintana GR, Clarke PBS, Pfaus JG. Ovarian hormones alter the expression of 50 kHz ultrasonic vocalizations induced by distributed clitoral stimulation in female rats. 2016, Program No. 539.14 / GGG5. Neuroscience Meeting Planner. San Diego, CA: Society for Neuroscience, 2016. Online.
23. Fiorani L, Maccarone R, Fernando N, Colecchi L, Bisti S, Valter K. Slow-release drug delivery through Elvax 40W to the rat retina: implications for the treatment of chronic conditions. J Vis Exp. 2014; 91: 51563.
24. Wong M, Moss RL. Long-term and short-term electrophysiological effects of estrogen on the synaptic properties of hippocampal CA1 neurons. J Neurosci. 1992; 12: 3217–3225. PMID: 1353794
25. Oberlander JG, Woolley CS. 17β-Estradiol Acutely Potentiates Glutamatergic Synaptic Transmission in the Hippocampus through Distinct Mechanisms in Males and Females. J Neurosci. 2016; 9: 2677–2690.
26. Barth C, Steele CJ, Mueller K, Rekkas VP, Arélin K, Pampel A, et al. In-vivo Dynamics of the Human Hippocampus across the Menstrual Cycle. Sci Rep. 2016; 6: 32833. https://doi.org/10.1038/srep32833 PMID: 27713470
27. Stryker MP, Harris WA. Binocular impulse blockade prevents the formation of ocular dominance columns in cat visual cortex. J Neurosci. 1986; 6: 2117–2133. PMID: 3746403
28. Henderson TA, Woolsey TA, Jacquin MF. Infraorbital nerve blockade from birth does not disrupt central trigeminal pattern formation in the rat. Dev brain Res. 1992; 66: 146–152.

29. Chiaia NL, Fish SE, Bauer WR, Bennett-Clarke CA, Rhoades RW. Postnatal blockade of cortical activity by tetrodotoxin does not disrupt the formation of vibrissa-related patterns in the rat's somatosensory cortex. Dev Brain Res. 1992; 66: 244–250.

30. Carter CS, Witt DM, Kolb B, Whishaw IQ. Neonatal decortication and adult female sexual behavior. Physiol Behav. 1982; 4:763–6.

31. Whishaw IQ, Kolb B. The mating movements of male decorticate rats: evidence for subcortically generated movements by the male but regulation of approaches by the female. Behav Brain Res. 1985; 3:171–91.

32. Contreras JL, Agmo A. Sensory control of the male rat's copulatory thrusting patterns. Behav Neural Biol. 1993; 3: 234–40.

33. Vandenbergh JG. Acceleration of sexual maturation in female rats by male stimulation. J Reprod Fertil. 1976; 2: 451–453.

34. Drickamer LC. Contact stimulation, androgenized females and accelerated sexual maturation in female mice. Behav. Biol. 1974; 12: 101–110. PMID: 4473977

35. Sisk CL, Foster DL. The neural basis of puberty and adolescence. Nat Neurosci. 2004; 10: 1040–1047.

36. Vetter-O'Hagen CS, Spear LP. Hormonal and physical markers of puberty and their relationship to adolescent-typical novelty-directed behavior. Dev Psychobiol. 2012; 54: 523–535. https://doi.org/10.1002/dev.20610 PMID: 21953609

37. Silberstein GB, Daniel CW. Elvax 40P implants: sustained, local release of bioactive molecules influencing mammary ductal development. Dev Biol. 1982; 93: 271–278.

38. Graber KD, Prince DA. A critical period for prevention of posttraumatic neocortical hyperexcitability in rats. Ann Neurol. 2004; 55: 860–870. https://doi.org/10.1002/ana.20124 PMID: 15174021

39. Lauer SM, Lenschow C, Brecht M. Sexually selected size differences and conserved sexual monomorphism of genital cortex. J Comp Neurol. 2017, 12: 2706–2718.

40. Divac I, Mojsilovic-Petrovic J, López-Figueroa MO, Petrovic-Minic B, Møller M. Improved contrast in histochemical detection of cytochrome oxidase: metallic ions protocol. J Neurosci Methods. 1995; 56: 105–113 PMID: 7752676

Table S1: Variation coefficient

	P25	P42	OVX at P20	OVX at P42
Clitoris cortex % of S1	0.183	0.142	0.271	0.252
Clitoris cortex % of PMBSF	0.232	0.189	0.280	0.268

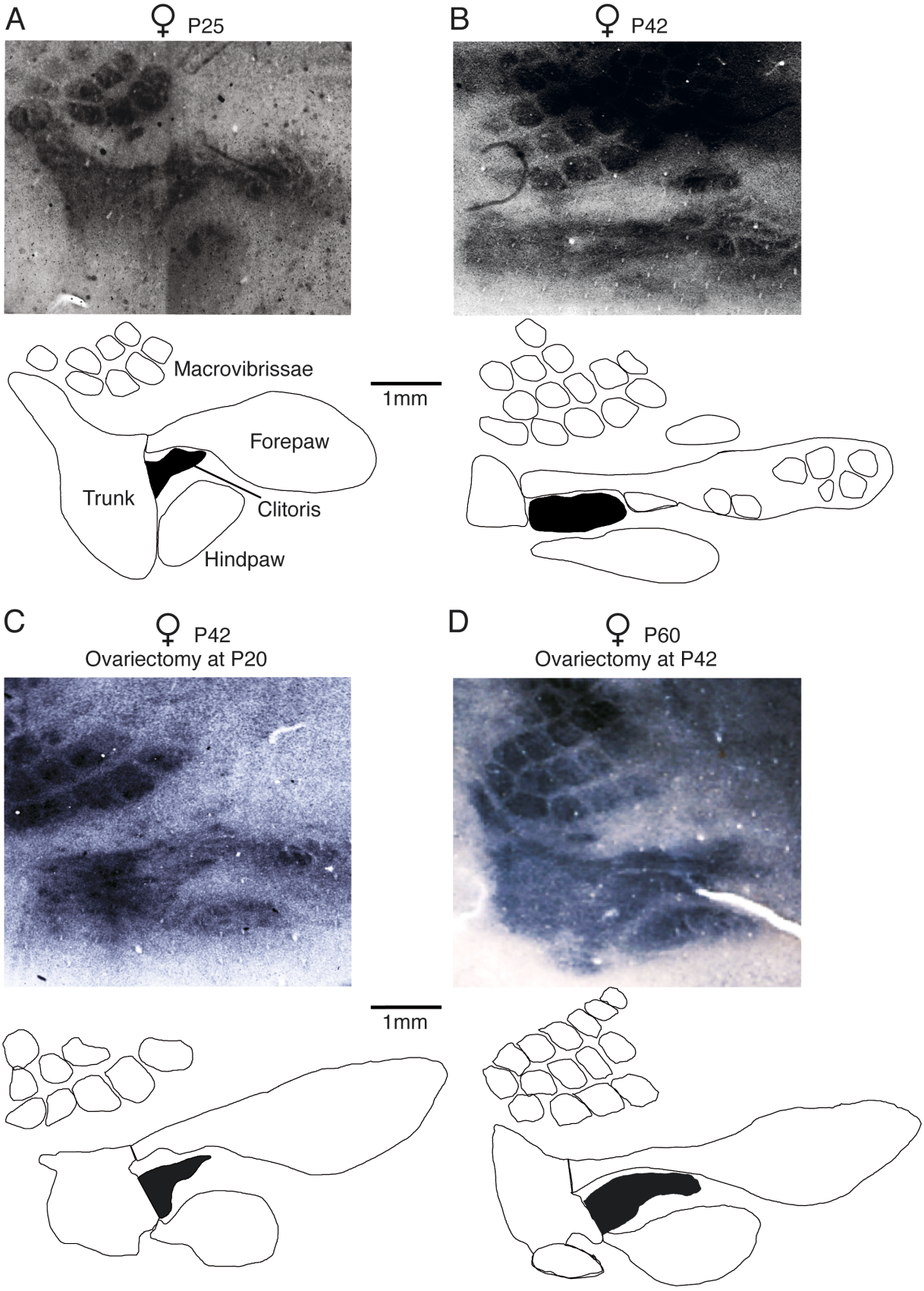
A
♀ P25
B
♀ P42
Macrovibrissae
Forepaw
Trunk
Clitoris
Hindpaw
1mm
C
♀ P42
Ovariectomy at P20
D
♀ P60
Ovariectomy at P42
1mm

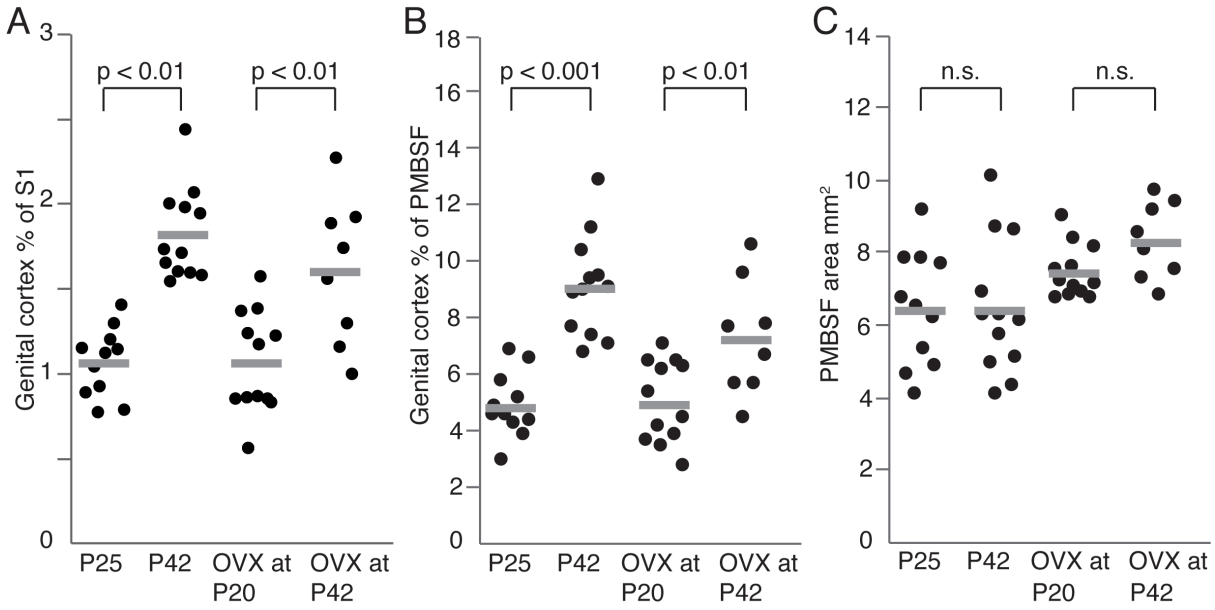
A
Genital cortex % of S1
p < 0.01
p < 0.01
P25
P42
OVX at P20
OVX at P42
B
Genital cortex % of PMBSF
p < 0.001
p < 0.01
C
PMBSF area mm²
n.s.
n.s.

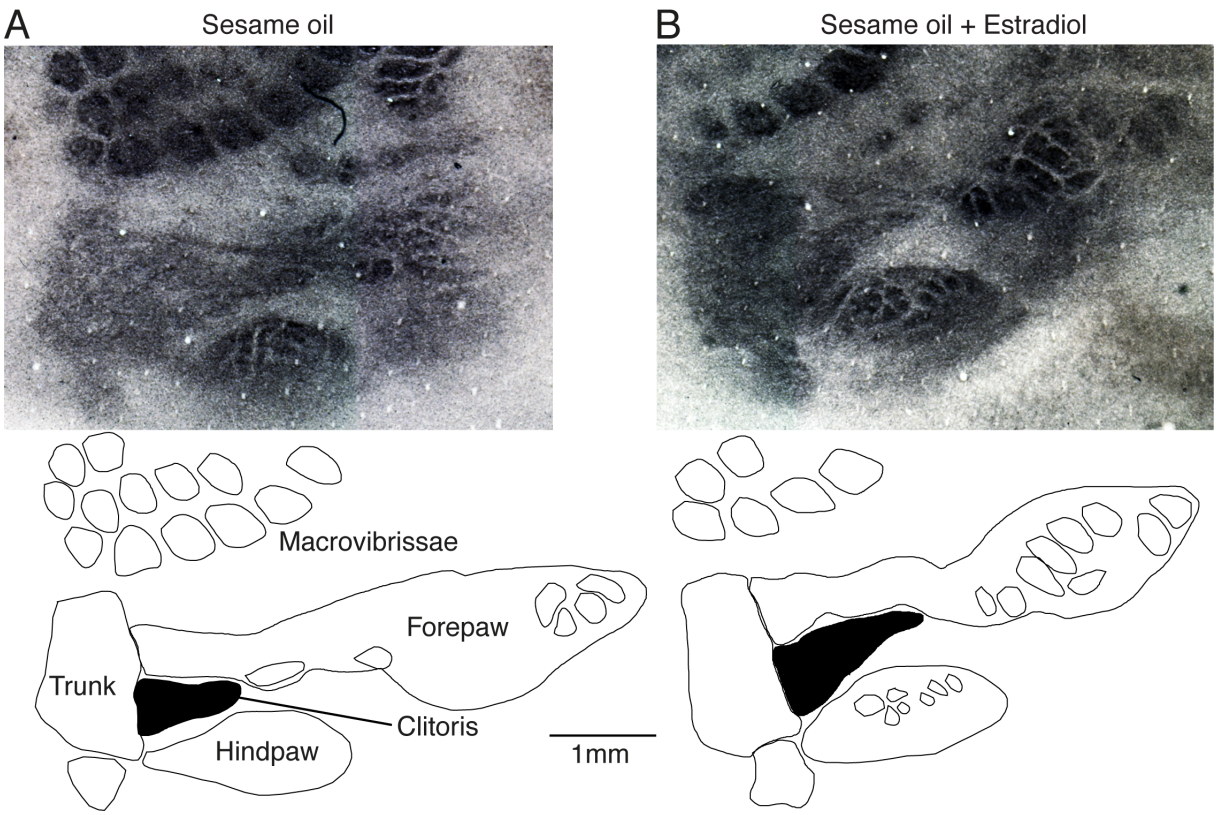
A
Sesame oil
B
Sesame oil + Estradiol
Macrovibrissae
Forepaw
Trunk
Clitoris
Hindpaw
1mm

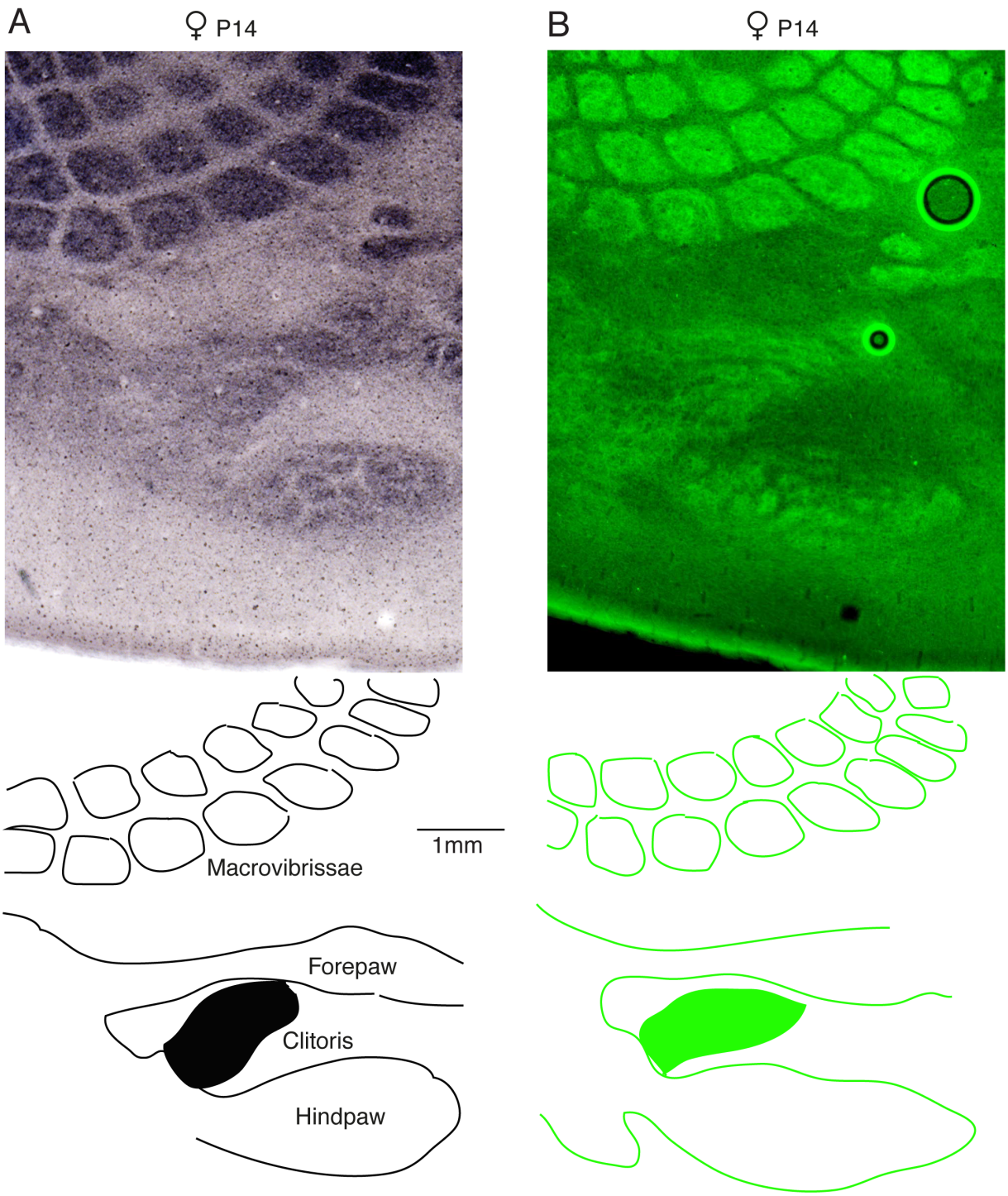
A
♀ P14
B
♀ P14
Macrovibrissae
1mm
Forepaw
Clitoris
Hindpaw

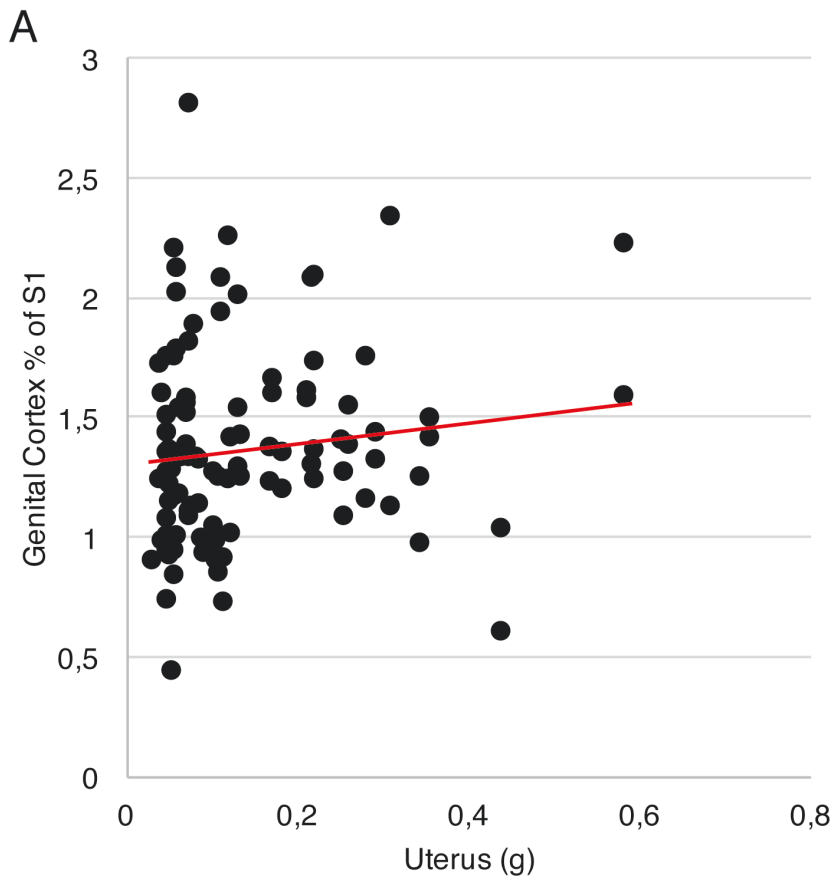
A
Genital Cortex % of S1
3
2,5
2
1,5
1
0,5
0
0
0,2
0,4
0,6
0,8
Uterus (g)

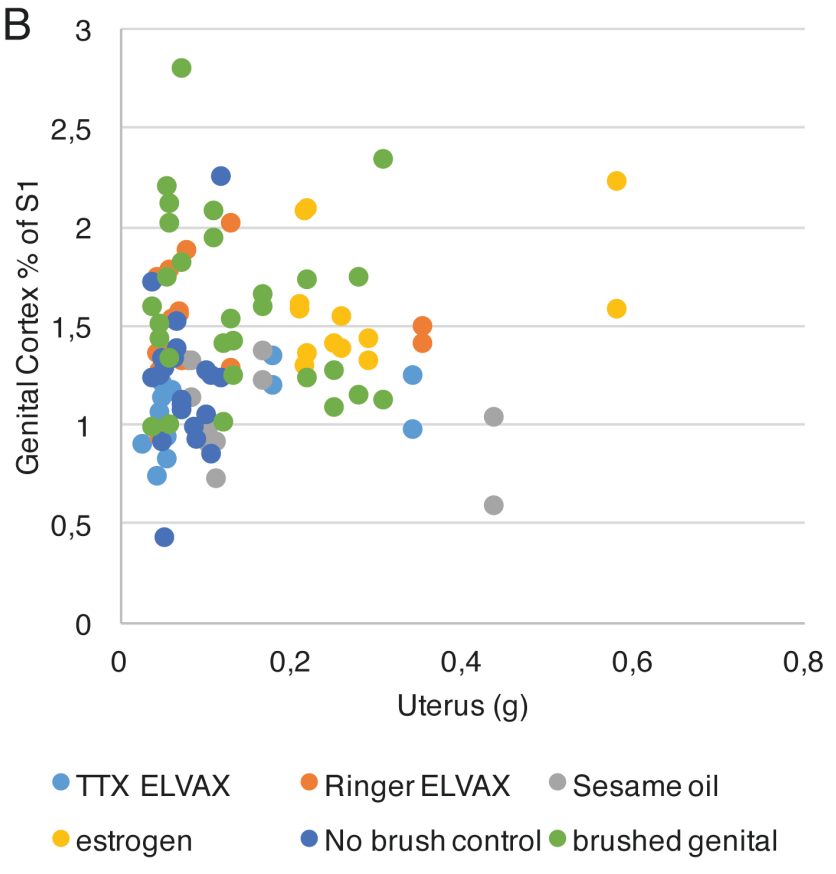
B
Genital Cortex % of S1
3
2,5
2
1,5
1
0,5
0
0
0,2
0,4
0,6
0,8
Uterus (g)
TTX ELVAX
Ringer ELVAX
Sesame oil
estrogen
No brush control
brushed genital

3 Peripheral innervation of the mouse penis

This work was published in revised form as:

Purkart, L., **Sigl-Glöckner, J**. & Brecht, M. (2020, Online ahead of print). Constant innervation despite pubertal growth of the mouse penis. *Journal of Comparative Neurology* https://doi.org/10.1002/cne.24892

This is the authors version of the manuscript.

3.1 Summary

The sexual characteristics of the vertebrate body change under the control of sex hormones. In mammals, genitals undergo major changes in puberty. While such bodily changes have been well documented, the associated changes in the nervous system are still poorly understood. To address this issue we studied the growth and innervation of the mouse penis throughout puberty. To this end, we measured length and thickness of the mouse penis in prepubertal (3 – 4 week old) and adult (8 – 10 week old) mice and performed fiber counts of the dorsal penile nerve. We obtained such counts with confocal imaging of proximal sections of the mouse penis after paraffin embedding and antibody staining against Protein-Gene-Product-9.5 or Neurofilament-H in combination with antigen retrieval procedures. We find that the mouse penis grows roughly 1.4 times in both thickness and length. Fiber counts in the dorsal penile nerve were not different in prepubertal (1620 ± 165 fibers per penis) and adult (1572 ± 383 fibers per penis) mice, however. Quantification of the area of mouse somatosensory penis cortex allowed us to compare cortical magnification of the penile nerve / genital cortex and the whisker / barrel cortex systems. This comparison suggested that 2 to 4 times less cortical area is devoted to a penile-nerve-fiber than to a whisker-nerve-fiber. The constant innervation of mouse penis through puberty suggests that pubertal changes in the cortical penis representation are not simply a reflection of peripheral change.

3.2 Introduction

During puberty, the external genitals undergo significant morphological and physiological changes which can easily be assessed by the external inspection of the body (Han & Lee, 2014; Tomova et al., 2010). Beyond physical maturation, the pubertal surge in sex hormones also controls the sexual differentiation of the brain (Juraska, Sisk, & DonCarlos, 2013; Schulz & Sisk, 2016). Therefore, the neuro-humoral mechanisms that control puberty have been intensely investigated (Terasawa & Kurian, 2012). Interestingly, it has been shown that puberty is not simply a rigid, age-dependent developmental program; instead puberty is in mammals heavily influenced by social cues (Bronson & Maruniak, 1975; Lenschow, Sigl-Glöckner, & Brecht, 2017; Levin & Johnston, 1986; Vandenbergh, 2012): the smell of male urine (Drickamer & Murphy, 1978; Mucignat-Caretta, Caretta, & Cavaggioni, 1995) or tactile cues such as genital touch (Lenschow et al., 2017) can powerfully advance the sexual maturation of rodents. Besides advancing the physical maturation, recent studies have shown that puberty also changes the central representation of the genitals in primary somatosensory cortex. After identifying the genital field in primary somatosensory using anatomical methods combined with microelectrode mapping (Lenschow et al., 2016), it was shown that this area undergoes a significant expansion during puberty, not only in rats but also in other mammals (Lenschow et al., 2016; Lauer et al., 2017; Lenschow et al., 2017).

This observation was highly unusual, because the topographic map in layer 4 of primary somatosensory cortex is conceived as particularly stable (Feldman & Brecht, 2005; Glazewski & Fox, 1996). It raises the question, what determines the size of different body parts within primary somatosensory cortex. Typically, the size of the cortical field is proportional to the density of nerve fibers innervating the peripheral surface. Accordinlgy, the more richtly innervated body parts occupy larger shares of cortical surface resulting in an afferent magnification of the body part. In rodents for example, the representation of the whisker pad occupies the majority of the primary somatosensory cortex (Lee & Woolsey, 1975; Welker & Van der Loos, 1986). Given this relationship and the pubertal expansion of genital cortex, we wondered whether there is a concurrent increase in the number of nerve fibers innervating the sex organs.

We decided to address this question in male mice, for which we have already analyzed pubertal changes in genital cortex (Lauer et al., 2017; Sigl-Glöckner et al. in press). In males, genital cortex receives input from the dorsal nerve of the penis (Calaresu, 1970), which is a branch of

the pudendal nerve and runs centrally along the dorsal surface of the penis, superior to the cavernous bodies. It contains mainly sensory fibers providing afferent sensory signals to the brain and some motor fibers for contracting muscles during erection. This somatic (sensory and motor) innervation is critical for sexual function (Chen et al., 2018; Larsson & Södersten, 1973; Weech & Ashurst, 2019). The autonomic innervation of the penis on the other hand is mainly provided by the cavernous nerves, which control neurovascular events during erection. However, staining with nitric oxide synthase has suggested that the dorsal penile nerve does also contain some autonomic fibers (Carrier et al., 1995), yet these seem to be mainly located at the penile helium (Colombel, Droupy, Paradis, Lassau, & Benoît, 1999). As a result, the dorsal penile nerve is considered as containing mostly sensory afferents that relay sensory input to the skin of the penis to the brain. Whether the density of these fibers changes during puberty is however still unknown.

In our current analysis we therefore investigate the mouse dorsal penile nerve and specifically asked the following questions: (i) What procedure should be applied to reveal and count individual nerve fibers in the mouse penis? (ii) How many nerve fibers are in the mouse dorsal penile nerve in prepubertal and adult animals? (iii) What is the relationship between fibers in the dorsal penile nerve and the cortical area representing the penis in the brain?

3.3 Results

3.3.1 Size measurements of prepubertal and adult mouse penises

First, we assessed the overall appearance of pre- and post-pubertal mouse penises. Prepubertal mice were three weeks of age, while adult mice were around eight weeks. Overall, prepubertal and adult penises were similar in appearance (Figure 2A). However, adult penises were both, thicker (mean diameter: 1.3 mm ± 0.1 mm (prepubertal) vs. 1.8 mm ± 0.2 mm (adult), X^2 = 10.89, p = 0.001, Figure 2B) and longer (mean length: 7.3 mm ± 0.7 mm (prepubertal) vs. 10.5 mm ± 0.9 mm (adult), X^2 = 11.29, p = 0.001, Figure 2C). Note that these measurements refer only to flaccid, dissected penises and we have no information about the effects of puberty on erected penises. We conclude that there is a major size increase of the mouse penis in puberty.

3.3.2 Identification of dorsal penile nerve in the mouse penis

To identify the course of the dorsal penile nerve along the proximo-distal extent of the mouse penis, we stained tissue sections with the pan-neuronal markers Protein Gene Product 9.5 (PGP 9.5, Figure 3). We took fluorescent micrographs along the proximo-distal axis of the penis (Figure 3A). Proximal to the body, the corpora cavernosa were the largest and surrounded the intercrural septum ventrally and laterally so that all nerve bundles were close to the midline (Figure 3B left). The urethra and the associated cavernous body were arranged at the ventral end of the section. A closer look at the intercrural septum shows the well-marked dorsal vein, one dorsal artery and several bundles of the dorsal nerve of the penis (Figure 3B, white arrows, right). More distal, some of the smaller dorsal penile nerve bundles spread laterally of the intercrural septum (Figure 3C, left) and the dorsal vein diameter was reduced (Figure 3C, right). Even more distal sections (Figure 3D, left) showed nerve bundles further lateral that approached the ventral side of the penis. Furthermore, additional single nerve fibers appeared within the corpora cavernosa, which in turn were considerably decreased in size. In the intercrural septum, there were few nerve bundles left, while some fibers appeared (Figure 3D, right). The very distal part of the penis appears almost devoid of nerve bundles. Instead, it is densely covered with single fibers (Figure 3E, right). The center is filled with the baculum, which is laterally surrounded by the diminishing corpora cavernosa (Figure 3E, left, Phillips, Wright, Gradie, Johnston, & Pask, 2015). The canal of the urethra is compressed and horizontally elongated. In these more distal regions (Figure 3A, D-E), the dorsal penile nerve branches out and mingles with other nerve fibers from the cavernous nerve and the perineal nerve. Here, single bundles belonging to the dorsal penile nerve can no longer be identified. Similar to the description of Chen et al. (2018), we find that proximal to the body, the dorsal nerve of the penis is compact

in the area of the intercrural septum (Figure 3A). We conclude that in the proximal penis, the dorsal nerve of the penis consisted of four to five main bundles on each side of the dorsal vein, which are easily and reliably identified and well suited for quantification.

3.3.3 Single nerve fiber counts

Using pan-neuronal antibody staining (PGP 9.5 or Neurofilament H), we were able to reveal single nerve fibers within each bundle, which we captured using confocal microscopy (Figure 4A, red dots). Single fibers were counted in z-stacks. Bundles located outside of the intercrural septum were not considered as part of the dorsal penile nerve and were therefore excluded. Hence, we identified the main bundles of the dorsal nerve of the penis (Figure 4B and C) in sections of prepubertal and adult penises. Usually, there were two to four large ones, containing more than 100 fibers and two to four small ones with 10 to 100 fibers. All bundles were located lateral to the dorsal vein, so a subdivision by side was easy to make (Figure 4B and C). The number of nerve fibers was similar between left and right side in both, prepubertal and adult penises. Figure 4D shows counts for all bundles on the left and right side, for both, prepubertal and adult penises, the fiber count between both sides was weakly but not significantly correlated ($r = 0.44$, $p = 0.089$ n.s.). Next, we compared the overall number of fibers in all bundles of the dorsal nerve of the penis in eight prepubertal and eight adult males. In order to avoid confounds owing to suboptimal staining, anatomical irregularities or damaged tissue, we counted in three sections within the proximal penis region identified in Figure 3A and derived the mean for each animal. Overall, different sections had similar numbers of fibers for the same mouse (data not shown). However, there was no difference in the number of nerve fibers within the dorsal penile nerve between prepubertal and adult mouse penises (Figure 4E, mean fiber number: 1620 ± 165 (prepubertal) vs. 1572 ± 383 (adult), $X^2 = 0.04$, $p = 0.916$). We conclude that the innervation of the mouse penis as measured by dorsal penile nerve fiber counts does not change during puberty.

3.3.4 Cortical magnification of penile and whisker nerve fibers

Sensory signals from the body surface reach the cortex in the cortical input layer 4, which contains a topographic map of the body surface with corresponding subfields for different body parts. To measure the size of subfields receiving sensory input from the penis, we used a transgenic mouse line, expressing the red fluorescent marker Td-tomato in Scnn1a-positive neurons. In somatosensory cortex Scnn1a expression is layer 4 specific and restricted to areas receiving strong lemniscal input; hence, within cortical layer 4 such expression nicely reveals

the somatosensory homunculus (Figure 5A). Using serial sections of flattened cortices, we reconstructed the full body map and focused our analysis of the genital cortex (orange) and the C2 barrel field (green, Figure 5B). Overall, genital cortex is larger than the C2 barrel (n = 7 adult mice, genital: 0.17 ± 0.02 mm^2 vs C2 barrel: 0.10 ± 0.02 mm^2, Figure 5C). Our estimates of the C2 barrel field were larger than those previously reported by Welker et al. (1986), shown in light green. We believe that this discrepancy stems from substantial differences in the histological procedures. Specifically, the flattening of the cortical sheet is likely result in an increase in the size of cortical areas. Next, we pooled the fiber counts for all 32 "hemi-penises" (half-penises) from 8 prepubertal and 8 adult mice and compared the results to the reported mean number of nerve fibers innervating the C2 barrel (Welker & Van der Loos, 1986). While a hemi-penis is innervated by 799 ± 167, the average C2 whisker follicle receives only 117 ± 5 nerve fibers. Finally, we calculated ratio between the cortical area (in the tangential / horizontal plane) and the number of innervating fibers for the penis and the C2 whisker. Welker et al. (1986) also estimated this ratio (shown in light green). However, for a fairer comparison to our current results from the genital cortex, we think one needs to consider the larger barrel and genital size in our flattened cortices. Hence, we also calculated this ratio using our own estimate of C2 barrel field size divided by the number of fibers counted by Welker et al. (1986), shown here in dark green. Overall, the cortical magnification of C2 whisker fiber is ~2-4 times larger than that of a dorsal penile nerve fiber.

3.4 Discussion

We found that the mouse penis grows substantially in puberty. We developed a methodology, which allows resolving and counting single nerve fibers in the mouse dorsal penile nerve. Our nerve fiber counts revealed a bilaterally symmetric innervation of the mouse penis, which does not change in puberty. Finally, we suggest that the somatosensory cortical area receiving peripheral inputs from a dorsal penile nerve fiber is smaller, compared to the cortical area receiving input from a whisker follicle nerve fiber.

Our methodology combined a variety of conventional techniques such as decalcification, antibody staining with the pan-neuronal markers PGP-9.5 or Neurofilament H, antigen retrieval and paraffin embedding. This approach allowed reliably identifying the proximo-distal course and architecture of the mouse dorsal penile nerve. We found dorsal penile nerve consists of several subbundles on each side of the intercrural septum. Our observations confirm the description of Chen et al. (2018), but contrast with the picture generally conveyed by text-books, where the dorsal nerve of the penis is invariably depicted as a single bundle running bilateral to the dorsal vein. Furthermore, the branching of the dorsal nerve of the penis appears similar in both, pre- and post-pubertal mice with no visible morphological differences. Our methodology also allowed the quantitative analysis of penile innervation in the mouse with single fiber resolution.

We found that the adult mouse penis is symmetrically innervated and that the mouse dorsal penile nerve contains about 1600 fibers per penis. Our data on fiber numbers in sub-bundles appear to be similar to those counted by other authors (Chen et al., 2018). This total fiber count is similar and slightly higher than counts of myelinated fibers in dorsal penis nerve obtained from adult rats, where 1423 myelinated fibers in total were counted (Calaresu, 1970). The larger number of fibers in the mouse penis than in the rat penis is surprising considering the ten times larger body weight of rats and the size of the rat penis, which is more than two times bigger than that of mice. The most obvious explanation for the larger number of fibers in our study on the mouse penis is that our antibody stains detected a large fraction of un-myelinated fibers, which were not detectable in the osmium stains performed by Calaresu et al. (Calaresu, 1970). The only other study we could find on dorsal penile nerve fiber counts comes from rhesus monkeys. In rhesus monkeys a higher nerve fiber count (3200-5600 myelinated fibers per penis) was reported (Herbert, 1973). This rhesus monkey number is clearly higher than the nerve fiber counts observed by us in the mouse. Still, also this difference (a factor of ~2.5) is remarkably

small if one considers the approximately ~100x larger body weight of rhesus monkeys compared to mice. Optic nerves fiber counts of mouse (~64000, Honjin et al., 1977) and rhesus monkey (~1600000; Sandell and Peters, 2001) differ by a factor of 25. These considerations suggest the possibility that the number of dorsal penile nerve fibers is relatively similar across species. This is a very preliminary conclusion, however, and we need more information about dorsal penile nerve fiber numbers. In particular, it would be worth determining dorsal penile nerve fiber counts in humans, who have a quite specialized sex life and no baculum (Diamond, 1998).

Our data also show that there is no difference in the number of nerve fibers within the dorsal penile nerve between prepubertal and adult male mice. While our data argue against major changes in penile innervation during puberty in mice, they do not totally rule out this possibility. Our analysis focused on the proximal penis, where the dorsal penile nerve is rather compact. Within the dorsal nerve of the penis, there are sympathetic, parasympathetic and sensory fibers, expressing the neuropeptides/transmitters tyrosine hydrolase (TH), neural nitric oxide synthase (nNOS) and calcitonin gene-related peptide (CGRP), respectively (Chen et al., 2018). Sympathetic and sensory fibers originate from the pudendal nerve, whereas parasympathetic fibers originate from the cavernous nerve (Colombel, Droupy, Paradis, Lassau, & Benoît, 1999; Rea, 2016; Yucel & Baskin, 2003). Puberty associated remodeling of genital innervation might be associated with certain subtypes of sensory fibers. It has been shown, that after nerve crushing, there is a decrease in parasympathetic fibers that are contributed by the cavernous nerve to the dorsal nerve of the penis. Therefore, peripheral nerve damage can lead to selective plasticity of fiber subtypes within the dorsal penile nerve. Given that the length of the prepuce changes during puberty, it is possible more distal nerve branches do exhibit puberty dependent plasticity. Such observations have also been made in female rodents, where the density and sensitivity of sensory axons is modulated by the estrous cycle and pregnancy (Adler, Davis, & Komisaruk, 1977; Liao & Smith, 2011; Zoubina, Fan, & Smith, 1998). The authors quantified the relative density of distributed, single axons in the vaginal wall. In contrast to them, we counted fibers in the region of the dorsal nerve of the penis, where it is well integrated. While this allowed us to count absolute numbers of nerve fibers, that certainly belonged to the dorsal nerve of the penis, hormone dependent plasticity may instead remodel more distal branches of dorsal never fibers or dendrites of sensory neurons in the spinal dorsal horn.

Recent studies revealed plasticity of genital somatosensory cortex. Due to the hormone dependent expansion of genital cortex during puberty (Lenschow et al., 2017), we asked if there is a similar change to be observed in the periphery. However, careful quantification of nerve fibers belonging to the proximal part of the dorsal nerve of the penis, using pan-neuronal staining, did not reveal a difference between prepubertal and adult mice. This is surprising, given that the primary somatosensory cortex is thought to represent the density of sensory fibers in the skin. Hence, the expansion of the genital region observed by Lenschow et al. (2017) might be independent of the density of nerve fibers in the genital.

We also performed an ad hoc assessment of cortical magnification of penis nerve fibers / penis cortex area and C2 whisker fibers / C2 barrel area (as quantified by Welker and Van der Loos, 1986) in the somatosensory cortex. The data suggest that there is less somatosensory cortex devoted to a dorsal penile nerve fiber than to a C2 whisker fiber. Multiple reasons might account for this difference. First of all, the dorsal penile nerve is a mixed nerve, which contains numerous descending fibers, whereas the C2 whisker fibers quantified by Welker and van der Loos (1986) were purely sensory. Thus, it may not be surprising that sensory fibers are more extensively represented in sensory cortex. In addition, it may be the case that C2 whisker fibers project more selectively to the somatosensory cortex, whereas penis fibers heavily project to subcortical centers controlling sexuality. To further investigate the relationship of periphery and cortex in the genital system, further experiments are needed, in which both, peripheral innervation and genital cortex size are quantified simultaneously.

In summary, our results suggest that there is no difference in fiber counts in the dorsal nerve of the penis between pre- and post-pubertal mice, despite a significant increase in the size of the penis.

3.5 Method

Animals. All experimental procedures were performed according to German guidelines on animal welfare under the supervision of local ethics committees. Prepubertal and adult C57BL/6JRj mice were purchased from Janvier Labs (St Berthevin Cedex, France) and perfused within one day upon arrival. Prepubertal mice were three weeks of age and adult mice were between six and ten weeks of age. We ensured, that in no prepubertal males balanopreputial separation had already occurred. For measuring the size of the primary somatosensory cortex, we purchased adult transgenic animals that express cre-recombinase in cortical layer 4 (Scnn1a-Tg3-Cre, #009613) and Ai9-reporter mice (#007909) mice from Jackson Labs and crossed those lines. The resulting offspring constitutionally expresses the fluorescent marker Td-tomato in excitatory neurons of cortical layer 4. Animals were killed under permits T0078/16 and T0215/18.

Penile tissue preparation. Mice were anaesthetized with isofluran and injected with an overdose of urethane (20%, 1ml/100g). Subsequently, animals were transcardially perfused with phosphate buffer, followed by a 4% paraformaldehyde (PFA) solution and genitals where removed, cleaned from connective tissue and stored in a 4% PFA solution for ~24h. Depending on the protocol, the solution was then changed to 30% sucrose for frozen sections or 70% ethanol for paraffin embedding. Frozen sections were cut at 40 µm on a Frigomobil (Leica) and kept free floating in 0.1 M phosphate buffer saline (PBS). For paraffin embedding, penises were cut into halves and put into a 20% ethylenediaminetetraacetic acid (EDTA) solution (EDTA-Entkalkungslösung ~20%, pH 7.4, Morphisto, Art. Nr. 13412) for ~7 days for decalcification. This step dissolves the baculum to avoid it damaging sections during slicing. Subsequently, the tissue was transferred to a Leica TP 1020 tissue processor, running an ascending alcohol series (Table 1). Next, penises were kept in a furnace at 60 °C for 24h and embedded in paraffin blocks using the Leica HistoCore Arcadia H. Blocks were cut into 16 µm sections, which were left to floated in a 45 °C preheated water-bath. The sections were then mounted on Thermo Scientific Superfrost Ultra Plus® slides, dried on a warming plate at 35 °C and stored overnight in a furnace at 42 °C. Before applying the immunohistochemistry protocol, sections were deparaffinized and rehydrated in a descending ethanol series (Table 2).

Brain tissue preparation. Some experiments were conducted in layer 4 transgenic reporter mice (Scnn1a x Ai9) to measure the size of the primary somatosensory cortex. Brains were removed, hemispheres were separated, subcortical brain areas removed and cortices were flattened between two glass slides separated by clay spacers. Glass slides were weighed down with small ceramic weights for 3h. Afterwards, flattened cortices were left free flouting in 4% PFA overnight. On the next day, slices were transferred in a 30% sucrose solution for cryoprotection. Afterwards, 40 µm sections were cut using a Frigomobil (Leica) and sections were mounted on gelatin coated glass slides.

Immunohistochemical staining. For immunohistochemical staining of penile tissue, we performed heat induced epitope retrieval (HIER) using a citrate buffer (Antigen Unmasking Solution, Citric Acid Based, pH6, 100x concentrated stock solution, Vector Laboratories Cat# H-3301, RRID:AB_2336227). A water-bath with a staining dish, containing the antigen retrieval solution, was preheated to 95-100 °C. Mounted sections were placed in the dish, heated for ~60 min and left to cool for 30 min at room temperature. For free floating sections, it was not necessary to perform HIER so that we could continue with immunohistochemistry. Antibody staining was performed according to standard procedures. In summary, penis sections were pre-incubated for an hour at room temperature in a blocking solution (0.1 M PBS, 2.5% Bovine Serum Albumin and 0.5% Triton X-100). Afterwards, primary antibodies were diluted

in a solution containing 0.5% Triton X-100 and 1% Bovine Serum Albumin. The primary antibodies against PGP 9.5 (Rabbit polyclonal, Agilent Cat# Z5116, RRID:AB_2622233, n = 4 brains) and Neurofilament H (Chicken polyclonal, Millipore Cat# AB5539, RRID:AB_11212161, n = 12 brains) were incubated for at least 48 h under gentle agitation at 4 °C. Incubation with the primary antibodies was followed by detection with secondary antibodies, coupled to the fluorophores Alexa 488 (Donkey anti rabbit: Thermo Fisher Scientific Cat# A-21206, RRID:AB_2535792; Goat anti chicken: Thermo Fisher Scientific Cat# A-11039, RRID:AB_2534096) or Alexa 546 (Donkey anti rabbit: Thermo Fisher Scientific Cat# A10040, RRID:AB_2534016). The secondary antibodies were diluted (1:1000) in 1% Bovine Serum Albumin in 0.1 M PBS and the reaction was allowed to proceed overnight in the dark at 4 °C. We mounted the free floating frozen sections on Superfrost glass slides and covered them with Fluoromount G® (Biozol, Eching, Germany) mounting medium. The same was done for the already mounted, paraffin embedded sections.

Microscopy. Z-stacks were taken on a Leica DM5500B epifluorescence microscope and on a Leica TCS SP5 confocal microscope. The z-planes were 0.1 µm and 1 µm apart, respectively. Stacks were analysed using ImageJ (RRID:SCR_003070).

Analysis and statistics. Localisation and analysis of nerve fiber counts is described in the following results section. Descriptive statistics were calculated in Excel and are expressed as mean ± standard deviation (STD). Data were tested for normality and compared using independent t-tests in MATLAB (Mathworks, RRID:SCR_001622).

Optimization of a staining / imaging protocol for a dorsal penile nerve fiber counts. Our initial attempts to count nerve fibers in the mouse dorsal penile nerve failed. In particular, we encountered the following problems: (i) the baculum (the penis bone) would disrupt sectioning and impose the need for decalcification procedures. (ii) Free floating tissue sections dissociated (Figure 1A, left), preventing the anatomical localization of the dorsal nerve of the penis. Specifically, the intercrural septum (IS), which contains blood vessels (dorsal vein (DV), dorsal arteries (DA)) and the bundles of the dorsal nerve of the penis completely detached from connective tissue. Therefore, we turned to paraffin embedding (Figure 1A, right), which maintained all anatomical structures very well. (iii) During the embedding process antigens are chemically modified and masked. As a result, they can no longer be detected by antibodies and the signal to noise ratio staining was insufficient for nerve fiber counts (Figure 1B, left). Therefore, we had to perform antigen retrieval procedures, i.e. we treated sections, mounted on highly adhesive slides, at 95 C° in citrate buffer. Subsequent antibody staining nicely revealed single fibers within bundles of the DNP (Figure 1B, right). (iv) Furthermore, we had to adjust the antibody concentration for optimal staining. An antibody dilution of 1:1000 resulted in high background staining (Figure 1C, left). Hence, we employed antibody dilution of 1:500, which greatly improved the contrast (Figure 1C, right). (v) Finally, confocal microscopy (Figure 1D, left) was superior to standard epifluorescence microscopy (Figure 1D, right) in resolving single nerve fibers.

Measurement of cortical areas. To quantify the relationship between nerve fibers in the DNP and the cortical area representing the penis in primary somatosensory cortex, we analyzed the brains of transgenic mice, which expressed Td-tomato in the cortical input layer 4 (the Scnn1a mouse line). The expression in this mouse line is limited to areas recieving strong lemniscal input, and therefore nicely reveals the somatosensory homunculus. We then identified the subfield representing the genitals by superimposing the Scnn1a / Td-tomato layer 4 map with functional signals from in vivo Ca-imaging or intrinsic imaging of sensory responses to genital

stimulation (Sigl-Glöckner et al. in preparation). We also identified C2 whisker barrel based on the known topography of the barrel field.

Acknowledgments
We thank Ann Clemens, Jean Simmonet, Constanze Lenschow and Andreea Neukirchner for comments on the manuscript and Undine Schneeweiß and Tanja Wölk for outstanding technical assistance. We also thank Casten Lüter and Jutta Zeller from Naturkundemuseum, Berlin for assistance in tissue preparation.

Conflict of Interest
All authors declare they have no conflict of interest.

Role of authors
All authors had full access to all the data in the study and take responsibility for the integrity of the data and the accuracy of the data analysis. Study concept and design: LP, JSG, MB. Acquisition of data: LP. Analysis and interpretation of data: LP, JSG, MB. Drafting of the manuscript: LP, JSG, MB Statistical analysis: LP, JSG. Obtained funding: MB. Administrative, technical, and material support: MB. Study supervision: MB.

Data availability statement
The data in the manuscript will be made available upon request to the corresponding author.

3.6 References

Adler, N. T., Davis, P. G., & Komisaruk, B. R. (1977). Variation in the size and sensitivity of a genital sensory field in relation to the estrous cycle in rats. *Hormones and Behavior*, *9*(3), 334–344. https://doi.org/10.1016/0018-506X(77)90068-X

Bronson, F. H., & Maruniak, J. A. (1975). Male-induced puberty in female mice: Evidence for a synergistic action of social cues. *Biology of Reproduction*, *13*(1), 94–98. https://doi.org/10.1095/biolreprod13.1.94

Calaresu, F. R. (1970). Experimental studies on the dorsal nerve of the penis of the rat. *American Journal of Anatomy*, *127*(4), 415–421. https://doi.org/10.1002/aja.1001270406

Carrier, S., Zvara, P., Nunes, L., Kour, N. W., Rehman, J., & Lue, T. F. (1995). Regeneration of Nitric Oxide Synthase-Containing Nerves After Cavernous Nerve Neurotomy in the Rat. *The Journal of Urology*, *153*(5), 1722–1727. https://doi.org/10.1016/S0022-5347(01)67512-8

Chen, Y. L., Chao, T. T., Wu, Y. N., Chen, M. C., Lin, Y. H., Liao, C. H., … Chiang, H. S. (2018). NNOS-positive minor-branches of the dorsal penile nerves is associated with erectile function in the bilateral cavernous injury model of rats. *Scientific Reports*, *8*(1). https://doi.org/10.1038/s41598-017-18988-2

Colombel, M., Droupy, S., Paradis, V., Lassau, J. P., & Benoît, G. (1999). Caverno-pudendal nervous communicating branches in the penile hilum. *Surgical and Radiologic Anatomy*, *21*(4), 273–276. https://doi.org/10.1007/s00276-999-0273-9

Diamond, J. (1998). *Why is sex fun?: the evolution of human sexuality*. Basic Books.

Drickamer, L. C., & Murphy, R. X. (1978). Female mouse maturation: Effects of excreted and bladder urine from juvenile and adult males. *Developmental Psychobiology*, *11*(1), 63–72. https://doi.org/10.1002/dev.420110110

Feldman, D. E., & Brecht, M. Map plasticity in somatosensory cortex, 310 Science § (2005). American Association for the Advancement of Science. https://doi.org/10.1126/science.1115807

Glazewski, S., & Fox, K. (1996). Time course of experience-dependent synaptic potentiation and depression in barrel cortex of adolescent rats. *Journal of Neurophysiology*, *75*(4), 1714–1729. https://doi.org/10.1152/jn.1996.75.4.1714

Han, S. H., & Lee, S.-H. (2014). Differential Growth of the Reproductive Organs during the Peripubertal Period in Male Rats. *Development & Reproduciton*, *17*(4), 469–475. https://doi.org/10.12717/dr.2013.17.4.469

Herbert, J. (1973). The role of the dorsal nerves of the penis in the sexual behaviour of the male rhesus monkey. *Physiology and Behavior*, *10*(2), 293–300. https://doi.org/10.1016/0031-9384(73)90313-2

Honjin, R., Sakato, S., & Yamashita, T. (1977). Electron microscopy of the mouse optic nerve: a quantitative study of the total optic nerve fibers. *Archivum Histologicum Japonicum = Nihon Soshikigaku Kiroku*.

Juraska, J. M., Sisk, C. L., & DonCarlos, L. L. (2013). Sexual differentiation of the adolescent rodent brain: Hormonal influences and developmental mechanisms. *Hormones and Behavior*, *64*(2), 203–210. https://doi.org/10.1016/j.yhbeh.2013.05.010

Larsson, K., & Södersten, P. (1973). Mating in male rats after section of the dorsal penile nerve. *Physiology & Behavior*, *10*(3), 567–571. https://doi.org/10.1016/0031-9384(73)90223-0

Lauer, S. M., Lenschow, C., & Brecht, M. (2017). Sexually selected size differences and conserved sexual monomorphism of genital cortex. *Journal of Comparative Neurology*, *525*(12), 2706–2718. https://doi.org/10.1002/cne.24237

Lee, K. J., & Woolsey, T. A. (1975). A proportional relationship between peripheral innervation density and cortical neuron number in the somatosensory system of the mouse. *Brain Research*, *99*(2), 349–353. https://doi.org/10.1016/0006-8993(75)90035-9

Lenschow, C., Copley, S., Gardiner, J. M., Talbot, Z. N., Vitenzon, A., & Brecht, M. (2016). Sexually Monomorphic Maps and Dimorphic Responses in Rat Genital Cortex. *Current Biology*. https://doi.org/10.1016/j.cub.2015.11.041

Lenschow, C., Sigl-Glöckner, J., & Brecht, M. (2017). Development of rat female genital cortex and control of female puberty by sexual touch. *PLoS Biology*, *15*(9), 1–22. https://doi.org/10.1371/journal.pbio.2001283

Levin, R. N., & Johnston, R. E. (1986). Social mediation of puberty: an adaptive female strategy? *Behavioral and Neural Biology*, *46*(3), 308–324.

Liao, Z., & Smith, P. G. (2011). Adaptive plasticity of vaginal innervation in term pregnant rats. *Reproductive Sciences*, *18*(12), 1237–1245. https://doi.org/10.1177/1933719111410706

Mucignat-Caretta, C., Caretta, A., & Cavaggioni, A. (1995). Acceleration of puberty onset in female mice by male urinary proteins. *The Journal of Physiology*, *486*(2), 517–522. https://doi.org/10.1113/jphysiol.1995.sp020830

Phillips, T. R., Wright, D. K., Gradie, P. E., Johnston, L. A., & Pask, A. J. (2015). A Comprehensive Atlas of the Adult Mouse Penis. *Sexual Development*, *9*(3), 162–172. https://doi.org/10.1159/000431010

Rea, P. (2016). *Essential Clinically Applied Anatomy of the Peripheral Nervous System in the Head and Neck*. *Essential Clinically Applied Anatomy of the Peripheral Nervous System in the Head and Neck*. https://doi.org/10.1016/C2014-0-05021-6

Sandell, J. H., & Peters, A. (2001). Effects of age on nerve fibers in the rhesus monkey optic nerve. *Journal of Comparative Neurology*. https://doi.org/10.1002/1096-9861(20010122)429:4<541::AID-CNE3>3.0.CO;2-5

Schulz, K. M., & Sisk, C. L. (2016). The organizing actions of adolescent gonadal steroid hormones on brain and behavioral development. *Neuroscience and Biobehavioral Reviews*, *70*, 148–158. https://doi.org/10.1016/j.neubiorev.2016.07.036

Terasawa, E., & Kurian, J. R. (2012). Neuroendocrine mechanism of puberty. In *Handbook of Neuroendocrinology* (pp. 433–484). Academic Press. https://doi.org/10.1016/B978-0-12-375097-6.10019-8

Tomova, A., Deepinder, F., Robeva, R., Lalabonova, H., Kumanov, P., & Agarwal, A. (2010). Growth and development of male external genitalia: A cross-sectional study of 6200 males aged 0 to 19 years. *Archives of Pediatrics and Adolescent Medicine*, *164*(12), 1152–1157. https://doi.org/10.1001/archpediatrics.2010.223

Vandenbergh, J. G. (2012). Pheromonal Regulation of Puberty. In *Pheromones and Reproduction in Mammals*. https://doi.org/10.1016/b978-0-12-710780-6.50010-8

Weech, D., & Ashurst, J. V. (2019). *Anatomy, Abdomen and Pelvis, Penis Dorsal Nerve*. *StatPearls*. StatPearls Publishing. Retrieved from http://www.ncbi.nlm.nih.gov/pubmed/30247841

Welker, E., & Van der Loos, H. (1986). Quantitative correlation between barrel-field size and the sensory innervation of the whiskerpad: a comparative study in six strains of mice bred for different patterns of mystacial vibrissae. *The Journal of Neuroscience : The Official Journal of the Society for Neuroscience*, *6*(11), 3355–3373. https://doi.org/10.1523/JNEUROSCI.06-11-03355.1986

Yucel, S., & Baskin, L. S. (2003). Identification of communicating branches among the dorsal, perineal and cavernous nerves of the penis. *Journal of Urology*, *170*(1), 153–158. https://doi.org/10.1097/01.ju.0000072061.84121.7d

Zoubina, E. V., Fan, Q., & Smith, P. G. (1998). Variations in uterine innervation during the estrous cycle in rat. *Journal of Comparative Neurology*, *397*(4), 561–571. https://doi.org/10.1002/(SICI)1096-9861(19980810)397:4<561::AID-CNE8>3.0.CO;2-#

3.7 Figures

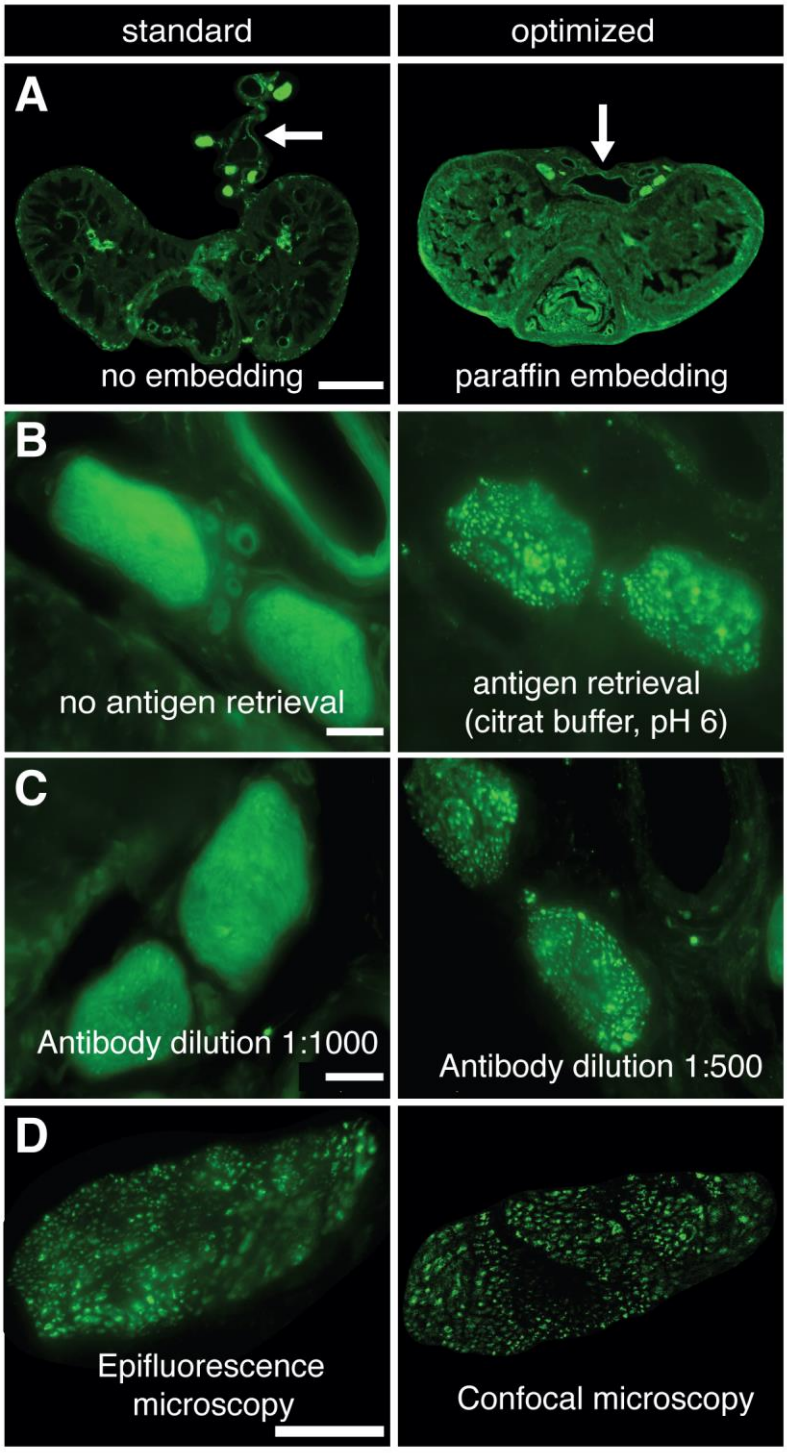

Figure 1. Protocol development for dorsal penile nerve fiber counts based on Protein Gene Product (PGP) 9.5 antibody staining of the mouse penis

A) Left, proximal cross section of an adult mouse penis, which was not embedded. Anatomical structures are poorly preserved. The intercrural septum (arrows) is almost completely detached from the corpora cavernosa (CC). Urethra and the surrounding cavernous bodies are dislocated. Right, section cut after paraffin embedding. Structures are well preserved and in their correct anatomical position. Scale bar = 400 µm.

B) Left, nerve bundles of the dorsal nerve of the penis stained without antigen retrieval. Detailed structures within the bundles are not discernable. Scale bar = 30 µm. Right, same as left panel, but following antigen retrieval using citrate buffer. Note the clearly visible single fibers within the bundles.

C) Same as (B), but using different antibody dilutions. Left, dilution of 1:1000 was not sufficient to stain single fibers within bundles of the dorsal nerve of the penis. Right, dilution of 1:500 reveals single fibers. Scale bar = 30 µm.

D) Left, An epifluorescence micrograph of a single dorsal nerve of the penis bundle. Due to high background fluorescence the image appears blurry. Scale bar = 40 µm. Right, same as left, but the micrograph was acquired using a confocal microscope.

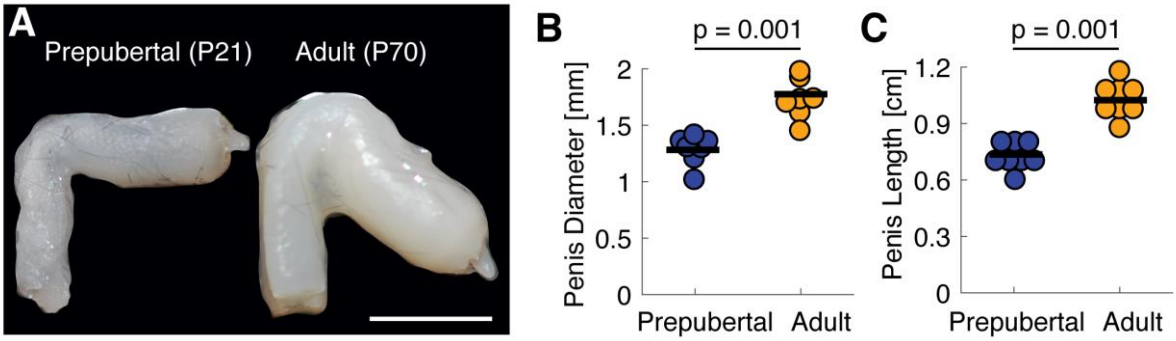

Figure 2. Pubertal growth of the mouse penis

A) Dissected penises of a prepubertal (P21, left) and an adult mouse (P70, right). The penises were dissected directly after perfusion and detached from connective tissue. Scale bar = 2 mm.

B) The mean diameter (black) of adult penises (orange, n = 8) was larger than that of prepubertal penises (blue, n = 8).

C) The mean length (black) of adult penises (orange, n = 8) was also longer than that of prepubertal penises (blue, n = 8).

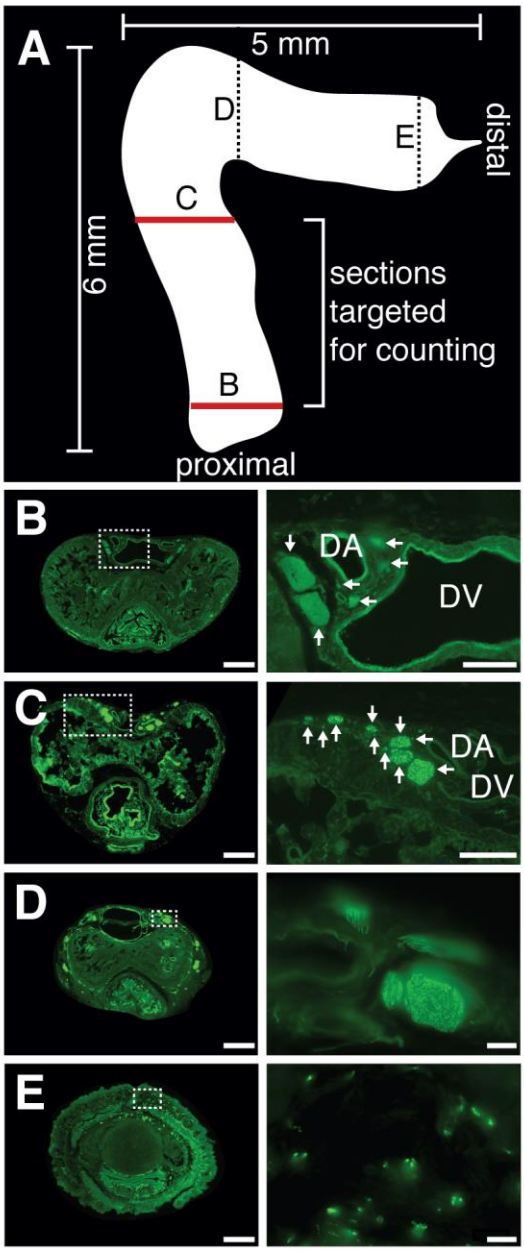

Figure 3. Localization of the dorsal penile nerve along the proximal-distal axis of the mouse penis

A) Schematic drawing of the mouse penis. Dashed and red lines indicate the approximate positions of the cross-sections shown in B to E.

B) Left, proximal penis cross-section. The corpora cavernosa are slightly bent dorsally and surround the intercrural septum laterally. Right, inset of intercrural septum with dorsal vein, dorsal arteries and bundles of the dorsal nerve of the penis (arrows). Bundles are always located left and right of the dorsal vein.

C) Note that the intercrural septum is more flattened than in (B) and laterally elongated. Right panel: dorsal vein and dorsal arteries are constricted and dorsal nerve of the penis branches out.

D) Left, corpora cavernosa are decreased in size and nerve bundles are migrating laterally. Right, only few bundles are left in the area of the intercrural septum.

E) Distal section. Left, baculum covering the center with lateral leftovers of the corpora cavernosa. Urethra is flattened. Right, no bundles of the dorsal nerve of the penis are left. Single fibers of various nerves are visible. Scale bars = 300 µm (left column), 150 µm (B), 150 µm (C), 25 µm (D), 25 µm (E)

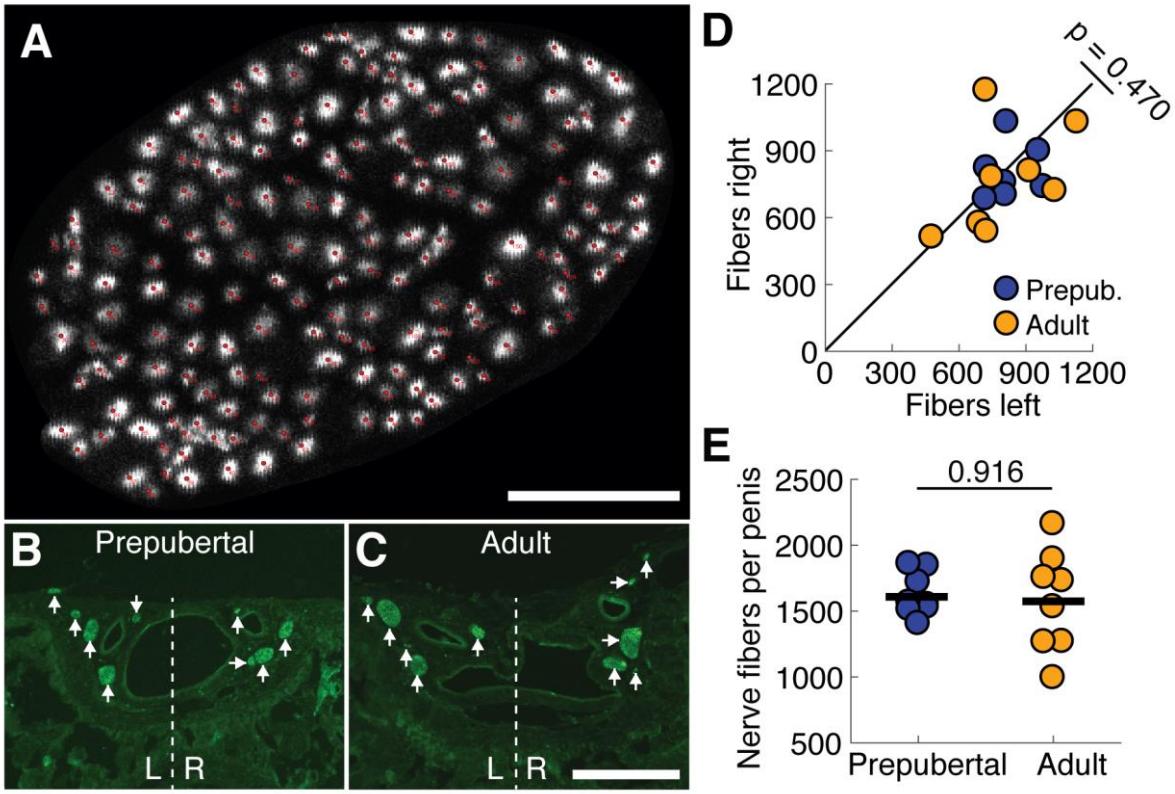

Figure 4. Nerve fiber counts are bilaterally symmetric and the same in prepubertal and adult mouse dorsal penile nerve sections

A) Confocal micrograph of dorsal nerve of the penis bundle of male aged P56. Red dots mark single fibers, that were counted. Scale bar = 15 µm.

B) Cross-section of an adult penis. The intercrural septum is subdivided in left and right, bundles of the DNP (arrows) are clearly visible on each side. Scale bar = 300 µm.

C) Same as (B), but for a prepubertal penis (from a P21 animal).

D) The fiber distribution on the left and right side of the mouse penis. There is no significant difference ($p = 0.470$). There is a correlation between the fiber count of both sides ($r = 0.44$) with no significant difference ($p = 0.089$).

E) There is no significant ($p = 0.916$) difference between the mean number of fibers within bundles of the dorsal nerve of the penis between prepubertal (blue) and adult (orange) animals ($n = 8$ each).

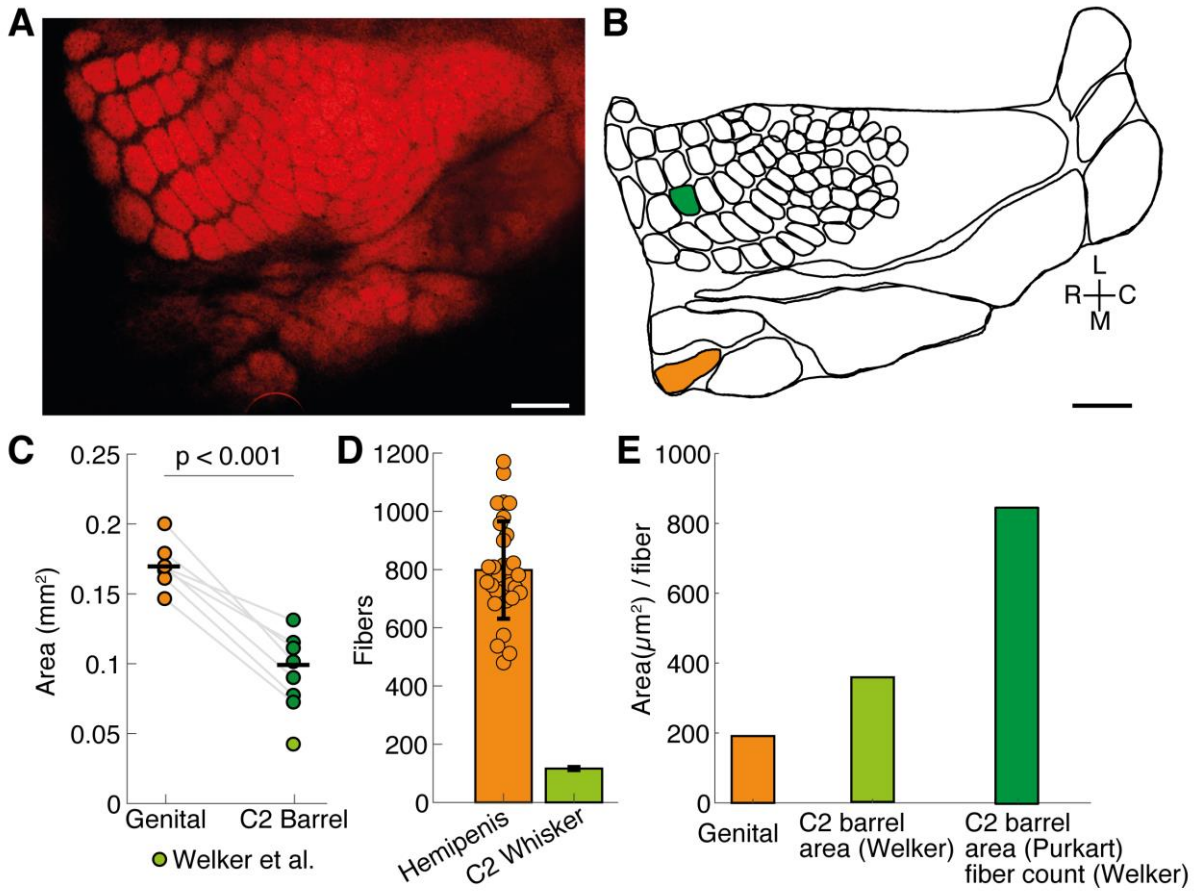

Figure 5. Cortical magnification of whisker and penile fibers

A) Flattened tangential section of a Scnn1a-Tg3-Cre x Ai9 mouse somatosensory cortex. Scnn1a+ expression reveals the homunculus within L4 of primary somatosensory cortex. Scale bar = 500 µm

B) Drawing through several serial tangential sections showing the complete homunculus in the primary somatosensory cortex of the mouse. Cortical areas receiving peripheral inputs form the C2 whisker (green) and from the genital (orange) are highlighted. Scale bar = 500 µm

C) Cortical area devoted to the genital representation (orange, left, 0.17 ± 0.02 mm^2) is larger than the C2 barrel (right, green, 0.10 ± 0.02 mm^2) in mouse primary somatosensory cortex ($n = 7$, $p < 0.001$). Black bars indicate the mean. As a reference the mean area of the C2 barrel from an unflattened mouse cortex as reported by Welker et al., 1986 is shown in light green.

D) The number of fibers counted in the dorsal nerve of 32 hemi-penises (left, orange, 799 ± 167 fibers) and the mean number of fibers innervating the C2 whisker follicle (117 ± 5 fibers), data are replotted from Welker et al., 1986.

E) Cortical area (μm^2) per nerve fiber for the genital (orange) and the C2 barrel (green). Light green: C2 barrel area estimate and C2 whisker fiber count by Welker et al., 1986. Dark green: C2 barrel area estimated by Purkart et al. divided by C2 whisker fiber count reported by Welker et al., 1986.

3.8 Tables

Table 1. Dehydration program Leica TP 1020 for penile tissue sections. Y = yes, N = no.

Step	Reagent	Vacuum	Duration
1	80% ethanol	N	1h
2	90% ethanol	Y	2h
3	96% ethanol	Y	1h
4	96% ethanol	Y	1h
5	96% ethanol	Y	1h
6	100% ethanol	Y	2h
7	100% ethanol	Y	2h
8	100% ethanol	Y	2h
9	Neo-Clear (xylene substitute)	Y	2h
10	Neo-Clear (xylene substitute)	Y	2h
11	paraffin	Y	3h
12	paraffin	Y	5h

Table 2. Deparaffinization und rehydration protocol for penile tissue sections.

Step	Reagent	Duration
1	Xylene	5 min
2	Xylene	5 min
3	100% ethanol	3 min
4	100% ethanol	3 min
5	96% ethanol	1 min
6	80% ethanol	1 min
7	60% ethanol	1 min
8	running cold tap water	3-5 min

4 Chronic imaging of genital cortex

This work was published as:

Sigl-Glöckner J., Meier E., Takahashi N., Sachdev, R. Larkum M. & Brecht M. (2019). Effects of sexual experience and puberty on mouse genital cortex revealed by chronic imaging. *Current Biology* 29(21): 3588-3599.e4.
https://doi.org/10.1016/j.cub.2019.08.062

This is the authors version of the manuscript.

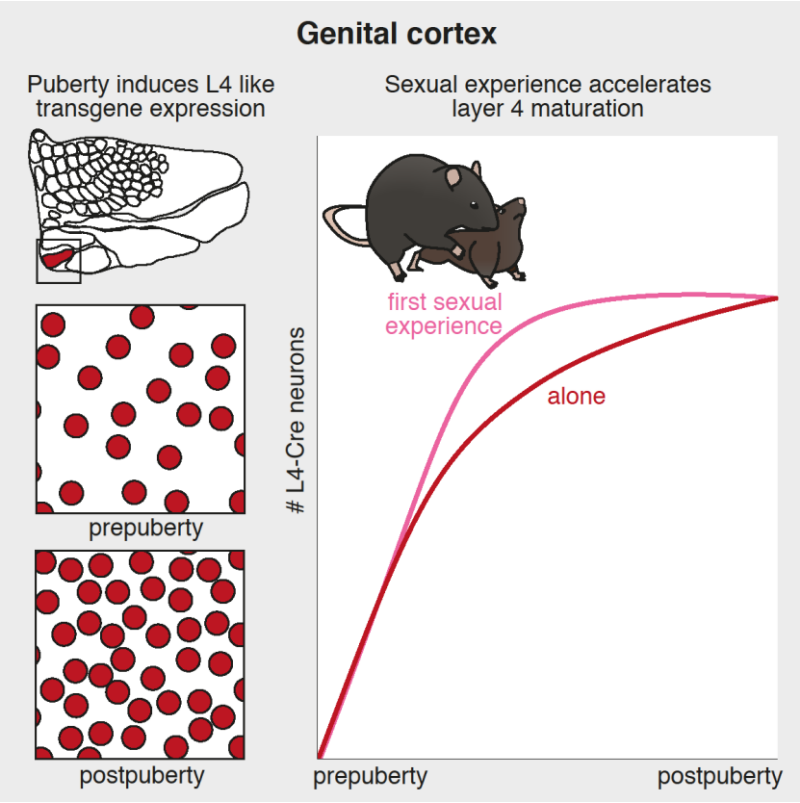

Figure 4. Graphical abstract illustrating the main findings of Chapter 4.

4.1 Summary

The topographic map in layer 4 of somatosensory cortex is usually specified early postnatally and stable thereafter. Genital cortex, however, undergoes a sex-hormone and sexual-touch-dependent pubertal expansion. Here we image pubertal development of genital cortex in Scnn1a-Tg3-Cre mice, where transgene expression has been shown to be restricted to layer 4 neurons with primary sensory cortex identity. Interestingly, during puberty, the number of Scnn1a+ neurons roughly doubled within genital cortex. The increase of Scnn1a+ neurons was gradual and rapidly advanced by initial sexual experience. Neurons that gained Scnn1a expression comprised stellate and pyramidal neurons in layer 4. Unlike during neonatal development, pyramids did not retract their apical dendrites during puberty. Calcium imaging revealed stronger genital-touch responses in Scnn1a+ neurons in males vs. females and a developmental increase in responsiveness in females. The first sexual interaction is a unique physical experience that often creates long lasting memories. We suggest such experience uniquely alters somatosensory body maps.

4.2 Introduction

For many years it has been recognized, that the precise topographic representation of the body surface by the cortical input layer 4 is determined by peripheral inputs [1]. Based on findings from the barrel cortex, a consensus emerged that this topographic map of the body is established within the first postnatal week [2,3] and shows little plasticity later in life [4]. However, there appears to be one exception to this rule of early and experience-independent map specification in layer 4 of somatosensory cortex: The region of rat somatosensory cortex that responds to genital stimulation, genital cortex, undergoes an unusually late expansion during puberty [5–7]. Furthermore, much like the onset of puberty [8], this expansion was dependent on sexual maturation and could be advanced by cohousing prepubertal female rats with adult males [6]. This plasticity of genital cortex is remarkable in several respects: (i) it occurs at a late postnatal stage. (ii) The extent of remodeling is large. (iii) It can be induced by physiological stimuli, whereas macroscopically detectable cortical plasticity usually requires drastic interference with incoming sensory signals, such as amputation or nerve transection [9]. (iv) It can be detected anatomically, unlike other somatosensory plasticity phenomena which can only be revealed physiologically [4]. The expansion has been quantified by measuring the area receiving thalamic afferents within this somatosensory field [6].

The observation that during puberty, thalamic fibers invade surrounding dysgranular regions of layer 4 [6] is particularly interesting because of the intricate relationship between thalamocortical axons and postsynaptic cortical neurons. In 1782 Francesco Gennari described the thick band of highly myelinated thalamic axons terminating in layer 4 [10]. After discovering fundamental differences in the physiology of primary and secondary (or higher order) cortical areas [11] their neurogenetic underpinnings have become evident more recently. Within somatosensory cortex, areal specification depends on various molecular cues and input from the ventral posteromedial nucleus of the thalamus [12–14]. Postsynaptically, thalamocortical axons target excitatory pyramidal and spiny stellate cells, the latter being a hallmark of primary somatosensory cortex [15–17]. Within layer 4, all excitatory neurons appear pyramidal-like at birth [18]. By postnatal day 5, however, the majority of neurons has a spiny stellate shape, suggesting that pyramidal neurons retract their apical dendrite to become stellates within the first postnatal week [18,19]. Without thalamocortical input, stellate cells fail to develop appropriately [12,14,20].

We have previously shown that rat genital cortex grows during puberty, which we revealed by visualizing antibody-stained thalamocortical afferents within layer 4 [6]. Therefore, we wonder, whether there are concurrent, cell type specific changes within layer 4. To address this question, we now turn to mice, where we can combine chronic two-photon imaging with the genetically targeted expression of fluorescent indicators. Specifically, we use the layer 4 specific transgenic mouse line Scnn1a-Tg3-Cre mice, where cre-recombinase expression resembles the homunculus in primary somatosensory cortex while septa are lacking Scnn1a+ neurons [21,22]. Moreover, Scnn1a+ neurons exhibit the transcriptional profile of primary somatosensory layer 4 neurons [19]. Scnn1a+ neurons express the RAR-related orphan receptor beta (RORβ), a layer 4 marker [12,23], whose ectopic expression is necessary and sufficient to orchestrate the acquisition of morphological, physiological and circuit properties of primary layer 4 neurons [19]. Using this mouse line, we investigate the following questions: First, does Scnn1a expression, which resembles the mouse homunculus, change in genital cortex during puberty? If so, what are the dynamics of this process? Second, do excitatory neurons in genital cortex remodel during puberty? Third, does puberty modulate the activity of genital cortex neurons? And finally, are there experience-dependent effects on pubertal maturation of layer 4 in genital cortex? More specifically, we want to find out whether initial sexual experience, usually conceptualized as particularly dramatic and memorable, modulates genital cortex maturation [24,25].

4.3 Results

4.3.1 Functional identification of genital cortex in Scnn1a-tdTomato mice

To investigate the cellular development of layer 4 (L4) in genital cortex, we used L4 specific Scnn1a-Tg3-cre mice [21], which we crossed with an Ai9 reporter line to label all cre-expressing neurons with td-Tomato. Tangential histological slices through cortical L4 of such Scnn1a-tdTomato brains reveal transgene expression limited to primary sensory cortices (Figure 1A, female, postnatal day (P) 40), with the homunculus being clearly visible within primary somatosensory cortex (S1). Coronal sections (Figure 1B) showed that Scnn1a expression is restricted to L4, where it is high in whisker (S1w) and paw (S1p) barrels and low in the dysgranular zone (DZ), secondary somatosensory cortex (S2) and absent from motor cortex (M1) [26]. Furthermore, Scnn1a+ neurons are confined to barrels, while septa do not contain Scnn1a+ neurons (Figure 1C). We conclude, that Scnn1a+ is a marker for primary sensory L4 neurons located in zones of dense lemniscal innervation [19,22].

The S1 homunculus is clearly visible in a magnified tangential section (Figure 1D, male, P25). Based on our mappings in rats [5], we suspected genital cortex within the dashed square in Figure 1D. Two-photon imaging of this area in Scnn1a-tdTomato mice also showed S1 subfields delineated by septa (Figure 1E). Next, we used intrinsic signal imaging to locate the genital, hindpaw, forepaw, tail, ventral and dorsal trunk cortex [27,28]. We sequentially stimulated these body parts with a small circular vibration motor. The resulting intrinsic signal for each body part is shown in Figure 1F and Figure S1. Based on the blood vessel pattern on the surface of the craniotomy (Figure 1G) we aligned these fields. We matched the blood vessel pattern captured during intrinsic imaging with blood vessels captured during two-photon imaging to superimpose intrinsically identified fields onto the pattern of Scnn1a+ neurons in layer 4 (Figure 1H). Intrinsically identified borders between body parts aligned well with septa lacking Scnn1a+ neurons (Figure 1H and S1A) and allowed us to assign the mouse homunculus to the expression of tdTomato (Figure 1I). Similar to the rat [5], the genital area is located close to the hindpaw. Intrinsic mapping showed very consistent alignment with the pattern of Scnn1a expression (Figure S1B,C).

4.3.2 Chronic imaging of Scnn1a+ expression across puberty

To investigate the pubertal development of genital cortex, we conducted chronic two-photon imaging of Scnn1a expression in genital cortex of anaesthetized Scnn1a-tdTomato mice (Figure 2A). Mice underwent imaging sessions every 4 to 7 days starting at the earliest possible time after weaning until early adulthood (approximately P25 to P63, Figure 2B). Simultaneously,

we tracked pubertal development (see below). Genital and hindpaw cortex were either located using intrinsic signal imaging (Figure 1F - I) or based on the clear topographic layout Scnn1a expression. During each imaging session we took a structural z-stack of the same field of view (FOV) in genital cortex (Figure 2C, top and middle). Stacks were approximately 200 x 200 μm size and covered the 400 μm between the bottom of L4 and the pia with 2 μm z-spacing. Similarly, we acquired stacks of a FOV in hindpaw cortex as a control region (Figure 2C, bottom). Within genital cortex, we observed that some neurons became fluorescent over time (Figure 2C, middle, red arrows), i.e. acquired Scnn1a expression. We counted Scnn1a+ neurons in the acquired series of stacks (Figure 2C, left to right), taking precautions to correct for small shifts in the xy-plane or imaging angle (see method). The absolute size of the acquired series of stacks varied between mice, depending on the quality of the craniotomy. Therefore, we expressed the resulting cell counts as percentage of the number of cells counted on P35 (5 weeks of age) for both genital and hindpaw cortex. The resulting percentages are then plotted as a line against age for each animal (Figure 2D), always reaching 100 % on P35. We found that in genital cortex the number of Scnn1a+ neurons roughly doubled between weaning and early adulthood in females (Figure 2D, red, left) and males (Figure 2D, blue, middle). In contrast, the number of neurons in hindpaw cortex only increased by ~ 40 % (Figure 2D, grey, right). Next, we calculated the mean slope for each cell count line shown in Figure 2D. To this end, we computed slope at each timepoint along each line and derived the mean. The mean also included negative values displayed for hindpaw cortex cell counts. The resulting mean slopes for female and male genital cortex as well as hindpaw cortex show that in female and male genital cortex there are significantly more Scnn1a+ neurons added in comparison to hindpaw cortex (Figure 2E, slope (mean ± SEM): female genital (n = 8): 1.78 ± 0.47; male genital (n = 7): 2.30 ± 0.69; hindpaw (n = 9): 0.76 ± 0.45; ANOVA, $F(2,21) = 17.2$, $p = 3.73 \times 10^{-5}$, p-values in Figure 2E indicate Tukey-Kramer pairwise comparisons between female genital cortex, male genital cortex and hindpaw cortex).

We also tracked the sexual development of mice. Weight increased from ~ 8 g to ~ 20 g in females (Figure 2F, left) while males reached up to ~ 23g (Figure 2F, right). We monitored vaginal opening in females and anogenital distance (AGD) in males, two markers for pubertal maturation [29,30]. Vaginal opening occurred around P40 (Figure 2F, left; 40.4 ± 3.1 days). In line with the tight relationship between sexual maturation and weight in females [31], vaginal opening was associated with mice reaching approximately 16 g. In males the AGD increased from prepubertal 7 mm to adult 16 mm (Figure 2G) [29]. The first ovulation usually occurs seven days after vaginal opening [32]. In line with this continuous process of sexual maturation,

the number of Scnn1a+ neurons did not show a sharp step-like increase. Instead the increase was gradual, rising steeply before P40 and leveling off towards early adulthood (Figure 2D).

4.3.3 Scnn1a+ expression increases while neuron density remains stable

To determine the origin of newly appearing Scnn1a+ neurons we performed immunostaining. Tangential brain sections of pre and postpubertal Scnn1a-tdTomato brains were counterstained with the neuron selective antibody NeuN conjugated to a green secondary antibody. Fluorescent micrographs show that neither in genital cortex (Figure 3A) nor in hindpaw cortex (Figure 3B) all L4 neurons (NeuN+, green) express Scnn1a (tdTomato+, red). However, in genital cortex, the number of Scnn1a+ neurons increases from pre to postpuberty (Figure 3A). We counted the number of Scnn1a+ neurons relative to all neurons (NeuN+) in z-stacks (xyz: 100 x 200 x 40 µm, 1 µm z-spacing, n = 12 hemispheres) of genital cortex of mice between P24 and P100. While the percentage of Scnn1a+ neurons increases in genital cortex with age (Figure 3C), it remains stable in hindpaw cortex (Figure 3D). Binning these data into three age groups shows that in genital cortex (Figure 3E, red,), the percentage of Scnn1a+ neurons is significantly lower at prepubertal ages (< P40: 8.47 ± 1.35) compared to postpuberty (P40 to P80: 18.0 ± 1.69) and adulthood (> P80: 20.5 ± 2.05), while there was no significant difference between the latter two age groups (ANOVA: $F(2,11) = 54.5$, $p = 9.35 \times 10^{-6}$, p-values in Figure 3E indicate pairwise comparisons between age groups). In comparison, the percentage of Scnn1a+ neurons remains consistently around 60 % in hindpaw cortex (ANOVA: $F(2,11) = 0.26$, $p = 0.77$, Figure 3E, grey). Finally, neuron density (all NeuN+ per mm^3) is similar and remains stable with age in both genital and hindpaw cortex (Figure 3F). While the density of Scnn1a+ neurons increases significantly with age, the density of Scnn1a– neurons decreases marginally and not significantly (Pearson's correlation coefficient: Scnn1a+ : $r = 0.900$, $p = 0.0001$; Scnn1a– : $r = -0.133$, $p = 0.681$) . These findings are in line with a conversion scenario, where previously Scnn1a– neurons acquire Scnn1a expression during puberty.

4.3.4 Apical dendrites of pyramidal neurons in genital cortex do not remodel during puberty

Within L4, excitatory neurons can be broadly categorized into stellate and pyramidal neurons, defined by the absence and presence of an apical dendrite respectively [15,17,33,34]. However, at birth all excitatory L4 neurons appear as pyramids [18], suggesting many retract their apical dendrite to become stellates in the first postnatal week [18]. This process seems to be a hallmark of layer 4 somatosensory map development [19]. To find out, whether pyramidal neurons in genital cortex lose their apical dendrite during puberty, we acquired high magnification two-

photon z-stacks of neurons within genital cortex of 5 mice. Stacks covered the entire distance from the bottom of L4 to the pia (xyz: 133 x 133 x 400 µm, 2 µm z-spacing). We captured the same Scnn1a+ neurons pre puberty (Figure 4A, left top, P30) and post puberty (Figure 4A, left bottom, P60) and reconstructed all neurons within these stacks (n = 5 pre and 5 post). We identified neurons that were present at both ages and those that newly appeared during adulthood. We further classified each neuron as either stellate (orange) or pyramidal (green) shaped, based on the absence and presence of an apical dendrite respectively. The high magnification micrographs (Figure 4A, right) show examples of a pyramidal and a stellate neuron, which evidently do not undergo morphological remodeling during puberty. In fact, 100 % of stellate cells (n = 51) retained their stellate cell morphology and 100 % of pyramids (n = 63) retained their apical dendrite throughout puberty (Figure 4B). Overall, there were more spiny stellates than pyramids in genital cortex L4 before puberty and their ratio was not different after puberty (Figure 4C, Fishers Exact test, $X^2 = 0.95$, $p = 0.91$).

4.3.5 Stronger genital-touch responses in layer 4 of males compared to females and a developmental increase of responsiveness in females

To understand how puberty shapes evoked responses in L4 of genital cortex, we performed calcium imaging of Scnn1a+ neurons during sensory stimulation of the genitals. Three weeks after neonatal injection (P0 to P1), Scnn1a-cre mice showed extensive cre-dependent expression of the activity dependent calcium indicator flex-GCaMP6s in genital cortex (Figure 5A). Overall, the labelling of Scnn1a+ neurons with flex-GCaMP corresponded well with labelling by genetic crossing of Scnn1a-cre and Ai9-reporter mice (see methods). For two-photon imaging, mice were lightly anaesthetized using isoflurane and head-fixed, while genitals were stimulated with a small circular vibration motor for 300 trials (Figure 5B). Care was taken to position the stimulation the exact same way during all experiments (see methods). For each cell, we computed a $\Delta F/F_0$ trace. Neurons varied in responsiveness to genital stimulation (green dashes, Figure 5C). Since imaging conditions varied, we z-scored all traces acquired during a session. To quantify the responsiveness of neurons in genital cortex, we first analyzed all detectable neurons, which also includes Scnn1a+ neurons that acquired Scnn1a expression during puberty. For each cell we computed a mean Ca^{2+} trace across all trails. The average of these mean traces shows that neurons in males respond more strongly to genital stimulation compared to females (Figure 5D), which is in line with previous findings from rats [5]. Calculating the response index (RI) for male and female neurons $((F_{max(stim)} - F_{mean(bsl)}))/ STD (F_{bsl})$, see methods) showed that this difference was highly significant (RI (mean ± SEM): Males

(990 neurons in 5 mice), 9.02 ± 0.357 vs. females (734 neurons in 5 mice), 5.67 ± 0.124, Rank-Sum test, $Z = 10.2$, $p = 2.74 \times 10^{-24}$).

To determine if response strength changes in genital cortex over the course of puberty, we performed functional imaging experiments between weaning and early adulthood. In females (n = 5) we split neurons according to whether they were recorded before or after vaginal opening. In accordance with previous reports of male puberty onset and the notion that male sexual maturation is independent of weight [31], we used the mean age at vaginal opening (P39) as an approximation in males (n = 5). Evoked responses in males were similar before and after P39 (Figure 5E, top). In contrast, responsiveness increased from before to after vaginal opening in females (Figure 5E, bottom). Accordingly, response indices of prepubertal males were greater than that of prepubertal females (Figure 5E, left, Males: n = 551 vs. Females: n = 465, Rank-Sum test, $Z = 10.9$, $p = 1.04 \times 10^{-27}$). Furthermore, neurons imaged in adult males responded more strongly to genital stimulation than neurons imaged in adult female mice (Figure 5E, right, Males: n = 418 vs. Females n = 255, Rank-Sum test, $Z = 2.77$, $p = 0.006$). Response indices of neurons in genital cortex of males only slightly increased before and after P39 (Figure 5F, top, RI (Mean ± SEM): < P39: 8.79 ± 0.394 vs. > P39: 9.45 ± 0.665, Rank-Sum test, $Z = 1.31$, $p = 0.190$). In contrast, in females stimulation of the external genitals elicited significantly larger responses after vaginal opening as compared to before vaginal opening (Figure 5F, bottom, RI (Mean ± SEM): before vaginal opening: 5.24 ± 0.126 vs. after vaginal opening: 6.49 ± 0.265, Rank-Sum test, $Z = 4.78$, $p = 1.74 \times 10^{-6}$). Given that pubertal maturation is temporally extended, we also correlated the response indices with the age at imaging for males (Figure 5G, top) and females (Figure 5G, bottom). Interestingly, response indices increased with age in females (Pearson's correlation coefficient: $r = 0.102$, $p = 0.006$), but not in males (Pearson's correlation coefficient: $r = 0.017$, $p = 0.600$). Together these results show that neurons in genital cortex show sex and age dependent response properties.

4.3.6 Newly appearing Scnn1a+ neurons respond to genital stimulation

Our data suggests that during puberty, many neurons in genital cortex gain Scnn1a+ expression (Figure 2). To determine whether these newly Scnn1a expressing neurons are functionally active we performed Ca^{2+} imaging experiments. We identified the newly appearing Scnn1a+ neurons by comparing z-stacks acquired before puberty (Figure 6A, top) to stacks acquired post puberty (Figure 6A, bottom). To ensure that the cellular gain of GCaMP fluorescence after puberty reflected the gain of Scnn1a expression and not a delay in viral transfection, prepubertal stacks were acquired at least four weeks after injection. Similar to results observed in Scnn1a-

tdTomato mice, many neurons expressed flexed GCaMP6s both before and after puberty (Figure 6A, purple arrows). Other neurons expressed GCaMP only after puberty (Figure 6A, green arrows). We limited our analysis to newly appearing Scnn1a+ neurons that clearly did not express GCaMP before puberty (28 neurons in 2 male and 2 female mice) and compared those to all other recorded neurons (1689 neurons in 5 male and 5 female mice). The average evoked response of these newly appearing Scnn1a+ neurons was similar to the response evoked in all other neurons (Figure 6B,C).

4.3.7 Scnn1a+ and Scnn1a− neurons respond similarly to genital stimulation

To determine whether Scnn1a+ and Scnn1a− neurons differ in their responsiveness to genital stimulation, we performed acute two-photon targeted juxtacellular recordings in Scnn1a-tdTomato mice under urethane anesthesia. We visualized L4 of genital cortex using two-photon microscopy and stimulated the external genital region as before (Figure 5). For juxtacellular recordings, we inserted a pipette filled with a green fluorescent dye (Alexa Fluor 488) and recorded evoked responses of both putative Scnn1a+ (Figure S2A, red) and putative Scnn1a− neurons, which were identifiable as dark shadows within the fluorescently labelled neuropil (Figure S2A, white arrows). After recording, neurons were electroporated (see methods) with Alexa Fluor 488 to identify the recorded neuron (Scnn1a+ vs. Scnn1a−). Scnn1a− neurons turned from not fluorescent (Figure S2B, top) to green fluorescent after electroporation (Figure S2B, bottom). In contrast, the Scnn1a-tdTomato+ neurons (Figure S2C, top) became red-and-green after electroporation (Figure S2C, bottom). Labeling efficacy was high (> 90 %) and multiple cells could be recorded and identified within the same animal (21 identified Scnn1a+ neurons, 25 identified Scnn1a− neurons in 2 males and 4 females). The mean firing rate of Scnn1a− (Figure S2D) and Scnn1a+ neurons (Figure S2E) in response to 200 ms of genital stimulation (shaded grey box) were overall similar. Mean firing rate differences were calculated by subtracting the mean firing rate during the 200 ms preceding stimulus onset from the mean firing rate during genital stimulation (200 ms) for each cell (Figure S2F). Overall, Scnn1a+ neurons responded slightly more strongly to genital stimulation than Scnn1a− neurons, but this difference was not statistically significant (Kruskal-Wallis test, $p = 0.154$).

4.3.8 Co-housing prepubertal females with adult males advances the gain of Scnn1a+ neurons in genital cortex

Pubertal development of female mice can be accelerated by co-housing them with adult males via the synergistic effect of male pheromones and touch [8]. Specifically, three days of co-housing resulted in a tripling of uterine weight. We have previously shown that this induced

advance in pubertal maturation by male conspecifics also accelerates the expansion of genital cortex in prepubertal female rats [6]. Therefore, we wondered, whether co-housing with adult males and the concomitant first sexual experience would also accelerate the gain of Scnn1a expression in genital cortex. To test this, we performed chronic imaging experiments of Scnn1a-tdTomato mice similar to Figure 2. Now, female mice were co-housed with sexually mature males between P36 and P39 (Figure 7A). At P36 females had just reached 15 g of bodyweight (Figure 7B), a timepoint where the uterine response to adult males is maximal [8] while vaginal opening had not yet occurred. While weight gain was similar between single and co-housed females, vaginal opening occurred slightly, albeit not significantly, earlier in co-housed females (Figure 7C, Alone (n = 8): P 40.4 ± 3.1 vs. +Male (n = 7): P 38.7 ± 1.5 days of age, unpaired t-test, p = 0.209). Scnn1a+ neurons were imaged in genital cortex of co-housed females and counted in series of stacks of the same FOV captured between P25 and P63. In females sitting alone, fewer neurons gained Scnn1a expression between P36 and P39 (Figure 7D) compared to females co-housed with adult males (Figure 7E). We quantified this increase in Scnn1a+ cells for females sitting alone (Figure 7F, left, same as Figure 2D) and for females co-housed with males (Figure 5F, right). A close examination of P36 to P39 (Figure 7G) highlights the steep increase in Scnn1a+ neurons for co-housed females in this short time window (Figure 7G right). Between P36 and P39, the slope of cell counts is significantly steeper for co-housed females compared to single housed females (Figure 7H, Alone (n = 8): 1.89 ± 0.69 vs. +Male (n = 7): 3.91 ± 1.60, unpaired t-test, p = 0.006). To examine, whether this steep increase during co-housing results in an overall increased number of Scnn1a+ neurons in genital cortex or represents an acceleration of Scnn1a+ expression gain, we compared cell counts at P50 (Figure 7I), 11 days after co-housing ended. Interestingly, there was no difference in the relative cell count of Scnn1a+ neurons between single housed and co-housed females at this stage (Figure 7I, Alone (n = 8): 127 ± 8 vs. +Male (n = 7): 136 ± 9, unpaired t-test, p = 0.111). Overall these data suggest that initial sexual experience has a strong effect on Scnn1a expression. This gain of Scnn1a+ cells appears to reflect an accelerating effect on the maturation rather than a life-long expansion of genital cortex.

To examine whether this effect of co-housing is specific to genital cortex, we also captured series of stacks in the hindpaw cortex of co-housed females and compared those to single house females (Figure S3A). In the hindpaw area the gain of Scnn1a+ neurons between P36 and P39 is minimal and similar between single and co-housed females (Figure S3B). Similarly, the slope of cell counts within the co-housing period is not different between the two groups in hindpaw cortex (Figure S3C, Alone (n = 6): 1.06 ± 0.82 vs. +Male (n = 7): 0.88 ± 0.79, unpaired t-test,

p = 0.695). Finally, the relative cell count of Scnn1a+ neurons was not different at P50 between co-housed and single housed females in hindpaw cortex (Figure S3D, Alone (n = 6): 109 ± 4 vs. +Male (n = 7): 111 ± 8, unpaired t-test, p = 0.668).

4.4 Discussion

Our findings reveal that layer 4 of the primary somatosensory genital field undergoes unusually late remodeling during puberty. We showed that the number of Scnn1a+ neurons almost doubles during pubertal maturation and that this gain is gradual rather than step-wise. Our data suggests that within genital cortex only a fraction of all neurons expresses Scnn1a+ and that this fraction grows during puberty while neuron density is stable. In contrast to developmental processes [18], Scnn1a+ neurons in genital cortex retain their original morphology as stellate or pyramidal neurons. Calcium imaging further showed that neurons in male genital cortex respond more vigorously to genital touch compared to females. It also revealed, that newly appearing Scnn1a+ neurons also respond to genital touch. Most interestingly however, we observed that initial sexual experience drastically accelerated the gain of Scnn1a expression in genital cortex neurons.

During pre and early postnatal development, extrinsic and intrinsic factors shape the distinct identity of layer 4 primary somatosensory cortex within a brief window of cortical plasticity [35,36]. Thereafter, the somatosensory homunculus remains particularly stable [9]. Compared to other body parts, genitals significantly change in shape and relevance much later in life [37,38]. While recent studies have demonstrated that activity in primary somatosensory cortex does not only reflect the physical properties of touch [39–41], few have yet examined the effect of sexual maturation and, more importantly, sexual experience on the cortical representation of genitals. We specifically targeted layer 4 of genital cortex to build on our previous findings [5–7], while we do not rule out puberty dependent changes in other layers of genital cortex.

We show that more Scnn1a+ neurons are gained in genital cortex compared to hindpaw cortex and that this increase represents a change in Scnn1a expression and not a gain of new neurons. Scnn1a+ neurons cluster densely in layer 4 of primary somatosensory cortex [19,22] and pattern it in the shape of the mouse homunculus, suggesting that neurons newly appearing as Scnn1a+ during puberty may resemble a late acquired layer 4 cell identity. New Scnn1a+ neurons did not appear abruptly but rather gradually, with an initial steep rise that levels off thereafter. This observation is in line with the view that sex hormones act within one temporally extended sensitive period during brain development [42], and not only during one brief perinatal and one brief pubertal pulse [43]. Moreover, we show that initial sexual experience can increase the gain of Scnn1a+ neurons in genital cortex. We suggest, that this immediate and drastic effect represents a developmental acceleration rather than a permanent increase, as the relative gain

of Scnn1a+ neurons was not different once animals reached adulthood. We wonder if this imminent accelerating effect of sexual experience on cortical circuitry is related to the great psychological and social significance of initial sexual experience [24,25], although we cannot exclude the possibility that other kinds of sexual experience (later or premature) also have an effect on genital cortex.

A key property of many excitatory neurons in layer 4 of primary somatosensory cortex is their spiny stellate morphology [18], which depends on the appropriate transcriptional expression [19]. Nevertheless, some excitatory neurons within the granular areas of somatosensory cortex retain their pyramidal morphology [15,16,18]. We find that in genital cortex, there were more spiny stellates compared to pyramids. While the number of Scnn1a+ neurons almost doubles during sexual maturation in genital cortex, the ratio between stellates and pyramids did not change from prepuberty to postpuberty. We also examined the morphology of pre and postpubertal Scnn1a+ neurons to find out if pyramidal Scnn1a+ neurons in genital cortex retract their apical dendrite as some of them do during early development [18]. However, we did not observe any pyramidal neurons that retracted their dendrites during this late stage. Alternatively, neurons in genital cortex may have already undergone morphological remodeling just prior to gaining Scnn1a expression. Unfortunately, we cannot investigate this scenario because layer 4 neurons do not express all viral constructs well and can be more easily visualized in vivo by using a transgenic mouse line.

Using two-photon calcium imaging we show that responses of layer 4 neurons in genital cortex to genital touch are more complex than anticipated. Similar to previous observations in rats [5], we found greater responsiveness of genital cortex neurons in males compared to females. In addition, we also observed a positive correlation between age at recording and response strength in females but not in males. Given that genital cortex appears anatomically monomorphic in males and females, this physiological dimorphism is particularly surprising. Differences in the anatomy of male and female genitals may contribute to this result. In males the surface area of the external genitals (penis and scrotum) is significantly larger than that of female genitals, where stimulation of the skin as it is applied here, does not resemble the sensory input that female genitals receive during natural intercourse. Moreover, males are usually heavier than females, possibly resulting in differences in depth of anesthesia. To further elucidate how genital cortex processes sensory inputs in an age, sex and possibly hormone dependent manner,

it will be key do develop approaches to exert precise local (vagina vs. clitoris) and naturalistic (external vs. internal) sexual stimulation on the female genital tract [44].

Finally, we cannot rule out the possibility that Scnn1a+ constitute a special subpopulation of layer 4 neurons, at least in genial cortex. While it would have been of great interest to investigate Scnn1a– neurons in vivo, there is currently no feasible strategy to target these neurons optically. Therefore we turned to two-photon guided juxtacellular recordings to investigate if Scnn1a+ and Scnn1a– neurons differ in their response properties to genital stimulation. The results suggested similar response strengths of Scnn1a+ and Scnn1a– neurons. Yet, it is conceivable that our experimental approach was insufficient to resolve differences between these cell types. For one, we cannot rule out that sensory responses of Scnn1a– neurons arise from excitatory network activity. We suggest to probe thalamic input to layer 4 more precisely by selectively activating primary thalamic afferents while recording from postsynaptic targets in layer 4. Alternatively, it would also be interesting to selectively label layer 4 neurons that receive thalamic input in Scnn1a-cre mice to find out how these neurons map onto Scnn1a expression. In a similar vein, comparing the molecular profile of Scnn1a+ and Scnn1a – neurons as well as the factors that lead to the gain of Scnn1a+ expression during puberty will be important. For example, hormone level changes during puberty might influence Scnn1a expression and cellular functions of Scnn1a+ neurons: The Scnn1a gene encodes for the alpha subunit of a well-known non-voltage gated epithelial sodium channel (ENaC) in various organs. Interestingly the activity of this channel is dependent on estrogen in several tissues [45–47].

Conclusion

In line with earlier observations our novel results show that layer 4 of genital cortex follows a unique developmental trajectory. Rather than being fully developed after the first postnatal week, many of its principal neurons assume their primary cortex layer 4 cell identity only in the course of puberty. Our data show genital cortex maturation can be dramatically accelerated the initial sexual experience. We wonder, if the molding out of the genital representation by the initial sexual interaction is part of what brings about its huge mnemonic weight and its powerful effects on the first-person perception of the own sexuality.

Acknowledgments

We thank Eduard Maier, Constanze Lenschow and Konstantin Hartmann for comments on the manuscript. We thank Undine Schneeweiß, Juliane Diederichs and Tanja Wölk for excellent technical assistance. We thank Jean-Sebastien Jouhanneau for advice for targeted juxta-cellular recordings.

JSG was funded by the Böhringer Ingelheim Fonds. JSG, EM and MB were funded by the Humboldt-Universität zu Berlin, BCCN Berlin (German Federal Ministry of Education and Research BMBF, Förderkennzeichen 01GQ1001A), a grant from the DFG (BR 3479/11-1), NeuroCure, the Gottfried Wilhelm Leibniz Prize of the DFG. MB, NT & ML were funded by the Deutsche Forschungsgemeinschaft (DFG, German Research Foundation) – Project number 327654276 – SFB 1315.

Author Contributions

JSG and MB designed the experiments, JSG and EM performed the experiments, NT assisted with two-photon imaging and analysis, RS and ML provided transgenic lines and other equipment, JSG, EM and MB analyzed the data and JSG and MB wrote the manuscript.

Declaration on Interests

The authors declare no competing interests.

4.5 Method

LEAD CONTACT AND MATERIALS AVAILABILITY

This study did not create new unique reagents or mouse lines. Further information and requests for resources and reagents should be directed to and will be fulfilled by the Lead Contact, Michael Brecht, michael.brecht@bccn-berlin.de.

EXPERIMENTAL MODEL AND SUBJECT DETAILS

Animals. All experimental procedures were performed according to the German guidelines on animal welfare under the supervision of local ethics committee (animal permit number G0244/16). Adult Scnn1a-Tg3-Cre (B6;C3-Tg(Scnn1a-cre)3Aibs/J, RRID: IMSR_JAX:009613) and Ai9-reporter mice (B6;Cg-Gt(ROSA)26Sor$^{tm9(CAG-tdTomato)Hze}$/J, RRID: IMSR_JAX:007909) mice were purchased from Jackson Labs. Wildtype C57BL/6JRj mice were purchased from Janvier. For intrinsic and chronic imaging, juxta cellular experiments and histology, heterozygous Scnn1a-cre mice were bred with homozygous Ai9-reporter mice. Scnn1a x Ai9 positive offspring constitutively expressed tdTomato in all cre-positive cells (Scnn1a-tdTomato). Males and females between postnatal day (P) 25 and P90 were used. For calcium imaging experiments, we used single transgenic Scnn1a-cre mice injected with flexed GCaMP6s. All animals were weaned at P20 and genotyped by Transnetyx (Cordova, TN). Mice were housed alone or in pairs under a 12-hour light and dark cycle in temperature controlled cabinets with ad libitum chow and water.

METHOD DETAILS

Assessment of pubertal development. Throughout chronic experiments (P25 - P60), weight and external parameters of pubertal development were closely monitored. Weights were smoothed with a three-day sliding window and plotted across days for each animal. Females were inspected daily starting at weaning to record vaginal opening. For males, we recorded the distance between anus and penis (anogenital distance, AGD). Both, vaginal opening and AGD are dependent upon the activation of the hypothalamic-pituitary-gonadal axis [29].
Sensory stimulation of the body surface
For stimulation of the body surface, in particular the external genitals, we used a small circular vibration motor, usually found in mobile phones (Ø 8 mm, 3 mm thick, Eckart Electronics, PO1637), which emits 10 Hz vibrations. The vibration motor was attached to a costume made control box, which could be triggered by TTL pulses during intrinsic imaging, two-photon calcium imaging and juxtacellular recordings. The vibration motor was held by a micro-manipulator which allowed precise positioning on the genital or other body parts. To stimulate the genital in males, the vibration motor was positioned on top of the penis and the scrotum. In females, it was positioned to cover the exit of the urethra, the clitoris and the vulva.

Headpost and window surgery. For all chronic imaging experiments, mice underwent headpost and window surgeries following weaning approximately at P25. Mice were anaesthetized with isoflurane (1.5 – 2 % in O2). Body temperature was maintained at 36°C using a heatpad. After removing the skin covering the skull, a circular 3 mm craniotomy was made positioned between the coronal suture and the midline. The dura was left intact and the craniotomy was sealed with a stack of three coverslips, 3 mm, 3 mm and 4 mm glued together with light Norland optic adhesive 71 (Norland products) and affixed using superglue. A light-weight, two-point fixation headpost was glued on the skull surrounding the craniotomy, before sealing everything with dental cement.

Intrinsic imaging of genital cortex. Topographic maps in S1 were functionally identified using intrinsic optical imaging (iOS) as previously described [27,28]. For this purpose, mice were lightly anesthetized with isoflurane (0.5 – 1 % in O2) and placed on a heatpad. We sequentially identified several body parts in each mouse which included the genital, hindpaw, forepaw, genital, tail, ventral and dorsal trunk. To limit the duration of anesthesia per experiment not all body parts were mapped in all mice. For identifying each body part, we placed the small circular vibration motor on it using a micromanipulator. Care was taken to prevent the vibration motor to touch anything but the body part under investigation. To reach the ventral side of the paws, they were minimally suspended. To reach the ventral trunk and the genital, the lower body was slightly twisted. After appropriate positioning, the blood vessel pattern on the surface of the craniotomy was captured using green illumination (530 nm). Next, the craniotomy was illuminated by a ring of small red LEDs (600 nm) mounted around the objective. Illumination was set so that the craniotomy was homogenously enlightened without saturation. Images were captured using a CCD camera coupled to a 50 nm and 25 nm lens. The signal was measured before and during sensory stimulation (1 sec stimulation, 5 sec ISI) for 20 sweeps. The intrinsic signal was measured as the difference between reflected light before and during stimulation and was mapped onto the blood vessel pattern (Figure 1F). The signal was then analyzed using ImageJ. Images were converted to grey scale and smoothed using a Gaussian filter (sigma = 10). The area of evoked activity was identified by thresholding the image to binary black and white, where the darkest pixels (strong activity) appeared as black and the remaining image in white. The threshold was set so that pixels within the darkest 10 % of the grey scale appeared in black. The resulting fields of activation were superimposed into the blood vessel pattern of the craniotomy (Figure 1G).

Two-photon imaging. Imaging was performed with a Thorlabs B-Scope or a costume built resonant scanning two-photon microscope equipped with GaAsP photomultiplier tubes (assembled by INSS, UK). tdTomato and GCaMP6s were excited at 940 nm (typically 30 to 40 mW at the sample) with a Ti:Sapphire laser (Spectra Physics) and imaged through a 16x 0.8 NA water immersion objective. Images (512 × 512 pixels) were acquired at 30 Hz using ScanImage software. During all imaging experiments, mice were lightly anaesthetized using isofluorane (0.5-1.0 % in O2) and body temperature was maintained using a heatpad.

Chronic imaging of Scnn1a+ neurons. Following window and headpost surgery, animals were allowed to recover for two days. In order to quantify Scnn1a+ cells in L4 of genital cortex, two-photon imaging carried out in Scnn1a-tdTomato transgenic mice, were excitatory neurons in L4 express tdTomato. Starting around P25, mice were imaged at least once per week until approximately 60 days of age. The exact start and endpoint of chronic imaging experiments varied between animals, depending on the quality of the craniotomy. Genital cortex was first identified either using intrinsic imaging (in 9 mice) or the topographic layout of the body map within L4, which is clearly visible in Scnn1a-tdTomato mice used here. To provide an overview of the whole genital field (1065 μm x 1065 μm), a stack was taken at minimal magnification first. Next, a representative subfield was captured at high magnification (~ 200 μm x 200 μm), which was used to quantify fluorescent cells. In addition, a similar stack was acquired in the somatosensory hindpaw cortex to serve as a control area. Care was taken to capture stacks at the center of the genital or hindpaw area. Stacks were always taken at the same angle and a two-point fixation headpost was used to minimize shifts in the imaging angle. To achieve optimal structural resolution, 60 to 200 images were acquired per z-plane and averaged online. Z-stacks were acquired starting below layer 4, densely populated by tdTomato+ neurons, moving upwards towards the pia. Stacks covered an overall distance of 400 μm with individual z-planes acquired every 2 μm. Following the first imaging day, the exact same field of view

was captured on subsequent imaging days. Image stacks were analyzed using ImageJ as follows: Acquired z-stacks were first minimally cropped in the xy-plane to ensure that they included the same FOV across days. With regards to the z-axis (depth), neurons were neither cut at the top or bottom due to the large vertical distance that they covered. Cells bodies were then traced by hand throughput the z-stacks to quantify the number of fluorescent cells in the genital and hindpaw region throughout puberty. Only neurons that were fully included in the stacks were counted. After counting, we took additional precautions to account for small shifts in the imaging angle, which resulted in Scnn1a+ neurons moving in and out of the stacks across timepoints. To avoid biases in counting such cells, we created maximum projections of the z-stacks after counting cells and made sure that the same neurons were systematically included or excluded. Because stacks were not exactly of the same xy-area (due to posthoc alignment or issues with the quality of the craniotomy), cell counts for each animal are expressed relative to the number of cells counted on P35 (7 weeks).

For morphological classification of Scnn1a+ neurons we captured structural z-stacks as described above (xyz: ~ 133 x 133 x 400 µm, 2 µm z-spacing). In 5 mice we acquired z-stacks of the same FOV in genital cortex around P30 and around P60. Stacks were reconstructed in 3D using ImageJ to reveal apical dendrite morphology between L4 and the pial surface. Scnn1a+ positive neurons were classified as either pyramidal or stellate cells, depending on the presence or absence of an apical dendrite, respectively. We further distinguished between neurons that were Scnn1a+ already before puberty (visible at P30 and P60) and those that only appeared after puberty (P60 only).

Manipulation of pubertal development. For manipulation experiments, female mice underwent chronic imaging sessions as described above. In addition, mice were co-housed with sexually mature wildtype mice for three days just prior to onset of puberty. Co-housing started once mice reached a weight of 15g [8] which occurred at P36. Males were removed again three days later on P39.

Neonatal viral injections. For functional imaging of Scnn1a neurons during puberty, we injected neonatal Scnn1a-cre mice (P0 – P3) with pAAV-Syn-Flex-GCaMP6s-WPRE (Addgene plasmid #100843, RRID: Addgene_100843). For injections, cryoanaesthesia was induced by placing pups wrapped in a lab glove on a metal plate on ice for 10 minutes, taking care to avoid pups directly contacting the ice [48]. Pups were positioned dorsal side up, lightly fixed using an adhesive bandage. AAV injections were made using a 10 µL Hamilton syringe (Hamilton) and a 32-gauge needle. For injections the head was held gently and the tip of the needle was inserted carefully through skin and cranium. Between 3 and 5 injections (~ 50 nl) were made into the left hemisphere directly below the cranium, covering the area between Bregma and Lambda close to the midline (visible through the skin) to cover S1. Pups recovered on a heat pad and were returned to their home cage once awake and re-warmed. All pups survived this procedure and dams did not reject any pups. Pups were weaned at P21 and underwent head-post implantation and window surgery as described above.

Functional 2-photon imaging. Following neonatal injections, two-photon calcium imaging was used to capture sensory evoked activity of Scnn1a+ L4 neurons expressing GCaMP6s throughout puberty. Mice were imaged between 25 and 60 days of age, whereby we sampled different neurons within mice during multiple imaging session. Despite the long duration of GCaMP6s expression, only few cells acquired nuclear filling. Those were excluded from the analysis. Furthermore, we ensured that viral injection of flex-GCaMP6s labelled the same neurons as genetic crossing of Scnn1a-cre and Ai9- reporter mice (resulting in td-Tomato expression). Injecting flex-GCaMP6s in Scnn1a-tdTomato mice showed a good, albeit not

perfect, correspondence between both transfection strategies (td-Tomato + GCaMP double labelling: 85.9 ± 2.1%, td-Tomato only: 3.7 ± 2.1%, GCaMP only: 10.4 ± 2.1%). To identify newly appearing Scnn1a+ neurons during adulthood, we took z-stacks at 840nm at a prepubertal timepoint, to be able to identify all neurons that already expressed Scnn1a. During each imaging session, we imaged neurons in the genital while stimulating the external genital with a small vibration motor (see above), triggered by TTL pulses. Time-series movies were acquired at 30 Hz and aligned with stimulations using Spike2 software. The vibration motor was held by a micromanipulator and placed either on the genital area. During each trial, calcium activity was recorded for 2s (baseline), followed by 1s of stimulation and a 5s inter-trial-interval. During each session, we recorded ~ 300 trials. Calcium traces were extracted using the Suite2p software [49], which performs motion correction and provides neuropil traces for each cell. Automated cell detection by the suite2p software was hand curated. This software uses adequate levels of Ca^{2+} fluorescence as a criterion for detecting neurons. Neurons that acquired nuclear filling by GCaMP6s were therefore automatically disregarded by the algorithm, which was confirmed during hand curation. Neuropil signals were weighed with a factor of 0.7 and subtracted for each cell. The fluorescent change ($\Delta F/F_0$) was calculated as $(F - F_0) / F_0$ where F_0 was the baseline fluorescence value in the ROI throughout the whole imaging session [50]. To account for differences in imaging quality across days, we z-scored all traces acquired during one session and pooled traces afterwards across sessions. This ensures that the structure within an imaging session is retained while particularly good or bad imaging sessions cannot distort the overall result. For analysis of event-related calcium activity, we further normalized traces for individual trials by subtracting a baseline comprising the mean fluorescence during the 50 frames preceding the stimulus onset from the entire trial. A response index was calculated for each trial by dividing the maximum $\Delta F/F_0$ during the stimulus by the standard deviation of the 10 frames preceding stimulus onset.

Targeted Juxta-cellular recording. Targeted juxtacellular experiments were carried out using Scnn1a-tdTomato (5 females, 2 males, P25 to P41) transgenic mice. The above surgical protocol for headpost and window implantation was slightly adjusted. On the day preceding the experiment, mice underwent headpost surgery while leaving the skull intact. After implantation, mice were placed under the 2-photon microscope and the topographic layout of L4 (tdTomato positive) was captured by imaging through the skull. On the day of the experiment, mice were anesthetized with 10 % urethane (0.01 g/g i.p.). A small craniotomy (1 mm diameter) was made above genital cortex and the dura was removed. Mice were placed under the two-photon microscope, where the body temperature was maintained at 36°C using a rectal probe and a homeothermic blanket (FHC). For sensory stimulation, the vibration motor was positioned on the genital. For simultaneous imaging and electrophysiology, the two-photon objective was positioned at 73° relative to the recording stage. The pipette for juxtacellular recording was controlled by micromanipulators (SM6, Luigs & Neumann) and positioned at 45° relative to the recording stage. Pipettes (4 - 6 MOhm; pulled with P-97; Sutter Instrument) were filled with intracellular solution containing the following (in mM): K-gluconate 130, Na-gluconate 10, HEPES 10, phosphocreatine 10, Mg-ATP 4, GTP 0.3, NaCl 4 and Alexa-488 hydrazine 10 (ThermoFisher, #10436) at pH 7.2.

We first visualized the pipette tip with the two-photon microscope above the pia, before lowering it down to the surface of the brain, 400-500 µm medial of genital cortex, were we set the vertical micromanipulator to 0. Following insertion into the brain, the pipette was lowered in 3-µm steps until it reached genital cortex layer 4, which was identified by simultaneous two-photon imaging. Once the pipette was positioned in reach of cells of interest, the craniotomy was covered with 1 % agarose to improve recording stability and a 3 mm circular glass coverslip for better visibility. We approached Scnn1a+ (tdTomato +) and Scnn1a– (visible as black holes

within the tdTomato + neuropil) in an alternating fashion. The distance from the pipette tip to a cell was visualized using two-photon microscopy and monitored by current step (1 nA)-induced voltage deviations, resulting from an increased resistance at the tip of the pipette in the proximity of cells. Cells were recorded in current-clamp mode. Once spike signals were between 0.5 mV and 1.5 mV, stimuli were delivered every 2 s with 200 ms stimulation length for 50 trials. After recording, cells were labelled by applying one 1 s long electroporation pulse train (-10V, 0.5 ms pulse width, 20 ms inter-pulse interval). This labelling procedure was adapted from Judkewitz et al., 2009. However, distance of the pipette tip to the cell was kept as close as during juxtacellular recording as long-term survival of the cell was not necessary and labeling success was > 90 % with this protocol. The labelling procedure was captured using two-photon microscopy: If the labelled neuron at the pipette tip was previously red and appeared yellow after electroporation with Alexa-488 hydrazine, it was classified as a Scnn1a + neuron. If it was non-fluorescent during recording and turned green upon electroporation, it was identified as a Scnn1a - neuron. We excluded recordings with unsuccessful or ambiguous labeling attempts or if two or more cells were labeled. Overall we recorded 21 Scnn1a + and 28 Scnn1a - neurons in 2 males (P25 and P41) and 4 females (2 x P25, P34 and P38), with a similar number of both cell types recorded in each mouse. The recorded signal was amplified by a patch-clamp amplifier (ELC-03XS; NPI, Tamm, Germany) and sampled at 50 kHz by a Power1401 analog to digital converter under the control of Spike2 software (CED). Recordings were analyzed in MATLAB 2015a (MathWorks, MA) using descriptive statistical methods.

Immunohistochemistry. At the end of the above described experiment, animals were anaesthetized using 20 % urethane solution and perfused with phosphate buffer followed by 4 % paraformaldehyde solution (PFA). Brains were removed, hemispheres were separated, subcortical brain areas removed and cortices were flattened between two glass slides separated by clay spacers. Glass slides were weighed down with small ceramic weights for 3 h. Afterwards, flattened cortices were left free floating in 4 % PFA overnight. On the next day, PFA was replaced with a 30 % sucrose solution for cryoprotection. Afterwards, brains were embedded and 40 µm sections were cut on a freezing microtome.

For quantifying the density of Scnn1a+ neurons relative to all other neurons, which were stained with an antibody against the neuron specific protein NeuN. Briefly, sections were washed four times for 10 minutes in 1XPBS and then incubated in a blocking solution containing 1XPBS and 0.5% Triton X-100 (PBS-X) and 10% goat serum for two hours at room temperature. Next, free-floating sections were incubated in the primary antibody mouse anti-NeuN (Millipore, Darmstadt, Germany) diluted (1:1000) in a solution containing PBS-X, 1 % BSA and 10 % goat serum for at least 24 h under mild shaking at 4 °C. Washing sections in 1XPBS was followed by incubation with the secondary antibody (donkey anti-mouse Alexa Fluor 488, Technologies, Darmstadt, Germany) diluted (1:500) in PBS-X and 2 % goat serum for at least 24 h in the dark. Finally, sections were mounted on gelatine coated glass slides with Fluoromount mounting medium.

An epifluorescence microscope (DM5500B, Leica Microsystems, Mannheim, Germany) equipped with a camera was used to acquire z-stacks of immunofluorescently labelled sections. Fluorophores were excited using the appropriate filter cubes (Alexa 488: L5, tdTomato: N3). Fluorescent images were acquired with a 100x oil-immersion objective. NeuN+ and Scnn1a+ neurons were counted in z-stacks of genital and hindpaw cortex layer 4 (xyz: 100 x 200 x 40 µm, 1 µm z-spacing) using the ROI-manager in ImageJ.

QUANTIFICATION AND STATISTICAL ANALYSIS

Data were analyzed in MATLAB (MathWorks, Natick, MA) and are shown as mean ± SEM. The sample size (n) refers to either mice, neurons or hemispheres. Details are provided where appropriate. To quantify the overall increase in the Scnn1a+ neurons in Figure 2E, we applied the MATLAB gradient function to the increase for each mouse plotted in Figure 2D. This function provides the gradient at each time point. These values (both positive and negative) were then averaged to provide the mean slope. Data was tested for normality using the Lilliefors test. Normally distributed data was compared using an unpaired t-test or an ANOVA for comparing two or more groups respectively. Non-normally distributed data were analyzed using Rank-Sum or Kruskal-Wallis tests. Differences were considered statistically significant when $p < 0.05$. Posthoc pairwise comparisons were performed using the Tukey-Kramer approach.

DATA AND CODE AVAILABILITY

Raw two-photon data imaging data have not been deposited in a publicly available repository due to file size, but all relevant data and code for this study can be made available by the Lead Contact Michael Brecht, michael.brecht@bccn-berlin.de upon reasonable request.

4.6 References

1. Van Der Loos, H., and Woolsey, T.A. (1973). Somatosensory cortex: Structural alterations following early injury to sense organs. Science *179*, 395–398.
2. Agmon, A., Yang, L., Jones, E., and O'Dowd, D. (2018). Topological precision in the thalamic projection to neonatal mouse barrel cortex. J. Neurosci. *15*, 549–561.
3. S.Erzurumlu, R., Jhaveri, S., Erzurumlu, R., and Jhaveri, S. (1990). Thalamic axons confer a blueprint of the sensory periphery onto the developing rat somatosensory cortex. Dev. Brain Res. *56*, 229–234.
4. Feldman, D.E., and Brecht, M. (2005). Map plasticity in somatosensory cortex (American Association for the Advancement of Science).
5. Lenschow, C., Copley, S., Gardiner, J.M.M., Talbot, Z.N.N., Vitenzon, A., Brecht, M., and Correspondence, M.B. (2016). Sexually Monomorphic Maps and Dimorphic Responses in Rat Genital Cortex. Curr. Biol. *26*, 106–113.
6. Lenschow, C., Sigl-Glöckner, J., and Brecht, M. (2017). Development of rat female genital cortex and control of female puberty by sexual touch. PLoS Biol. *15*, 1–22.
7. Lauer, S.M., Lenschow, C., and Brecht, M. (2017). Sexually selected size differences and conserved sexual monomorphism of genital cortex. J. Comp. Neurol. *525*, 2706–2718.
8. Bronson, F.H., and Maruniak, J.A. (1975). Male-induced puberty in female mice: Evidence for a synergistic action of social cues. Biol. Reprod. *13*, 94–98.
9. Kaas, J. (1991). Plasticity Of Sensory And Motor Maps In Adult Mammals. Annu. Rev. Neurosci. *14*, 137–167.
10. Gennari, F. (1782). De peculiari structura cerebri nonnullisque ejus morbis (Ex Regio Typographeo).
11. Woolsey, C.N., and Fairman, D. (1946). Contralateral, ipsilateral, and bilateral representation of cutaneous receptors in somatic areas I and II of the cerebral cortex of pig, sheep, and other mammals. Surgery *19*, 684–702.
12. Pouchelon, G., Gambino, F., Bellone, C., Telley, L., Vitali, I., Lüscher, C., Holtmaat, A., and Jabaudon, D. (2014). Modality-specific thalamocortical inputs instruct the identity of postsynaptic L4 neurons. Nature *511*, 471–474.
13. Moreno-Juan, V., Filipchuk, A., Antón-Bolaños, N., Mezzera, C., Gezelius, H., Andrés, B., Rodríguez-Malmierca, L., Susín, R., Schaad, O., Iwasato, T., *et al*. (2017). Prenatal thalamic waves regulate cortical area size prior to sensory processing. Nat. Commun. *8*, 14172.
14. Li, H., Fertuzinhos, S., Mohns, E., Hnasko, T.S.S., Verhage, M., Edwards, R., Sestan, N., and Crair, M.C.C. (2013). Laminar and Columnar Development of Barrel Cortex Relies on Thalamocortical Neurotransmission. Neuron *79*, 970–986.
15. Staiger, J.F., Flagmeyer, I., Schubert, D., Zilles, K., Kötter, R., and Luhmann, H.J. (2004). Functional diversity of layer IV spiny neurons in rat somatosensory cortex: Quantitative morphology of electrophysiologically characterized and biocytin labeled cells. Cereb. Cortex *14*, 690–701.
16. Scala, F., Kobak, D., Shan, S., Bernaerts, Y., Laturnus, S., Cadwell, C.R.C.R., Hartmanis, L., Castro, J., Tan, Z.H.Z.H., Sandberg, R., *et al*. (2018). Neocortical layer 4 in adult mouse differs in major cell types and circuit organization between primary sensory areas. bioRxiv, 507293.

17. Elston, G.N., Pow, D. V., and Calford, M.B. (1997). Neuronal composition and morphology in layer IV of two vibrissal barrel subfields of rat cortex. Cereb. Cortex *7*, 422–431.

18. Callaway, E.M., and Borrell, V. (2011). Developmental Sculpting of Dendritic Morphology of Layer 4 Neurons in Visual Cortex: Influence of Retinal Input. J. Neurosci. *31*, 7456–7470.

19. Klingler, E., Rossa, A. De, Devaraju, K., Abe, P., Jabaudon, D., Devaraju, K., Abe, P., Jabaudon, D., De la Rossa, A., Fièvre, S., *et al*. (2018). A Translaminar Genetic Logic for the Circuit Identity of Intracortically Projecting Neurons Report A Translaminar Genetic Logic for the Circuit Identity of Intracortically Projecting Neurons. Curr. Biol. *29*, 1–8.

20. Vue, T.Y., Lee, M., Tan, Y.E., Werkhoven, Z., Wang, L., and Nakagawa, Y. (2013). Thalamic Control of Neocortical Area Formation in Mice. J. Neurosci. *33*, 8442–8453.

21. Madisen, L., Zwingman, T.A., Sunkin, S.M., Oh, S.W., Zariwala, H.A., Gu, H., Ng, L.L., Palmiter, R.D., Hawrylycz, M.J., Jones, A.R., *et al*. (2010). A robust and high-throughput Cre reporting and characterization system for the whole mouse brain. Nat. Neurosci. *13*, 133–140.

22. De La Rossa, A., Bellone, C., Golding, B., Vitali, I., Moss, J., Toni, N., Lüscher, C., and Jabaudon, D. (2013). In vivo reprogramming of circuit connectivity in postmitotic neocortical neurons. Nat. Neurosci. *16*, 193–200.

23. Oishi, K., Aramaki, M., and Nakajima, K. (2016). Mutually repressive interaction between Brn1/2 and Rorb contributes to the establishment of neocortical layer 2/3 and layer 4. Proc. Natl. Acad. Sci. *113*, 3371–3376.

24. Bozrm, M., and Kontula, O. (2014). Sexual initiation and gender in Europe: A cross-cultural analysis of trends in the twentieth century. Sex. Behav. HIV/AIDS Eur. Comp. Natl. Surv., 37.

25. Simon, W. (2017). Sexual conduct: The social sources of human sexuality (Routledge).

26. Lein, E.S., Hawrylycz, M.J., Ao, N., Ayres, M., Bensinger, A., Bernard, A., Boe, A.F., Boguski, M.S., Brockway, K.S., Byrnes, E.J., *et al*. (2007). Genome-wide atlas of gene expression in the adult mouse brain. Nature *445*, 168–76.

27. Palmer, L.M., Schulz, J.M., Murphy, S.C., Ledergerber, D., Murayama, M., and Larkum, M.E. (2012). The Cellular Basis of GABAB-Mediated Interhemispheric Inhibition. Science *335*, 989–993.

28. Grinvald, A., Lieke, E., Frostig, R.D., Gilbert, C.D., and Wiesel, T.N. (1986). Functional architecture of cortex revealed by optical imaging of intrinsic signals. Nature *324*, 361–364.

29. DiVall, S.A., Williams, T.R., Carver, S.E., Koch, L., Brüning, J.C., Kahn, C.R., Wondisford, F., Radovick, S., and Wolfe, A. (2010). Divergent roles of growth factors in the GnRH regulation of puberty in mice. J. Clin. Invest. *120*, 2900–2909.

30. Safranski, T., Lamberso, W.R., and Keisler, D.H. (2005). Correlations among Three Measures of Puberty in Mice and Relationships with Estradiol Concentration and Ovulation1. Biol. Reprod. *48*, 669–673.

31. Falconer, D.S. (1984). Weight and age at puberty in female and male mice of strains selected for large and small body size. Genet. Res. *44*, 47–72.

32. Gaytan, F., Morales, C., Leon, S., Heras, V., Barroso, A., Avendaño, M.S., Vazquez,

M.J., Castellano, J.M., Roa, J., and Tena-Sempere, M. (2017). Development and validation of a method for precise dating of female puberty in laboratory rodents: The puberty ovarian maturation score (Pub-Score). Sci. Rep. *7*, 46381.

33. Brecht, M., and Sakmann, B. (2002). Dynamic representation of whisker deflection by synaptic potentials in spiny stellate and pyramidal cells in the barrels and septa of layer 4 rat somatosensory cortex. J. Physiol. *543*, 49–70.

34. Guillamon-Vivancos, T., Tyler, W.A., Medalla, M., Chang, W.W., Okamoto, M., Haydar, T.F., and Luebke, J.I. (2018). Distinct Neocortical Progenitor Lineages Fine-tune Neuronal Diversity in a Layer-specific Manner. Cereb. Cortex *29*, 1–18.

35. Antón-Bolaños, N., Espinosa, A., and López-Bendito, G. (2018). Developmental interactions between thalamus and cortex: a true love reciprocal story. Curr. Opin. Neurobiol. *52*, 33–41.

36. Simi, A., and Studer, M. (2018). Developmental genetic programs and activity-dependent mechanisms instruct neocortical area mapping. Curr. Opin. Neurobiol.

37. Han, S.H., and Lee, S.-H. (2014). Differential Growth of the Reproductive Organs during the Peripubertal Period in Male Rats. Dev. Reprod. *17*, 469–75.

38. Tomova, A., Deepinder, F., Robeva, R., Lalabonova, H., Kumanov, P., and Agarwal, A. (2010). Growth and development of male external genitalia: A cross-sectional study of 6200 males aged 0 to 19 years. Arch. Pediatr. Adolesc. Med. *164*, 1152–1157.

39. Lenschow, C., and Brecht, M. (2015). Barrel Cortex Membrane Potential Dynamics in Social Touch. Neuron *85*, 718–725.

40. Bobrov, E., Wolfe, J., Rao, R.P., and Brecht, M. (2014). The representation of social facial touch in rat barrel cortex. Curr. Biol. *24*, 109–115.

41. Ishiyama, S., and Brecht, M. (2016). Neural correlates of ticklishness in the rat somatosensory cortex. Science *354*, 757–760.

42. Schulz, K.M., and Sisk, C.L. (2016). The organizing actions of adolescent gonadal steroid hormones on brain and behavioral development. Neurosci. Biobehav. Rev. *70*, 148–158.

43. Sisk, C.L., and Zehr, J.L. (2005). Pubertal hormones organize the adolescent brain and behavior. Front. Neuroendocrinol.

44. Adler, N.T., Davis, P.G., and Komisaruk, B.R. (1977). Variation in the size and sensitivity of a genital sensory field in relation to the estrous cycle in rats. Horm. Behav. *9*, 334–44.

45. Greenlee, M.M., Mitzelfelt, J.D., Yu, L., Yue, Q., Duke, B.J., Harrell, C.S., Neigh, G.N., and Eaton, D.C. (2013). Estradiol activates epithelial sodium channels in rat alveolar cells through the G protein-coupled estrogen receptor. Am. J. Physiol. Cell. Mol. Physiol. *305*, L878-89.

46. Yusef, Y.R., Thomas, W., and Harvey, B.J. (2014). Estrogen increases ENaC activity via PKCδ signaling in renal cortical collecting duct cells. Physiol. Rep. *2*, e12020.

47. Yang, G.Z., Nie, H.G., Lu, L., Chen, J., Lu, X.Y., Ji, H.L., and Li, Q.N. (2011). Estrogen regulates the expression and activity of epithelial sodium channel in mouse osteoblasts. Cell. Mol. Biol. *57 Suppl*, OL1480-6.

48. Kim, J.-Y., Grunke, S.D., Levites, Y., Golde, T.E., and Jankowsky, J.L. (2014). Intracerebroventricular Viral Injection of the Neonatal Mouse Brain for Persistent and Widespread Neuronal Transduction. J. Vis. Exp., 1–7.

49. Pachitariu, M., Stringer, C., Dipoppa, M., Schröder, S., Rossi, L.F., Dipoppa, M., Rossi, L.F., Carandini, M., Harris, K.D., Callaway, E.M., *et al*. (2016). Suite2p : beyond 10 , 000 neurons with standard two-photon microscopy. bioRxiv *53*, 639–647.

50. Takahashi, N., Oertner, T.G., Hegemann, P., and Larkum, M.E. (2016). Active cortical dendrites modulate perception. Science *354*, 1587–1590.

51. Judkewitz, B., Rizzi, M., Kitamura, K., and Häusser, M. (2009). Targeted single-cell electroporation of mammalian neurons in vivo. Nat. Protoc. *4*, 862–869.

4.7 Figures

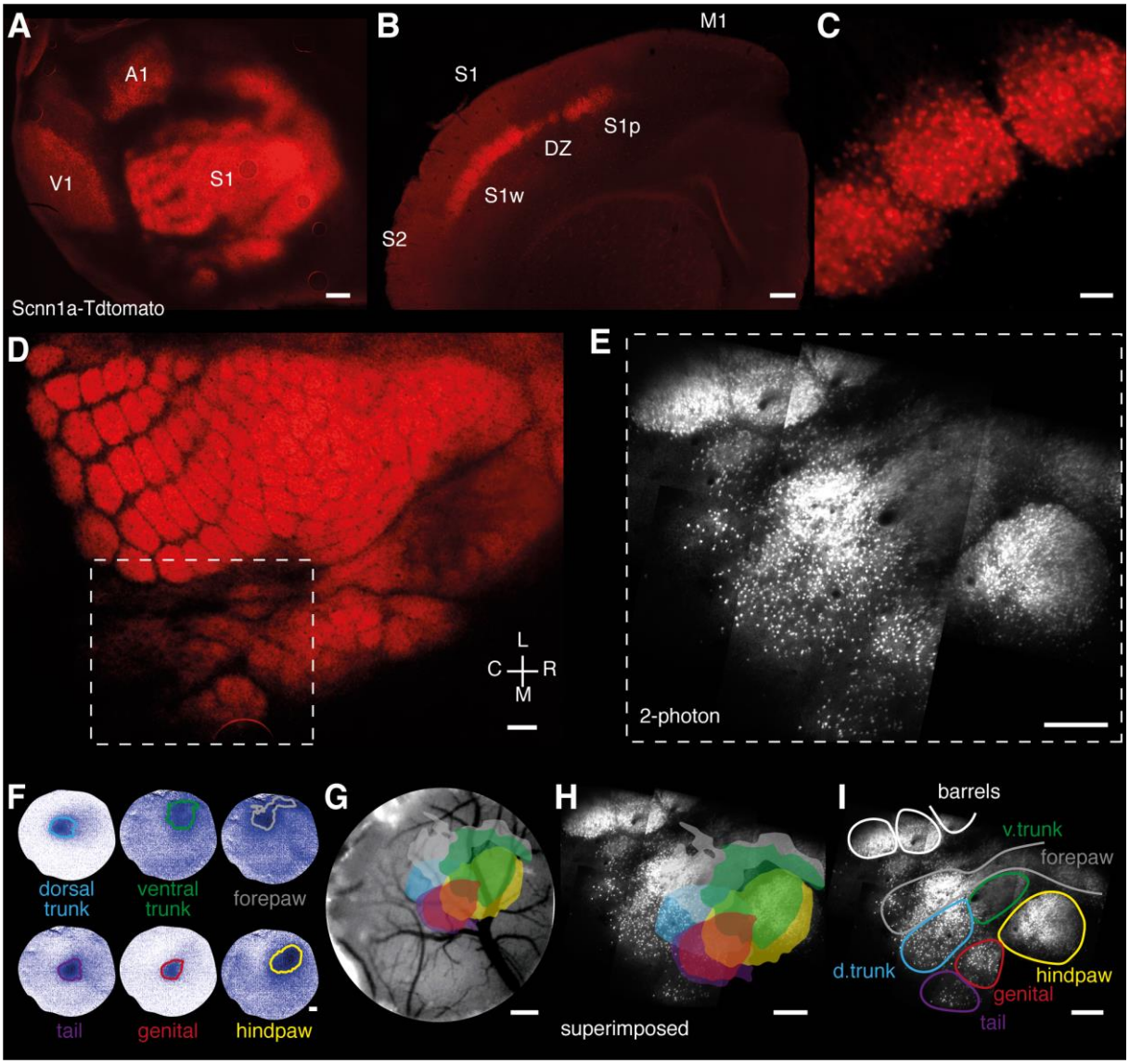

Figure 1. Mapping Scnn1a-expression and genital cortex in Scnn1a-tdTomato mice.

A) Scnn1a-tdTomato tangential section. Scnn1a expression is dense in primary somatosensory (S1), auditory (A1) and visual (V1) cortex. Scale bar = 500 µm.

B) Scnn1a-tdTomato coronal section. Scnn1a expression is high in L4 whisker (S1w) and paw barrels (S1p), but low in the dysgranular zone (DZ), primary motor cortex (M1), secondary somatosensory cortex (S2) and non-layer 4 cells. Scale bar = 250 µm.

C) Within L4 Scnn1a+ neurons are confined to barrels and are absent from septa between barrels. Scale bar = 50 µm.

D) Scnn1a-tdTomato tangential section. Scnn1a expression reveals the S1 homunculus (male, P25). Scale bar = 250 µm.

E) The region of S1 highlighted by the dashed box in panel D imaged using two-photon microscopy. Multiple z-stacks were acquired at minimal magnification (1065 µm x 1065 µm) and tiled together. Scale bar = 250 µm.

F) Intrinsic imaging (male, P25) revealed S1 subfields (dark blue) on the surface of the craniotomy representing the dorsal and ventral trunk, forepaw, tail, genital and hindpaw. Scale bar = 250 µm.

G) Regions circled in panel F were aligned to each other based on the blood vessel pattern on the surface of the craniotomy. Scale bar = 250 μm.
H) Superimposing intrinsically mapped body parts (F, G) onto the expression of Scnn1a+ neurons in L4 of S1 as shown in panel E based on the blood vessel pattern. The topographic arrangement of subfields revealed by intrinsic imaging aligns with Scnn1a+ dense areas in L4. Scale bar = 250 μm.
I) Based on the alignment in panel H, we infer that the barrel-like subfields of Scnn1a+ neurons within L4 represent the mapped body parts as shown. Scale bar = 250 μm. See also Figure S1.

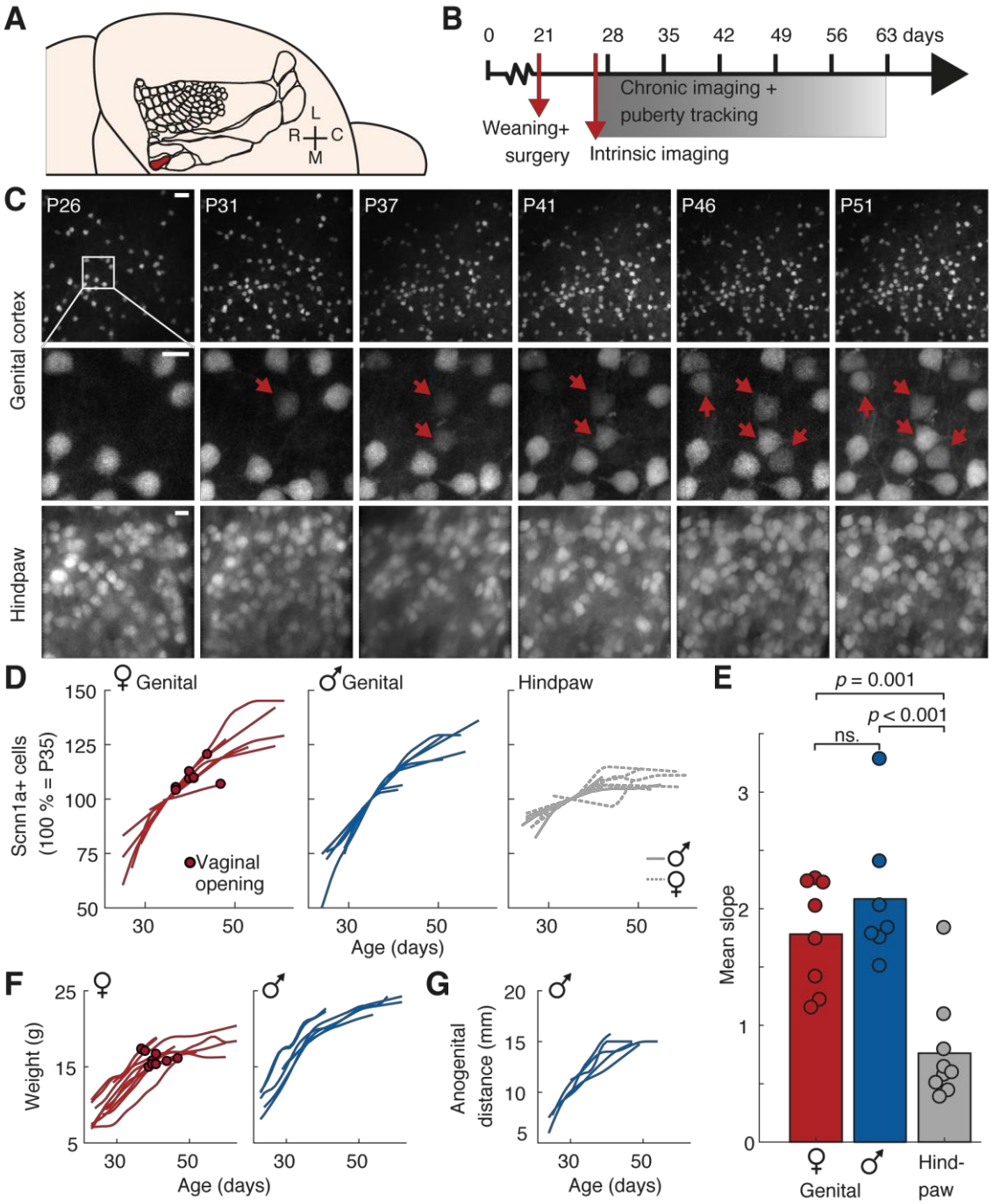

Figure 2. The number of Scnn1a+ neurons increases in genital cortex during puberty.

A) Schematic of the somatosensory homunculus and genital cortex (red).

B) Experimental timeline for chronic imaging experiments. Mice undergo two-photon imaging sessions every 4 to 7 days.

C) Two-photon stacks capturing Scnn1a+ neurons in the same field of view in genital cortex (top) and hindpaw cortex (bottom) between P26 and P51 (from left to right). In genital cortex additional Scnn1a+ neurons appear over time (middle, arrows). Scale bars: 20 µm (top) and 10 µm (middle, bottom). Arrows mark newly appearing Scnn1a+ neurons.

D) Scnn1a+ neurons were counted in stacks of genital cortex and hindpaw cortex. Counts are expressed as P35 = 100 %. Resulting relative counts increase steeply in female (left, n = 8) and male genital cortex (middle, n = 7) compared to hindpaw cortex (right, grey, n = 9).

E) The average slope was calculated for each line in D. The slope of cell counts was greater for female (n = 8, 1.78 ± 0.47) and male (n = 7, 2.30 ± 0.69) genital cortex, compared to hindpaw cortex (n = 9, 0.76 ± 0.45, ANOVA, $F(2,21) = 17.2$, $p = 3.73 \times 10^{-5}$, superscripted p-values indicate Tukey-Kramer posthoc comparisons).
F) During chronic imaging experiments, weight of females increased from approximately 8 g to 20 g (left, n = 10) while males reached up to 23 g (right, n = 8).
G) In males, the anogenital distance increased from 7 mm pre puberty to 16 mm post puberty (n = 5).

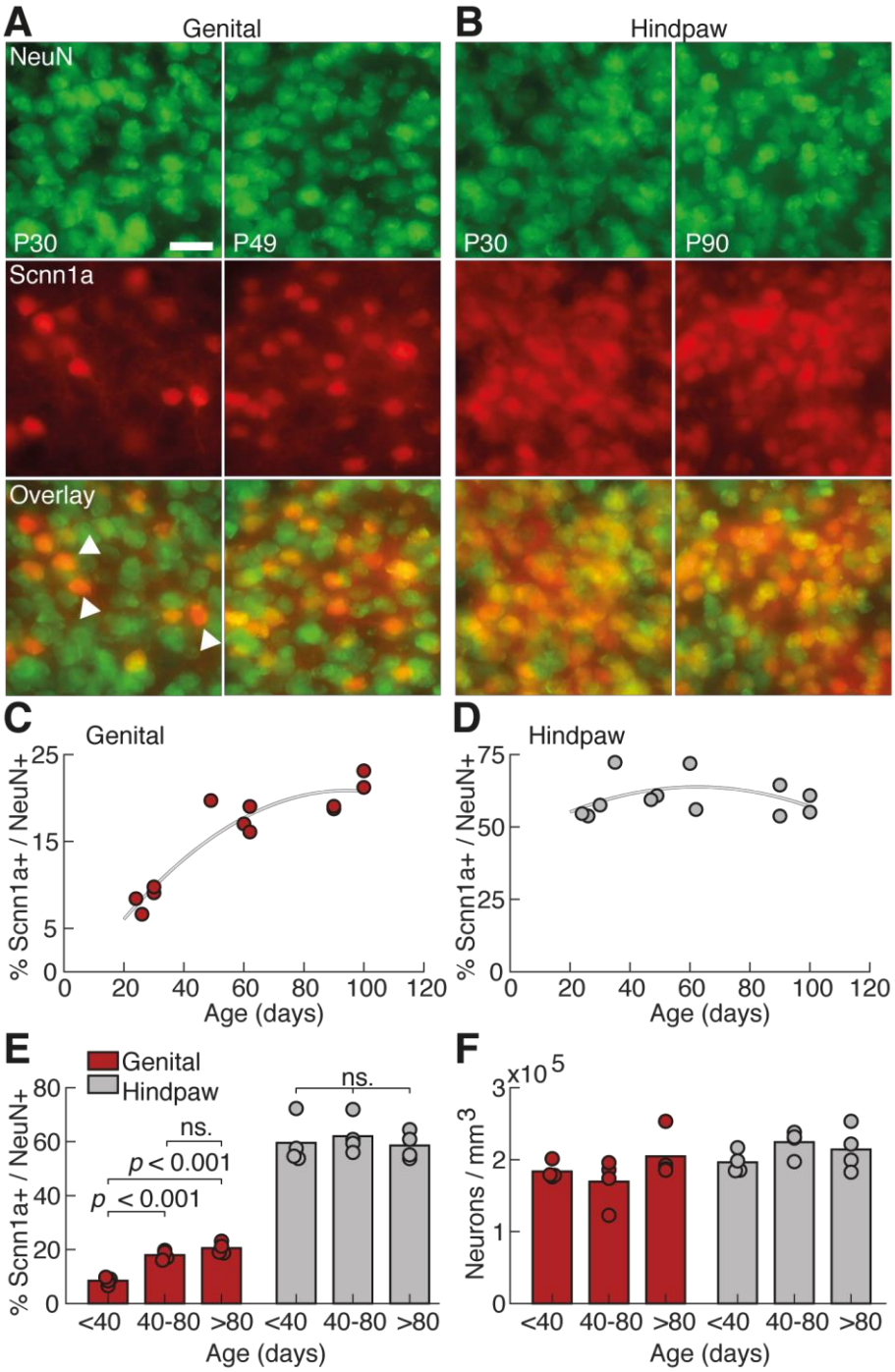

Figure 3. Genital cortex Scnn1a+ expression increases while neurons density remains stable.

A) Tangential Scnn1a-tdTomato sections (40 µm) of genital cortex layer 4. Sections were stained against NeuN (top, green) to reveal the density of Scnn1a+ neurons (red, middle) relative to all NeuN+ neurons. Scnn1a+ neurons appear as orange in the overlay (white arrows, bottom). Left: pre puberty (P30), right: post puberty (P49).

B) Same as panel A but for hindpaw cortex. Left: pre puberty (P30), right: post puberty (P90). Scale bar (A,B) = 25 µm.

C) The number of Scnn1a+ neurons relative to all NeuN+ neurons counted in z-stacks of genital cortex plotted against age (days), n = 12 hemispheres. Grey = polynomial fit line.

D) Same as panel C for hindpaw cortex, n = 12 hemispheres.

E) Data shown in panel C and D binned into three age groups (< P40, P40 to P80, > P80). Left: genital cortex (red), right: hindpaw cortex (grey). P-values indicate Tukey-Kramer pairwise comparisons between age groups.
F) Neuron density per 1 mm^3 for hemispheres shown in panels C and D. Left: genital cortex (red), right: hindpaw cortex (grey).

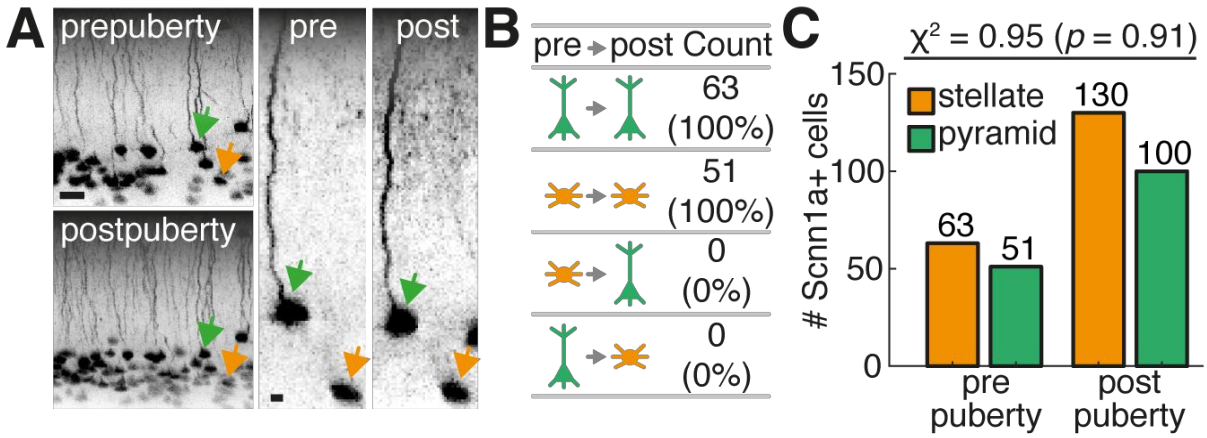

Figure 4. No evidence for a loss of apical dendrites in pubertal development of Scnn1a+ neuron.

A) Structural stacks (xyz: 133 x 133 x 400 µm, 2 µm z-spacing) of Scnn1a+ neurons in genital cortex were vertically reconstructed to reveal dendritic morphology. Stacks of the same FOV were compared pre and post puberty in 5 mice. There are fewer fluorescent cells pre puberty (left, top) compared to post puberty (left, bottom). Stellate cells (no apical dendrite, orange arrows) remain stellate cells and pyramidal cells (with apical dendrite, green arrows) remain pyramidal cells. The same cells are shown at a higher magnification on the right. Scale bars: 50 µm (left) and 10 µm (right).

B) Scnn1a+ neurons were reconstructed in 5 pre and 5 post pubertal stacks and identified as stellate or pyramidal shaped. All neurons that were captured before puberty (63 pyramids and 51 stellates in 5 mice) retained their original morphology. No cell underwent a conversion from either stellate to pyramid or vice versa during puberty.

C) There were slightly more stellates (orange) than pyramids (green) both before (left) and after puberty (right). The number of both stellates and pyramids approximately doubled during puberty. There was no association between age and cell type (Fisher's exact test, $\chi^2 = 0.95$, $p = 0.91$).

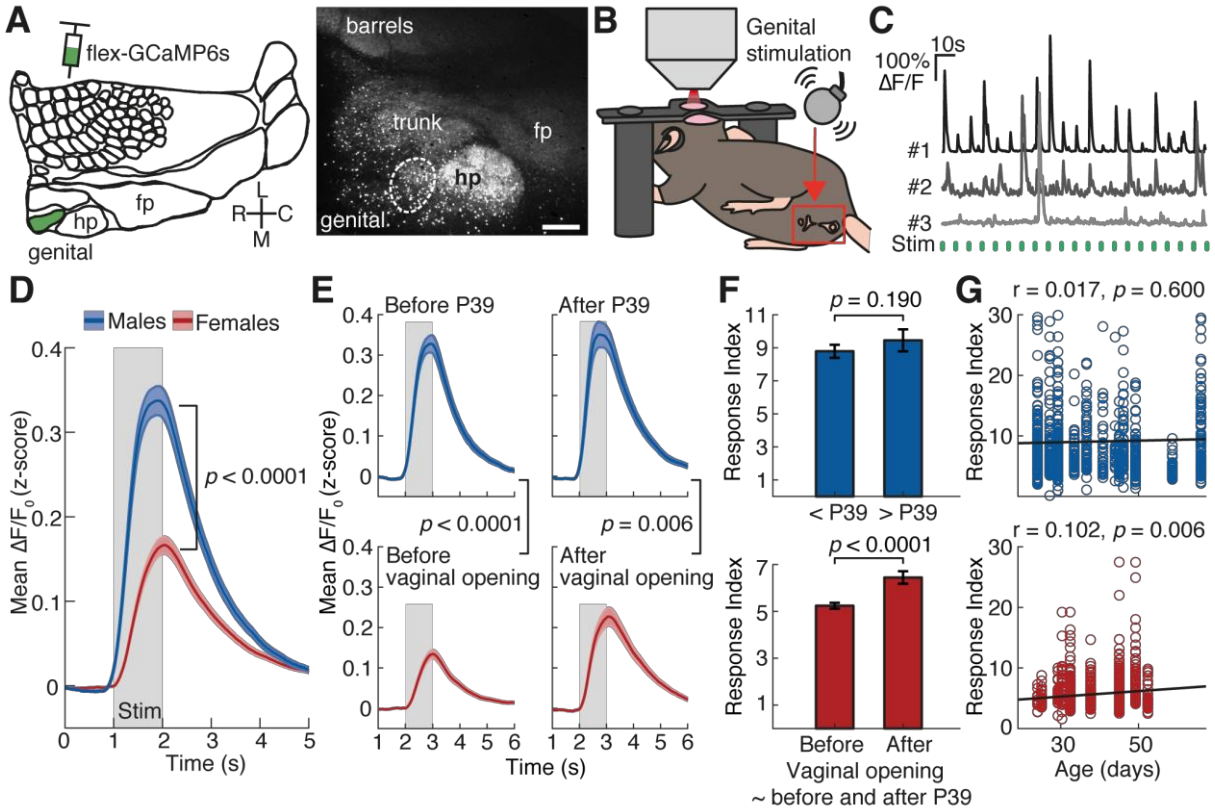

Figure 5. Calcium imaging reveals sex and development responses in genital cortex.

A) GCaMP expression in S1 of Scnn1a-cre mice. Scale bar = 250 µm.

B) Genitals were stimulated with a small vibration motor during Ca^{2+} imaging.

C) Example Ca^{2+} traces. #1: Strongly responding, #2: weakly responding, #3: non-responding. Stimulation = green.

D) Average evoked Ca^{2+} response in males (blue, 990 neurons) and in females (red, 734 neurons). Shown is the mean (line) and SEM (shaded) of the mean responses of all cells. Response indices (RI, see methods) were greater for males than for females (Rank-Sum test, Z = 10.2, p = 2.74 x 10^{-24}).

E) Same as D, split according to age at vaginal opening for females (red). Mean age at vaginal opening (P39) was used as approximation for puberty in males (blue). Prepubertal male neurons (top left, 551 neurons) responded more strongly to genital stimulation than female neurons (bottom left, 465 neurons, Rank-Sum test, Z = 10.9, p = 1.04 x 10^{-27}). This was also true after puberty (right, males: 418 neurons vs. females 255 neurons, Rank-Sum test, Z = 2.77, p = 0.006).

F) RIs for males (top) and females (bottom) before and after putative puberty onset. The mean RI increased marginally for males (Rank-Sum test, Z = 1.31, p = 0.190) but strongly for females (Rank-Sum test, Z = -4.78, p = 1.74 x 10^{-6}).

G) Males (top) and female (bottom) genital response indices as a function of age. See also Figure S2.

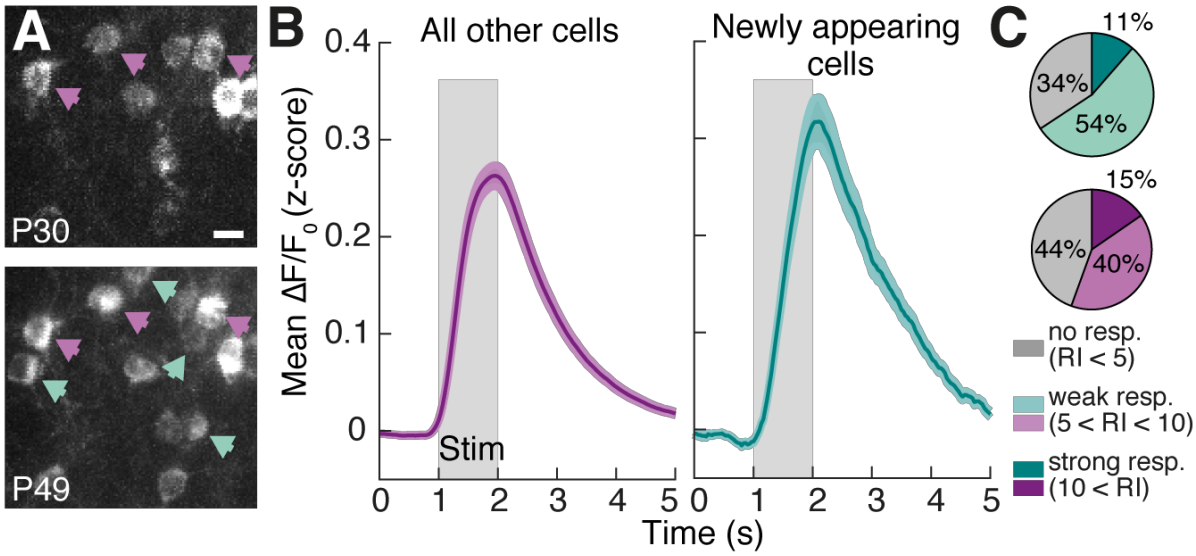

Figure 6. Newly appearing Scnn1a+ neurons respond to genital stimulation.

A) Maximum projection of two-photon micrographs of Scnn1a+ neurons in genital cortex expressing GCaMP6s acquired before puberty (P25, top) and after puberty (P49, bottom). In contrast to neurons which can be identified at both time points (purple arrows), there are some neurons appearing as Scnn1a+ at P49, which were not visible at P25 (green arrows, bottom). Scale bar = 20 μm.

B) Mean evoked responses of newly appearing Scnn1a+ neurons (right, 28 neurons in 4 mice) and all other imaged neurons (right, 1689 neurons in 10 mice) to genital stimulation (grey). For each cell the mean z-scored $\Delta F/F_0$ was computed across trials. Shown is the mean (line) and SEM (shaded) of these mean responses of each cells.

C) The evoked responses of newly appearing neurons (green) and all other neurons (purple) were classified into three categories according to their RI. Strongly responding: 10 < RI (dark green/purple), weakly responding: 5 < RI < 10 (light green/purple) or non-responding: RI < 5 (grey).

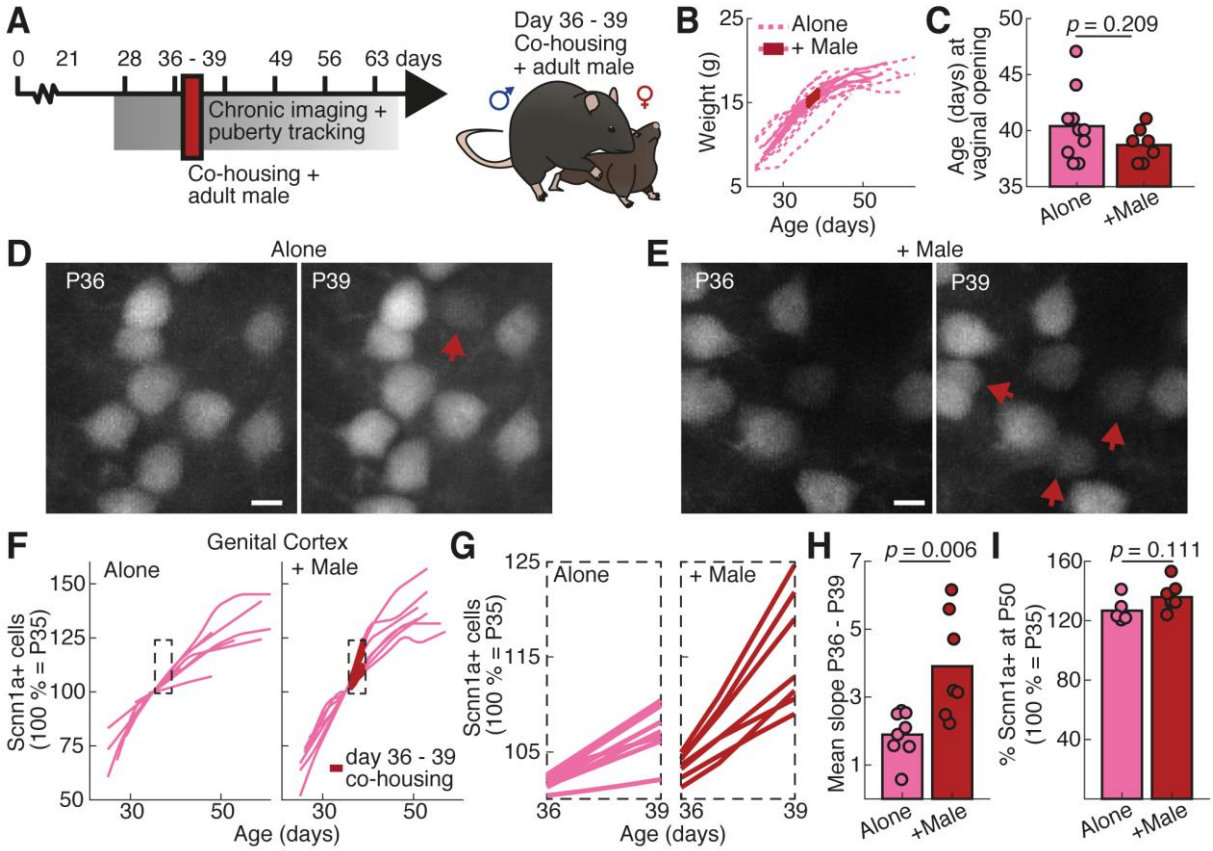

Figure 7. Co-housing prepubertal females with adult male mice advances the gain of Scnn1a+ neurons in genital cortex.

A) Prepubertal females were co-housed with adult males, when females were between 36 and P39. Chronic imaging was performed as before (Figure 2).

B) Females sitting alone (dashed pink, n = 10) and females co-housed with males (solid pink, n = 7) gained weight at a similar rate. Co-housing started when female mice reached 15g and continued for three days (red).

C) Age at vaginal opening was slightly but not significantly advanced in co-housed females (+ Male, red, n = 7, 38.7 ± 1.5 vs. Alone, pink, n = 8, 40.4 ± 3.1, unpaired t-test, p = 0.209).

D) Scnn1a+ neurons in females sitting alone on P36 (left) and P39 (right). Arrows mark newly appearing Scnn1a+ neurons. Scale bar = 10 µm.

E) Same as (D) for females co-housed with adult males. Scale bar = 10 µm.

F) Scnn1a+ neurons in genital cortex (P35 = 100 %) of females sitting alone (left, n = 8, same as Figure 2D) and females co-housed with males (right, n = 7). Days of co-housing = red.

G) Magnification of dashed boxes in (D). The gain of Scnn1a+ neurons is greater in females sitting with a male (right) compared to females sitting alone (left).

H) Between P36 and P39 the mean slope of Scnn1a+ cell counts is smaller for single housed females (left, n = 8, 1.89 ± 0.69) compared to co-housed females (right, n = 7, 3.91 ± 1.60, unpaired p = 0.006).

I) At P50 relative Scnn1a+ cell counts of females sitting alone (left) and females co-housed with males (right) are not different (unpaired t-test, p = 0.111).

See also Figure S3.

4.8 Supplementary Figures

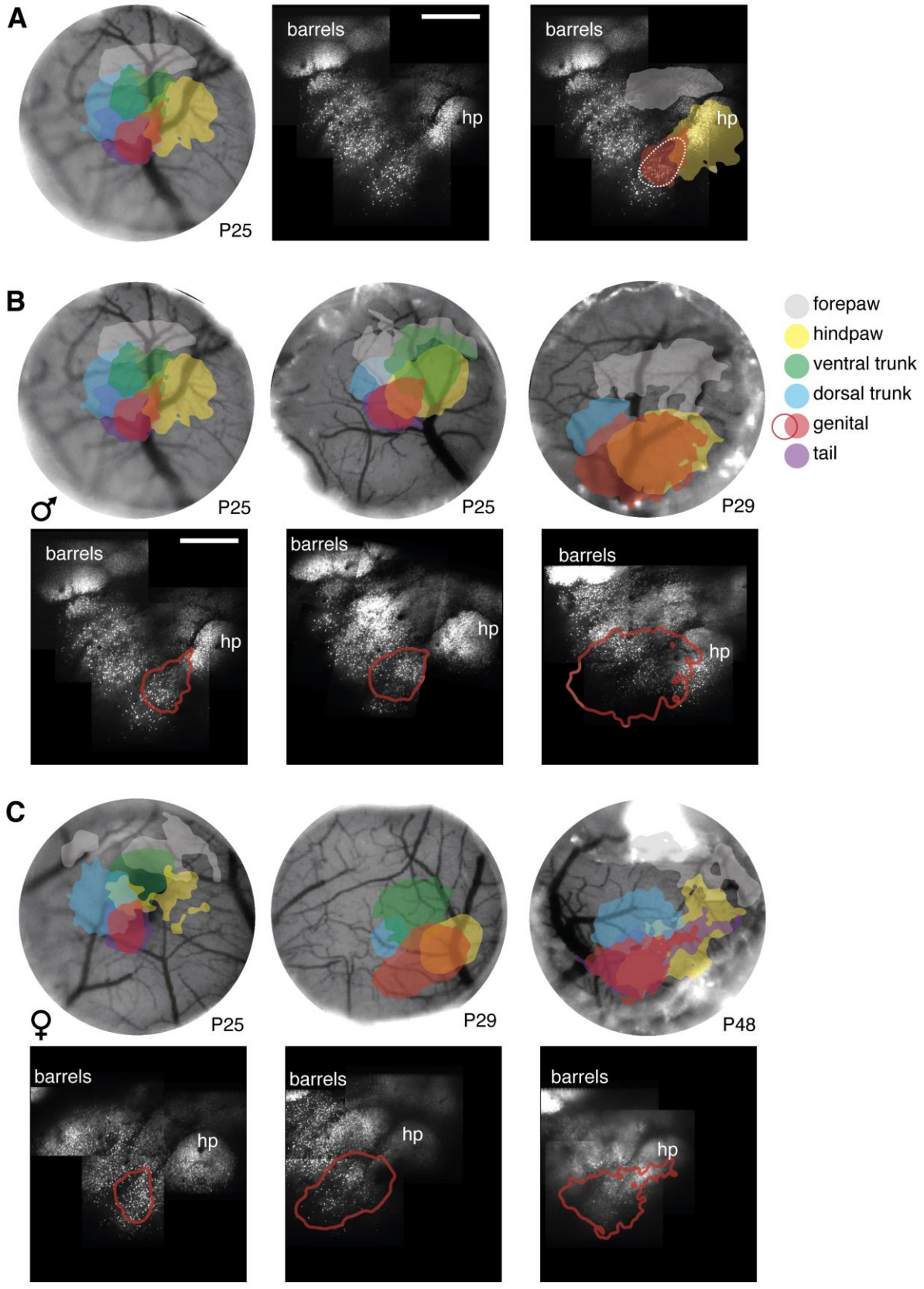

Figure S1. Intrinsically identified somatosensory subfields consistently map onto Scnn1a dense areas in layer 4. Related to Figure 1.

A) Left: Intrinsically identified areas that respond to the stimulation of the forepaw (grey), hindpaw (yellow), ventral trunk (green), dorsal trunk (blue), genital (red) and tail (purple), overlaid onto the blood vessel pattern on the surface of the circular craniotomy of a male mouse (P25). Middle: Pattern of the underlying Scnn1a+ expression in layer 4 of the same mouse. Barrels and hindpaw cortex (hp) are labelled. Right: Fields identified for the genital (red) and hindpaw (yellow) aligned with the expression of Scnn1a in layer 4. White dashed: inferred genital field that is later imaged for cell number quantification. is Scale bar = 500 μm.

B) Intrinsic imaging results for three male mice (P25, P25 and P29). Intrinsically mapped fields are first superimposed on the craniotomy (top) and then aligned with the expression of Scnn1a in layer 4 based on the blood vessel patterns (bottom). Here we only mark the genital (red) for visibility. Scale bar = 500 μm.

C) Same as panel B for three female mice (P25, P29 and P48).

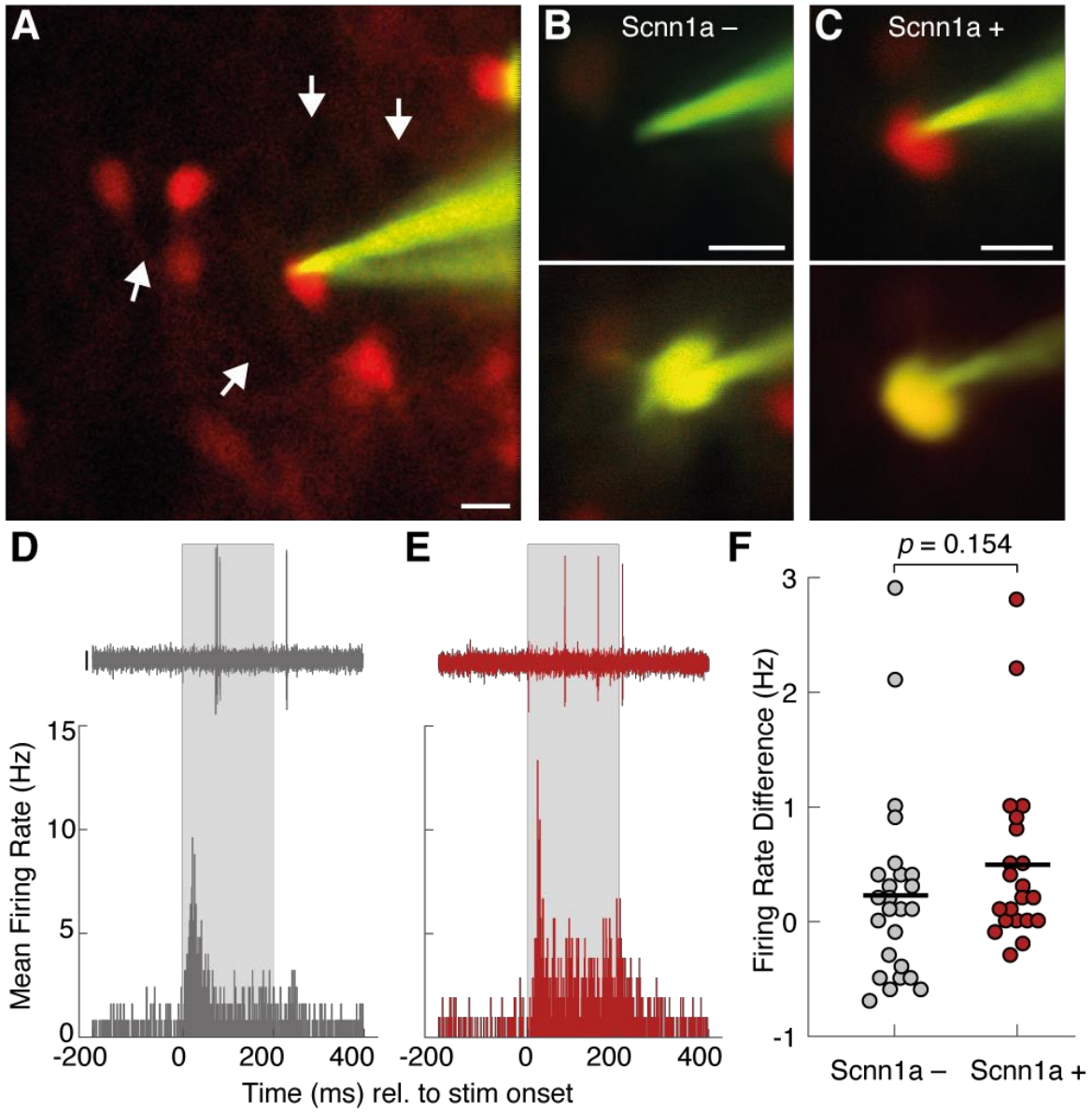

Figure S2. Two-photon targeted juxtacellular recordings reveal similar sensory evoked responses of Scnn1a+ and Scnn1a– neurons. Related to Figure 5.

A) Juxtacellular recordings were performed in Scnn1a-tdTomato mice while stimulating the genital as shown in Figure 5. Two-photon microscopy was used to visualize Scnn1a+ neurons (red). The recording pipette was filled with Alexa Fluor 488 (green) to label recorded neurons. Scnn1a– neurons were identifiable as black holes within the red labelled neuropil (white arrows). Scale bar = 10 µm.

B) Two-photon micrographs of a Scnn1a– neuron during juxtacellular recoding (top, no fluorescence) and after labelling with Alexa Fluor 488 (bottom, green).

C) Two-photon micrographs of a Scnn1a+ neuron during juxtacellular recoding (top, red) and after electroporation with Alexa Fluor 488 (bottom, yellow).

D) Example trace (top) and mean firing rate depicted in a peristimulus-time histogram (1 ms bins) of all identified Scnn1a– neurons (bottom, n = 25). Time is expressed relative to the onset of genital stimulation, which lasted from 0 ms to 200 ms (shaded, grey). Scale bar = 1mV.

E) Same as panel (D) for Scnn1a+ neurons (n = 21).

F) The firing rate difference of identified Scnn1a– (left, grey) and Scnn1a+ (right, red) neurons is not significantly different (Kruskal-Wallis test, $p = 0.154$). Firing rate difference was calculated by subtracting the mean firing rate during the 200 ms preceding stimulus onset form the mean firing rate during genital stimulation (200 ms) for each cell. Black bars indicate the mean.

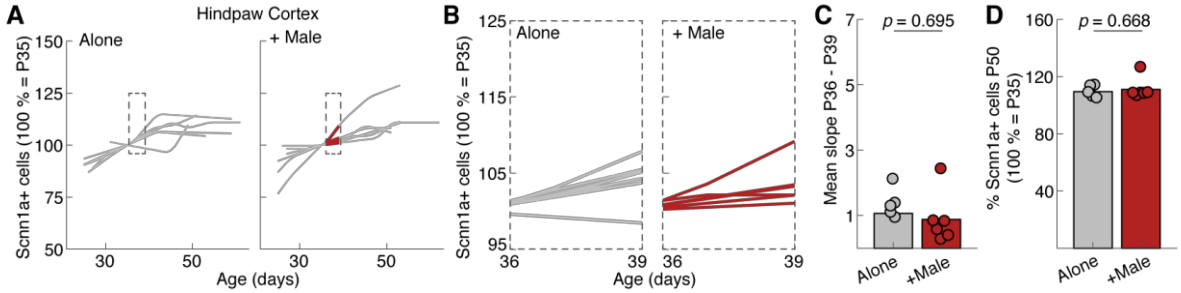

Figure S3. Co-housing prepubertal females with adult male mice does not affect the number of Scnn1a+ neurons in hindpaw cortex. Related to Figure 7.

D) Number of Scnn1a+ neurons counted in stacks of hindpaw cortex of females sitting alone (left, n = 6) and females co-housed with males (right, n = 7). Days of co-housing (P36 and P39) are marked in red.

E) High magnification of Scnn1a+ neuron counts between P36 and P39 as indicated by dashed boxes in (A).

F) In hindpaw cortex the slope of Scnn1a+ cell counts between P36 and P39, as shown in (B) is similar for single housed females (left, grey, n = 6, 1.06 ± 0.82) compared to co-housed females (right, red, n = 7, 0.88 ± 0.79, unpaired t-test p = 0.695).

G) At 50 days of age, relative Scnn1a+ cell counts in hindpaw cortex of females sitting alone (left, grey, 109 ± 4) and females co-housed with males (red, right, 111 ± 8) are also not different (unpaired t-test, p = 0.668).

5 Polyploidy in rat cortical layer 5

This work was originally published as:

Sigl-Glöckner J. & Brecht M. (**2017**) Polyploidy and the Cellular and Areal Diversity of Rat Cortical Layer 5 Pyramidal Neurons. *Cell Reports* 20.11: 2575-2583.
https://doi.org/10.1016/j.celrep.2017.08.069

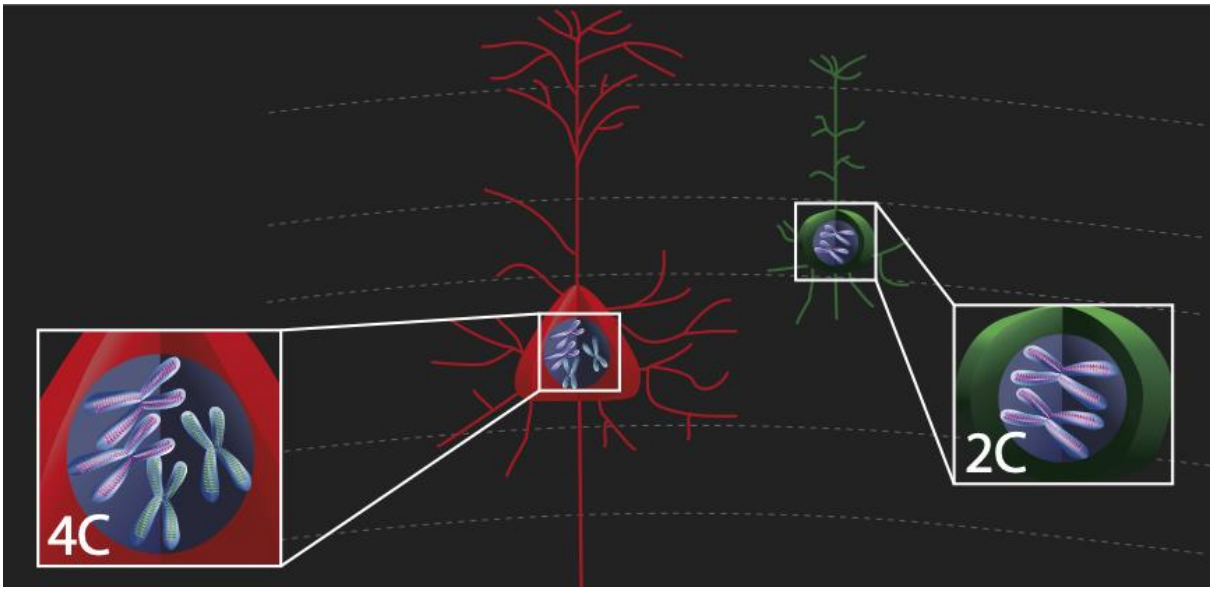

Figure 5. Illustration of cortical polyploidy.

Report

Cell Reports

Polyploidy and the Cellular and Areal Diversity of Rat Cortical Layer 5 Pyramidal Neurons

Graphical Abstract

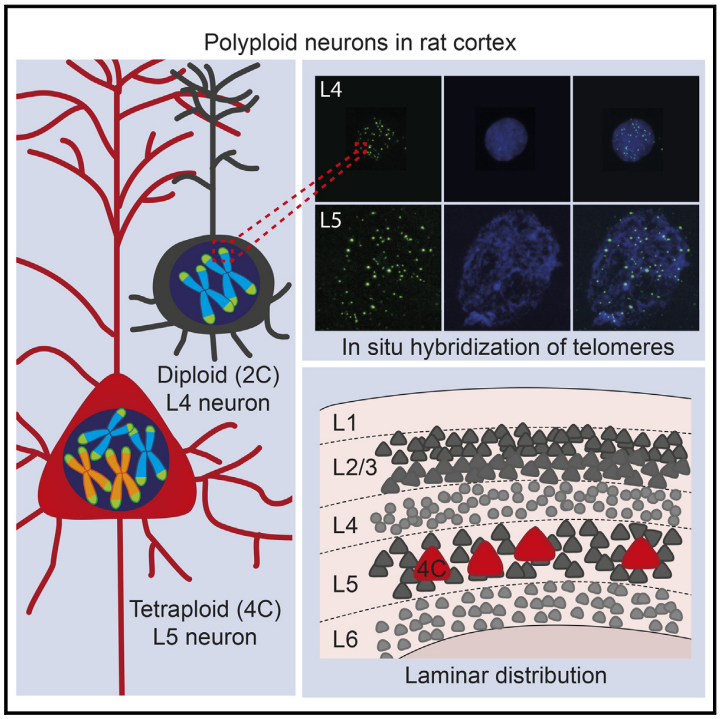

Authors

Johanna Sigl-Glöckner, Michael Brecht

Correspondence

michael.brecht@bccn-berlin.de

In Brief

Cortical principal cell diversity is poorly understood. Sigl-Glöckner and Brecht find that very large principal neurons in layer 5 of rat cortex are polyploid. Putatively tetraploid neurons are differentially distributed across cortical areas and functional subdivisions.

Highlights

- Integrated DAPI fluorescence and chromocenters report 2C jumps in ploidy
- We find putatively polyploid neurons only in layer 5
- The distribution of polyploid neurons varied across cortical areas
- In situ hybridization and flow cytometry also support cortical polyploidy

Sigl-Glöckner & Brecht, 2017, Cell Reports *20*, 2575–2583
September 12, 2017
http://dx.doi.org/10.1016/j.celrep.2017.08.069

Cell Reports
Report

Polyploidy and the Cellular and Areal Diversity of Rat Cortical Layer 5 Pyramidal Neurons

Johanna Sigl-Glöckner[1] and Michael Brecht[1,2,3,*]
[1]Bernstein Center for Computational Neuroscience, Humboldt University of Berlin, 10115 Berlin, Germany
[2]NeuroCure Cluster of Excellence, Humboldt University of Berlin, 10115 Berlin, Germany
[3]Lead Contact
*Correspondence: michael.brecht@bccn-berlin.de
http://dx.doi.org/10.1016/j.celrep.2017.08.069

SUMMARY

In many species, polyploidy, in which an increase in nuclear DNA content is accompanied by an increase in cell size, contributes to cellular diversity. In the rat visual cortex, most neurons are small and homogeneous in size, while layer 5 cells are heterogeneous, containing some very large neurons. To measure DNA content, we quantified nuclear chromocenters and integrated DNA/DAPI fluorescence. The results suggest that most cortical neurons, non-neuronal cells, parvalbumin-positive interneurons, and large entorhinal layer 2 stellate projection neurons are diploid. In contrast, chromocenter counts and integrated fluorescence are ~2-fold higher for some excitatory neurons in layer 5, suggesting that large Ctip2-negative and Ctip2-positive layer 5 neurons might be tetraploid. The distribution of putatively tetraploid neurons differed between areas and showed sharp borders aligned with functional subdivisions of the somatosensory cortex. Telomere counting and flow cytometry supported layer 5 polyploidy. We conclude that polyploidy contributes to cellular and areal diversity of rat cortex.

INTRODUCTION

Ever since the dawn of neuroanatomy, there has been an extensive quest to understand how neuronal subtypes differ between cortical areas and layers. With the aid of molecular biology and transgenic animal technologies, cellular markers for many subtypes, especially for interneurons have been identified (Monyer and Markram, 2004). In contrast, our understanding of principal cell diversity is much less advanced. Although the labeling of transcription factors (Arlotta et al., 2005; Chen et al., 2008; Tarabykin et al., 2001) and large-scale gene expression analysis (Zeisel et al., 2015) hold promise for a clearer subdivision of principal neurons, an unambiguous classification of excitatory cortical cells is still missing.

In many species, genomic differences contribute to cellular diversity (Lee et al., 2009). One type of genomic alteration observed in the cortex is an increase in the number of sets of chromosomes in the nucleus (López-Sánchez and Frade, 2013). This phenomenon, referred to as polyploidy, can be detected by quantifying DNA content. Although vertebrate neurons are usually diploid (2C), doubling of chromosomes results in a tetraploid cell (4C). Polyploidy is often associated with increased cell size, in which the amplification of the genome is accompanied by a proportional increase in cell size (Epstein, 1967; Beaulieu et al., 2008). Furthermore, polyploidy fosters species adaption and evolutionary fitness, allowing large cells to respond to high metabolic demand in terms of macromolecules and transcripts (Edgar and Orr-Weaver, 2001; Selmecki et al., 2015). Tetraploidy has previously been described in rat Purkinje neurons (Lentz and Lapham, 1969), giant Betz cells in layer 5 of motor cortex, neurons in the cat spinal cord (Herman and Lapham, 1969), and the human entorhinal cortex (Mosch et al., 2007). In mouse cortex, 3% of neurons are tetraploid, of which many expressed the transcription factor Ctip2, specific to subcortical projection neurons (López-Sánchez and Frade, 2013; Arlotta et al., 2005). In cortical layer 5, Ctip2-positive cells are large pyramidal projection neurons with thick-tufted apical dendrites (Chagnac-Amitai et al., 1990).

In light of large-scale efforts to understand neuron diversity, it seems astonishing that our insight into the abundance, distribution, and function of polyploid neurons in the cortex is so limited. Because of the lack of robust techniques to measure the DNA content of interphase cells in tissue sections, systematic surveys across the vertebrate brain are challenging. Hence, we combined a variety of methods to find out how genome amplification contributes to laminar, cellular, and areal diversity of rat cortex. We asked (1) Is polyploidy confined to one cortical layer? (2) How is polyploidy related to cell size and specific neuronal subtypes, such as large projection neurons? (3) Is an increase in DNA content associated with certain cortical areas? We find that polyploidy is associated with large neurons of cortical layer 5, without being clearly confined to one cellular subtype. We find sharp boundaries in the distribution of polyploid neurons along functional borders, even within cortical areas.

RESULTS

Layer 5 Contains the Biggest Neurons in Rat Primary Visual Cortex

To assess a possible contribution of polyploidy to neuronal diversity, we first studied basic cellular properties in neuronal and non-neuronal cells of the cortex. We initially focused on primary visual cortex (V1). To visualize nuclei, we stained sections of rat cortex (~P60) with the blue fluorescent dye DAPI, which binds to AT-rich regions of DNA (Figure 1A, left). Staining cell

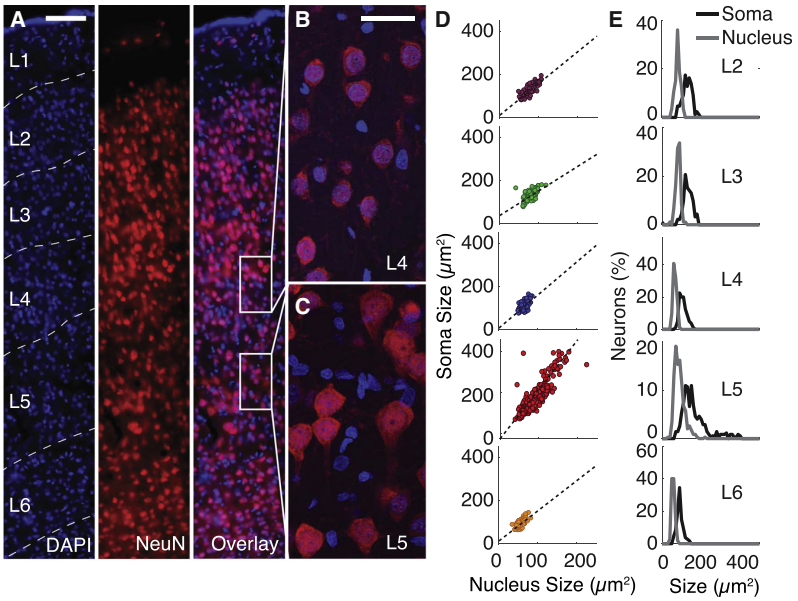

Figure 1. Neurons in L5 of Visual Cortex Have Larger Nuclei and Somata than Neurons in Other Layers

(A) Coronal section of primary visual cortex (V1) stained with DAPI (left) and an anti-NeuN antibody (middle) revealing neuronal somata (overlay, right). White squares indicate the position of sections shown in (B) (L4) and in (C) (L5).

(B) Section through cortical L4 of V1 stained with DAPI and NeuN.

(C) Section through cortical L5 of V1.

(D) Soma size versus nucleus size for L2 (purple, n = 86), L3 (green, n = 92), L4 (blue, n = 124), L5 (red, n = 348), and L6 neurons (orange, n = 107). Dashed lines indicate a linear fit.

(E) Frequency distribution histograms for soma and nucleus size of cortical layers 2 to 6.

Scale bars represent 100 μm (A) and 30 μm (B and C).

bodies with an anti-NeuN antibody (Figure 1A, middle) allowed differentiation of neuronal and non-neuronal cells in overlays (Figure 1A, right). Cell size differs markedly between layer 4 (L4; Figure 1B) and layer 5 (L5; Figure 1C). Soma and nucleus size are plotted in Figure 1D. Neurons in layer 6 (L6) and L4 were smallest, followed by layer 2 (L2) and layer 3 (L3) (L2 [n = 86]: soma 129 ± 24 μm^2, nucleus 81 ± 13 μm^2; L3 [n = 92]: soma 132 ± 26 μm^2, nucleus 83 ± 12 μm^2; L4 [n = 124]: soma 114 ± 22 μm^2, nucleus 69 ± 10 μm^2; L6 [n = 107]: soma 92 ± 16 μm^2, nucleus 57 ± 8 μm^2). In contrast, somata and nuclei in L5 were heterogeneous, and some were very large (L5 [n = 348]: soma 167 ± 67 μm^2, nucleus 89 ± 26 μm^2). Although L2–L4 and L6 contain homogeneous cell populations, L5 consists of neurons that vary immensely in size (Figure 1E). We will explore the idea that the large size of some L5 neurons is a reflection of polyploidy.

Approximating DNA Content Using Integrated DAPI Fluorescence and Chromocenter Counts

As cortical neurons are constitutively postmitotic, one cannot easily resolve their karyogram. Measuring DNA content often requires tissue homogenization, preventing insight into areal origin or cellular subtype. To overcome these limitations, we applied two alternative approaches to assess ploidy in tissue sections. First, we measured integrated DAPI fluorescence of cell nuclei. DAPI binds to DNA stoichiometrically (Darzynkiewicz, 2010; Dann et al., 1971). Therefore, integrated DAPI fluorescence ought to vary proportionally to DNA content. To validate this assumption, we measured integrated DAPI fluorescence of cells of known genotype, namely, germ cells. Testes contain seminiferous tubules, which are lined by spermatogonia and spermatids (Figures S1A and S1B). These cell types are easily recognized by their characteristic shape and position in the seminiferous tubules (Figures S1A and S1B). Spermatogonia are diploid germ cells (2C), which undergo meiosis to generate haploid spermatids (1C; Figure S1B). For integrated fluorescence measurements of spermatogonia and spermatid nuclei, we prepared sections of rat testes stained with DAPI (Figures S1A and S1B) and obtained image stacks with a z-spacing of 1 μm. In each focal section, we measured the mean fluorescent intensity of the nuclear area and took a background measurement close to the nucleus for background subtraction. Background-subtracted intensities were multiplied by the nuclear area and added up across the relevant focal planes to obtain an integrated DAPI fluorescence measurement for each nucleus. Despite our best efforts, absolute values differed between image stacks as a result of varying illumination strength and staining quality. The distribution of integrated DAPI fluorescence measurements, however, was consistent across image stacks. Hence, integrated DAPI fluorescence was normalized to the average obtained for spermatogonia in the same stack. The mean normalized integrated DAPI fluorescence value for spermatids was 0.5, that is, half of the mean value obtained for diploid spermatogonia (normalized integrated fluorescence: spermatogonia [n = 155] 1.00 ± 0.23 [by definition], spermatids [n = 79] 0.49 ± 0.11; Figure S1C). According to these data, integrated DAPI fluorescence accurately represents the 1C DNA content of spermatids when compared with spermatogonia (Figure S1C).

We also examined nuclear chromocenters. Chromocenters appear as bright spots of heterochromatic DNA upon DAPI staining. In organisms with few chromosomes, the number of chromocenters is typically slightly smaller than chromosome number. In organisms with more chromosomes, chromocenters fuse together, albeit still correlated with chromosome number (Fransz et al., 2002; Laibach, 1907). Consistent with other reports (Dyuzhikova et al., 2003), we found that rats have clearly visible chromocenters (Figures 2C and 2D, white arrows). In order to validate this approach, we quantified chromocenters of diploid spermatogonia from rat testes (Figures S1B and S1D).

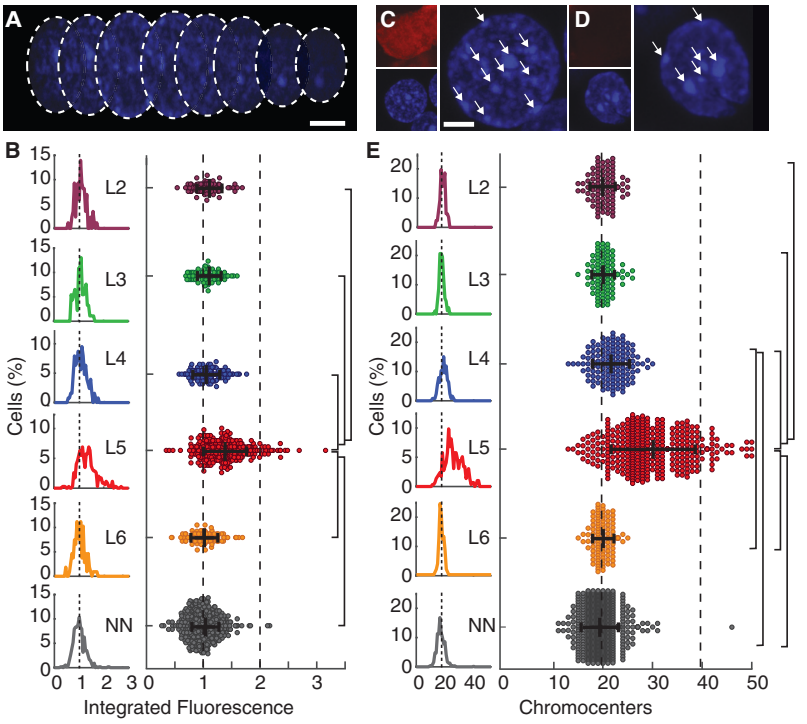

Figure 2. Integrated DAPI Fluorescence and Chromocenter Counts for Cortical Layers 2 to 6

(A) Schematic illustrating how integrated fluorescence is measured. Z-stack of a nucleus stained with DAPI. Fluorescence of each optical plane is integrated, normalized, and summed up across all sections.

(B) Frequency distribution and univariate plot of DAPI fluorescence of neurons in L2 (purple, n = 86), L3 (green, n = 92), L4 (blue, n = 126), L5 (red, n = 347), and L6 (orange, n = 107) and non-neuronal cells (gray, n = 556; NeuN−) in V1. Cellular fluorescence measurements are normalized to the mean normalized fluorescence of non-neuronal cells (by definition = 1) in each section analyzed.

(C) L5 neuron stained with NeuN (red, top left) and DAPI (blue, bottom left). White arrows indicate 10 chromocenters in the displayed section. In total, this nucleus has 27 chromocenters.

(D) Non-neuronal nucleus, as in (C). Note the absence of NeuN staining (red channel). There are 6 chromocenters in the displayed section. In total this nucleus has 19 chromocenters.

(E) Frequency distributions and univariate plots of chromocenter counts of cells in (B).

Dashed lines indicate mean integrated fluorescence and chromocenter counts of non-neuronal cells (1.0 by definition and 20) and twice this number. Black crosses indicate mean ± SD. Black lines indicate significant pairwise comparisons (Kruskal-Wallis ANOVA, $p < 0.05$). Scale bars represent 5 μm. See also Figure S1.

Spermatids were excluded, because their DNA is too condensed. We counted bright spots of DAPI fluorescence and added them up across sequential focal planes through the nucleus. We took care to track chromocenters to avoid counting the same chromocenter twice in adjacent sections. We also limited our analysis to well-stained sections and image stacks of excellent quality to prevent differences in contrast and brightness to confound the results. Spermatogonia had a mean of 19 ± 3 chromocenters (n = 54), suggesting that ~20 chromocenters are associated with a 2C DNA content (Figure S1D).

Assuming that differences in integrated DAPI fluorescence accurately represent differences in DNA content, we analyzed tissue sections of rat V1 stained with DAPI and the neuronal marker NeuN (Figure 2A). The experimenter was blind to cellular identity while quantifying integrated fluorescence. Post hoc, nuclei were identified as neuronal or non-neuronal on the basis of NeuN staining. All neuronal measurements were normalized to the mean of non-neurons in each stack. We found that neurons in L5 had significantly greater integrated DAPI fluorescence than neurons of other layers and non-neuronal cells (Kruskal-Wallis ANOVA, p = 0.00000; normalized integrated fluorescence: L5 [n = 347] 1.34 ± 0.38, L2 [n = 86] 1.06 ± 0.22, L3 [n = 92] 1.07 ± 0.21, L4 [n = 126] 1.06 ± 0.24, L6 [n = 107] 1.01 ± 0.24, non-neuronal cells [n = 556] 1.00 ± 0.24 [by definition]; Figure 2B, right). Neurons in L2–L4 and L6 and non-neuronal cells showed similar integrated DAPI fluorescence, resulting in a narrow distribution centered on the mean of 1 (Figure 2B, left). In contrast, L5 neurons gave rise to a much broader distribution, with 6% of cells having integrated fluorescence greater than 2 (twice the mean of non-neuronal cells). The narrow distribution of normalized integrated DAPI fluorescence in non-neuronal cells is remarkable given that this population is made up of very different cell types (epithelial cells, glia, microglia, etc.) with distinct nuclei.

We also quantified chromocenters of cells in V1. Chromocenters were counted before cells were identified as either neuronal (NeuN+; Figure 2C) or non-neuronal (NeuN−; Figure 2D; note the absence of NeuN staining). Figure 2C shows a L5 neuron with a total of 27 chromocenters. Similarly, we counted 19 chromocenters in a non-neuronal cell (Figure 2D). Non-neuronal cells had a mean of 20 chromocenters (n = 556, 20 ± 3 chromocenters; Figure 2E, right). As we expected, this number is smaller than the total number of chromosomes (42) but similar to previous reports of chromocenter counts in non-neuronal rat cells (approximately 17 chromocenters; Snapp et al., 2013). L5 had significantly more chromocenters than all other layers and non-neuronal cells (Kruskal-Wallis ANOVA, p = 00000; mean chromocenters: L5 [n = 350] 30 ± 7, L2 [n = 86] 20 ± 2, L3 [n = 92] 20 ± 2, L4 [n = 126] 22 ± 3, L6 [n = 107] 20 ± 2; Figure 2E). Like integrated fluorescence, chromocenters were differentially distributed across layers (Figure 2E, left). L5 neurons varied substantially in their number of chromocenters: 9% of cells with had more than 40 chromocenters (double the number of non-neuronal cells). On the other hand, chromocenter counts of L2–L4 and L6 neurons, and non-neuronal cells resulted in a narrow distribution with one peak around 20 chromocenters.

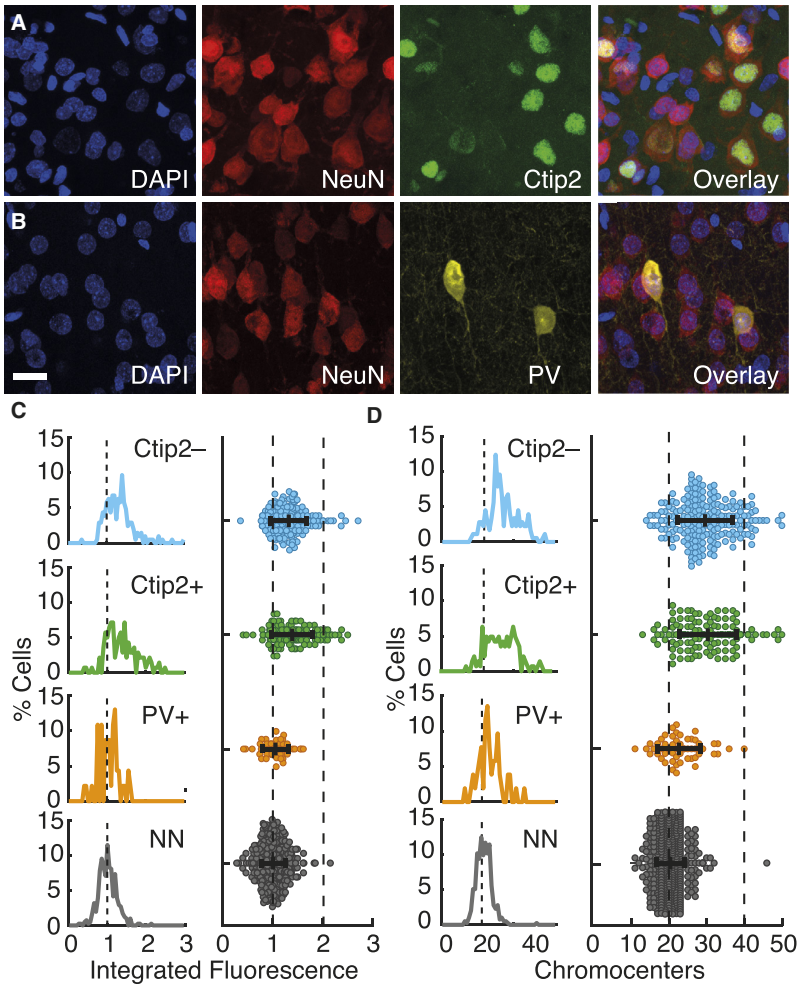

Figure 3. Integrated DAPI Fluorescence and Chromocenter Counts of Identified Cell Types in L5

(A) Confocal image of rat V1 L5 stained with DAPI (blue), NeuN (red), an antibody against the transcription factor Ctip2 (green), and overlay.

(B) Same as (A), stained with DAPI (blue), NeuN (red), an antibody against parvalbumin (yellow), and overlay.

(C) Distribution and univariate plot of integrated DAPI fluorescence of neurons negative for the transcription factor Ctip2 (Ctip2−, blue, n = 207), neurons positive for the transcription factor Ctip2 (Ctip2+, green, n = 142), parvalbumin-positive interneurons (PV+, yellow, n = 54), and non-neuronal cells (NN, gray, n = 365).

(D) Chromocenter counts of identified cells in (C). Dashed lines indicate mean integrated fluorescence and chromocenter counts (by definition 1.00 and 20) and twice this number. Black crosses indicate mean ± SD. Scale bar represents 20 μm. See also Figure S2.

Overall, L2–L4 and L6 and non-neuronal cells had similar mean values and distributions according to both DNA content markers, forming small, homogeneous clusters (Figures 2B and 2E).

DNA Content and Cell Size of Identified Neuronal Subtypes

To determine if neurons with greater integrated fluorescence and chromocenter counts belonged to a particular cellular subtype within L5, we combined DAPI and NeuN staining with immunofluorescent labeling of the transcription factor Ctip2 (Figure 3A, green) and the calcium-binding protein parvalbumin (PV+; Figure 3B, yellow). Ctip2 is largely expressed in deep L5 and L6 and marks a subset of subcortically projecting L5 pyramidal neurons (Chen et al., 2008), while PV colocalizes with many fast-spiking inhibitory interneurons. Post hoc, four types of L5 cells were identified (Ctip2+, Ctip2−, PV+, and non-neuronal cells; Figures 3A and 3B). The distributions of integrated fluorescence (Figure 3C) and chromocenter counts were similar (Figure 3D). PV+ interneurons were like non-neuronal cells (Figures 3C and 3D), which are homogeneous with a narrow distribution, pointing to diploidy. In contrast, integrated fluorescence and chromocenters were greater and more widely distributed for Ctip2+ and, to a slightly lesser degree, for Ctip2− neurons (Figures 3C and 3D). 2-fold higher fluorescence was observed in 4% and 9% of Ctip2− and Ctip2+ neurons, respectively, compared with non-neuronal cells. Accordingly, some Ctip2− and Ctip2+ cells had twice as many chromocenters compared with PV+ and non-neuronal cells (>40 = 11% and 8% respectively). Putatively diploid PV+ interneurons were also smallest, followed by Ctip2− and Ctip2+ cells, which are very heterogeneous. In this population, we also observed a steep correlation between integrated DAPI fluorescence and soma size (data not shown).

Given previous observations (López-Sánchez and Frade, 2013), we wondered if polyploidy may be a general feature of cortical projection neurons. We examined two types of projection neurons in L2 of medial entorhinal cortex (MEC), namely, the very large reelin-positive stellate cells and calbindin-positive pyramidal neurons. This analysis should provide insight as to whether polyploidy is associated with a projection neuron cellular phenotype or if it is specifically linked to cortical L5. Tangential sections of MEC (Figure S2A, left) were stained with DAPI and antibodies against reelin (Figure S2A, green) and calbindin (Figure S2A, red). Multicolor overlays were used to post hoc identify reelin-positive stellates, calbindin-positive pyramids, and cells negative for both markers (Figure S2A, others). Projection neurons had significantly bigger nuclei than other cells (data not shown). However, mean integrated fluorescence (Figure S2B) and chromocenters (Figure S2C) were not different

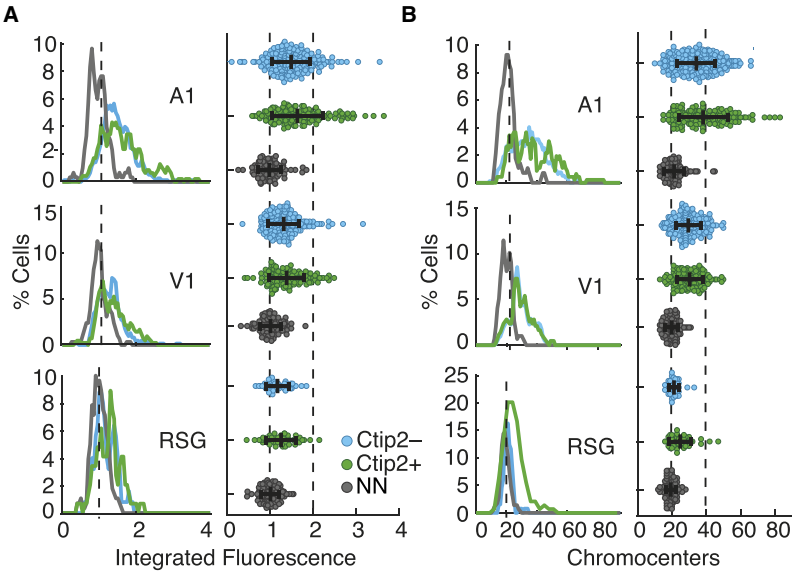

Figure 4. Integrated DAPI Fluorescence and Chromocenter Counts of L5 Cells in Three Different Cortical Areas

(A) Frequency distribution and univariate plot of integrated DAPI fluorescence of Ctip2− (blue), Ctip2+ (green), and non-neuronal cells (NN, gray) in L5 of three cortical areas with large, medium, and small mean neuronal size: primary AI (n = 261 Ctip2−, n = 156 Ctip2+, n = 101 NN), V1 (n = 207 Ctip2−, n = 140 Ctip2+, n = 98 NN), and granular retrosplenial cortex (RSG; n = 42 Ctip2−, n = 49 Ctip2+, n = 94 NN).

(B) Chromocenter counts of cells in (A).

Dashed lines indicate mean integrated fluorescence and chromocenter counts (by definition 1.00 and 20) and twice this number. Black crosses indicate mean ± SD. See also Figures S3 and S4.

to that of other cells, pointing to diploidy of stellates and pyramids in MEC.

DNA Content and Cell Size across Cortical Areas

Measuring neuron size across 24 cortical areas revealed substantial variations (Figure S3). Therefore, we extended the analysis of DNA content beyond V1 (contains mostly medium-sized L5 neurons) to auditory cortex (A1; contains very large L5 neurons) and to retrosplenial cortex (RSG; contains the smallest L5 neurons). These three areas showed striking differences in integrated fluorescence (Figure 4A) and chromocenter counts (Figure 4B) for Ctip2+ and Ctip2− neurons but not for non-neuronal cells (Figures 4A and 4B). We observed numerous neurons with integrated DAPI fluorescence values >3 and chromocenter counts >60 in AI, which were mostly Ctip2+. Such cells were rare or absent from V1 and RSG and may represent a hexaploid neuronal population (Figure 4).

Next, we determined if changes in polyploidy markers align with functional borders in the cortex. We prepared flattened sections of rat cortex (Figure S4A), stained with antibodies against Vglut2, a marker of thalamocortical inputs to L4, in addition to Ctip2, NeuN, and DAPI. On the basis of the Vglut2 staining, we reconstructed the sensory homunculus in primary somatosensory cortex (S1; Figure S4A) and aligned the tracing with slices of Ctip2+ stained L5. We focused on the borders of the hindpaw and forepaw region (Figure S4A, right), because we have previously observed large differences in cell size between those areas (Figure S3). We measured cell size, integrated fluorescence, and chromocenters of S1 hindpaw, forepaw, and the intermediate septum (interlimb cortex). Nuclear size, integrated fluorescence, and chromocenter counts of neurons were smallest in the septum, followed by the forepaw and the hindpaw (data not shown). For Ctip2+ neurons, we observed significant differences between forepaw and hindpaw regions (integrated fluorescence: 1.08 ± 0.28 [forepaw], 1.38 ± 0.59 [hindpaw]; chromocenters: 22 ± 3 [forepaw], 25 ± 6 [hindpaw]; Figures S4B and S4C). Therefore, the distribution of polyploidy shows sharp borders, even within subregions of S1.

In Situ Hybridization of Telomeres and Flow Cytometry

Our observations suggest that some cortical L5 neurons have an increased DNA content. To complement these findings, we turned to more established techniques to measure ploidy. We use fluorescence in situ hybridization (FISH) of telomeres, which are located at the end of each chromosome and therefore make it possible to indirectly count chromosomes. Preparing single-cell suspensions of adult cortical neurons is very challenging. Therefore, we used single-nucleus suspensions. Because the neuronal marker NeuN is expressed in the cytoplasm, neurons and non-neurons cannot be differentiated in FISH. We chose L4 as a putatively diploid comparison and made single-nucleus suspensions of L4 (Figure 5A, top) and L5 (Figure 5A, bottom). To separate L4 and L5, we prepared flattened sections of rat cortex and stained every second slice with cytochrome oxidase to identify L4 (Wong-Riley, 1989). Thereafter unstained slices were assigned to L4 or L5. Single-nucleus suspensions were hybridized with a green fluorescent peptic nucleic acid (PNA) probe against rat telomeres (Figure 5A, middle) and counterstained with DAPI (Figure 5A, left). Telomeres appeared as bright green spots. Suspended L4 nuclei were homogeneous and small (n = 84; size 113 ± 69 μm^2, range 37 to 395 μm^2; Figure 5B). In contrast, L5 nuclei were heterogeneous, containing some very large nuclei (n = 126; size 399 ± 237 μm^2, range 31 to 1,121 μm^2; Figure 5B). Overall, nuclear size was bigger than in tissue sections (Figure 1D), because of differences in fixation and other histochemical treatments. L4 nuclei had a mean of 52 ± 8 telomere spots, with a narrow distribution (Figure 5C), which was less than expected in a postmitotic diploid rat cell with 84 telomeres. This is likely due to limitations in image resolution. Much like L4, many L5 nuclei also had between 50 and

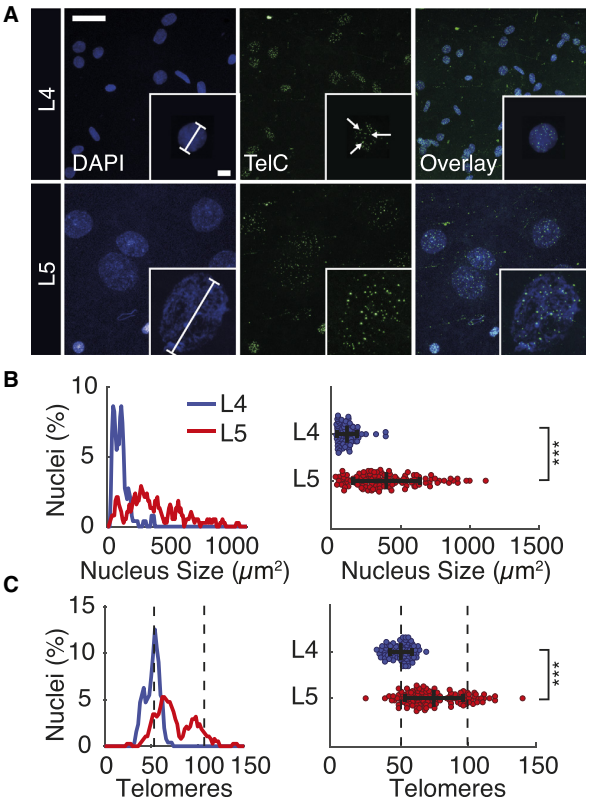

Figure 5. Fluorescent In Situ Hybridization of Telomeres in Suspended Interphase Nuclei of Cortical L4 and L5

(A) Suspended nuclei of L4 (top) and L5 (bottom) stained with DAPI (blue, left), a PNA probe against rat telomere (TelC; green, middle), and overlay (right). Insets show a representative L4 nucleus (top, 11 μm diameter, 53 telomere spots) and a large L5 nucleus (bottom, 30 μm diameter, 104 telomere spots). White arrows indicate green telomere spots.

(B) Frequency distribution and univariate plot of nucleus size for L4 (blue, n = 84) and L5 (red, n = 126).

(C) Telomere counts for cells in (B).

Dashed lines indicate the mean number of telomeres of L4 (52) and twice this number. Black crosses indicate mean ± SD. Stars indicate significant pairwise comparisons (Kruskal-Wallis ANOVA, $p < 0.0005$). Scale bars represent 25 and 5 μm (all insets). See also Figure S5.

60 telomeres. However, 15% had more than 100 telomere spots (twice the number of an average L4 nucleus), suggesting that these cells are tetraploid instead of diploid (76 ± 21 telomeres; Figure 5C).

Finally, we applied flow cytometry as a gold standard for measuring DNA content. Nuclei suspensions required for flow cytometry also did not allow neurons and non-neurons to be differentiated. We prepared live suspensions of rat cortical nuclei stained with the DNA dye Höchst (Figure S5A). Amount of dye incorporated into the nucleus was analyzed using a flow cytometer. Doublets and clumps were excluded by a series of gating steps (Figure S5B; López-Sánchez and Frade, 2013). According to DNA histograms, most brain cells were diploid (n = 82 samples from 23 brains, 93.7 ± 2.7%; Figures S5C and S5D), but there was also a small tetraploid population (3.6 ± 1.7%; Figure S5D, middle) and even a few hexaploid cells (0.6 ± 0.4%; Figure S5D, right). Nuclear size (measured by forward scatter [FSC-A]) increased with DNA content (Figure S5E). As a control, we analyzed Höchst-stained nuclei from rat testes (Figure S5F). DNA histogram showed three peaks, corresponding to haploid spermatids (1C), diploid spermatogonia (2C), and tetraploid spermatocytes (4C) (Figure S5G). Both peaks in the DNA histogram of cortical nuclei aligned well with the two rightmost peaks in the sperm DNA histogram, which represent 2C and 4C cells, respectively (Figures S5H and S5I). Thus, FISH and flow cytometry provide further support polyploid neurons in the rat cortex.

DISCUSSION

Differences in integrated DAPI fluorescence and chromocenter counts between L5 and all other cortical layers mirrored differences in cell size. In visual cortex, the data suggest that non-neuronal cells, small neurons, parvalbumin-positive interneurons and projection neurons in the MEC are putatively diploid, while some Ctip2-negative and Ctip2-positive principal cells in L5 are putatively tetraploid. Such very large, putatively tetraploid neurons were distributed in a highly specific manner across cortical layers and areas. Finally, in situ hybridization of telomeres and flow cytometry confirmed the presence of a small tetraploid cell population in rat cortex.

Polyploidy in L5 Neurons

Although they have the largest nuclear and soma size in visual cortex, L5 principal neurons show sometimes even 2-fold greater integrated DAPI fluorescence and chromocenter counts compared with other cortical neurons. Furthermore, areal differences in L5 neuron size are correlated with DAPI fluorescence and chromocenter counts, even on a subregion scale. Although individual observations reported here are not by itself conclusive, collectively our findings are best explained by the polyploidy of a subgroup of L5 neurons. Specifically, we suggest that differences in somatic size of L5 neurons are due to 2C jumps in DNA content (indicated by DAPI fluorescence and flow cytometry) and chromosome number (indicated by telomere and chromocenter counts).

Related Work on Cortical Polyploidy

Our work builds on the early work of Lapham and colleagues (Herman and Lapham, 1969; Lentz and Lapham, 1969), who argued that some cortical L5 neurons are polyploid. In line, we propose that rat cortex tetraploidy appears to be a relatively rare condition of few large L5 neurons. Recent results from flow cytometry and FISH also found a small fraction of often Ctip2-positive cortical projection neurons to be tetraploid (López-Sánchez and Frade, 2013). Our observations do not support a strong link between Ctip2-positive neurons and tetraploidy. Instead, we also observed, albeit fewer, large, Ctip2-negative neurons that are putatively tetraploid. We further find no evidence for polyploidy in large stellate cells, suggesting that polyploidy is not a general feature of cortical projection neurons.

Implications for Cortical Principal Cell Diversity

Given the accumulating evidence for genomic mosaicism in the brain (Rosenkrantz and Carbone, 2017), we argue that determination of DNA content should complement classic methods of cell classification, such as morphological analysis, connectivity analysis, and characterization of membrane properties. We wonder whether a distinction based on DNA content will lead to the establishment of novel L5 principal cell classes. So far, L5 principal cell types have only broadly been subdivided (Chagnac-Amitai et al., 1990; Arlotta et al., 2005). However, our analysis indicates the presence of diploid, tetraploid, and possibly also hexaploid cells. Cell biology has identified numerous instances in which polyploidy leads to functionally distinct cell types (D'Amato, 1989).

Implications for Cortical Areal Diversity

Early observations from Lapham and colleagues pointed toward area specific polyploidy (Herman and Lapham, 1969; Lentz and Lapham, 1969). In particular, these authors argued for a polyploidy of Betz cells, giant output neurons in the motor cortex of many mammals. Similarly, we observe that neuron size and polyploidy markers are distributed in a highly specific manner across the cortical sheet. Overall, we observed that all areas contain mostly putatively diploid L5 neurons. Yet the density of tetra- and hexaploid L5 neurons differs markedly across the cortex and even within the same sensory area (Figure S4). We find more putatively tetraploid L5 neurons in the hindpaw region of S1, which likely constitute the much investigated thick tufted L5 pyramidal neurons (Romand et al., 2011; Markram, 1997). Moreover, polyploidy has previously been associated with long-range projection neurons in a target-dependent manner (Morillo et al., 2010). It has been proposed that endoreduplication is actually supported by neurotrophic factors retrogradely incorporated into neurons from the target tissue (Matsuo et al., 2013). This could be a potential mechanism to support the high metabolic demands of long-range projection neurons. Thus, it will be important to investigate putative tetraploid L5neurons according to their specific projection targets.

Methodological Considerations

Classical methods to measure DNA content require the dissociation of cortical tissue, which limits insight into spatial information and marker expression. To systematically investigate the spatial distribution of polyploid neurons across cortical layers and areas, we focused on the measurement of DAPI fluorescence and the counting of chromocenters in immuno-labeled cortical sections. We validated this approach in rat testis cells of known genotype and therefore argue that this approach holds great promise for cortical cell classification. Assessment of DNA content in this way led to very similar but not identical results. More specifically, chromocenter counts usually indicated slightly higher degrees of polyploidy. Future work is needed to resolve this discrepancy. To corroborate our findings, we also used FISH of telomeres, which marks all chromosomes, resulting in a better signal-to-noise ratio compared with single-chromosome painting. We observed nuclei with a 2-fold increase in telomere spots only in L5. The percentage of such cells was relatively high, potentially because of the small sample size. We also applied FISH to cortical slices. However, large neurons in L5 were ruptured systematically in sufficiently thin tissue sections. This may also have also led to largely contradictory results from previous studies based on FISH (Rosenkrantz and Carbone, 2017). Finally, flow cytometry allows extremely accurate and high-throughput measurement of ploidy, despite lacking insight into cellular and areal distributions. In line with our other observations, DNA histograms showed two clearly separable peaks for diploid and tetraploid cells, as opposed to a broadened diploid peak, which would indicate a DNA increase in the Mb range (Westra et al., 2010).

Conclusion

We present and validate several approaches to assess cortical polyploidy on the basis of DAPI fluorescence measurements, chromocenter counting, FISH, and flow cytometry. The data suggest an unexpected genomic heterogeneity of L5 neurons, which contributes to the laminar and areal cell diversity of the rat cerebral cortex.

EXPERIMENTAL PROCEDURES

All experimental procedures were performed according to the German guidelines on animal welfare under the supervision of local ethics committees.

Immunohistochemistry

Antibody staining and image acquisition were prepared according to standard procedures.

Somatic and Nuclear Size

Neuronal and nuclear size of antibody-stained cells were measured in 2D in the focal z-plane with maximal intersection with the cell. In order to reduce potential observer bias, all measurements were obtained prior to establishing cellular identity.

Quantification of Integrated DAPI Fluorescence and Chromocenters

Average fluorescent intensity of all pixels within an ROI drawn around a nucleus was measured. For background correction, average fluorescence of a nearby background ROI was subtracted from the nuclear ROI fluorescence. Background subtracted intensities were multiplied with the area of the nuclear ROI in each focal plane. The net integrated fluorescent intensity was added up across all relevant focal planes to obtain an integrated DAPI fluorescence measurement for each nucleus. All fluorescent measurements were normalized to the average fluorescence of non-neuronal cells within a section. Chromocenters appeared as bright spots of DAPI fluorescence. They were counted and summed across all focal planes of a nucleus. In some cases, chromocenters appeared in more than one optical plane, in which case they were tracked to avoid double counting. Analysis was done blind to cellular identity and restricted to well stained sections and image stacks of excellent quality.

Fluorescent In Situ Hybridization of Telomeres

Subcortical areas were removed from fresh brains and each hemicortex was sliced tangentially. Every second slice was stained for cytochrome oxidase to reveal L4 (Wong-Riley, 1989). Every other slice was placed in a 50 μL Eppendorf tube on dry ice, paying particular attention to the order in which slices were collected. To make separate nuclei suspensions of either L4 or L5 cells, cytochrome oxidase stained sections were inspected to reveal which frozen sections contained either L4 or L5. Frozen sections of L4 or L5 were homogenized and fixed using Carnoy's fixative. For fluorescent in situ hybridization (FISH) of rat telomeres, an Alexa 488 conjugated PNA probe against rat telomere was used (PNA Bio, Thousand Oaks, CA). The manufacturer's instructions were followed. Nuclei were counterstained with DAPI, and size was measured. In single-cell suspensions, nuclei are

distorted, and therefore absolute size cannot be compared with measurements from intact tissue sections. Telomeres were counted by hand, and care was taken to separate overlapping telomeres in the 3D stack while avoiding double counting.

Flow Cytometry

Live nuclear suspensions were made similar to Halder et al. (2016). After removing subcortical areas, fresh-frozen tissue was homogenized in low-sucrose buffer. The homogenized suspension was layered onto high-sucrose buffer and centrifuged. The supernatant was discarded, and the pellet was resuspended in 1× PBS. The nuclei suspension was filtered through a 40 μm nylon mesh. All steps were performed on ice. Nuclei were then stained with Höchst. Flow cytometry was performed with a BD LSR II flow cytometer (BD Biosciences, San Jose, CA) equipped with a UV laser (405 nm). Data were collected using FACSDiva (BD Biosciences) and FlowJo (FlowJo, Ashland, OR) and displayed using biexponential scaling. Single nuclei were gated according to the DAPI-H-to-DAPI-A ratio (López-Sánchez & Frade, 2013). The percentages of diploid, tetraploid, and hexaploid nuclei were derived from the DNA histogram.

Statistics

Statistical analysis was done in MATLAB (The MathWorks). Lilliefors tests were used to test if the data were normally distributed. If data were not normally distributed or had unequal variances, a Kruskal-Wallis ANOVA was conducted instead of an ANOVA. P values represent pairwise comparisons according to Dunn's approach.

SUPPLEMENTAL INFORMATION

Supplemental Information includes Supplemental Experimental Procedures and five figures and can be found with this article online at http://dx.doi.org/10.1016/j.celrep.2017.08.069.

AUTHOR CONTRIBUTIONS

J.S.-G. and M.B. designed the experiments. J.S.-G. performed the experiments. J.S.-G. and M.B. analyzed the data and wrote the manuscript.

ACKNOWLEDGMENTS

We thank Andreea Neukirchner, Juliane Steger, and Undine Schneeweiß for outstanding technical assistance; Aarti Swaminathan for her help making live nuclei suspensions; and Christian Ebbesen, Jean Simmonet, and Saikat Ray for valuable comments. This work was supported by Humboldt-Universität zu Berlin, BCCN Berlin (German Federal Ministry of Education and Research BMBF, Förderkennzeichen 01GQ1001A), NeuroCure, the Gottfried Wilhelm Leibniz Prize of the DFG, and Böhringer Ingelheim Fonds. J.S.G. was part of the Medical Neuroscience PhD program of the Charité during this work.

Received: March 26, 2017
Revised: July 11, 2017
Accepted: August 20, 2017
Published: September 12, 2017

REFERENCES

Arlotta, P., Molyneaux, B.J., Chen, J., Inoue, J., Kominami, R., and Macklis, J.D. (2005). Neuronal subtype-specific genes that control corticospinal motor neuron development in vivo. Neuron *45*, 207–221.

Beaulieu, J.M., Leitch, I.J., Patel, S., Pendharkar, A., and Knight, C.A. (2008). Genome size is a strong predictor of cell size and stomatal density in angiosperms. New Phytol. *179*, 975–986.

Chagnac-Amitai, Y., Luhmann, H.J., and Prince, D.A. (1990). Burst generating and regular spiking layer 5 pyramidal neurons of rat neocortex have different morphological features. J. Comp. Neurol. *296*, 598–613.

Chen, B., Wang, S.S., Hattox, A.M., Rayburn, H., Nelson, S.B., and McConnell, S.K. (2008). The Fezf2-Ctip2 genetic pathway regulates the fate choice of subcortical projection neurons in the developing cerebral cortex. Proc. Natl. Acad. Sci. U S A *105*, 11382–11387.

D'Amato, F. (1989). Polyploidy in cell differentiation. Caryologia *42*, 183–211.

Dann, O., Bergen, E., and Volz, G. (1971). Trypanocide diamidine des 2-phenyl-benzofurans, 2-phenyl-indens und 2-phenyl-indols. Justus Liebigs Ann. Chem. *749*, 68–89.

Darzynkiewicz, Z. (2010). Critical aspects in analysis of cellular DNA content. Curr. Protoc. Cytom. *Chapter 7*, Unit 7.2.

Dyuzhikova, N.A., Dudkin, K.N., Mironov, S.V., Vaido, A.I., Shiryaeva, N.V., and Lopatina, N.G. (2003). Characteristics of interphase chromatin in hippocampal neurons in rats with different excitability of the nervous system exposed to stress at different time of the day. Bull. Exp. Biol. Med. *135*, 161–163.

Edgar, B.A., and Orr-Weaver, T.L. (2001). Endoreplication cell cycles: more for less. Cell *105*, 297–306.

Epstein, C.J. (1967). Cell size, nuclear content, and the development of polyploidy in the mammalian liver. Proc. Natl. Acad. Sci. U S A *57*, 327–334.

Fransz, P., De Jong, J.H., Lysak, M., Castiglione, M.R., and Schubert, I. (2002). Interphase chromosomes in Arabidopsis are organized as well defined chromocenters from which euchromatin loops emanate. Proc. Natl. Acad. Sci. U S A *99*, 14584–14589.

Halder, R., Hennion, M., Vidal, R.O., Shomroni, O., Rahman, R.U., Rajput, A., Centeno, T.P., van Bebber, F., Capece, V., Garcia Vizcaino, J.C., et al. (2016). DNA methylation changes in plasticity genes accompany the formation and maintenance of memory. Nat. Neurosci. *19*, 102–110.

Herman, C.J., and Lapham, L.W. (1969). Neuronal polyploidy and nuclear volumes in the cat central nervous system. Brain Research *15*, 35–48.

Laibach, F. (1907). About the individuality of chromosomes in the plant kingdom. Botan Zentralbl *22*, 191–210.

Lee, H.O., Davidson, J.M., and Duronio, R.J. (2009). Endoreplication: polyploidy with purpose. Genes Dev. *23*, 2461–2477.

Lentz, R.D., and Lapham, L.W. (1969). A quantitative cytochemical study of the DNA content of neurons of rat cerebellar cortex. J. Neurochem. *16*, 379–384.

López-Sánchez, N., and Frade, J.M. (2013). Genetic evidence for p75NTR-dependent tetraploidy in cortical projection neurons from adult mice. J. Neurosci. *33*, 7488–7500.

Markram, H. (1997). A network of tufted layer 5 pyramidal neurons. Cereb. Cortex *7*, 523–533.

Matsuo, R., Yamagishi, M., Wakiya, K., Tanaka, Y., and Ito, E. (2013). Target innervation is necessary for neuronal polyploidization in the terrestrial slug Limax. Dev. Neurobiol. *73*, 609–620.

Monyer, H., and Markram, H. (2004). Interneuron diversity series: molecular and genetic tools to study GABAergic interneuron diversity and function. Trends Neurosci. *27*, 90–97.

Morillo, S.M., Escoll, P., de la Hera, A., and Frade, J.M. (2010). Somatic tetraploidy in specific chick retinal ganglion cells induced by nerve growth factor. Proc. Natl. Acad. Sci. U S A *107*, 109–114.

Mosch, B., Morawski, M., Mittag, A., Lenz, D., Tarnok, A., and Arendt, T. (2007). Aneuploidy and DNA replication in the normal human brain and Alzheimer's disease. J. Neurosci. *27*, 6859–6867.

Romand, S., Wang, Y., Toledo-Rodriguez, M., and Markram, H. (2011). Morphological development of thick-tufted layer V pyramidal cells in the rat somatosensory cortex. Front. Neuroanat. *11*, 5.

Rosenkrantz, J.L., and Carbone, L. (2017). Investigating somatic aneuploidy in the brain: why we need a new model. Chromosoma *126*, 337–350.

Selmecki, A.M., Maruvka, Y.E., Richmond, P.A., Guillet, M., Shoresh, N., Sorenson, A.L., De, S., Kishony, R., Michor, F., Dowell, R., and Pellman, D. (2015). Polyploidy can drive rapid adaptation in yeast. Nature *519*, 349–352.

Snapp, R.R., Goveia, E., Peet, L., Bouffard, N.A., Badger, G.J., and Langevin, H.M. (2013). Spatial organization of fibroblast nuclear chromocenters: component tree analysis. J. Anat. *223*, 255–261.

Tarabykin, V., Stoykova, A., Usman, N., and Gruss, P. (2001). Cortical upper layer neurons derive from the subventricular zone as indicated by Svet1 gene expression. Development *128*, 1983–1993.

Westra, J.W., Rivera, R.R., Bushman, D.M., Yung, Y.C., Peterson, S.E., Barral, S., and Chun, J. (2010). Neuronal DNA content variation (DCV) with regional and individual differences in the human brain. J. Comp. Neurol. *518*, 3981–4000.

Wong-Riley, M.T.T. (1989). Cytochrome oxidase: an endogenous metabolic marker for neuronal activity. Trends Neurosci. *12*, 94–101.

Zeisel, A., Muñoz-Manchado, A.B., Codeluppi, S., Lönnerberg, P., La Manno, G., Juréus, A., Marques, S., Munguba, H., He, L., Betsholtz, C., et al. (2015). Cell types in the mouse cortex and hippocampus revealed by single-cell RNA-seq. Science *347*, 1138–1142.

Cell Reports, Volume *20*

Supplemental Information

Polyploidy and the Cellular and Areal Diversity of Rat Cortical Layer 5 Pyramidal Neurons

Johanna Sigl-Glöckner and Michael Brecht

Supplemental Figures and Supplemental Experimental Procedures

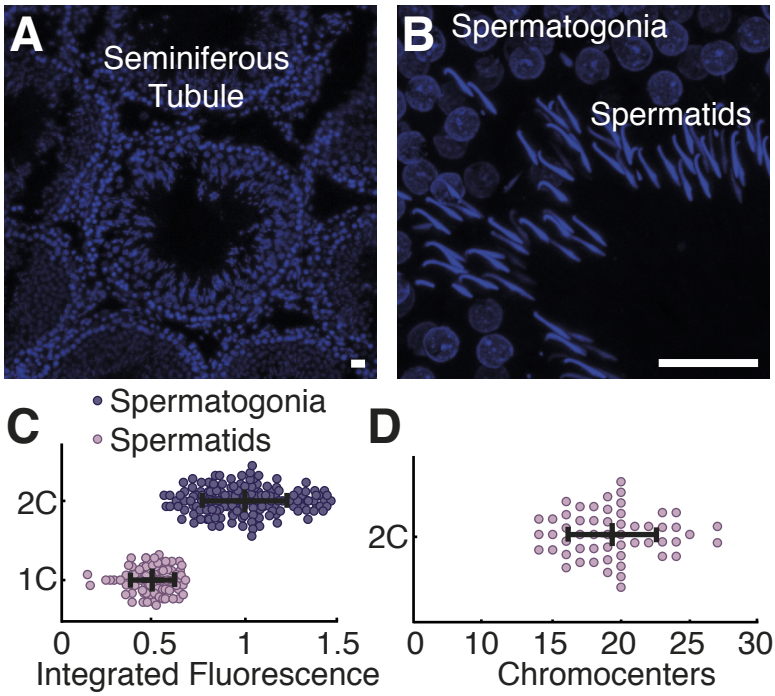

Figure S1. Integrated DAPI Fluorescence and chromocenter counts in testis cells of defined genotype, related to Figures 2.

(**A**) Confocal image of a section through seminiferous tubules in the rat testis stained with DAPI.

(**B**) High magnification view of diploid spermatogonia and haploid spermatids.

(**C**) Integrated DAPI fluorescence of spermatogonia (blue, n = 155) and spermatids (pink, n = 79). All cellular fluorescence measurements were normalized to the mean fluorescence of spermatogonia in each section analysed (1.0 by definition).

(**D**) Chromocenters counts of spermatogonia (n = 54).

Black lines indicate mean ± STD. Scale bars = 25 μm.

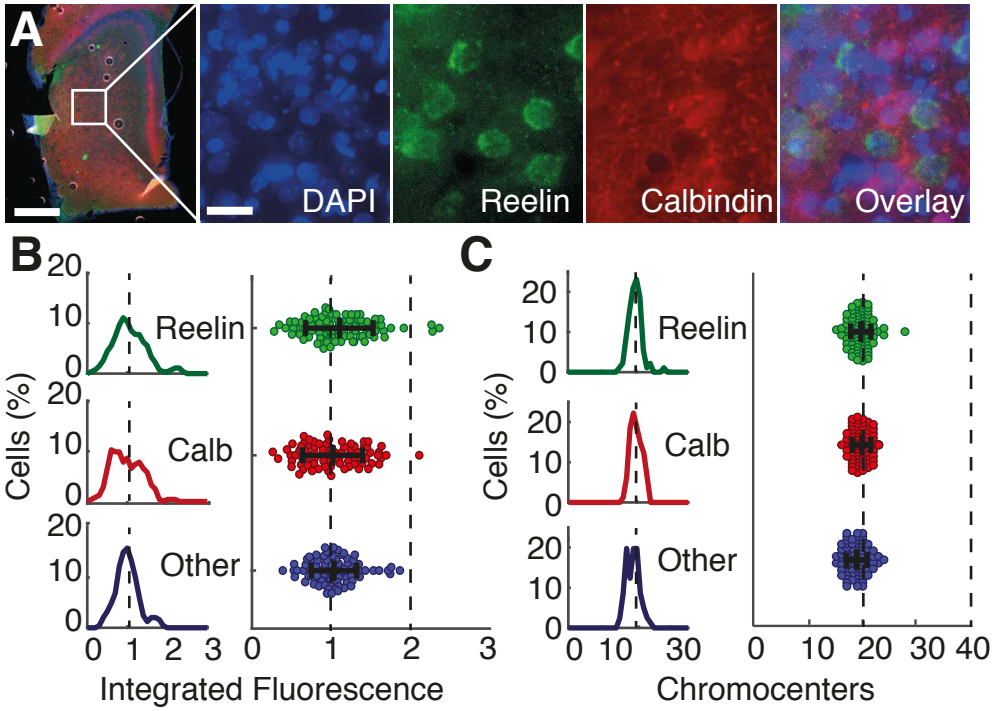

Figure S2. Integrated fluorescence and chromocenters of projection neurons in layer 2 of medial entorhinal cortex, related to Figure 3.

(**A**) Triple stained tangential section of medial entorhinal cortex layer 2 (left). Projection neurons are either positive for reelin (green, stellate cells) or for calbindin (red, pyramidal cells). Multicolour overlays were used to identify stellates and pyramids. Unstained nuclei were identified as others.

(**B**) Frequency distribution and univariate plot of integrated DAPI fluorescence of stellate neurons (reelin+, green, n = 92), pyramidal neurons (calb+, red, n = 88) and other cells (blue, n = 52) in medial entorhinal cortex layer 2. All cellular fluorescence measurements were normalized to the mean fluorescence of other cells (by definition = 1) in each section analysed.

(**C**) Same as B for chromocenters.

Dashed lines indicate the mean of other cells (1.00 and 19 respectively) and twice this number. Black crosses indicate mean ± STD. Scale bars = 1mm and 25µm.

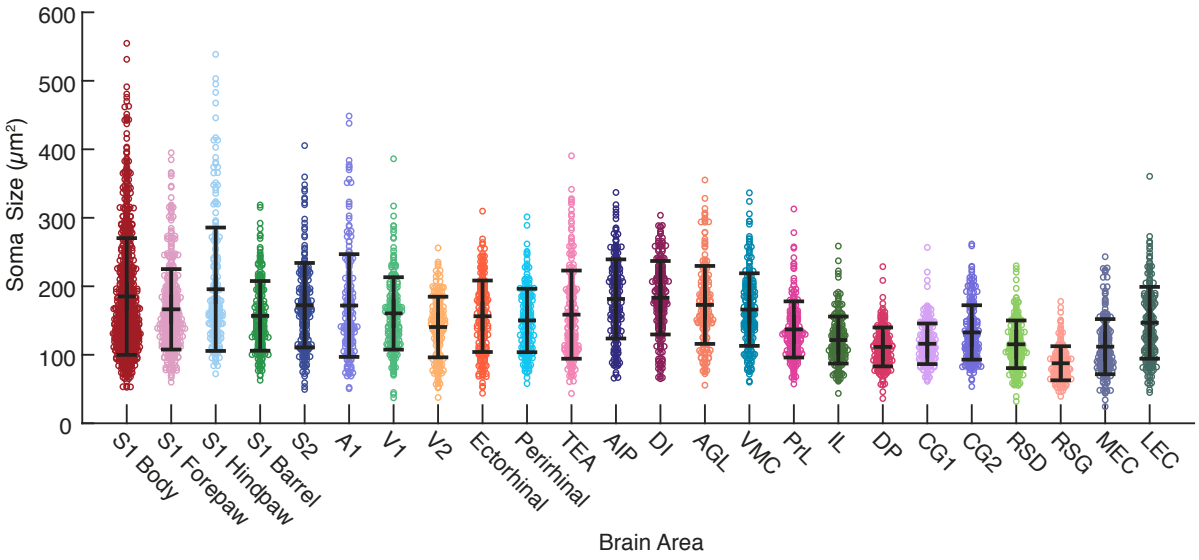

Figure S3. Soma size of L5 neurons across cortical areas, related to Figure 4.

Soma size of L5 neurons across 24 regions of the rat cortex. Primary somatosensory cortex (S1) shows a lot of areal heterogeneity and four distinct regions were analyzed in this area. S1 body = body area of primary somatosensory cortex, S1 forepaw = forepaw area of primary somatosensory cortex, S1 hindpaw = hindpaw area of primary somatosensory cortex, S1 barrel = barrel cortex, S2 = secondary somatosensory cortex, A1 = primary auditory cortex, V1 = primary visual cortex, V2 = secondary visual cortex, ectorhinal = ectorhinal cortex, perirhinal = perirhinal cortex, TEA = temporal association cortex, AIP = agranular insular cortex, DI = dysgranular insular cortex, AGL = agranular primary motor cortex, VMC = vibrissa motor cortex, PrL = prelimbic cortex, IL = Infralimbic cortex, DP = dorsal peduncular cortex, CG1 = cingulate cortex, area 1, CG2 = cingulate cortex area 2, RSD = retrosplenial dysgranular cortex, RSG = retrosplenial granular cortex, MEC = medial entorhinal cortex, LEC = lateral entorhinal cortex. Black crosses indicate mean ± STD

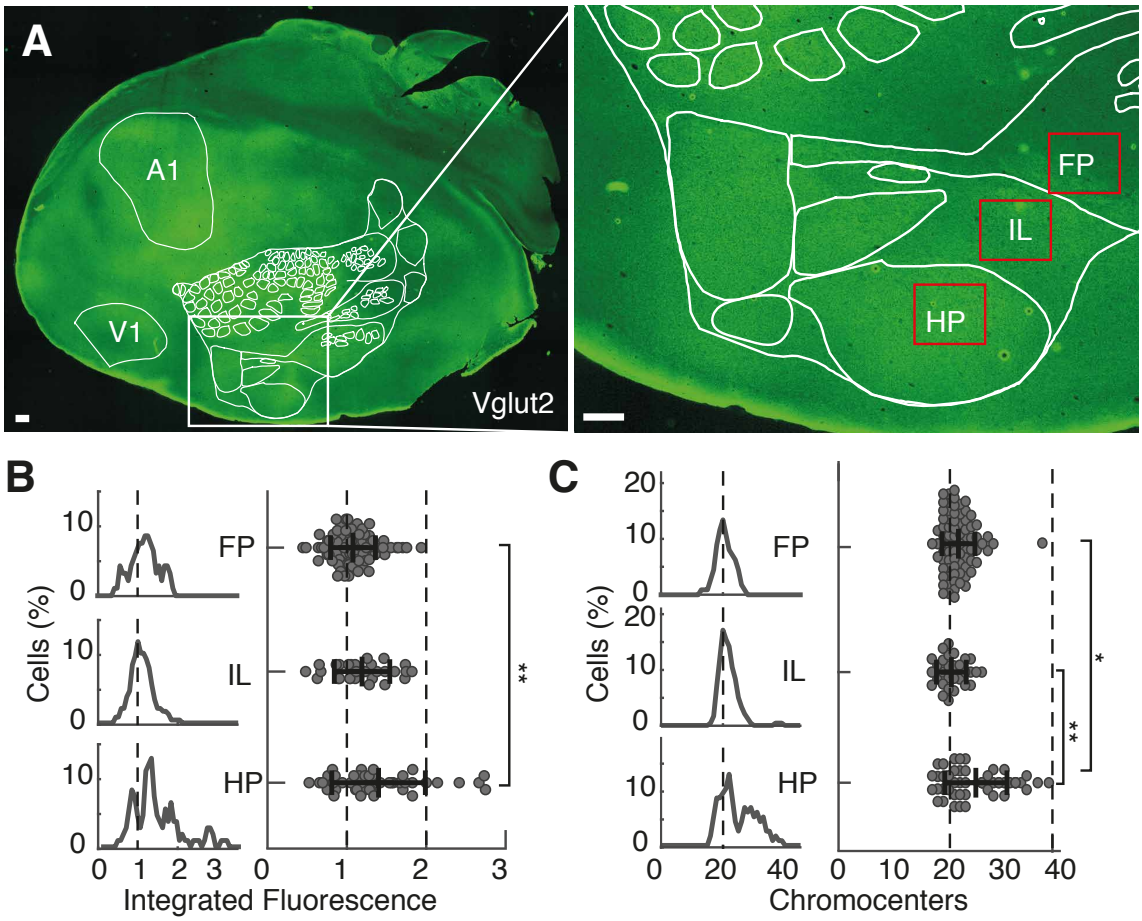

Figure S4. Integrated fluorescence and chromocenters of Ctip2+ neurons show sharp borders aligned with functional subdivisions of primary somatosensory cortex, related to Figure 4.

(**A**) Tangential section of rat cortex stained with Vglut2 to reveal thalamocortical axons to cortical L4. Primary somatosensory cortex was reconstructed based on Vglut2 staining. Subsequent analysis focuses on the borders between the forepaw (FP) and hindpaw (HP) region and the intermediate septum (interlimb, IL).

(**B**) Frequency distribution and univariate plot of integrated DAPI fluorescence of Ctip2+ neurons in the forepaw (n = 80), interlimb (n = 31) and hindpaw (blue, n = 51) region of primary somatosensory cortex. All cellular fluorescence measurements were normalized to the mean fluorescence of non-neurons in each section analysed (by definition = 1, not shown).

(**C**) Same as B for chromocenters.

Dashed lines indicate the means of integrated fluorescence or chromocenter counts of non-neurons (1.00 and 19 respectively) and twice this number. Black crosses indicate the mean ± STD. Stars indicate significant pairwise comparisons (Kruskal Wallis ANOVA, $P < 0.005$**, $P < 0.0005$***). Scale bars = 500 µm.

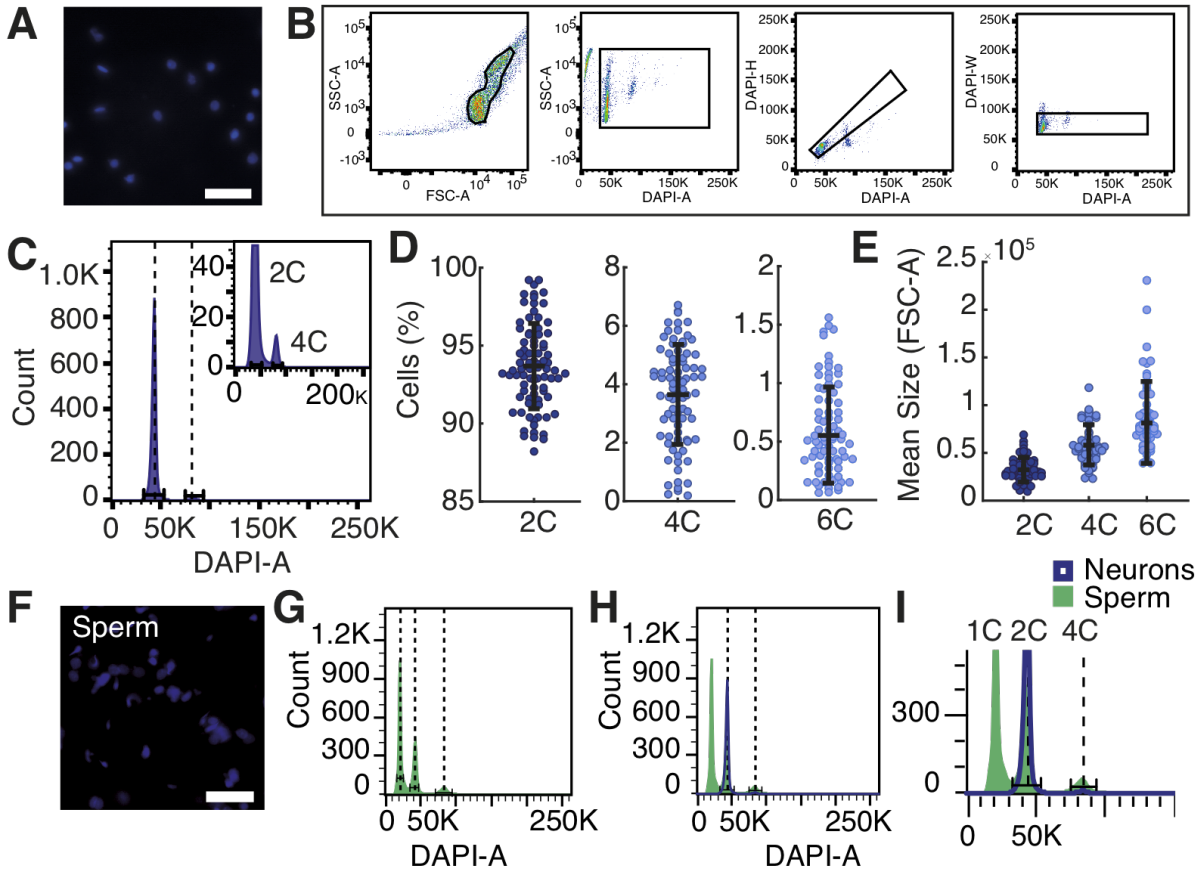

Figure S5. Flow cytometry of live cell nuclei isolated from rat cortex and testes, related to Figure 5.

(**A**) Confocal image of suspended nuclei from rat cortex stained with Höchst.

(**B**) Cell nuclei stained with the DNA dye Höchst were subjected to flow cytometric analysis. Particles were gated (polygonal box) on a forward scatter (FSC-A, particle size) versus sideward scatter (SSC-A, internal complexity) plot. Höchst positive particles were selected (square gate) on a SSC-A versus DAPI-A (intensity of Höchst staining) plot. Single cells were selected (square gate) on a DAPI-H versus DAPI-A plot. DAPI-H measures the height of the voltage pulse. For single cells DAPI-H increases proportionally to DAPI-A, the area of the voltage pulse. Doublets and clumps are disregarded. To ensure the complete exclusion of doublets, gated single nuclei were plotted on a DAPI-W (voltage pulse width) versus DAPI-A plot. DAPI-W of single cells does not increase proportionally to DAPI-A. All nuclei selected in the square gate in D are further processed as single nuclei.

(**C**) Example DNA histogram for live nuclei isolated from the adult rat cortex, showing a sharp peak for diploid nuclei and another small peak for tetraploid nuclei.

(**D**) Percent of diploid (left), tetraploid (middle) and hexaploid (right) nuclei reported by flow cytometry for 82 samples from 23 brains of suspended nuclei.

(**E**) Nuclear size as measured by FSC-A increases from diploid to tetraploid to hexaploid nuclei.

(**F**) Suspended live nuclei from rat testis stained with Höchst.

(**G**) DNA content histogram of nuclei from rat testis shows three peaks referring to haploid spermatids, diploid spermatogonia and tetraploid spermatocytes.

(**H**) DNA content histogram of nuclei from rat testes (green) and rat cortex (blue).

(**I**) Enlarged view of DNA histogram in E shows that the second and third sperm peak coincide with the first and second neuronal peak, confirming that the distance between both neuronal peaks represents a twofold increase in DNA content.

Black crosses indicate mean ± STD. Scale bars = 50µm

Supplemental Experimental procedures

All experimental procedures were performed according to German guidelines on animal welfare.

Brain and testes tissue preparation for immunohistochemistry
Male Wistar rats (~ P60, 250-400g) were anesthetized using isoflurane and euthanized by an intraperitoneal injection of 20% urethane. Rats were perfused transcardially 0.1 M phosphate buffered saline (1XPBS) followed by 4% paraformaldehyde (PFA) in 0.1 M phosphate buffer (PB). After perfusion, brains were removed from the skull and postfixed in PFA overnight. On the next day brains were washed in PB and transferred into a 30% sucrose solution in PB and left for at least 24 hours for cryoprotection. For cryosectioning, brains were embedded in Jung Tissue Freezing Medium. Coronal sections (40 µm) were obtained using a freezing microtome.

For the analysis of germ cells, rat testes were excised and immediately decapsulated following perfusion and the removal of the brain. Testes were treated alike brains. Overnight fixation in PFA was followed by immersion in 30 % sucrose for at least 24 hours. Testes were embedded in Jung Tissue Freezing Medium and 40 µm thick sections were obtained using a freezing microtome.

For the analysis of stellate and pyramidal projection neurons, tangential sections (40 µm) of the MEC were obtained by separating the entorhinal cortex from the remaining hemisphere by a cut parallel to the surface of the MEC. For subsequent sectioning the surface of the entorhinal cortex was attached to the block face of the microtome.

For the analysis of areal borders (Figure S6), brains were removed after perfusion, hemispheres were separated and subcortical structures detached. Cortices were flattened in phosphate buffer between two glass slides separated by clay spacers. Glass slides were weighed down with small ceramic weights for 3–5h at 48C. Flattened cortices (Figure 1c) were then stored overnight in a 4% PFA solution. Hemispheres were cut into 40 µm sections on a Vibratome.

Immunohistochemistry
Immunohistochemical staining was performed according to standard procedures. Briefly, sections were washed four times for 10 minutes in 1XPBS followed by incubation in 10mM citrate buffer (pH 7) in a 60°C water bath. After one hour wells were removed from the water bath and left to cool for 30 minutes. Next, sections were incubated in a blocking solution containing 1XPBS and 0.5% Triton X-100 (PBS-X) and 10% goat serum for two hours at room temperature. Primary antibodies against the neuron specific protein NeuN (1:1000, Millipore, Darmstadt, Germany), the calcium-binding albumin protein Parvalbumin (PV, 1:1000, Millipore, Darmstadt, Germany), the zinc-finger transcription factor Ctip2 (1:1000, Abcam, Cambridge, UK), the calcium binding protein calbindin (1:5000) and the extracellular matrix protein reelin (1:1000) were used. Free-floating sections were incubated with primary antibodies in a solution containing PBS-X, 1% BSA and 10% goat serum for at least 24 hours under mild shaking at 4°C. Washing sections in 1XPBS was followed by detection with secondary antibodies coupled to different fluorophores (Alexa 488, 546 and 633, Life Technologies, Darmstadt, Germany). Sections were incubated in secondary antibodies diluted (1:500) in PBS-X and 2% goat serum for at least 24h in the dark. For multiple antibody staining, antibodies raised in different host species were used. After antibody staining, sections were washed in 1XPBS and incubated with the nuclear acid dye DAPI diluted in 1XPBS (5 µg/ml) for 30 minutes. Finally, sections were mounted on gelatine coated glass slides with Fluoromount mounting medium.

For histological analysis of germ cells, rat testes sections were stained with DAPI for 30 minutes and mounted on gelatine coated glass slides using Fluoromount.

Image Acquisition
Epifluorescence and confocal microscopes equipped with a camera were used to acquire z-stacks (0.3 to 1.0 µm z-spacing) of immunofluorescently labelled sections. Fluorophores were excited using the appropriate filter cubes (Alexa 488-L5, Alexa 546-N3, Alexa 633-Y5, DAPI-A3). Fluorescent images were acquired with a 63x (confocal) or a 100x (epifluorescence) oil-immersion objective.

Somatic and nuclear size
Our initial analysis focused on primary visual cortex, which was localized using the rat brain atlas (Paxinos & Watson, 1980). Visual cortex contains a prominent and densely packed layer 4, which eases differentiation of layer 4 and layer 5. To analyse the distribution of neuronal and nuclear size across layer cortical layers, epifluorescent image stacks of NeuN (red), Ctip2 (yellow), PV (green) and DAPI (blue) fluorescence were obtained with optical sections 1 µm apart. Stacks were analysed using the commercially available software Neurolucida. To approximate neuronal and nuclear size, a region of interest (ROI) was drawn around NeuN positive cell somata and DAPI

stained nuclei in the focal z-plane with maximal intersection with the cell. Cells were identified as neuronal (NeuN+) or non-neuronal (NeuN−) and for further analysis as interneurons (PV+) or Ctip2−positive (Ctip2+) or Ctip2−negative (Ctip2−) principal cells on the basis of the multi-colour overlap. Similarly, stacks of MEC were acquired and stellates and pyramids were identified according to positive staining for reelin and calbindin, respectively. In order to reduce a potential observer bias, all nuclear measurements (size, fluorescence and chromocenters) were obtained prior to establishing the cellular identity.

Quantification of integrated DAPI fluorescence
In order to assess nuclear DNA content in intact brain sections, DAPI fluorescence was quantified. DAPI binds to double stranded DNA stoichiometrically and therefore variation in fluorescence intensity between individual nuclei represents differences in DNA content. In order to measure DAPI fluorescence for a nucleus, average fluorescent intensity of all pixels within a ROI, drawn around a nucleus, was measured. Next, average fluorescence of a nearby ROI in the background was measured and subtracted from the nuclear ROI fluorescence for background correction. Background subtracted intensities were multiplied with the area of the nuclear ROI in each focal plane. The net integrated fluorescent intensity was added up across all relevant focal planes to obtain an integrated DAPI fluorescence measurement for each nucleus. Despite very stringent control of staining and imaging procedures, absolute values of integrated fluorescence varied across sections and image stacks. Nevertheless, the distribution of fluorescent measurements was consistent across stacks. Therefore, all fluorescent measurements were normalized to the average fluorescence of non-neuronal cells. Integrated DAPI fluorescence was compared between neuronal and non-neuronal cells and for further analysis between PV+ interneurons, Ctip2+ and Ctip2− pyramidal neurons as identified by the multicolour overlap.

Analysis of chromocenters
In order to further verify that variation in integrated fluorescence is due to differences in nuclear DNA content, we counted chromocenters, which are spots of heterochromatic DNA that correlate in number with the number of chromosomes. Since chromosomes cannot be quantified in postmitotic neurons in intact brain sections, such counts were obtained to approximate chromosome number. Upon DAPI staining chromocenters appear as bright fluorescent spots. Hence chromocenters were counted in fluorescent image stacks and summed across all focal planes of a nucleus. In some cases, chromocenters appeared in more than one optical plane, in which case they were tracked to avoid double counting. Given the subjective nature of this measurement, analysis was restricted to well-stained sections and image stacks of excellent quality. Chromocenters were compared between neuronal and non-neuronal nuclei and for further analysis between PV+ interneurons and Ctip2+ and Ctip2− principal neurons as identified by the multicolour overlap.

Further analysis of cell and nuclear size, integrated DAPI fluorescence and chromocenter counts in cortical layers was extended to other cortical areas, including the primary auditory cortex, retrosplenial cortex, somatosensory cortex and medial entorhinal cortex, identified using a rat brain atlas.

Integrated fluorescence and chromocenters in rat testes tissue
In order to confirm integrated DAPI fluorescence measurements and chromocenter counts as valid methods to assess DNA content, we also examined germ cells in rat testes sections, namely spermatogonia and spermatids, which are easily recognized by their characteristic shape. Spermatogonia are by definition diploid germ cells, which give rise to haploid spermatids. Henceforth, a twofold increase in integrated DAPI fluorescence and chromocenters between spermatids and spermatogonia is expected in order to validate this approach as a DNA quantification method. Epifluorescent image stacks of DAPI stained testes sections were acquired, displaying cross-sections of seminiferous tubules, which contained diploid spermatogonia and haploid spermatids. DAPI fluorescence of spermatogonia and sperm cells was integrated in the same way as was done for brain cells and measurements were normalized to the average fluorescence of spermatogonia. Chromocenters were also counted in spermatogonia in the same way as was done for brain cells. Chromocenters were not counted in sperm cells, since their DNA is too condensed making chromocenters invisible.

Fixed nuclear suspension for fluorescent in situ hybridization
Male Wistar rats (150-400g) were anesthetized using isoflurane and euthanized by decapitation. Brains were removed, hemispheres were separated and subcortical areas removed. Each hemicortex was then flattened and sliced tangentially on a vibratome into 100 µm sections. Every second slice was added to a 24 well plate and stained for cytochrome oxidase to reveal layer 4 (Wong-Riley, 1989) . Every other slice was placed in a 50µl Eppendorf tube on dry ice, paying particular attention to the order in which slices were collected. To make separate cell suspensions containing either layer 4 or layer 5 cells, cytochrome oxidase stained sections were inspected to reveal which frozen sections contained either layer 4 or layer 5. Frozen sections of layer 4 or of layer 5 were transferred to a dounce tissue grinder and minced using small pestles. After adding 2ml of 1XPBS, tissue was further homogenized using large pestles. Next, samples was transferred to a 15 ml Eppendorf tube and 1ml of 60%

glacial acetic acid was added and left to incubate for 3 to 5 minutes. Further 9ml of ice could (-20°C) Carnoys fixative (methanol/acetic acid 3:1 freshly prepared at 4°C) were added. Samples was centrifuged at 1000 x g for 5 minutes at room temperature. The supernatant was discarded and 9ml of ice cold Carnoys fixative was added before centrifuging again at 1000xg for 8 minutes at room temperature. This step was repeated 4 times. After checking the nuclear density of the suspension on a microscopic slide, 50 to 100 µm of suspension were dropped on a superfrost slide and air dried for 15 minutes at RT.

Fluorescent in situ hybridization

For fluorescent in situ hybridization (FISH) of rat telomeres, an Alexa-488 conjugated peptide nucleic acid (PNA) probe against the C rich region of rat telomere was used (PNA Bio, Thousand Oaks, CA). For hybridization, the manufacturer's instructions were followed. In short, slides were incubated in 1XPBS for 2 minutes and then in 0.01M HCl for 5 minutes on a shaker at room temperature. Next, slides were digested in pepsin solution at 37°C in a water bath for 5 to 10 minutes. Pepsin solution was freshly prepared: 1ml of 1M HCl was added to 99ml ddH_2O in a cuvette and heated to 37°C in a water bath. Next 50 µl of pepsin stock solution (10% w/v) was added and the solution was left in the water bath for 20 minutes before slides were added. Afterwards slides were washed in 1XPBS three times at room temperature before postfixing in 1% PFA for 10 minutes at room temperature with gentle agitation. Slides were washed in 1XPBS three times and then dehydrated in an ethanol series (70, 90 and 100%, 3 minutes each) and air dried. Slides were baked at 85°C for 10 minutes together with 200 µl of hybridization buffer (20mM Tris, 60% formamide, 0.5% blocking reagent, 11096176001 Roche, Berlin, Germany). Next, 5 µl of a peptide nucleic acid probe were added to the hot hybridization buffer and 25 µl were added to each slide. Slides were covered with cover glasses, sealed with fixogum and placed in the heat cupboard for 10 minutes at 85°C. Slides were left in a humidifying chamber at room temperature overnight. On the next day, cover glasses were removed and slides were washed in 2X SSC and 0.1% Tween-20 twice at 55°C for 10 minutes and once at room temperature. Slides were then incubated in DAPI solution (0.5mg/ml DAPI in 2XSSC) for 10 minutes, washed with 2XSSC, 1XSSC and finally ddH_2O for two minutes each. Slides were air dried and mounted using Fluoromount and cover slipped.

Quantification of telomeres

Upon FISH, telomeres appeared as bright green spots in the nucleus counterstained with DAPI (blue). Image stacks (z-spacing of 0.3 µm) of single nuclei were captured on a confocal microscope using 100x magnification and an optical zoom of 7. ImageJ was used to measure nuclear area (μm^2) at the maximum intersection with the imaging plane. In single cell suspensions, nuclei are distorted and therefore absolute size cannot be compared to measurements form intact tissue sections. Telomeres were counted by hand and care was taken to separate overlapping telomeres in the three dimensional stack while avoiding double counting.

Live nuclear suspension for flow cytometry

Male Wistar rats (150-400g) were anesthetized using isoflurane and euthanized by decapitation. Brains were isolated and subcortical areas were removed. Cortical tissue was frozen at -80°C until used. On the day of the experiment, tissue was homogenized in 250 µm of low sucrose buffer (0.32M sucrose, 10mM HEPES (pH 8), 5mM CaCl2, 2mM Mg(Ac)2, 1mM DTT, 0.1mM EDTA, 0.1%Triton X-100) with small pestles till big chunks of tissue were dissociated and then with large pestles. The homogenized suspension (1ml) was carefully layered onto 6ml of high sucrose buffer (1M sucrose, 10mM HEPES (pH 8), 3mM Mg(Ac)2, 1mM DTT) in a 15ml Eppendorf tube followed by centrifugation at 4000rpm for 10 minutes at 4°C. A light yellow pellet appeared on the bottom of the tube. The supernatant was discarded and the pellet was resuspended in 500µl 1XPBS. The nuclei suspension was filtered through a 40µm nylon mesh. All steps were performed on ice. Nuclei were then stained with Höchst.

Flow cytometry

Flow cytometry was performed with a BD LSR II Flow cytometer (BD Biosciences, San Jose, CA) equipped with an ultra violet laser (405nm). The emission filter used was BP440/40. Data was collected using FACSDiva (BD Biosciences) and FlowJo (FlowJO, LLC, Ashland, OR) and displayed using biexponential scaling. Single nuclei were gated as follow: first, a clean-up gate was placed on the forward (FSC-A) versus sideward (SSC-A) scatter plot. Next, nuclei that incorporated DAPI were gated from cellular debris in the SSC-A versus DAPI-A plot. Next, doublets and clumps were excluded by gating the DNA pulse area (DAPI-A) versus its corresponding height (DAPI-H) (Nunez, 2001). The exclusion of doublets was confirmed/refined by checking the DNA pulse area (DAPI-A) versus the pulse width (DAPI-W) of the selected population. The percentage of diploid, tetraploid and hexaploid nuclei was derived from the DNA histogram (DAPI-A) using horizontal gates.

6 General Discussion

This thesis consists of two parts, which investigate novel forms of cellular specialization within functionally defined structures of the neocortex. The first part (**Chapters 2 to 4**) reveals that the cortical input layer, layer 4, of the genital somatosensory field undergoes some remarkable changes during puberty, which are not seen in other parts of the somatosensory cortex. Our findings suggest that genital touch might be processed uniquely in the cortex, possibly providing a substrate for the great salience genital touch has in our society. The second part of the thesis (**Chapter 5**) examines the cellular architecture of the cortical output layer, layer 5. Our findings suggest, that some remarkably large neurons in cortical layer 5 have an increased DNA content, potentially providing them with the cellular machinery to serve their high metabolic demands. In this chapter we will first separately discuss these two parts of the thesis before highlighting some important shared themes that bridge these apparently remote fields of research.

6.1 Sexual maturation of genital cortex layer 4

In **Chapters 2 to 4** we investigated puberty and experience dependent development of genital cortex. Layer 4 is a unique cortical structure, where sensory input from the body surfaces reaches the first relay of cortical processing, namely excitatory stellate and pyramidal neurons. Typically, somatosensory layer 4 is conceived as particularly stable to perturbations (Harding-Forrester and Feldman, 2018). However, we find that within genital cortex layer 4, thalamic afferents expand during puberty in a hormone dependent manner (**Chapter 2**). Moreover, we show that in females this expansion can be advanced by sexual experience or by repeated sensory stimulation of the genital elicited with brushing (**Chapter 2**). Investigating the underlying mechanism of this expansion, we find the maturation of genital cortex is not accompanied by a gain in peripheral innervation of the mouse penis (**Chapter 3**). Finally, we

showed that during puberty, there are cell specific changes within cortical layer 4, where some neurons gain the expression of a layer 4 specific transgene (**Chapter 4**). Similar to our observations in **Chapter 2**, the gain of transgene expression neurons was accelerated by sexual experience.

6.1.1 Genital touch shapes body and brain

Our research suggests that, unlike other areas of primary somatosensory cortex, genital cortex undergoes late, experience dependent maturation during puberty. These findings add to a growing body of literature, which is starting to uncover a number of key neurodevelopmental processes occurring during puberty (Piekarski et al., 2017; Walker et al., 2017), an important time for physical, cognitive, social and emotional maturation (Juraska and Willing, 2017; Dahl et al., 2018; Worthman and Trang, 2018). In humans, there is evidence that the timing of puberty is shaped by environmental factors (Walvoord, 2010). This notion is corroborated by animal studies showing that social experience, pheromones as well as touch, have a strong effect on the onset of sexual maturation (Vandenbergh, 1967, 1969; Bronson and Maruniak, 1975; Drickamer, 1977; Massey and Vandenbergh, 1980). In **Chapter 2** we were able to show, that in rats co-housing prepubertal females with sexually mature males not only advances sexual maturation but also genital cortex expansion. Interestingly, this observation was dependent on touch and could be mimicked by supplementing conspecific touch with gentle stroking of female genitals by a human experimenter. Using cell-specific in vivo imaging (**Chapter 4**), we were further able to show that even a co-housing period as short as three days accelerated the gain of layer 4 like transgene expression in genital cortex. Together, these observations highlight that experience not only modulates sexual maturation but also shapes puberty associated neuronal dynamics in genital cortex.

The importance of these findings is highlighted by the observation that similar to mice, early inappropriate genital touch may be linked to precocious puberty in humans (Herman-Giddens et al., 1988; Boynton-Jarrett et al., 2013; Noll et al., 2017). Interestingly, the putative cortical genital field appears thinned in participants who have experienced early childhood sexual abuse (Heim et al., 2013). Besides the unconceivable, detrimental emotional consequences of sexual abuse, precocious puberty often has negative behavioral as well as physical consequences (Carel et al., 2004; Colich et al., 2019). Early sexual maturation can result in prolonged estrogen exposure, which may be associated with an increase in reproductive cancers (Bernstein, 2002; McLachlan et al., 2006). Interestingly, there is also evidence showing that sex hormones are directly associated with differences in thickness of somatosensory cortex in humans (Nguyen

et al., 2013, 2016). Integrating our findings in rodents with observations made in humans suggests that puberty represents an important period of neuronal and physical development, which is particularly susceptible to external modulators. Together, these findings highlight the often negative consequences of precocious puberty and the need to increase public awareness to ensure appropriate adolescent maturation.

6.1.2 From periphery to cortex

Besides investigating how pubertal maturation and sexual experience shape the expansion of genital cortex, we also examined the underlying cellular mechanisms. Based on the functional identification of genital cortex (Lenschow et al., 2016), we first measured the size of this area in sections of pre- and postpubertal rats based staining with the metabolic marker cytochrome oxidase (**Chapter 2**). We find that genital cortex undergoes a significant expansion during puberty. Furthermore, antibody staining of thalamocortical afferents suggests that this expansion is due to an invasion of the dysgranular zone that surrounds the genital field, causing an overall increase in size. Typically, the size of a cortical field represents the density of sensory receptors on the peripheral sensory surface (Lee and Woolsey, 1975; Welker and Van der Loos, 1986). In the somatosensory system, highly innervated regions of the skin therefore occupy proportionally larger areas of the cortical surface, assuming that neuronal density is similar. Therefore, we asked, whether the expansion of genital cortex in terms of thalamic afferents might be accompanied by an increase in peripheral sensory fibers innervating the genitals. In **Chapter 3** we quantified the absolute numbers of fibers in the mouse dorsal penile nerve. However, we did not find a difference comparing pre- and postpubertal males. One possible explanation is that puberty associated plasticity of the dorsal penile nerve is only detectable at the nerve endings. Using a similar histological approach, it has been shown that peripheral nerve terminals exhibit sprouting in hairy skin of the trunk (Botchkarev et al., 1997). Similarly, a number of studies have shown that hormonal fluctuations are associated with changes in the density of free nerve endings innervating the female genital tract (Ting et al., 2004; Liao and Smith, 2014; Mónica Brauer and Smith, 2015). Accordingly, it is conceivable that our approach was not able to detect plasticity of the peripheral penile innervation during puberty.

Besides potential plasticity, it is also conceivable that genital cortex maturation involves more central processes. Therefore, we applied a new approach in **Chapter 4**, where we used chronic imaging to visualize genital cortex layer 4 in vivo while mice were sexually maturing. Given the intricate relationship between thalamocortical axons and excitatory pyramidal and stellate neurons in layer 4 (Callaway and Borrell, 2011; Antón-Bolaños et al., 2018), we used a

transgenic mouse, Scnn1a-Cre, that labels layer 4 excitatory neurons, which cluster densly in areas receiving strong lemniscal input (Madisen et al., 2010; Pouchelon et al., 2014). The density of such Scnn1a+ neurons varies between body parts of the primary somatosensory cortex. Moreover, in genital cortex the number of Scnn1a+ neurons increased steadily over the course of puberty. We propose that this increase is a result of an increase in thalamocortical input to this area (**Chapter 2**). Assuming that the peripheral plasticity is limited in genitals, one might speculate about the central processes underlying the observed changes within layer 4. Remodeling of thalamocortical axons has previously been shown in the adult cortex (De Paola et al., 2006; Gogolla et al., 2007), which could result in new synapses formed with layer 4 neurons, which did not receive thalamic input previously. Interestingly, nursing behavior is associated with significant plasticity of trunk receptive fields (Xerri et al., 1994; Rosselet et al., 2006). While nursing behavior definitely involves a great increase of sensory stimulation of the trunk and might therefore result in use-dependent plasticity, it is possible that the hormonal status of nursing females contributes or facilitates such plasticity. Similarly, the current results demonstrate genital cortex remodeling not only as result of increased sensory stimulation, but also as part of natural pubertal development. Given the wide distribution of steroid receptors in the cortex (Simerly et al., 1990; Shughrue et al., 1997; Kritzer, 2002), it may therefore be possible that during puberty the combination of steroid activation as well as increased thalamic input might result in the observed changes time course of genital cortex maturation. Additional experiments will be key to understand how pubertal hormones and experience interact to shape both thalamic afferents and cortical layer 4 in this area.

6.1.3 Technical considerations and future directions

Finally, we would like to discuss some technical aspects of the experiments performed as part of the **Chapters 2 to 4**, which further highlight specific questions that remain to be answered. While chronic imaging provides a unique opportunity to access a 2D structure like genital cortex, it would have been great to simultaneously visualize additional circuit components, such as the thalamic afferents or transgene negative layer 4 neurons (Scnn1a–). Unfortunately, there were no feasible transgenic strategies available to pursue these lines of research. Accordingly, it remains a conundrum how stellate, pyramidal neurons and the likely existing intermediate cell-type (Callaway and Borrell, 2011) map onto Scnn1a expression and which role these two cell-types have within genital cortex. Moreover, simultaneous access to the thalamic afferents arriving in genital cortex, possibly using optogenetics, would have advanced our understanding of the synaptic input to both, Scnn1a+ and Scnn1a– neurons. In a similar vein, our results

suggest that there may be some puberty related differences in the responsiveness of excitatory neurons in female genital cortex (**Chapter 4**). Despite the advantages of functional two-photon imaging, certain aspects of the experiments made it particularly challenging to chronically image sensory evoked responses in genital cortex. For one, imaging the same neurons over several weeks while not only the imaged area (gain of Scnn1a+) but also the entire brain (growth) change substantially was particularly demanding. In addition, the comparison of sensory evoked responses over weeks requires sensory stimulation to be similar across imaging days. Precise stimulation of the external genital as well as exerting behaviorally relevant sensory stimulation is difficult. Therefore further development of naturalistic stimulation as well as imaging techniques will be needed to provide more conclusive results on the physiological responses of excitatory neurons in this area during puberty. Nevertheless, the publications (**Chapter 2 to 4**) presented in this thesis significantly extend our previous insights into the maturation of the cortical genital field during this highly relevant period of physical and neuronal development. Overall, we demonstrate that layer 4 of somatosensory cortex does not represent a homogenous cortical structure, but instead exhibits some remarkable areal differences that might underly the differential salience of touch on different body parts.

6.2 Polyploidy as a novel mechanism to increase cellular diversity in layer 5

In the second part of this thesis (**Chapter 5**), we turn away from the cortical input layer, and instead focus on the corresponding output layer, layer 5. Here, we investigate diversity of excitatory cell-types from a novel point of view. Based on the observation that cell size differs strongly among excitatory projection neurons in this area (Chagnac-Amitai et al., 1990), we explored the possibility that a key determinant of cell size, namely ploidy (Kondorosi et al., 2000; Sugimoto-Shirasu and Roberts, 2003), contributes to excitatory cell diversity within cortical layer 5. Combining a number of different approaches to measure DNA content of layer 5 projection neurons, we were able to show that there is a small fraction of remarkably large, putatively polyploidy neurons, which are likely to correspond to subcortical projection neurons. To date this special type of genomic variation has received little attention in the nervous system (Lentz and Lapham, 1969; Mosch et al., 2007; Morillo et al., 2010; López-Sánchez and Frade, 2013) because of the great difficulty to systematically identify it, especially in intact adult neurons. While we can only speculate on the function of polyploidy in neurons, there are some interesting suggestions regarding other cell-types (Edgar and Orr-Weaver, 2001). Generally, the size of projection neurons is related to the their axodendritic properties, where greater somatic size is accompanied by a greater axon diameter and length, as well as a greater

conduction velocity (Cullheim, 1978; Lee et al., 1986). Therefore, a larger somatic size might be better suited to maintain efficient long-range projections. It has been shown, that polyploidy helps maintain such large soma size by increasing the amount of cellular machinery available and therefore provide an evolutionary mechanism to meet greater metabolic demands (Edgar and Orr-Weaver, 2001; Selmecki et al., 2015). Overall, the contribution of genomic variations to cell diversity of both, the healthy and diseased brain, is greatly understudied and hopefully the increasingly fast development of evermore intricate molecular techniques will soon provide more complete investigations of this unusual phenomenon.

6.3 Conclusion

Delineating functionally specialized brain areas according to cell-type is important to understand the processing of neuronal signals in the neocortex, dating back to the fathers of neuroanatomy, Broadman, Vogt and Campbell (Campbell, 1905; Brodmann, 1909; Vogt, 1910). The advent of molecular and cellular techniques brought about by the last two decades has, however, not provided the much desired, straightforward taxonomy of neocortical excitatory cell-types (Johnson and Walsh, 2017). Instead, the necessity to take into account numerous dimensions including gene expression, epigenomic state, morphology, electrophysiology and laminar and areal position make the recognition of neuronal subtypes excessively challenging (Mukamel and Ngai, 2019). Accordingly, the delineation of cortical areas based on their inhabitant cell-types has become exceptionally complex. The studies reported in this thesis contribute to this issue by revealing that there are novel forms of cellular specialization which distinguish not only the primary sensory cortices but, in the case of the somatosensory cortex, even highly specialized subfields. On the one hand, excitatory neurons in genital cortex, but not other subfields of somatosensory cortex, appear to undergo a unique developmental trajectory, which even involves changes in their gene expression. This observation adds to previous reports of neurons that change their gene expression pattern and epigenomic state in response to experience (Hrvatin et al., 2018) and suggests that neurons can transition through different classes of cell-types. On the other hand, our observations in layer 5 suggest that differences in ploidy also contribute to cellular diversity between cortical areas. Moreover, putatively polyploid neurons were not distributed evenly across the cortical sheet. Instead their distribution aligned sharply with cytoarchitectonic borders of and even within primary sensory cortices. We find this observation particularly interesting because it relates to our findings on genital cortex and highlights the cellular specialization of functional subdivisions of primary somatosensory cortex. Overall, our observations highlight the need to

investigate the cytoarchitectonic organization of the neocortex not only with respect to stable, large scale organizational principles, but also to focus on increasingly specialized local circuits, which can be shaped by evolutionary adaption, experience and development.

References

Adler NT, **Davis PG**, **Komisaruk BR** (1977) Variation in the size and sensitivity of a genital sensory field in relation to the estrous cycle in rats. *Horm Behav 9*:*334–344*.

Amunts K, **Zilles K** (2015) Architectonic Mapping of the Human Brain beyond Brodmann. Cell Press.

Antón-Bolaños N, **Espinosa A**, **López-Bendito G** (2018) Developmental interactions between thalamus and cortex: a true love reciprocal story. *Curr Opin Neurobiol 52*:*33–41*.

Beaulieu JM, **Leitch IJ**, **Patel S**, **Pendharkar A**, **Knight CA** (2008) Genome size is a strong predictor of cell size and stomatal density in angiosperms. *New Phytol 179*:*975–986*.

Bernstein L (2002) Epidemiology of endocrine-related risk factors for breast cancer. *J Mammary Gland Biol Neoplasia 7*:*3–15*.

Berthold AA (1849) Transplantation der hoden. *Arch Anat Physiol*:*42–46*.

Betz W (1874) Anatomischer Nachweis Zweier Gehinrzentren. *Zentralbl Med Wiss 12*.

Botchkarev VA, **Eichmüller S**, **Johansson O**, **Paus R** (1997) Hair cycle-dependent plasticity of skin and hair follicle innervation in normal murine skin. *J Comp Neurol 386*:*379–395*.

Boynton-Jarrett R, **Wright RJ**, **Putnam FW**, **Lividoti Hibert E**, **Michels KB**, **Forman MR**, **Rich-Edwards J** (2013) Childhood abuse and age at menarche. *J Adolesc Heal 52*:*241–247*.

Brodmann K (1909) Vergleichende Lokalisationslehre der Grosshirnrinde in ihren Prinzipien dargestellt auf Grund des Zellenbaues. Barth.

Bronson FH, **Maruniak JA** (1975) Male-induced puberty in female mice: Evidence for a synergistic action of social cues. *Biol Reprod 13*:*94–98*.

Calaresu FR (1970) Experimental studies on the dorsal nerve of the penis of the rat. *Am J Anat 127*:*415–421*.

Callaway EM, **Borrell V** (2011) Developmental Sculpting of Dendritic Morphology of Layer 4 Neurons in Visual Cortex: Influence of Retinal Input. *J Neurosci 31*:*7456–7470*.

Campbell AW (1905) Histological studies on the localisation of cerebral function. University Press.

Carel J-C, **Lahlou N**, **Roger M**, **Chaussain JL** (2004) Precocious puberty and statural growth. *Hum Reprod Update 10*:*135–147*.

Chagnac-Amitai Y, **Luhmann HJ**, **Prince D a.** (1990) Burst generating and regular spiking layer 5 pyramidal neurons of rat neocortex have different morphological features. *J Comp Neurol 296*:*598–613*.

Chapin JK, **Lin C -S** (1984) Mapping the body representation in the SI cortex of

anesthetized and awake rats. *J Comp Neurol 229*:*199–213*.

Chen YL, **Chao TT**, **Wu YN**, **Chen MC**, **Lin YH**, **Liao CH**, **Wu CC**, **Chen KC**, **Chou SSP**, **Chiang HS** (2018) NNOS-positive minor-branches of the dorsal penile nerves is associated with erectile function in the bilateral cavernous injury model of rats. *Sci Rep 8*.

Colich NL, **Platt JM**, **Keyes KM**, **Sumner JA**, **Allen NB**, **McLaughlin KA** (2019) Earlier age at menarche as a transdiagnostic mechanism linking childhood trauma with multiple forms of psychopathology in adolescent girls. *Psychol Med*:*1–9*.

Constantinople CM, **Bruno RM** (2013) Deep cortical layers are activated directly by thalamus. *Science (80-) 340*:*1591–1594*.

Cullheim S (1978) Relations between cell body size, axon diameter and axon conduction velocity of cat sciatic α-motoneurons stained with horseradish peroxidase. *Neurosci Lett 8*:*17–20*.

Dahl RE, **Allen NB**, **Wilbrecht L**, **Suleiman AB** (2018) Importance of investing in adolescence from a developmental science perspective. *Nature 554*:*441–450*.

De Carlos JA, **Borrell J** (2007) A historical reflection of the contributions of Cajal and Golgi to the foundations of neuroscience. *Brain Res Rev 55*:*8–16*.

De Paola V, **Holtmaat A**, **Knott G**, **Song S**, **Wilbrecht L**, **Caroni P**, **Svoboda K** (2006) Cell Type-Specific Structural Plasticity of Axonal Branches and Boutons in the Adult Neocortex. *Neuron 49*:*861–875*.

Douglas RJ, **Martin KAC** (2004) Neuronal Circuits of the Neocortex. *Annu Rev Neurosci 27*:*419–451*.

Drickamer LC (1977) Delay of sexual maturation in female house mice by exposure to grouped females or urine from grouped females. *Reproduction 51*:*77–81*.

Drickamer LC, **Murphy RX** (1978) Female mouse maturation: Effects of excreted and bladder urine from juvenile and adult males. *Dev Psychobiol 11*:*63–72*.

Edgar B a., **Orr-Weaver TL** (2001) Endoreplication cell cycles: More for less. *Cell 105*:*297–306*.

Epstein CJ (1967) Cell Size, Nuclear Content, and the Development of Polyploidy in the Mammalian Liver. *Proc Natl Acad Sci U S A 57*:*327–334*.

Feldman DE, **Brecht M** (2005) Map plasticity in somatosensory cortex. American Association for the Advancement of Science.

Fox K (1992) A critical period for experience-dependent synaptic plasticity in rat barrel cortex. *J Neurosci 12*:*1826–1838*.

Gerfen CR, **Economo MN**, **Chandrashekar J** (2018) Long distance projections of cortical pyramidal neurons. *J Neurosci Res 96*:*1467–1475*.

Glazewski S, **Fox K** (1996) Time course of experience-dependent synaptic potentiation and depression in barrel cortex of adolescent rats. *J Neurophysiol 75*:*1714–1729*.

Gogolla N, **Galimberti I**, **Caroni P** (2007) Structural plasticity of axon terminals in the adult. *Curr Opin Neurobiol 17*:*516–524*.

Hallman LE, **Schofield BR**, **Lin C -S** (1988) Dendritic morphology and axon collaterals of corticotectal, corticopontine, and callosal neurons in layer V of primary visual cortex of the hooded rat. *J Comp Neurol 272*:*149–160*.

Han SH, **Lee S-H** (2014) Differential Growth of the Reproductive Organs during the Peripubertal Period in Male Rats. *Dev Reprod 17*:*469–475*.

Harding-Forrester S, **Feldman DE** (2018) Somatosensory maps, 1st ed. Elsevier B.V.

Harris KD, **Mrsic-Flogel TD** (2013) Cortical connectivity and sensory coding. *Nature 503*:*51–58*.

Heim CM, **Mayberg HS**, **Mletzko T**, **Nemeroff CB**, **Pruessner JC** (2013) Decreased cortical representation of genital somatosensory field after childhood sexual abuse. *Am J Psychiatry 170*:*616–623*.

Herbert J (1973) The role of the dorsal nerves of the penis in the sexual behaviour of the male rhesus monkey. *Physiol Behav 10*:*293–300*.

Herman-Giddens ME, **Sandler AD**, **Friedman NE** (1988) Sexual Precocity in Girls. *Am J Dis Child 142*:*431*.

Hrvatin S, **Hochbaum DR**, **Nagy MA**, **Cicconet M**, **Robertson K**, **Cheadle L**, **Zilionis R**, **Ratner A**, **Borges-Monroy R**, **Klein AM**, **Sabatini BL**, **Greenberg ME** (2018) Publisher Correction: Single-cell analysis of experience-dependent transcriptomic states in the mouse visual cortex. *Nat Neurosci 21*:*1*.

Jabaudon D (2017) Fate and freedom in developing neocortical circuits. *Nat Commun 8*:*1–9*.

Johnson MB, **Walsh CA** (2017) Cerebral cortical neuron diversity and development at single-cell resolution. *Curr Opin Neurobiol 42*:*9–16*.

Juraska JM, **Sisk CL**, **DonCarlos LL** (2013) Sexual differentiation of the adolescent rodent brain: Hormonal influences and developmental mechanisms. *Horm Behav 64*:*203–210*.

Juraska JM, **Willing J** (2017) Pubertal onset as a critical transition for neural development and cognition. *Brain Res 1654*:*87–94*.

Kaneko N, **Debski EA**, **Wilson MC**, **Whitten WK** (1980) Puberty acceleration in mice. II. Evidence that the vomeronasal organ is a receptor for the primer pheromone in male mouse urine. *Biol Reprod 22*:*873–878*.

Kim EJ, **Juavinett AL**, **Kyubwa EM**, **Jacobs MW**, **Callaway EM** (2015) Three Types of Cortical Layer 5 Neurons That Differ in Brain-wide Connectivity and Function. *Neuron 88*:*1253–1267*.

Klein BG, **Mooney RD**, **Fish SE**, **Rhoades RW** (1986) The structural and functional characteristics of striate cortical neurons that innervate the superior colliculus and lateral posterior nucleus in hamster. *Neuroscience 17*:*57–78*.

Kondorosi E, **Roudier F**, **Gendreau E** (2000) Plant cell-size control: Growing by ploidy? *Curr Opin Plant Biol 3*:*488–492*.

Kritzer MF (2002) Regional, Laminar, and Cellular Distribution of Immunoreactivity for ER and ERss in the Cerebral Cortex of Hormonally Intact, Adult Male and Female Rats. *Cereb Cortex 12*:*116–128*.

Krubitzer L, **Campi KL**, **Cooke DF** (2011) All rodents are not the same: A modern synthesis of cortical organization. *Brain Behav Evol 78*:*51–93*.

Lauer SM, **Lenschow C**, **Brecht M** (2017) Sexually selected size differences and conserved sexual monomorphism of genital cortex. *J Comp Neurol 525*:*2706–2718*.

Lee KH, **Chung K**, **Chung JM**, **Coggeshall RE** (1986) Correlation of cell body size, axon size, and signal conduction velocity for individually labelled dorsal root ganglion cells in the cat. *J Comp Neurol 243*:*335–346*.

Lee KJ, **Woolsey TA** (1975) A proportional relationship between peripheral innervation density and cortical neuron number in the somatosensory system of the mouse. *Brain Res 99*:*349–353*.

Lee Weller W, **Johnson JI** (1975) Barrels in cerebral cortex altered by receptor disruption in newborn, but not in five-day-old mice (Cricetidae and Muridae). *Brain Res 83*:*504–508*.

Lenschow C, **Copley S**, **Gardiner JMM**, **Talbot ZNN**, **Vitenzon A**, **Brecht M**, **Correspondence MB** (2016) Sexually Monomorphic Maps and Dimorphic Responses in Rat Genital Cortex. *Curr Biol 26*:*106–113*.

Lenschow C, **Sigl-Glöckner J**, **Brecht M** (2017) Development of rat female genital cortex and control of female puberty by sexual touch. *PLoS Biol 15*:*1–22*.

Lentz RD, **Lapham LW** (1969) A quantitative cytochemical study of the DNA content of neurons of rat cerebellar cortex. *J Neurochem 16*:*379–384*.

Levin RN, **Johnston RE** (1986) Social mediation of puberty: an adaptive female strategy? *Behav Neural Biol 46*:*308–324*.

Li H, **Crair MC** (2011) How do barrels form in somatosensory cortex? *Ann N Y Acad Sci 1225*:*119–129*.

Liao Z, **Smith PG** (2011) Adaptive plasticity of vaginal innervation in term pregnant rats. *Reprod Sci 18*:*1237–1245*.

Liao Z, **Smith PG** (2014) Persistent Genital Hyperinnervation Following Progesterone Administration to Adolescent Female Rats1. *Biol Reprod 91*:*1–9*.

López-Muñoz F, **Boya J**, **Alamo C** (2006) Neuron theory, the cornerstone of neuroscience, on the centenary of the Nobel Prize award to Santiago Ramón y Cajal. *Brain Res Bull 70*:*391–405*.

López-Sánchez N, **Frade JM** (2013) Genetic evidence for p75NTR-dependent tetraploidy in cortical projection neurons from adult mice. *J Neurosci 33*:*7488–7500*.

Madisen L, **Zwingman TA**, **Sunkin SM**, **Oh SW**, **Zariwala HA**, **Gu H**, **Ng LL**, **Palmiter RD**, **Hawrylycz MJ**, **Jones AR**, **Lein ES**, **Zeng H** (2010) A robust and high-throughput Cre reporting and characterization system for the whole mouse brain. *Nat Neurosci 13*:*133–140*.

Mason A, **Larkman A**, **Mason A** (1990) Correlations between morphology and electrophysiology of pyramidal neurons in slices of rat visual cortex. II. Electrophysiology. *J Neurosci 10*:*1415–1428*.

Massey A, **Vandenbergh JG** (1980) Puberty delay by a urinary cue from female house mice in feral populations. *Science 209*:*821–822*.

McLachlan JA, **Simpson E**, **Martin M** (2006) Endocrine disrupters and female reproductive health. *Best Pract Res Clin Endocrinol Metab 20*:*63–75*.

Meyer HS, **Egger R**, **Guest JM**, **Foerster R**, **Reissl S**, **Oberlaender M** (2013) Cellular organization of cortical barrel columns is whisker-specific. *Proc Natl Acad Sci U S A 110*:*19113–19118*.

Molnár Z, **Cheung AFP** (2006) Towards the classification of subpopulations of layer V pyramidal projection neurons. *Neurosci Res 55*:*105–115*.

Molyneaux BJ, **Arlotta P**, **Menezes JRL**, **Macklis JD** (2007) Neuronal subtype specification in the cerebral cortex. *Nat Rev Neurosci 8*:*427–437*.

Mónica Brauer M, **Smith PG** (2015) Estrogen and female reproductive tract innervation: Cellular and molecular mechanisms of autonomic neuroplasticity. *Auton Neurosci Basic Clin 187*:*1–17*.

Morillo SM, **Escoll P**, **de la Hera A**, **Frade JM** (2010) Somatic tetraploidy in specific chick retinal ganglion cells induced by nerve growth factor. *Proc Natl Acad Sci U S A 107*:*109–114*.

Mosch B, **Morawski M**, **Mittag A**, **Lenz D**, **Tarnok A**, **Arendt T** (2007) Aneuploidy and DNA replication in the normal human brain and Alzheimer's disease. *J Neurosci 27*:*6859–6867*.

Mucignat-Caretta C, **Caretta A**, **Cavaggioni A** (1995) Acceleration of puberty onset in female mice by male urinary proteins. *J Physiol 486*:*517–522*.

Mukamel EA, **Ngai J** (2019) Perspectives on defining cell types in the brain. *Curr Opin Neurobiol 56*:*61–68*.

Nguyen T-V, **McCracken J**, **Ducharme S**, **Botteron KN**, **Mahabir M**, **Johnson W**, **Israel M**, **Evans AC**, **Karama S** (2013) Testosterone-Related Cortical Maturation Across Childhood and Adolescence. *Cereb Cortex 23*:*1424–1432*.

Nguyen T-V, **McCracken JT**, **Albaugh MD**, **Botteron KN**, **Hudziak JJ**, **Ducharme S** (2016) A testosterone-related structural brain phenotype predicts aggressive behavior from childhood to adulthood. *Psychoneuroendocrinology 63*:*109–118*.

Noll JG, **Trickett PK**, **Long JD**, **Negriff S**, **Susman EJ**, **Shalev I**, **Li JC**, **Putnam FW** (2017) Childhood Sexual Abuse and Early Timing of Puberty. *J Adolesc Heal 60*:*65–71*.

Petreanu L, **Mao T**, **Sternson SM**, **Svoboda K** (2009) The subcellular organization of neocortical excitatory connections. *Nature 457*:*1142–1145*.

Piekarski DJ, **Boivin JR**, **Wilbrecht L** (2017) Ovarian Hormones Organize the Maturation of Inhibitory Neurotransmission in the Frontal Cortex at Puberty Onset in Female Mice. *Curr Biol 27*:*1735-1745.e3*.

Pouchelon G, **Gambino F**, **Bellone C**, **Telley L**, **Vitali I**, **Lüscher C**, **Holtmaat A**, **Jabaudon D** (2014) Modality-specific thalamocortical inputs instruct the identity of postsynaptic L4 neurons. *Nature 511*:*471–474*.

Rosselet C, **Zennou-Azogui Y**, **Xerri C** (2006) Nursing-Induced Somatosensory Cortex Plasticity: Temporally Decoupled Changes in Neuronal Receptive Field Properties Are Accompanied by Modifications in Activity-Dependent Protein Expression. *J Neurosci 26*:*10667–10676*.

Selmecki AM, **Maruvka YE**, **Richmond PA**, **Guillet M**, **Shoresh N**, **Sorenson AL**, **De S**, **Kishony R**, **Michor F**, **Dowell R**, **Pellman D** (2015) Polyploidy can drive rapid adaptation in yeast. *Nature 519*:*349–352*.

Shughrue PJ, **Lane M V.**, **Merchenthaler I** (1997) Comparative distribution of estrogen receptor-? and -? mRNA in the rat central nervous system. *J Comp Neurol 388*:*507–525*.

Simerly RB, **Swanson LW**, **Chang C**, **Muramatsu M** (1990) Distribution of androgen and estrogen receptor mRNA-containing cells in the rat brain: An in situ hybridization study. *J Comp Neurol 294*:*76–95*.

Simi A, **Studer M** (2018) Developmental genetic programs and activity-dependent mechanisms instruct neocortical area mapping. Elsevier Current Trends.

Smith PH, **Uhlrich DJ**, **Manning KA**, **Banks MI** (2012) Thalamocortical projections to rat auditory cortex from the ventral and dorsal divisions of the medial geniculate nucleus. *J Comp Neurol 520*:*34–51*.

Sugimoto-Shirasu K, **Roberts K** (2003) “Big it up”: Endoreduplication and cell-size control in plants. *Curr Opin Plant Biol 6*:*544–553*.

Tasic B, **Menon V**, **Nguyen TN**, **Kim TK**, **Jarsky T**, **Yao Z**, **Levi B**, **Gray LT**, **Sorensen SA**, **Dolbeare T**, **Bertagnolli D**, **Goldy J**, **Shapovalova N**, **Parry S**, **Lee C**, **Smith K**, **Bernard A**, **Madisen L**, **Sunkin SM**, **Hawrylycz M**, **Koch C**, **Zeng H** (2016) Adult mouse cortical cell taxonomy revealed by single cell transcriptomics. *Nat Neurosci 19*:*335–346*.

Terasawa E, **Kurian JR** (2012) Neuroendocrine mechanism of puberty. In: Handbook of Neuroendocrinology, pp 433–484. Academic Press.

Ting AY, **Blacklock AD**, **Smith PG** (2004) Estrogen Regulates Vaginal Sensory and Autonomic Nerve Density in the Rat1. *Biol Reprod 71*:*1397–1404*.

Tomova A, **Deepinder F**, **Robeva R**, **Lalabonova H**, **Kumanov P**, **Agarwal A** (2010) Growth and development of male external genitalia: A cross-sectional study of 6200 males aged 0 to 19 years. *Arch Pediatr Adolesc Med 164*:*1152–1157*.

Udaka F, **Kameyama M**, **Tomonaga M** (1986) Degeneration of betz cells in motor neuron disease. A Golgi study. *Acta Neuropathol 70*:*289–295*.

Van Der Loos H, **Welker E**, **Dörfl J**, **Rumo G** (1986) Selective breeding for variations in patterns of mystacial vibrissae of mice: Bilaterally symmetrical strains derived from ICR stock. *J Hered 77*:*66–82*.

Van Der Loos H, **Woolsey TA** (1973) Somatosensory cortex: Structural alterations following early injury to sense organs. *Science 179*:*395–398*.

Vandenbergh JG (1967) Effect of the presence of a male on the sexual maturation of female mice. *Endocrinology 81*:*345–349*.

Vandenbergh JG (1969) Male odor accelerates female sexual maturation in mice. *Endocrinology 84*:*658–660*.

Vandenbergh JG (2012) Pheromonal Regulation of Puberty. In: Pheromones and Reproduction in Mammals.

Vogt O (1910) Die myeloarchitektonische Felderung des menschlichen Stirnhirns. *J Psychol Neurol 15*:*221–232*.

Waite PME, **Taylor PK** (1978) Removal of whiskers in young rats causes functional changes in cerebral cortex [24]. *Nature 274*:*600–602*.

Walker DM, **Bell MR**, **Flores C**, **Gulley JM**, **Willing J**, **Paul MJ** (2017) Adolescence and reward: Making sense of neural and behavioral changes amid the chaos. Society for Neuroscience.

Walshe FMR, **M R Walshe BF** (1942) The giant cells of betz, the motor cortex and the pyramidal tract: a critical review. *Brain 65*:*409–461*.

Walvoord EC (2010) The timing of puberty: Is it changing? Does it matter? *J Adolesc Heal 47*:*433–439*.

Welker C (1976) Receptive fields of barrels in the somatosensory neocortex of the rat. *J Comp Neurol 166*:*173–189*.

Welker C, **Woolsey TA** (1974) Structure of layer IV in the somatosensory neocortex of the rat: Description and comparison with the mouse. *J Comp Neurol 158*:*437–453*.

Welker E, **Van der Loos H** (1986) Quantitative correlation between barrel-field size and the sensory innervation of the whiskerpad: a comparative study in six strains of mice bred for different patterns of mystacial vibrissae. *J Neurosci 6*:*3355–3373*.

Wong-Riley MTT (1989) Cytochrome oxidase: an endogenous metabolic marker for neuronal activity. *Trends Neurosci 12*:*94–101*.

Woolsey TA, **Van der Loos H** (1970) The structural organization of layer IV in the somatosensory region (S I) of mouse cerebral cortex. The description of a cortical field composed of discrete cytoarchitectonic units. *Brain Res 17*:*205–242*.

Worthman CM, **Trang K** (2018) Dynamics of body time, social time and life history at adolescence. *Nature 554*:*451–457*.

Xerri C (2008) Imprinting of idyosyncratic experience in cortical sensory maps: Neural substrates of representational remodeling and correlative perceptual changes. *Behav Brain Res 192*:*26–41*.

Xerri C, **Stern JM**, **Merzenich MM** (1994) Alterations of the cortical representation of the rat ventrum induced by nursing behavior. *J Neurosci 14*:*1710–1721*.

y Cajal SR (1923) Recuerdos de mi vida:(obra ilustrada con numerosos fotograbados). Imprenta de Juan Pueyo.

Zilles K (2018) Brodmann: A pioneer of human brain mapping-His impact on concepts of cortical organization. *Brain 141*:*3262–3278*.

List of Publications

Purkart, L., **Sigl-Glöckner, J**. & Brecht, M. (**in revision**). Constant innervation despite pubertal growth of the mouse penis. *Journal of Comparative Neurology* *,†

Takahashi, N., Ebner, C., **Sigl-Glöckner, J**., Nierwetberg, S. & Larkum, M. (**in revision**). Active Dendritic Currents Gate Descending Cortical Outputs in Perception. *Nature Neuroscience* *

Sigl-Glöckner J., Meier E., Takahashi N., Sachdev, R. Larkum M. & Brecht M. (**in press**). Effects of sexual experience and puberty on mouse genital cortex revealed by chronic imaging. *Current Biology* *,†

Sigl-Glöckner J. & Seibt J. (**2018**) Peeking into the sleeping brain: how in vivo imaging in rodents contributes to the understanding of the relationship between sleep and cognition. *Journal of Neuroscience Methods*. *316: 71-82*.*

Seibt J., Richard C., **Sigl-Glöckner J**., Takahashi N., Doron G., Kaplan D., de Limoges D., Bocklisch C., & Larkum M. E. (**2017**) Cortical dendritic activity correlates with spindle-rich oscillations during sleep in rodents. *Nature Communications*. *8(1), 684*.*

Sigl-Glöckner J. & Brecht M. (**2017**) Polyploidy and the Cellular and Areal Diversity of Rat Cortical Layer 5 Pyramidal Neurons. *Cell Reports* 20.11: 2575-2583.*,†

Lenschow C., **Sigl-Glöckner J.**, Brecht M. (**2017**) Development of rat female genital cortex and control of female puberty by sexual touch. *PLoS Biol* 15(9): e2001283. *,†

Allgaier, A., Pietsch, K., Fruhe, B., **Sigl-Glöckner, J.** & Schulte-Körne, G. (**2012**) Screening for Depression in Adolescents: Validity of the Patient Health Questionnaire in Pediatric Care. *Depression and anxiety*, *29*.10: 906-913.

Allgaier, A., Pietsch, K., Fruhe, B., Prast, E., **Sigl-Glöckner, J.** & Schulte-Körne, G. (**2012**) Depression in pediatric care: Is the WHO-5 Well-Being Index a valid screening instrument for children and adolescents? *General hospital psychiatry* 34.3: 234-241.

* This research was done during the PhD studies.

† These papers are part of this thesis.

Acknowledgements

First of all, I would like to thank my supervisor Prof. Dr. Michael Brecht for sharing his infinite curiosity and great enthusiasm for neuroscience and biology. Michael is able to create a unique, familiar and most of all positive lab environment, where junior scientists can thrive, investigate unconventional questions and always feel like the effort and sometimes suffering is worthwhile, because all research questions are treated equally. In addition to this ubiquitous spirit it was his physical presence in the lab that helped me not to get lost in never-ending data collection and procedural polishing but to keep the bigger picture in sight. I learned that only a result that is visible in the raw data is convincing and that most of the time, the first, simplest and most straightforward experiment is the best. Throughout the last four years I was having a lot of fun and I cannot imagine a better mentor and supervisor.

Further, I would like to thank my outstanding friends and colleagues at the Brecht lab: Constanze Lenschow for sharing a room in Chicago, many early mornings in the lab and finally her research on genital cortex with me; Eddy Meier for his great spirit during dark hours in the two-photon room and never giving up on our juxtacellular recordings; Leo Purkart for being an absolutely outstanding undergraduate student, who independently set up an entire experimental network from the BCCN to the Naturkundemuseum to visualize those penis fibers; Ann Clemens for providing invaluable linguistic and scientific feedback on this thesis and innumerous other paper drafts; Undine Schneeweis for being the heart and soul of the lab, things would fall apart with her; Shimpei Ishiyama, Jean Simmonet, Edith Chorev and Christian Ebbesen, my office neighbors, for telling me that Excel is no longer an option and guiding me through the unknown waters of Matlab and other programming Grenzerfahrungen; Nacho Sanguinetti and Saikat Ray for making the last years a culinary breakthrough and Konstantin Hartmann for providing the drinks (and always a great spirit!); the new generation, Lena, Elcin, Katriona and Iovanna for rejuvenating the lab and ensuring that the future is female; Andreea Neukirchner, Tanja Wölk, Juliane Diederichs, Maik Kunert, Arnold Stern, Willi Schiegel, Karin Biermann and Denise Kaufmann for providing a great technical and administrative infrastructure that makes the lab run smoothly despite the never-ending bureaucratic hurdles; and to everyone else whose paths I crossed in and around the lab in the last years.

I would like to thank Prof. Dr. Matthew Larkum for welcoming me in his lab five years ago and for his great advice and fruitful discussion throughout my whole PhD. I also want to thank

his entire group, in particular Robert Sachdev, Naoya Takahashi and Julie Seibt for giving me a second home over at the Charite, sharing not only their endless knowledge on two-photon imaging but also their equipment, be it centrifuges, mice or microscopes, with me. Neither project would have been possible without them.

I would like to thank all current, past and future BIF fellows as well as everyone at the BIF office in Mainz. I am very grateful for being a part of this unique network of young scientists. Hirschegg and Lautrach are some of the most memorably days within the last four years.

I would like to thank my parents, Martina & Richard and Peter & Nicola, my siblings, Pippa, Lucas and Kilian, my grandmother Gossa and my friends, both in Berlin and in Munich, Carina, Nikolai, Philip, Lukas, Teresa, Anna, Anna, Eli, Konrad and Laurenz for listening to my highs and lows throughout the last for years and providing endless support and encouragement. In particular, I would like to thank my sister for sharing her home with me for the last couple of months and always keeping up my spirit throughout the final stretch. Finally, I would like to thank Felix for spending endless hours on the train and always letting me play office.

Eigenständigkeitserklärung

Hiermit versichere ich, dass ich die vorliegende Arbeit selbständig verfasst und keine anderen als die angegebenen Quellen und Hilfsmittel verwendet habe. Ich erkläre, dass ich sämtliche in der oben genannten Arbeit verwendeten fremden Quellen als solche kenntlich gemacht habe und gemäß den mir bekannten gängigen wissenschaftlichen Regeln korrekt zitiert habe. Ich bestätige, dass ich bei wörtlich übernommenen Aussagen bzw. bei unverändert übernommenen Grafiken als auch bei in eigenen Worten wiedergegebenen Aussagen bzw. von mir abgewandelten Grafiken anderer Autoren die Quelle angegeben habe. In dem Zusammengang, muss erwähnt werden, dass die in der vorgelegten Arbeit behandelten Themen bereits in wissenschaftlichen Zeitungen veröffentlicht wurden. Aus diesem Grund sind Ähnlichkeiten in Text und Abbildung unvermeidbar. Zu Beginn eines jeden Kapitels, wurde deshalb auch noch einmal explizit darauf verwiesen, dass das Thema bereits veröffentlicht wurde.
Ich habe diese Arbeit nicht anderweitig zu Prüfungszwecken vorgelegt und habe mich nicht anderwärts um einen Doktorgrad beworben. Des weiteren versichere ich, dass keine Zusammenarbeit mit gewerblichen Promotionsberatern stattgefunden hat. Bei Anfertigung der Arbeit wurden die Grundsätze der Humboldt-Universität zu Berlin zur Sicherung guter wissenschaftlicher Praxis eingehalten. Die dem Promotionsverfahren zugrunde liegende Promotionsordnung ist mir bekannt.

Datum:

Unterschrift: